THÈSE

Pour obtenir le grade de

DOCTEUR DE L'UNIVERSITÉ GRENOBLE ALPES

École doctorale : CSV- Chimie et Sciences du Vivant
Spécialité : Chimie Biologie
Unité de recherche : LPCV - Laboratoire de Physiologie Cellulaire Végétale

Capture Contrôlée de Goutelettes Lipidiques: Design de Compartiments pour Sonder les Contacts entre Organelles et les Flux Metaboliques

Controlled Trapping of Lipid Droplets: Engineered Compartments to Probe Organelle Contacts and Metabolic Flux

Présentée par :

Chems AMARI

Direction de thèse :

Juliette SALVAING CHARGEE DE RECHERCHE HDR, INRAE	Directrice de thèse
Zoher GUEROUI chercheur, CNRS	Co-directeur de thèse

Rapporteurs :

Yonghua LI-BEISSON
DIRECTRICE DE RECHERCHE, CEA Cadarache
Guillaume DRIN
DIRECTEUR DE RECHERCHE, CNRS Délégation Côte d'Azur

Thèse soutenue publiquement le **7 novembre 2025**, devant le jury composé de :

Juliette SALVAING, CHARGEE DE RECHERCHE, INRAE Grenoble	Directrice de thèse
Zoher GUEROUI, DIRECTEUR DE RECHERCHE, Ecole Normale Supérieure	Co-directeur de thèse
Yonghua LI-BEISSON, DIRECTRICE DE RECHERCHE, CEA Cadarache	Rapporteure
Guillaume DRIN, DIRECTEUR DE RECHERCHE, CNRS Délégation Côte d'Azur	Rapporteur
Marc JAMIN, PROFESSEUR DES UNIVERSITES, Université Grenoble Alpes	Président
Alice NICOLAS, DIRECTRICE DE RECHERCHE, CNRS Délégation Alpes	Examinatrice

Contents

Contents i

List of Figures iii

List of Tables v

Abbreviations vi

Preface 1

1 Manipulating organelle contacts: introducing lipid droplets 4
1 Communication between organelles at the center of cellular organization . . 5
2 Developing organelle probing tools for a perturbative approach 9
2.1 Traditional perturbation methods 9
2.2 Engineered synthetic tethers and proximity modules 11
2.3 Chemically induced dimerization for rapid and reversible control . . 12
2.4 Optogenetic control for light-induced perturbations 15
2.5 Optical tweezers and mechanical probing 19
3 The lipid droplet: a conserved organelle for lipid storage and metabolic regulation 21
3.1 General presentation of lipid droplets 21
3.2 Structure and composition 21
3.3 Formation and degradation mechanisms 24
3.4 Response to external stimuli 30
3.5 Biotechnological and biomedical relevance 33
4 PhD objectives 36
5 Review article: Lipid droplets degradation mechanisms from microalgae to mammals, a comparative overview 38

2 Designing artificial condensates to entrap lipid droplets 55
1 Liquid-liquid phase separation in synthetic biology 56
1.1 Physical Principles governing Liquid-Liquid Phase Separation (LLPS) 56
1.2 Quick overview of endogenous biological LLPS 59
2 Mimicking biological LLPS through protein engineering 61
3 Using synthetic condensates to control lipid droplet dynamics 69
4 Main findings 70
5 Main article: Controlling lipid droplet dynamics via tether condensates . . 73

6 Conclusion and transition . . . 92

3 Adaptation of ControLD to *Phaeodactylum tricornutum* 94
1 From mammalian cells to *Phaeodactylum tricornutum* . . . 96
2 Experimental strategies . . . 102
2.1 Adapting the ControLD scaffolds to *Phaeodactylum tricornutum* . . . 102
2.2 Pt transformation . . . 102
2.3 Choice of promoter . . . 103
2.4 Introducing Fm-Ft as an alternative scaffold for phase separation . . . 103
2.5 Development of a method for quantitative condensate localization and measurement . . . 105
3 Expression of non-targeted condensates in Pt . . . 108
3.1 Description of artificial condensates in Pt . . . 108
3.2 Quantitative analysis of condensate growth rate . . . 110
3.3 Concentration buffering effect of condensate formation . . . 111
3.4 Dynamic properties of condensates in Pt . . . 113
3.5 Development of a live-imaging setup for Pt . . . 115
3.6 Live dissolution of condensates in Pt . . . 117
4 Functionalization of condensates for lipid droplets targeting . . . 120
4.1 Functionalization with endogenous LD-associated proteins . . . 120
4.2 Optimization of LD-targeting strategies . . . 125
4.3 Induction of bigger LDs to favor StLDP recruitment . . . 129
5 Discussion and perspectives . . . 131
6 Material and methods . . . 135

Conclusion and perspectives 143

Annexes 150
1 Short communication: Condensate-mediated intracellular organelle sequestration . . . 151
2 Protein domains sequences . . . 152

References 155

List of Figures

1.1 Membrane contact sites as central organizing principles of cell biology . . . 6
1.2 Overview of loss-of-function approaches . . . 10
1.3 ChiMERA: a synthetic biology tether . . . 11
1.4 FKBP-FRB chemically induced dimerization . . . 13
1.5 CRY2-CIB1 optogenetic dimerization . . . 16
1.6 Optical tweezers to probe organelle contacts . . . 20
1.7 Lipid droplet general structure . . . 22
1.8 Lipid droplet biogenesis . . . 26
1.9 Lipid droplet degradation . . . 29
1.10 PhD general concept . . . 36

2.1 General principles of liquid-liquid phase separation. . . . 56
2.2 Examples of dynamic properties of LLPS condensates . . . 58
2.3 Examples of endogenous biomolecular condensates . . . 60
2.5 OptoDroplets as light-induced condensates . . . 64
2.6 The Corelet system, a high-valency photoinducible LLPS . . . 65
2.7 iPOLYMER: a chemically inducible condensate . . . 66
2.8 Modular Fm-Ft phase separation scaffold . . . 67
2.9 5Fm condensates as a pathological model . . . 68
2.10 Graphical abstract of the ControLD framework . . . 70

3.1 Endosymbiotic events in *Phaeodactyum tricornutum* evolution . . . 97
3.2 Change of cellular model: from HeLa to Pt . . . 101
3.3 Nitrate-induced GFP expression kinetics . . . 104
3.4 High-throughput condensate and cell segmentation . . . 106
3.5 Validation of inducible GFP expression . . . 108
3.6 Expression of LLPS condensates in Pt . . . 109
3.7 Condensate count distribution per cell . . . 110
3.8 Condensate growth dynamics over time . . . 111
3.9 Cytosolic fluorescence comparison between LLPS scaffolds . . . 112
3.10 DMSO concentration effects on condensates . . . 114
3.11 Microwell fabrication for live imaging . . . 116
3.12 Left: Daily imaging of Pt cell divisions using microwells . . . 117
3.13 Overnight live imaging of divisions . . . 117
3.14 Real-time DMSO-induced condensate dissolution . . . 118
3.15 StLDP-emGFP localization patterns . . . 120
3.16 StLDP-functionalized condensates dock to LDs . . . 121

3.17 GFP intensity kinetics post induction 122
3.18 Condensate-LD colocalization frequency quantification 123
3.19 PtLDP1 scaffold and its localization in cells 125
3.20 Truncated StLDP scaffold targeting effects 126
3.21 Using HOGP as an exogenous LD targeting protein 127
3.22 Dual scaffold expression localization analysis 128
3.23 Phosphate starvation for StLDP recruitment 129
3.24 Palmitoleic feeding for large LDs formation 130

List of Tables

3.1 Complete list of generated plasmids and Pt strains. Bltc.: number of biolistics performed; Scr.: number of screened colonies; Pos.: number of positive colonies showing fluorescence after nitrate induction. Blasti, blasticidine. . 105
5.2 Amino-acid sequences of protein domains, and nucleic sequences of promoters presented throughout the study. 152

Abbreviations

Acyl-CoA Acyl-coenzyme A

CID Chemically induced dimerization

CNN Convolutional neural network

DAG Diacylglycerol

DMSO Dimethylsulfoxide

emGFP Emerald Green Fluorescent Protein

ER Endoplasmic reticulum

fcpA (fcpB) Fucoxanthin chlorophyll protein A (B)

FKBP FK506 binding protein

Fm Human FKBP with point mutation F36M

FRAP Fluorescence recovery after photobleaching

Ft Human light-chain ferritin

HOGP *Haematococcus* oil globule protein

LD Lipid droplet

LLPS Liquid-liquid phase separation

NOA Norland optical adhesive 85S

PDMS Polydimethylsiloxane

Plin1/2/3 Perilipin 1/2/3

pNR Nitrate reductase promoter of *Pt*

Pt *Phaeodactylum tricornutum*

PtLDP1 *Phaeodactylum tricornutum* Lipid Droplet Protein 1

StLDP *Stramenopile*-type LD protein

TAG Triacylglycerol

Preface

Cells are nonequilibrium systems in constant flux. To stay alive, they must store energy, build new components, and respond to environmental changes. Much of this is coordinated by organelles, a set of specialized compartments that share materials and information through short-range contacts. With spatial and temporal organization, cells orchestrate thousands of biochemical reactions to maintain homeostasis and adapt to new conditions. Among organelles, lipid droplets (LDs) play a central role: beyond serving as neutral lipid reservoirs, they function as dynamic hubs that traffic fatty acids, recruit enzymes, and interface with the endoplasmic reticulum, mitochondria, peroxisomes, and other partners. A central challenge in cell biology is to understand how organelles communicate and cooperate to shape metabolism; accordingly, new methods are rapidly emerging to probe these interactions with causal precision.

In this context, my PhD project develops a targeted perturbation strategy to probe LD dynamics. Specifically, I engineer a protein-based system that uses principles of liquid-liquid phase separation to assemble directly at lipid droplet surfaces, transiently confining them and modulating their surface accessibility. By controlling access without globally altering lipid synthesis or degradation, I use this approach to test how limiting accessibility reshapes organelle contacts, redistributes lipid fluxes, and impacts LD behavior.

Organization of the manuscript

This manuscript is divided into three chapters.

In the first chapter, I describe the state-of-the-art tools used to investigate organelle dynamics, communication, and trafficking using perturbative approaches. These tools allow one to change a defined cellular element and reading out the consequences, and are therefore powerful for establishing causality. The focus narrows to lipid droplets, describing their structure, lipid and protein makeup, dynamics, and physiological roles, concluding with the rationale for selecting LDs as the central organelle of this thesis and the resulting design requirements for an LD-perturbation strategy.

In the second chapter, I develop and validate a synthetic methodology based on liquid-liquid phase separation to build protein condensates that can reversibly capture LDs in living mammalian cells. After a concise overview of phase separation and engineered condensates, I present the design of the ControLD system, its targeting logic, and its tunable, reversible behavior. This chapter details how ControLD perturbs LD accessibility and organization, the quantitative readouts used to characterize its action, and the main findings that establish its utility as a causal probe of LD function in mammalian cells.

In the third chapter, I adapt this strategy to the model microalga *Phaeodactylum tricornutum*. I outline the specific features that make diatoms an interesting model organism and describe the genetic and imaging methods used to port and assess the system in this organism. I first investigate the formation of artificial condensates in *P. tricornutum*, then functionalize them with LD-targeting proteins to achieve robust LD docking, and finally discuss the limits, trade-offs, and perspectives that arise from working in this divergent model.

Following a general conclusion and an outlook, the annex presents practical resources that support the main text, and a consolidated reference list closes the manuscript.

Chapter 1

Manipulating organelle contacts: introducing lipid droplets

Objectives

This chapter depicts the cell as a dynamic network of organelles wired by membrane contact sites and explains how these interfaces coordinate metabolism, signaling, and morphology. It then surveys perturbative strategies, from genetics and pharmacology to inducible synthetic tethers, that enable causal tests of inter-organelle communication. On this basis, lipid droplets are introduced as conserved, tractable model organelles, with an overview of their structure, life cycle, and functions. Finally the PhD aims are presented in this context.

Contents

1 Communication between organelles at the center of cellular organization **5**
2 Developing organelle probing tools for a perturbative approach **9**
2.1 Traditional perturbation methods 9
2.2 Engineered synthetic tethers and proximity modules 11
2.3 Chemically induced dimerization for rapid and reversible control 12
2.4 Optogenetic control for light-induced perturbations 15
2.5 Optical tweezers and mechanical probing 19
3 The lipid droplet: a conserved organelle for lipid storage and metabolic regulation . **21**
3.1 General presentation of lipid droplets 21
3.2 Structure and composition 21
3.3 Formation and degradation mechanisms 24
3.4 Response to external stimuli 30
3.5 Biotechnological and biomedical relevance 33
4 PhD objectives **36**
5 Review article: Lipid droplets degradation mechanisms from microalgae to mammals, a comparative overview **38**

1 Communication between organelles at the center of cellular organization

For much of the twentieth century, textbooks portrayed eukaryotic cells as archipelagos of specialized compartments, each executing a discrete subset of tasks behind sealed membranes. A more modern view emphasizes that organelles do not work in isolation: live imaging, electron tomography, and cell physiology converge on a paradigm where organelles operate as a *network* that constantly communicates and self-organizes at the mesoscale. Their membranes move, pause, undergo fission and fusion, and repeatedly come into close contact with partners. In this view, the cell's organization is less a static map than a circuit in motion, with information and material fluxes along specific paths[1].

A central motif of this network is the **membrane contact site** (MCS), a zone where two organelles approach to within tens of nanometers (typically 10-30 nm) without fusing. At this distance, the two membranes "kiss" but remain distinct, preserving identity while enabling proteins and lipids to transit. A canonical example is the contact sites between endoplasmic reticulum (ER) and mitochondria: ultrastructural studies first revealed striking images of ER cisternae wrapping around mitochondria; proteomics studies established that these contacts form at specific ER domains (the mitochondria-associated membrane, MAM). Over the past two decades, the field has moved from these descriptive beginnings to a functional understanding: contacts are platforms that intensify throughput and signaling locally, giving the cell speed and specificity that diffusion alone cannot provide [2].

This shift depicts therefore the cytoplasm as a wired landscape. Instead of isolated islands, the ER, mitochondria, lipid droplets, endosomes/lysosomes, peroxisomes, the Golgi and, in plants, plastids, form a web of short-range connections that open and close as physiological needs evolve. A small change in a tether's abundance, a local adjustment in lipid composition, or a tug from the cytoskeleton can alter how often two membranes meet and how long they remain engaged. Cells exploit this sensitivity to encode decisions: proliferating cells create contacts that favor biosynthesis and flux; differentiated or stressed cells favor contacts that support quality control and recycling. Fluxes across a contact alter the physical and chemical microenvironment at that same site, which in turn stabilizes or dismantles the connection, ensuring feedback. In this way, inter-organelle communication appears as a *central organizing principle* of eukaryotic cell biology.

What contact sites do: from descriptive to functional

Membrane contact sites have been extensively characterized over the past decades. While a comprehensive catalog is beyond the scope of this chapter, are highlights below selected examples that illustrate the span of their functional roles.

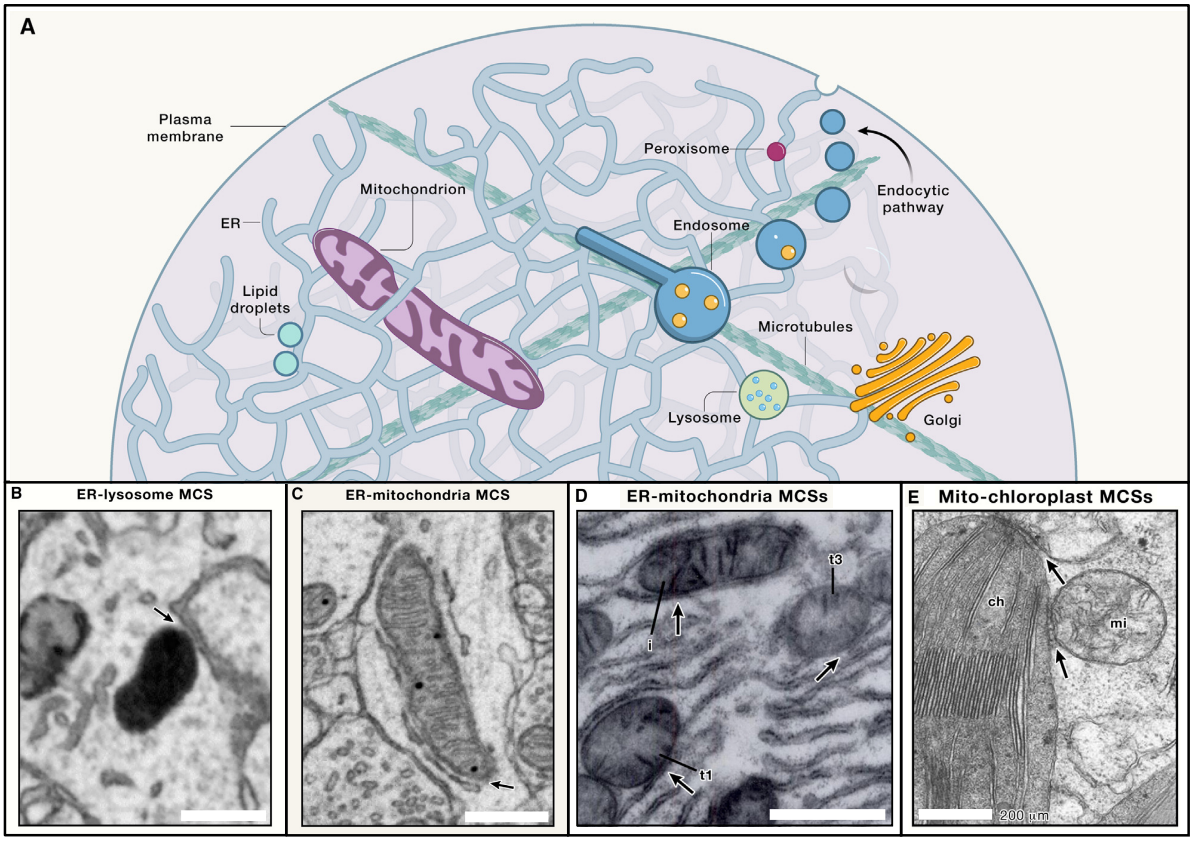

Figure 1.1: **A.** Organelles do not exist in isolation. Their locations are organized by the cytoskeleton and contacts formed between the membranes of different organelles. The endoplasmic reticulum (ER) in particular creates extensive contacts with other organelles. These contacts are major regulatory hubs in the cytoplasm. **B-E.** Electron micrographs reveal that organelle membranes contact each other within molecular distances (arrows). **B.** ER-lysosome MCS in the soma of a neuron. **C.** ER-mitochondria MCS in a dendrite. **D.** Abundant ER-mitochondria MCSs in a rat liver cell. l: mitochondrion shown in longitudinal section. t1, t3: mitochondria shown in transverse section. **E.** In plants, chloroplasts (ch) and mitochondria (mi) form MCSs marked by electron-dense bridges. Scale bars, 500 nm for B-D, 200 nm for E. Figure adapted from [Voeltz et al. 2024]

.

The best-studied example is the ER-mitochondria interface. These junctions couple three core processes that are otherwise distributed in space. First, they channel *lipid exchange*: phospholipids and precursors synthesized in the ER can be handed directly to mitochondria for membrane biogenesis and maintenance. Second, they confine *calcium signaling* to local microdomains: Ca^{2+} released from ER stores can be captured by mitochondrial uniporters within nanometers, tuning oxidative metabolism with high spatiotemporal precision. Third, they organize *mitochondrial morphogenesis*: thin ER tubules wrap mitochondria and mark future fission sites, aligning organelle division with metabolic state [1]. Through a single contact axis, metabolism, signaling and architecture are synchronized.

A second axis links the ER to lipid droplets (LDs). LDs bud from the ER and often

remain tethered to it; light and electron microscopy routinely show ER tubules embracing LDs, with shared proteins transiting across the interfacial bridge. These contacts govern both *storage* and *mobilization*: enzymes such as acyltransferases traffic from ER to LDs to build neutral lipids, while lipases and co-factors can be recruited in the opposite direction to release fatty acids when needed. Because LDs also engage mitochondria and peroxisomes, their contacts act as valves that direct fatty acids into β-oxidation on demand, minimizing cytosolic accumulation of toxic intermediates [4, 5]. LDs are therefore metabolic hubs at the crossroads of ER biosynthesis and mitochondrial/peroxisome catabolism.

Mitochondria-peroxisome contacts extend this division of tasks in lipid catabolism and redox control: very-long-chain or branched fatty acids can be shortened and detoxified with peroxisomal help before entering mitochondrial pathways. ER-endosome and ER-lysosome contacts add a logistics layer to trafficking and nutrient signaling: ER tubules can pause endosomes, change their maturation route, and provide conduits for cholesterol and phospholipid exchange; ER-lysosome junctions contribute to calcium homeostasis and tune autophagy capacity.

Across pairs and contexts, several generic functions recurrently emerge:

Metabolic channeling. By placing producers next to consumers, contact sites create efficient organization in metabolic fluxes. Lipids synthesized in the ER are delivered directly to mitochondria, LDs or endosomes; fatty acids released from LDs are fed straight into oxidation. Intermediates do not diffuse broadly into the cytosol, where they could be lost, mis-signaled or cause damage [4].

Spatially confined signaling. MCS generate privileged microdomains for second messengers (e.g. calcium signaling) so that signals are potent locally without perturbing global cytosolic levels. This yields fast, organelle-specific responses while preserving overall homeostasis [1].

Coordinated morphogenesis. Physical wrapping at interfaces aligns membrane remodeling across compartments. ER marks future mitochondrial fission sites; peroxisome and mitochondrial division can be coupled; autophagosome formation initiates at ER-rich interfaces that supply membrane.

Direct lipid and membrane exchange. Specialized tethers and lipid-transfer proteins shuttle phospholipids, sterols and signaling lipids across nanogaps orders of magnitude faster than bulk vesicular traffic. This maintains membrane composition and supports rapid remodeling when demands change.

These common roles explain how contact sites wire metabolism, signaling and structure into a coherent system. Because MCS can form and dissolve within seconds to minutes, the network balances itself in response to changing inputs. Under nutrient abundance, the

cell favors contacts that support synthesis and storage (ER-Golgi, ER-LD). Under starvation, LD-mitochondria and LD-peroxisome contacts often strengthen, routing stored fats to oxidation. During ER stress, ER-lysosome contacts can increase to boost degradation capacity. The same physical mechanism of adjustable proximity supports different physiological states without general rewiring of gene expression.

Physiology and diseases

When inter-organelle communication is operational, cells benefit from tight control over energy production, lipid balance and signaling homeostasis; when it fails, broad dysfunction follows. Defects at ER-mitochondria interfaces can decouple Ca^{2+} transfer from respiratory demand, producing energy shortfalls or stress signaling. Conversely, excessively tight coupling can drive Ca^{2+} overload and sensitize cells to apoptosis pathways. Genetic impairment of tether components highlights causality: altering levels or function of ER-mitochondria tethers such as VAPB-PTPIP51 changes contact frequency and impacts calcium handling and bioenergetics in neurons, pointing to mechanisms relevant for neurodegeneration [6]. On the metabolic side, misregulated ER-LD contacts can impair safe fat storage or timely mobilization, contributing to steatosis and insulin resistance; conversely, insufficient LD-mitochondria coupling can leave fatty acids stranded in the cytosol, where they damage membranes and organelles [5]. Similar themes recur in many contexts: skewed ER-endosome contacts alter cholesterol distribution; faulty mitochondria-peroxisome interplay perturbs fatty acid catabolism and redox balance. Because MCS sit at the junctions of pathways, their disruption propagates widely.

Two generic concepts emerge here. First, inter-organelle contacts give *speed* and *specificity* to cellular communication: they let compartments exchange information and material on the timescale of catalysis and ion flux. Second, MCS are inherently *regulation* levers: contact frequency, dwell time, and molecular composition can be tuned by modest changes in tethers, local lipids, or cytoskeletal forces. This is why the same cellular parts can support proliferation in one context, quiescence in another, and stress survival in a third without changing the population of organelles themselves.

This recognition has transformed cell biology from a descriptive atlas of compartments into a functional map of their conversations. With the central role of contact sites now established, the key challenge nowadays is to move beyond description and rigorously establish causal links between inter-organelle communication and cellular physiology.

2 Developing organelle probing tools for a perturbative approach

A common and effective way to study organelle interactions is the **perturbative approach**. One deliberately changes a defined element of the system, observes how contact architecture and function respond, and infers causality from the difference between the baseline and the perturbed state. This moves beyond descriptive colocalization. It tests what element is necessary for forming, stabilizing, or dissolving contacts and for supporting the fluxes that pass through them (lipids, ions, metabolites).

In practice, the workflow is direct. A mechanistic hypothesis is stated – for example, that a tether protein controls an ER-mitochondria junction. A targeted perturbation is applied. The experiment then tracks two classes of readouts in parallel: structural measures of contact geometry (frequency, lifetime, distance, ultrastructure when needed) and functional measures of throughput (calcium microdomains, lipid transfer rates, metabolite exchange, trafficking kinetics). Early responses on the scale of seconds to minutes are most informative about direct mechanisms. Slower changes over hours to days reveal instead compensation or remodeling. In this section, we will explore this logic and combine modalities to link changes in contact geometry to changes in function.

2.1 Traditional perturbation methods

In order to induce such perturbations, many different approaches co-exist nowadays. However, classical genetic approaches (gene knockout or knockdown) and chemical perturbations have long been the main tool for studying organelle functions. For example, genetic loss-of-function (LOF) methods ranging from classical mutagenesis and gene knockouts to newer CRISPR-based editing have been widely used to disrupt a specific protein or pathway, to gain a better understanding in various physiological events. The different methods described hereafter are summarized in figure 1.2.

Interestingly, each acts at different biological levels (DNA, RNA or protein) and with different durations[7]. The choice of method (e.g. CRISPR versus RNAi) can strongly affect outcomes. Knockdowns by RNAi or morpholinos typically produce partial, transient LOF, whereas null mutations irreversibly ablate function. In many systems (mouse, zebrafish, Arabidopsis, etc.) knockouts have triggered upregulation of other related genes that mask loss-of-function phenotypes, a phenomenon called genetic compensation[8]. Thus, interpreting LOF experiments requires care: one must consider differences in the depth, timing, reversibility and off-target effects of each tool.

CRISPR-based tools themselves come in multiple variants. Conventional CRISPR-Cas9 knockout creates DNA breaks and indels, permanently deleting gene function. By contrast, CRISPR interference (CRISPRi) and activation (CRISPRa) use nuclease-dead

dCas9 fused to repressors or activators to reversibly inhibit or upregulate transcription. In practice, CRISPRi often yields more uniform knockdown than RNAi, but like other methods it must deal with endogenous proteins and potential cellular adaptation over time.

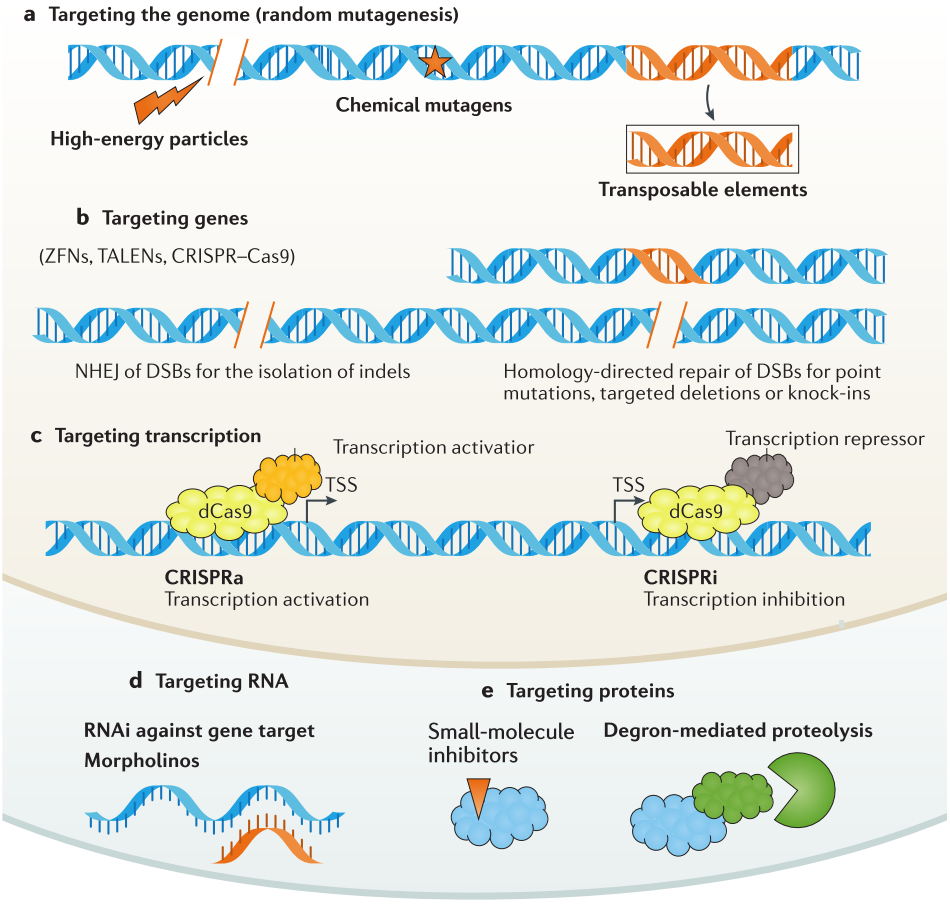

Figure 1.2: Overview of loss-of-function approaches, highlighting different levels of intervention (DNA, RNA, protein). Figure adapted from [Housden et al. 2017].

Complementing genetics, small-molecule inhibitors and drugs have proven another robust way to induce perturbations. These act directly on proteins or pathways and are typically fast, reversible, and tunable by dose[7]. Classic examples include metabolic inhibitors (e.g. ATP synthase inhibitors like oligomycin[7]), ER-stress inducers (thapsigargin to block SERCA calcium pumps[9]), or lipid metabolism blockers. Such chemicals can acutely modulate organelle functions such as electron transport, ion transport or lipid synthesis, and thus indirectly perturb inter-organelle communication. However, their specificity varies widely: some are highly specific enzyme inhibitors, while others have off-target toxicities. When possible, combining pharmacology with genetic perturbations (or using multiple drugs) helps validate which effects are on-target.

These classical genetic and pharmacological tools provide essential baseline approaches, but they often lack precise spatial or temporal control, and can trigger indirect compensation effects. In recent years, a new generation of methods inspired by synthetic and

optical biology has emerged to directly manipulate organelle contacts with high resolution. The following sections discuss modern strategies for acutely inducing or measuring inter-organelle contact and communication.

2.2 Engineered synthetic tethers and proximity modules

In order to explore new synthetic perturbative approaches, researchers have built various systems of fixed synthetic tethers to force proximity of organelles. These engineered connectors act like artificial membrane contact sites. A classic example is the ChiMERA construct from Kornmann et al. in 2009[10]. ChiMERA is a chimeric protein containing a mitochondrial targeting presequence, a fluorescent GFP core, and an ER membrane anchor tail (see figure 1.3). As such, ChiMERA physically spans the ER-mitochondrial gap: the N-terminal helix inserts into mitochondria and the C-terminal KDEL-like tail anchors to the ER. When expressed in yeast lacking the endogenous ER-mitochondria tethering complex (ERMES), ChiMERA rescued the defects effectively substituting for the native tether. This proof-of-concept showed that an engineered bifunctional protein can enforce organelle contact and restore exchange (e.g. phospholipid transfer) *in vivo*. Subsequent work has used similar strategies to modulate contact strength: for instance, synthetic linkers (of defined length or flexibility) have been used to tune the distance between organelles and assess effects on calcium flux and metabolism[1].

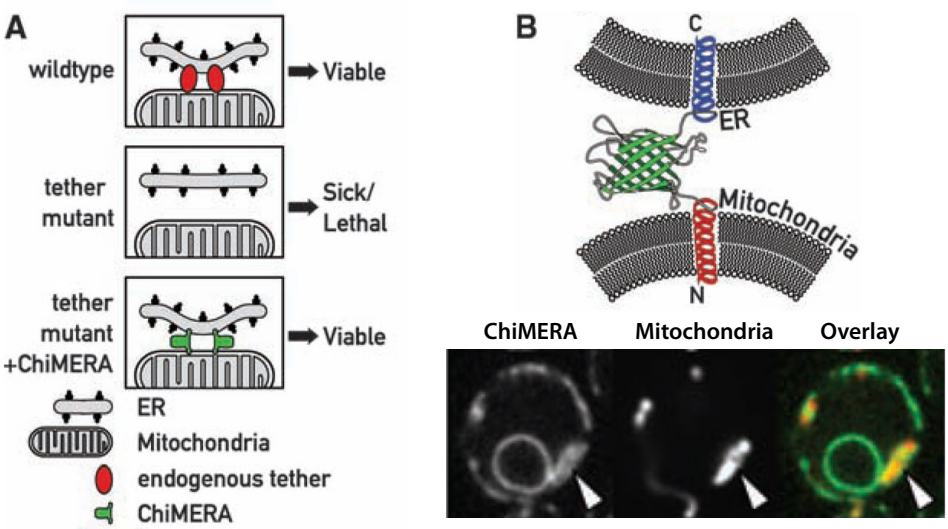

Figure 1.3: ChiMERA: a synthetic biology tether to uncover mutants of the ER-mitochondria connection. (A) Rationale of the tether. (B) Outline of the ChiMERA. A central GFP molecule (green) is flanked by the mitochondria-directed N-terminal Tom70 presequence and transmembrane sequence (red) and the ER-directed C-terminal Ubc6 tail anchor sequence (blue). (C) Confocal Z-series across a yeast cell expressing the ChiMERA and a mitochondrial marker (mt-dsRed). ChiMERA displays a characteristic ER staining with additional thicker structures (arrowheads), which colocalize with mitochondria and represent sites of artificial tethering. Adapted from [Kornmann et al. 2009]

Other synthetic modules include engineered protein scaffolds or heterodimers inserted

at membranes. For example, expressing membrane proteins with complementary leucine-zipper domains or with chemically inducible dimers provides a constant tether once induced. In higher eukaryotes, overexpression of tether components like VAPB-PTPIP51 can tighten ER-mitochondria contacts; although these are native proteins, their dose-dependent effect mimics a synthetic tether[6]. Additionally, synthetic lipid-binding domains fused to membrane anchors (e.g. adding a phosphoinositide-binding PH domain on one organelle and a matching binding motif on another) have been proposed to create lipid-mediated tethers. More recently, synthetic biology approaches have built completely artificial contact sites: one study inserted a chemically self-assembling protein to link two lipid bilayers in vitro, recapitulating SNARE-independent membrane tethering[11]. In general, these engineered proximity modules are designed as constant-on tethers, and serve to test how forced physical apposition alone (independent of native signaling) influences inter-organelle exchange.

These synthetic tethers have been applied to many organelle pairs. For example, linking lipid droplets to mitochondria or peroxisomes can be achieved by fusing an LD-targeting peptide to a peroxisome- or mitochondrion-targeting anchor. In mammalian cells, an endogenous example is M1 Spastin, which localizes to LDs and directly tethers them to peroxisomes; overexpressing Spastin mimics a synthetic LD-peroxisome bridge and promotes fatty acid trafficking to peroxisomes[12]. Such tools have elucidated the metabolic role of specific contacts. Therefore, these engineered tethers allow investigators to force organelle proximity and analyze the consequences of this physical coupling.

2.3 Chemically induced dimerization for rapid and reversible control

If engineered tethers provide a reliable way to statically link organelles, these systems lack dynamic properties such as rapid on/off switching. To address this, researchers have developed chemically induced dimerization (CID). These systems use bifunctional small molecules to force two engineered protein domains to bind with high affinity and specificity[13]. The most classical CID employs the natural product rapamycin, an immunosuppressive drug that binds simultaneously to the protein FKBP12 (FK506-binding protein) and FRB (FKBP-rapamycin binding domain of the mammalian target of mTOR kinase). This system, developed by Spencer et al. in 1993, was used to control protein position by oligomerization[14]. Structurally, rapamycin occupies a pocket in FKBP and presents an interface that captures FRB through complementary contacts[15]. This ternary complex (FKBP-rapamycin-FRB) is extremely stable, with a dissociation constant in the low nanomolar range. Importantly, FKBP and FRB are small domains (12 kDa and 11 kDa respectively) that can be genetically fused to other proteins without disrupting their function. Thus, by expressing an FKBP fusion on one organelle and an FRB fusion on another, addition of rapamycin rapidly brings the two organelles together.

In addition to rapamycin, several orthogonal CID modules have been developed using plant hormones. For instance, gibberellin (GA_3) binds its receptor GID1 and induces a conformational change that recruits the DELLA protein GAI[16]. The GA_3-AM prodrug, which is hydrolyzed in cells to GA_3, efficiently triggers GID1-GAI binding on a sub-minute timescale. Likewise, abscisic acid (ABA) acts as a molecular glue between ABA receptors (PYR/PYL family) and PP2C phosphatases (e.g. HAB1)[17]. These hormone-based CIDs are fully orthogonal to the FKBP/FRB system, allowing combinatorial control.

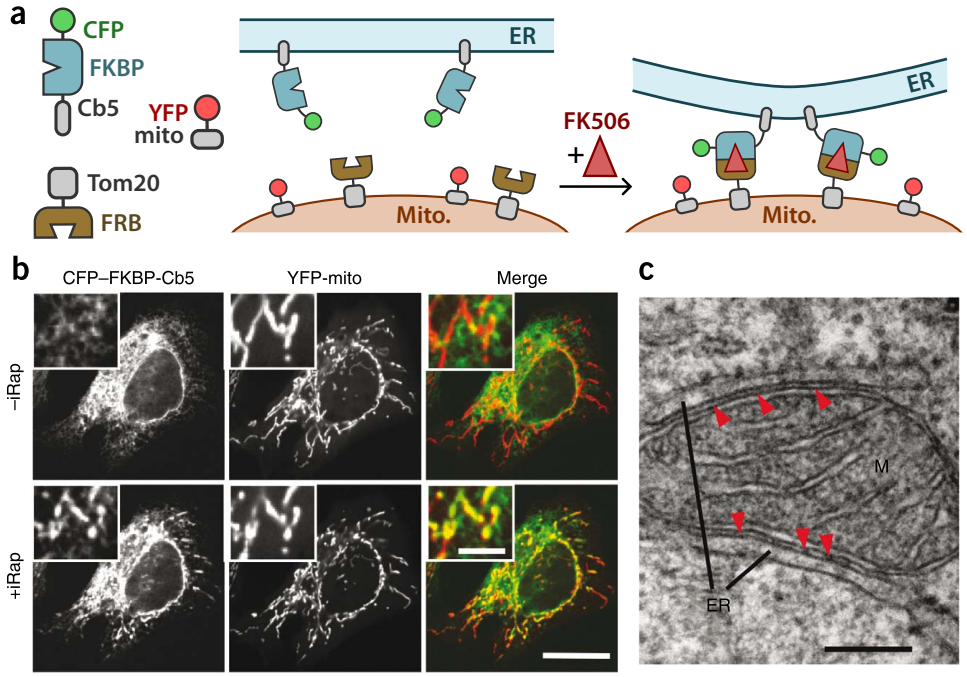

Figure 1.4: (a) Implementation of organelle recruiting system to probe the role of signaling molecules and inter-organelle interactions using rapamycin-induced FKBP-FRB dimerization. (b) Confocal fluorescence images of HeLa cells expressing CFP-FKBP-Cb5 (ER marker), Tom20-FRB and YFP-labeled mitochondrial marker (YFP-mito) before and after addition of 5 µM iRap (a rapamycin analog) for 5 min. Scale bars, 20 µm; 5µm for insets. (e) TEM images of membrane junction sites created by inducible ER-mitochondria connection. Cells were expressing Tom20-YFP-FRB and CFP-FKBP-Cb5 and were treated with 5 µM iRap for 15 min. Arrowheads mark junction sites. M, mitochondria. Scale bar, 500 nm. Images adapted from [Komatsu et al. 2010].

Organelle-targeted CID for tethering and recruitment. If these CID tools have also been broadly used for signal transduction and gene regulation, they have been especially useful regarding the field of organelle perturbation. CID tools are often targeted to specific organelles by fusing the dimerization domains to organelle-localizing sequences. One landmark application was by Komatsu *et al.*, who fused FKBP or FRB to proteins localized on different organelles. Using a membrane-anchored FRB (e.g. FRB fused to an ER membrane protein) and an FKBP-tagged mitochondrial anchor, rapamycin addition induced rapid ER-mitochondrial tethering[18], as depicted in figure 1.4. In that work, rapamycin drove colocalization of ER and mitochondrial markers within minutes, effec-

tively forming a synthetic contact site between the two organelles. A similar approach (the anchor-away strategy) has been used to translocate nuclear or cytosolic factors to various organelles. For example, tagging a protein of interest with FKBP and an organelle anchor with FRB allows recruitment upon ligand addition[19]. Another study developped a PEX3-FKBP peroxisome anchor and an FRB-tagged fragment of Dopey1 to test peroxisome dynamics[20]. Addition of rapamycin forced the FRB-Dopey1 fusion to peroxisomes via FKBP, and live imaging showed that this artificial tethering dramatically altered peroxisome positioning. Specifically, rapamycin recruited a Dopey1 fragment (lacking its membrane-binding DEC domain) to PEX3-FKBP on peroxisomes, causing the peroxisomes to move outward along microtubules, leading to a significant increase in the average radial distribution and velocity of peroxisomes after CID tethering. Thus, CID can be used to mechanically link proteins to organelles and observe functional outcomes, such as transport and clustering.

More complex CID designs have extended tethering to three-way junctions. Umehara and Inoue introduced chemically inducible trimerization (CIT) by splitting the FRB domain into two halves and co-expressing them with FKBP[13]. In a CIT system, rapamycin simultaneously binds FKBP and both FRB halves, bringing together three distinct components. This enabled synthetic tri-organellar junctions: co-targeting two split FRB halves to the ER and plasma membrane and FKBP to mitochondria, then adding rapamycin drove all three organelles to cluster together: 15 minutes after rapamycin, signals from plasma membrane, ER, and mitochondria became highly colocalized, demonstrating engineered contact formation between these organelles. This tri-tethering approach also allowed highly localized biochemical perturbation: for instance, recruiting a PI(4,5)P_2 phosphatase (INP54P) to ER-membrane junctions with CIT depleted PIP_2 specifically at those sites, while leaving the bulk membrane intact. CID can therefore be used not only to bring existing contacts together, but to create entirely new organelle contact sites on demand.

Recent innovations have enhanced CID versatility. Photocaged CID ligands allow light-activated control: for example, Shen *et al.* synthesized a photoactivatable rapamycin analog (pRap) and an engineered FKBP variant (iFKBP). In their system, cells expressing FKBP or iFKBP fusions remained inactive until a pulse of UV light uncaged rapamycin to trigger heterodimerization[21], leading to a localized dimerization and a finer temporal gating compared to adding drug. Similarly, photoresponsive versions of other CIDs (e.g. caged gibberellins or caged ABA) have been reported, enabling optogenetic-like control of chemically based dimerizers.

Synthetic variation of CID molecules adds further control. Mutant FRB domains have been generated that bind only to designed rapalogs (analogs of rapamycin), reducing crosstalk with endogenous mTOR. For example, an FRB(T2098L) mutation recognizes rapalog AP21967, which does not inhibit mTOR, enabling in vivo studies with minimal

toxicity[13]. The combination of multiple CID systems (e.g. FKBP/FRB + GID1/GAI) in the same cell is particularly powerful: Miyamoto *et al.* built intracellular AND/OR gates by requiring two separate ligands, achieving sub-minute logical control of protein localization and even cell shape[16]. In summary, modern CID technology includes photocaged CIDs, fully reversible dimers, split-protein designs (CIT), and libraries of synthetic ligands, all providing highly tunable and rapid modulation of protein and organelle interactions.

However, CID systems have caveats. The requirement for an exogenous ligand means that drug delivery, cell permeability, and dimerization kinetics become experimental variables. Rapamycin, in particular, is an immunosuppressant: it inherently binds endogenous mTOR and inhibits TOR signaling[22]. Use of mutant FRB and non-immunosuppressive rapalogs can mitigate this, but any small molecule used as a CID may have off-target effects or toxicity. Reversibility is also limited: many CIDs once activated stay dimerized until ligand is removed and even then, dissociation can be slow. In multi-cell or in vivo settings, homogeneous ligand delivery and light penetration (for photocaged CIDs) can be challenging. Finally, the engineered fusion proteins themselves may perturb membrane dynamics or recruit unintended partners. Careful controls are needed to ensure that observed phenotypes are due to the intended tethering or localization, instead of non-specific clustering or overexpression artifacts.

Despite these limitations, CID-based strategies have become indispensable for probing organelle communication. By providing fast, reversible, and localized control, CID enables tests of how contacts affect cellular physiology. As newer CIDs continue to emerge, they will only enhance our ability to understand the complex network of membrane contact sites that control cell organization.

2.4 Optogenetic control for light-induced perturbations

An innovative and powerful approach to perturb organelle contacts is using optogenetic tools. These systems use light-sensitive protein domains to control protein interactions with high spatiotemporal precision. By fusing light-inducible dimerization modules to organelle-targeting sequences, researchers can use light pulses to rapidly and reversibly induce or break membrane contacts between organelles.

The most widely used optogenetic dimerizers in mammalian cells derive from plant photoreceptors. The CRY2-CIB1 system, based on the blue-light photoreceptor cryptochrome 2 (CRY2) and its binding partner CIB1 from *Arabidopsis thaliana*, was first described in plant cells[23]. Upon illumination (450-490 nm), CRY2 binds to its FAD cofactor and undergoes a conformational change that enables high-affinity binding to CIB1. In vitro and in vivo studies showed that photoexcited CRY2 can also oligomerize into photobodies, but fusion to CIB1 generally promotes heterodimerization[24]. In mam-

malian cells, truncated CRY2 and N-terminal CIB1 have been used to recruit proteins or organelle membranes to one another. For example, Duan *et al.* used CRY2-CIB1 to attach kinesin or dynein motors to organelles: CRY2 was anchored to the mitochondrial, peroxisomal or lysosomal membrane and CIB1 was fused to a motor-adaptor, so that blue light rapidly drove those organelles along microtubules[25], as shown in figure 1.5. This CRY2-CIB1 system presents subsecond binding kinetics and the ability to reverse association when light is removed[24].

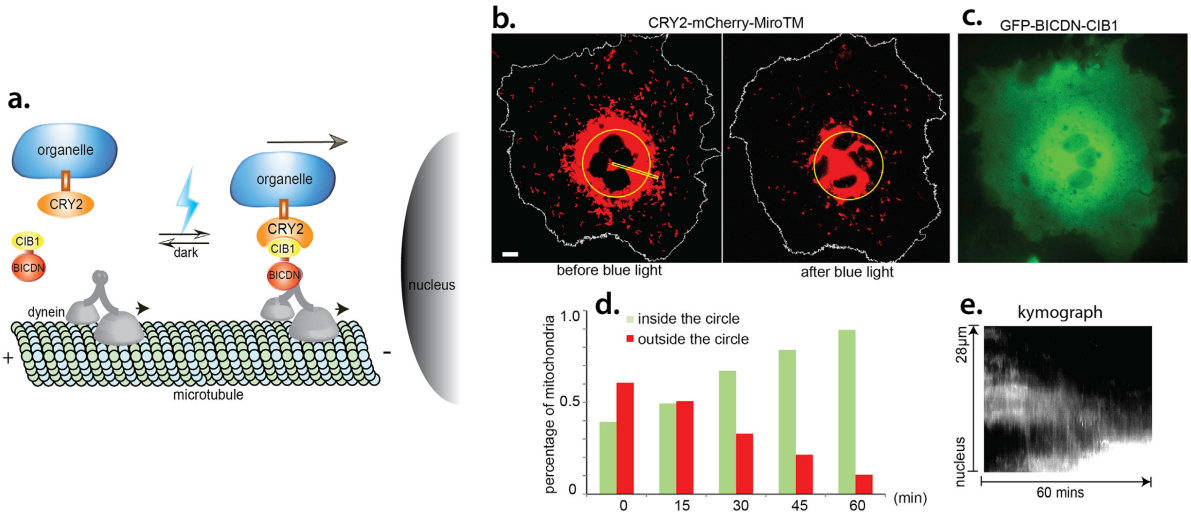

Figure 1.5: Light-induced redistribution of mitochondria by recruiting molecular motors. **a.** Schematic of light-controlled motor recruitment and organelle transport. COS-7 cells were transfected with CRY2-mCherry-MiroTM and GFP-BICDN-CIB1. **b.** Mitochondria were visualized in the red channel by CRY2-mCherry-MiroTM. Before blue-light illumination, some mitochondria were positioned close to the nucleus while others were spread throughout the cell. After blue-light illumination, most mitochondria moved toward the cell nucleus as indicated by the yellow circle. **c.** The green channel showed GFP-BICDN-CIB1 diffusing in the cytosol. **d.** The percentage of mitochondria inside the yellow circle in (A) increased from 39% to 89% after intermittent light exposure for 60 min. **e.** The kymograph extracted from the area indicated by yellow rectangle in (a.) showed the clear trend of mitochondria moving toward the nucleus. Scale bars, 10 μm. Adapted from [Duan et al. 2015].

The red-light activated PhyB-PIF is another widespread optogenetics system. This dimerizers exploit plant phytochrome B (PhyB) and its phytochrome-interacting factor (PIF) partner. In the dark or under far-red light (740-780 nm), PhyB is in the inactive Pr form and does not bind PIF. Red light (650 nm) photoisomerizes the attached linear tetrapyrrole chromophore, converting PhyB to the active Pfr state, which binds PIF proteins with high affinity. Switching to far-red light reverts PhyB to Pr and releases PIF[26]. For mammalian cells, it is mandatory to supply PCB, either by exogenous addition or by co-expressing heme oxygenase and phycocyanobilin synthase. Buckley et al. demonstrated that PhyB-PIF can be used in live zebrafish embryos: they anchored PhyB at the plasma membrane and showed rapid, reversible recruitment of a PIF6-fused protein

to specific cells and subcellular regions upon red light[27]. The PhyB-PIF interaction is highly specific to the light wavelength and is fully reversible on the order of seconds, enabling repeated cycles of binding and release. Thus, PhyB-PIF provides a powerful red-light optical switch complementary to blue-light systems.

Other optogenetic dimerizers have also been developed. The blue-light-sensitive LOV2 domain from *Avena sativa*[28] can be engineered as a light-inducible dimerizer, using a caging approach by fusing the LOV2 domain with the bacterial peptide SsrA[29]. In the dark, LOV2 N-terminal αhelix is anchored to SsrA, inducing a steric hindrance and preventing interactions with its natural binding partner, SspB. Upon blue light illumination LOV2 detaches, allowing SsrA and SspB to bind. This system was later improved through computational design to obtain a LOV2-SspB pair presenting a 50-fold affinity under blue light[30]. These LOV-based modules allow graded control of binding via light intensity and duration. Near-infrared optogenetics has also emerged: for example, bacterial phytochromes (BphP1-QPAS1 or BphP1-PpsR2 pairs) bind biliverdin and dimerize under 740 nm light, offering deeper tissue light penetration[31]. All these optogenetic platforms share a common mechanism of light-induced conformational change that toggles protein-protein affinity, with the CRY2-CIB1 (blue light) and PhyB-PIF (red/far-red light) pairs being the most established for mammalian cell engineering.

Optogenetic dimers enable precise control of inter-organelle or organelle-protein connections. By anchoring one dimer to one organelle and its partner to a second organelle, light pulses can create or remove membrane contacts on demand. Qiu *et al.* used CRY2-CIB1 to tether mitochondria and lysosomes: they fused CRY2 to a mitochondrial anchor and CIB to LAMP1 (a lysosomal protein), so that blue light drove acute formation of mitochondria-lysosome contacts (MLCs). This artificial MLC induction immediately increased mitochondrial fission rate, since lysosome contacts can create fission sites[32]. In cells lacking a fission regulator (SLC25A46$^{-/-}$), optically induced MLCs partially rescued normal mitochondrial morphology. Thus, the optogenetic MLC system provides a reversible platform to manipulate mitochondrial dynamics with spatiotemporal precision.

Similarly, optical tools have been applied to endoplasmic reticulum (ER) contacts and mechanobiology. For example, Song et al. engineered an inducible system called LIMER (light-inducible mechanostimulator of ER) in COS-7 cells: CRY2 and CIBN (the N-terminal domain of CIB1) were targeted to opposite sides of ER membranes, so that blue light generates a mechanical constraint on the ER network. Interestingly, this ER-specific optomechanical stimulus triggered a transient Ca^{2+} efflux from the ER lumen via stretch-sensitive channels (TRPV1 and PKD2). Thus optogenetics revealed that the ER is mechanosensitive: repeated blue-light pulses could tune Ca^{2+} release, and sustained activation induced ER stress markers and blocked ER-to-Golgi transport. In contrast to traditional mechanical agitation, optogenetic activation demonstrated rapid, reversible, and locally addressable.

In a similar fashion, Wu et al. showed that membrane-bound CRY2 can form extensive clusters when illuminated, implying that CRY2 tethering could dramatically reorganize membrane morphology[24]. This property has been harnessed as optoshaping tools. For instance, optogenetic clustering of CRY2 on mitochondria induced tubulation or fragmentation of the mitochondrial network[33]. Conversely, recruiting microtubule motors by light can reposition organelles: Duan *et al.* demonstrated blue-light-driven relocation of lysosomes, peroxisomes, or mitochondria by recruiting kinesin or dynein to those membranes[25]. More recently, Deng *et al.* created an optogenetic platform for lipid droplets called Opto-LDs: CRY2 fused to a droplet coat protein (either Plin2 or *Drosophila* Lsd-1) was paired with CIBN fused to kinesin or other motor adaptors. Blue light rapidly drove LDs to the cell periphery (kinesin) or perinuclear region (dynein) in hepatocytes[34]. This reversible control of LD position showed that peripherally localized LDs enhanced secretion of lipid vesicles (VLDL). Importantly, optogenetically moved LDs returned to normal distribution after illumination stopped, whereas genetic ablation of motors irreversibly disrupts transport.

These optogenetic approaches offer a temporal and spatial control far beyond conventional chemical dimerizers. Light activation can occur within milliseconds and stop immediately when illumination ends, providing sub-second kinetics. For instance, the PhyB-PIF system can recruit proteins in seconds upon red-light exposure and release them within seconds under far-red light[27]. This temporal control also aids dynamic studies: light pulses can be applied in controlled patterns to study fast processes such as vesicle trafficking or calcium release without chemical washout steps. Spatial precision is another unique feature: focused light can target single cells or even subcellular regions. Buckley *et al.* showed that PhyB-PIF recruitment could be confined to one region of a zebrafish neuroepithelial cell. By scanning light, one could selectively induce contacts in one part of the ER network or one cell in a tissue. Finally, optogenetics is noninvasive and tunable. No exogenous ligand must be added (except for plant chromophores in some systems), so endogenous signaling pathways remain unperturbed. For example, Deng et al. note that their LD-transport system is minimally invasive, avoiding broad disruption of the cytoskeleton as chemical drugs do[34]. Optogenetic perturbations can be reversed simply by turning off light, allowing recovery to be observed, whereas chemical crosslinks often require washout and have slow off-rates. However, one caveat is potential phototoxicity, but most dimerization systems require only low-intensity illumination for activation[32].

In summary, optogenetic heterodimerizers such as CRY2-CIB1 and PhyB-PIF enable unprecedented control over organelle interactions. By toggling dimerization on and off with light, researchers can induce or break membrane contacts, recruit motors, and probe organelle function in live mammalian cells with millisecond precision. As demonstrated in examples above, optical perturbation of ER-mitochondria, mitochondria-lysosome, and

LD-motor connections has provided new insights into organelle dynamics and physiology. Combined with its reversibility and spatial selectivity, optogenetics thus offers powerful capabilities for dissecting inter-organelle communication.

2.5 Optical tweezers and mechanical probing

Finally, a distinct class of methods uses physical force to test organelle contacts. Optical tweezers (laser traps) can immobilize and move single organelles within living cells. Because organelles have a different refractive index from the cytoplasm, a focused infrared laser can grab a mitochondrion or vesicle, hold it in place, and then pull it laterally. If the organelle is tethered to another, an extra force is required to overcome the adhesion. By incrementally increasing trap force on a Golgi or mitochondrion, one can measure whether it detaches or drags associated ER membranes with it[35] (see figure 1.6). Consistent co-movement of the neighboring organelle indicates a strong physical link. For instance, optical trapping revealed that some Golgi stacks in plant cells remain bound to ER via the CASP tether protein: when the trap pulls the Golgi, the ER moves in concert[2]. Likewise, peroxisomes tethered to chloroplasts in algae required greater force to separate under illumination. Optical tweezers therefore provide a quantitative readout of contact strength and dynamics.

Other mechanical tools include femtosecond laser ablation or micro-needle manipulation. A tightly focused femtosecond pulse can cut a membrane tether between organelles, and the resulting recoil velocity indicates the tension of the contact. Such laser microsurgery has been used in neurons to sever ER-mitochondria links and study calcium signaling consequences[36]. Micropipette aspiration (sucking on one organelle with a tiny pipette) can similarly assess membrane-cytoskeleton linkages at contact sites[37]. These physical methods are challenging but offer unique insight: they demonstrate directly that organelles are physically coupled and can quantify the forces involved in membrane apposition. In practice, they are used sparingly but provide a valuable complement to biochemical and imaging techniques.

By combining classical perturbations with these new techniques, researchers can more precisely dissect inter-organelle crosstalk. Through such integrative use of tools, it is now possible to probe both the physical architecture of contact sites and the functional signals that pass through them. Although researchers must remain mindful of limitations (e.g., compensation and off-target effects), these advances enable a paradigm in which dynamic, reversible control of organelle interactions is achievable.

From perturbative frameworks to a target organelle The previous section reviewed how modern cell biology moves from observation to controlled perturbation, using tools that acutely and reversibly perturb subcellular organization. In the present study, our aim is to engineer such a perturbative tool and use it to causally probe organelle

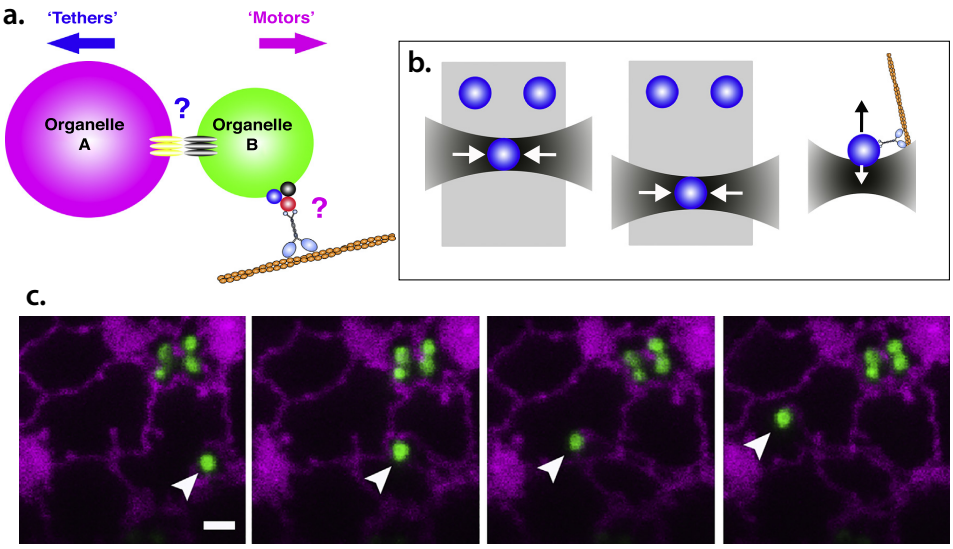

Figure 1.6: **a.** Schematic highlighting force components involved in controlling plant organelle dynamics. Organelle movement is driven by cytoskeletal components (mainly actin and myosin) and tethering between organelles, imposing opposing forces on organelle positioning (arrows). **b.** Objects (blue; bead or organelle) with a significantly different refractive index to the surrounding media are trapped by the forces (white arrows) from the focused optical beam (black cone), and can either be immobilized in the cell, or moved relative to its original position. Motor forces can be determined due to the force imparted by the motor (black arrow) compensating the force exerted by the trapping laser. **c.** Movement of a trapped Golgi drags the attached ER in leaf epidermal cells. the trapped Golgi is moved laterally within the cell, which in turn drags and remodels the ER (magenta) behind it. Scale bar, 2 µm. Adapted from [Sparkes 2018].

function. Choosing the right organelle is therefore strategic. The ideal target should (i) be central to cell physiology across models, (ii) form abundant, tractable structures with clear quantitative readouts (number, size, dynamics, proteome), (iii) engage in rich contact-site crosstalk so that perturbations have interpretable consequences on cellular fluxes.

Lipid droplets meet these requirements particularly well. They are ubiquitous and conserved organelles at the crossroads of lipid storage, detoxification and signaling, with their activities gated by regulated protein access at a phospholipid monolayer surface. Because LDs also form and remodel contact sites with the ER, mitochondria, lysosomes and peroxisomes, an intervention at their surface is likely to influence lipid fluxes and inter-organelle communication in a controlled, testable manner.

For these reasons, we adopt LDs as the primary object of study for developing a perturbative tool. The next section introduces LD structure, composition and dynamics to define measurable phenotypes and mechanistic hypotheses.

3 The lipid droplet: a conserved organelle for lipid storage and metabolic regulation

3.1 General presentation of lipid droplets

As noted above, lipid droplets (LDs) are ubiquitous, evolutionarily conserved organelles found in all eukaryotic cells from unicellular yeasts and algae to plants and animal tissues[5]. Under the microscope, LDs appear as spherical oil objects in the cytosol. First described by 19th-century microscopists as fat globules in cells, LDs were then considered as inert storage depots – essentially cytoplasmic fat reservoirs. For over a century after their initial description in the 1880s, these lipid globules were largely ignored in cell biology[38]. However, starting in the 1990s and 2000s a series of discoveries revealed that LDs are far from passive fat blobs[38]. Researchers identified specific proteins associated with LD surfaces and observed LD interactions with other organelles, raising new questions on LD functions.

The core function of LDs is to serve as intracellular lipid reservoirs for energy storage and lipid homeostasis[5]. Cells synthesize and sequester excess fatty acids into neutral lipids stored in LDs, thereby buffering fluctuations in nutrient availability. In this way, LD turnover is central to energy homeostasis, allowing cells to buffer excess of energy and later tap into these reserves when needed. However, diverse other roles of LDs have been highlighted beyond energy storage in cellular metabolism. By packaging hydrophobic molecules into an inert core, LDs shield the cell from the toxicity of excess free fatty acids and other lipids, which can disrupt membranes and organelles if left in the cytosol[39]. LDs also actively communicate with other organelles via membrane contact sites, exchanging lipids and signaling molecules[4]. They physically interact with the endoplasmic reticulum (ER), mitochondria, lysosomes/vacuoles, peroxisomes, and even the nucleus, allowing coordinated lipid metabolism across organelles. LDs also play a role in cellular signaling: in immune cells, LDs serve as platforms for the synthesis of eicosanoids (inflammatory lipid mediators), linking LDs to inflammation and immunity. Modern cell biology now recognizes LDs as dynamic, metabolically active organelles which play a central role in cellular physiology.

3.2 Structure and composition

Lipid droplets have a unique architecture that distinguishes them from other organelles. They consist of a hydrophobic core of neutral lipids surrounded by a single phospholipid monolayer[5]. This architecture can be visualized as a tiny oil droplet stabilized by a coat of amphipathic lipids. The core is composed predominantly of triacylglycerols (TAGs) and sterol esters (SEs) in most eukaryotes[5]. In plants, wax esters may also be present in certain LDs (e.g. in seeds or pollen), and in some algae or microbes unusual neutral lipids

can accumulate, but TAGs remain the primary component for energy storage[40]. Because the core is highly hydrophobic, it excludes polar molecules: unlike other organelles, LD inner part contains essentially only neutral lipids and no aqueous phase. This all-oil core is what led earlier microscopists to describe LDs as having a half-unit membrane, as they observed only a single boundary layer by electron microscopy, rather than a double-membrane boundary[41].

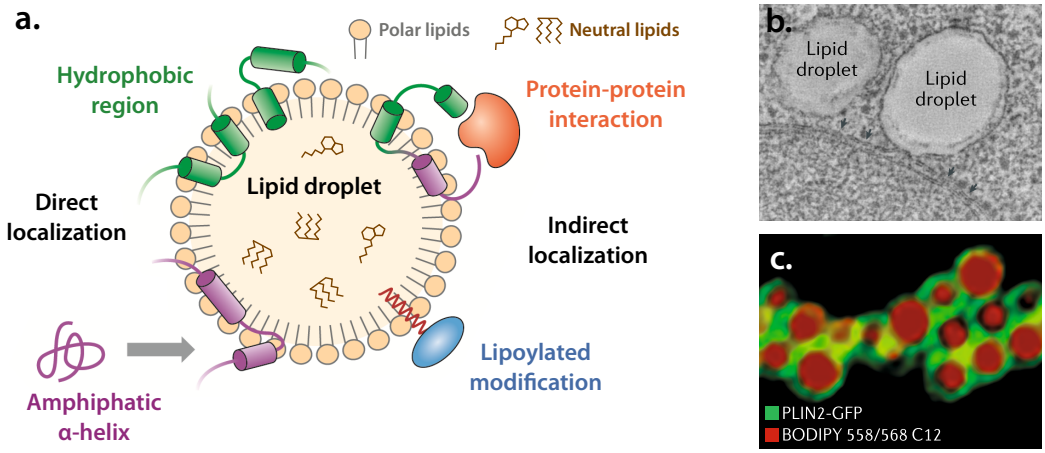

Figure 1.7: **a.** Schematic representation of lipid droplet structure and composition. Lipid droplets consist of a hydrophobic core of neutral lipids (mainly triacylglycerols and sterol esters) surrounded by a phospholipid monolayer embedded with specific proteins (e.g. perilipins in mammals, oleosins in plants). **b.** Tomogram of lipid droplets in yeast. **c.** Fluorescence microscopy image of liver cancer cells indicating the presence of the neutral lipid core labelled with a fluorescent fatty acid (BODIPY 558/568 C12 dye) and with a perilipin family member. Adapted from [42] for a., and [Olzmann et al. 2019] for b. and c.

The surface monolayer of a LD is derived from the ER membrane and is composed of phospholipids arranged with their hydrophobic fatty acyl tails facing inward toward the neutral lipid core, while their hydrophilic headgroups face the cytosol[5]. In mammals, phosphatidylcholine (PC) is typically the most abundant phospholipid in the LD monolayer, often comprising 50-60% of the monolayer lipids[41, 44]. Phosphatidylethanolamine (PE) is the next most common, along with smaller fractions of other phospholipids such as phosphatidylinositol (PI) and phosphatidylserine[45]. Interestingly, a sufficiently high PC content is critical for LD stability: PC acts as a surfactant that prevents LDs from coalescing into larger drops[46]. Cells with impaired PC synthesis show aberrant LD fusion and oversized droplets, as seen when key enzymes like CTP:phosphocholine cytidylyltransferase (CCT1) are disrupted[46]. Thus, the precise phospholipid composition of the monolayer influences LD size and number by modulating surface tension. Interestingly, the LD monolayer composition is broadly similar across heterotrophic species: for example, yeast LDs also have PC as 58% of monolayer lipids (with PI 22% and PE 17%)[45], which highlights a conserved physical requirement for surface lipids that can pack around a spherical oil droplet without exposing the core to cytosol.

Embedded within and peripherally attached to this phospholipid monolayer is a diverse set of proteins that define much of LDs functionality[5]. Among them, a crucial protein population is the structural proteins, which ensure correct shape and size of LDs. A key family of structural proteins in higher eukaryotes are the perilipins (Plin1-5 in mammals) which decorate the LD surface and regulate lipid storage and mobilization. Yeast and other fungi lack clear perilipin homologs, but they have their own coat proteins such as Pet10p in *Saccharomyces cerevisiae*, which behaves functionally like a perilipin by stabilizing LDs and possibly organizing surface enzymes[47]. In plants, especially oil-rich seeds, a distinct set of LD coat proteins called oleosins are the majoritary of proteins on the LD surface. Oleosins are small hydrophobic proteins in seed oil bodies (another term for LDs in plant seeds) that insert into the LD monolayer with a hairpin hydrophobic domain, effectively anchoring and stabilizing the droplet[48]. Oleosins prevent coalescence of oil bodies during desiccation and germination, maintaining numerous small oil droplets in seeds. Seeds also contain related proteins like caleosins and steroleosins on LDs. Caleosins carry a calcium-binding domain and enzymatic activity, whereas steroleosins have sterol-binding dehydrogenase activity, highlighting that plant seed LDs are also involved in signaling and metabolism beyond simple fat storage. Vegetative plant tissues, on the other hand, often express LD-associated proteins (LDAPs) rather than oleosins on LDs. LDAPs are a conserved family in land plants that coat LDs in leaves and roots; they appear to fulfill structural roles analogous to perilipins/oleosins in non-seed contexts[48]. Interestingly, during seed germination the oleosin coat is actively removed (via ubiquitin-proteasome system) and replaced by other proteins like LDAPs to allow oil mobilization.

This specialized set of proteins lead to different functions and sizes for LDs. In normal conditions, human adipocyte LDs present a central large LD which is almost entirely coated by perilipin 1 and filled with triglycerides as a dedicated long-term energy depot, often growing to tens of microns in diameter (nearly the entire cell volume). Yeast cells, by contrast, typically contain multiple small LDs (0.2-1 µm) that partition TAG and steryl esters; these LDs cluster near the vacuole or nucleus and carry enzymes for rapid lipid turnover during growth transitions[49]. Plant seeds contain myriad of LDs (0.5-2 µm) densely packed with TAGs, stabilized by oleosins, allowing seeds to remain viable under desiccation and then use the stored oil upon germination[48]. If each organism and cell type can adapt this collection of proteins to different physiological contexts, the LDs composition consisting in a neutral lipid core, a phospholipid monolayer, and a specific proteome is nonetheless conserved in principle across eukaryotes, as being highly efficient for safe lipid storage within the aqueous cytosolic environment.

Beyond structural proteins, LD proteomes include enzymes for lipid metabolism (such as lipases and acyltransferases) which are more highly conserved across species. Many enzymes of neutral lipid synthesis (e.g. DGAT2 in mammals, or Dga1 in yeast) and lipolysis (ATGL, HSL, or yeast Tgl lipases) dynamically localize to LD surfaces, ensuring that

LDs are metabolic hubs[5]. Additionally, a high number of proteins involved in membrane trafficking, signaling, and even protein quality control have been found on LDs. Proteomics studies reveal that LDs can bind chaperones, ubiquitin-proteasome components, and even chromatin-related proteins, suggesting roles in proteostasis and sequestration of proteins[5]. Some of these associations are transient or condition-dependent, which reinforces the idea that the LD is a hub organelle that dynamically engages in various cellular processes.

3.3 Formation and degradation mechanisms

Biogenesis of lipid droplets

In all eukaryotes, LD biogenesis is majorly tied to the endoplasmic reticulum. The ER is the site where neutral lipids are synthesized and where LDs start their growth[41]. The most canonical model of LD formation, called the budding model, describes that triglycerides and sterol esters are produced within the ER bilayer. They accumulate between the two leaflets of the membrane, forming a hydrophobic lens or oil droplet within the bilayer[5]. Once this neutral lipid lens reaches a critical size, it buds outwards from the cytosolic face of the ER, eventually pinching off as a distinct LD, which remains coated by a phospholipid monolayer continuous with the outer ER leaflet. Modern live-cell imaging and electron tomography have corroborated that LDs form at specific ER sites and often remain tethered to the ER after budding[50]. In fact, LDs can maintain continuity with the ER via a membrane bridge, allowing exchange of lipids and proteins even after their initial emergence[41].

Other models have been proposed to describe LD biogenesis. The budding model described above is widely accepted for cytosolic LD formation. An alternative "egg-cup" model suggests that in some cells, LDs form in a specialized dimple or pit on the ER surface (the cup), where certain proteins like perilipin-2 help transfer lipids into the droplet (the egg)[51]. This model arose from electron micrographs of adipocytes showing LDs wrapped in ER invaginations. Another is the enfolding model, based on observations of monocyte-derived LDs containing ribosomal patches, proposing that the ER membrane can wrap around a forming LD in a loop, contributing bilayer material that is later removed[52]. These models are not mutually exclusive and might reflect different degrees of ER involvement or droplet growth stages. For instance, a nascent LD might initially bud out (budding model), then remain in a cradle of ER membrane (egg-cup) or become partially surrounded by ER loops (enfolding) as it matures. Nonetheless, what is clear is that LD biogenesis often occurs at discrete ER subdomains rather than uniformly across the ER. Factors like local membrane curvature, lipid composition (e.g. enrichment of DAG or certain phospholipids), and protein assemblies like Seipin likely define these nucleation hotspots[53].

After formation, LDs can grow in size either by local lipid synthesis on their surface, by a lipid influx coming from the ER, or by the fusion/coalescence of LDs. Enzymes like DGAT2 not only create TAG at the ER, but can also relocalize to LDs and expand them by catalyzing TAG production using fatty acyl-CoA and DAG present at the droplet surface[54]. In adipocytes, as lipids accumulate after a meal, small LDs can fuse to form a single large droplet that dominates the cell (a process facilitated by proteins like cell death-inducing DFF45-like effector C, CIDEC, also known as fat-specific protein 27, in adipocytes)[55]. Conversely, LDs can also shrink or fragment when lipids are extracted (during lipolysis or membrane utilization). Throughout their life, most LDs remain functionally connected to the ER via contact sites. These LD-ER contacts allow bidirectional exchange: for example, excess phospholipids from an expanding LD can flow back into the ER membrane, or membrane proteins can traffic between the ER and LD surface[56]. Some LDs in specialized cells even form inside the nucleus: recent studies show that neutral lipid accumulation in the inner nuclear membrane can bud into the nucleoplasm as nuclear LDs under certain conditions (e.g., liver cells with cholesterol imbalance)[57]. These nuclear LDs remain tethered to the inner nuclear membrane and are thought to protect the nucleus from aberrant lipid accumulation at the nuclear envelope. Such variations underscore the plasticity of LD formation in different cellular compartments, although cytoplasmic LD biogenesis from the ER is the dominant pathway in most contexts.

At the molecular level, LD nucleation and growth are facilitated by several key protein factors. Seipin has emerged as one of the most important and conserved components of LD biogenesis[58]. Seipin is an ER membrane protein (forming oligomeric complexes) that localizes to ER domains where LDs form, and it is thought to organize or stabilize nascent lipid lenses[41]. In yeast (where Seipin is encoded by Fld1 and Ldb16), loss of seipin causes aberrant LD morphology: either a few supersized droplets or numerous tiny ones, indicating a defect in nucleation and growth of LDs[59]. Similarly, in mammals, Seipin mutations (such as those causing congenital lipodystrophy) lead to dysfunctional adipocyte LD formation and lipid dysregulation. How exactly Seipin works is an area of active study: it may act as a scaffold that recruits triglyceride-synthesizing enzymes and as a conduit to facilitate lipid flow into the growing droplet[41]. Recent structural studies suggest Seipin oligomers form a ring or pore at ER-LD junctions, helping to concentrate or trap neutral lipids to promote a nascent droplet's expansion[60]. Seipin also interacts with other proteins like LDAF1 (also called promethin in mammals) to form an LD assembly complex. This complex was shown to co-purify with triglycerides, implying it physically associates with the forming lipid globule[61]. Plant Seipin possess three homologs which similarly influence LD size in seeds: *Arabidopsis* Seipin2 triple-KO mutants have abnormally enlarged LDs in seeds[60], highlighting the conserved role of Seipin in regulating droplet morphology.

Another set of players in LD biogenesis are the enzymes that actually produce the neutral lipids. The terminal step in triglyceride synthesis is catalyzed by diacylglycerol acyltransferases (DGAT) enzymes, which esterify diacylglycerol (DAG) to form TAG. Mammals have two DGAT isoforms (DGAT1 and DGAT2) that reside in the ER (however, DGAT2 can also localize to LD surface)[62]. Yeast similarly have Dga1 (analogous to DGAT2) and an alternative pathway via phospholipid: diacylglycerol acyltransferase (PDAT, gene LRO1) that transfers an acyl chain from a phospholipid to DAG to make TAG[62]. Plants possess both DGAT and PDAT enzymes as well. For example, *Arabidopsis* has DGAT1 and PDAT1, both contributing to TAG biosynthesis in seeds and stress conditions[62]. These neutral lipid-synthesizing enzymes are critical for LD formation: if TAG synthesis is blocked cells cannot form LDs at all and become sensitive to fatty acid-induced lipotoxicity[63]. Altogether, active TAG and sterol ester production is the first step in generating the lipid core of LDs.

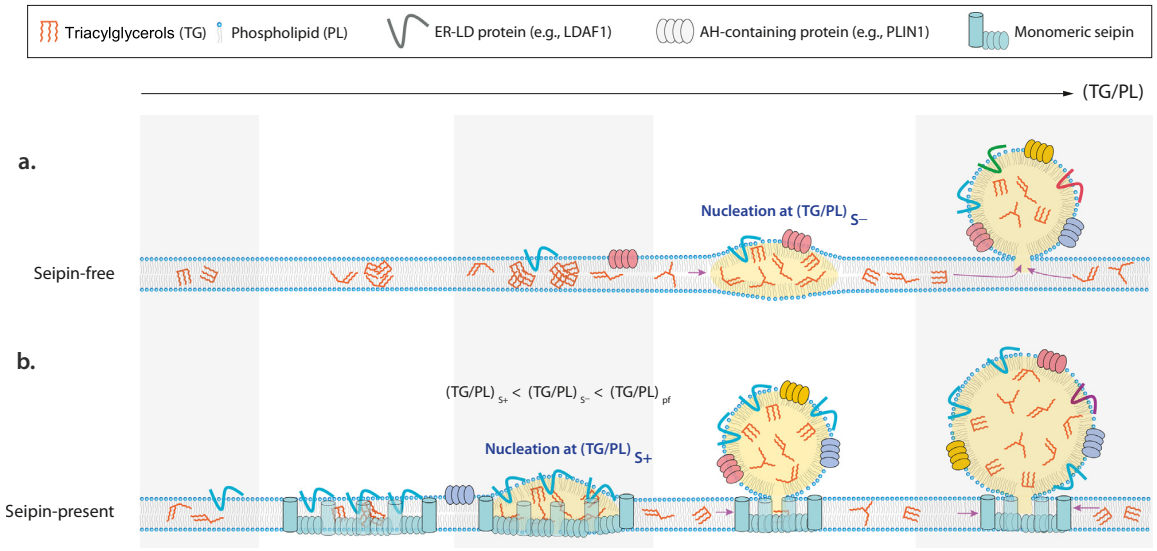

Figure 1.8: Schematic illustration of the Condensation of triacylglycerols, in Seipin-deficient vs Seipin-containing conditions. Increasing the concentration of TGs per phospholipid [TG/PL] leads to the formation of transient clusters that are bigger and steadier for larger TG concentrations. Proteins, in particular seipin, might decrease the critical nucleation concentration. AH, amphipathic helix. Adapted from [Thiam et al. 2021].

Once a neutral lipid lens forms in the ER, other factors ensure it buds off properly. Fat storage-inducing transmembrane protein 2 (FIT2) is one such factor. FIT2 is an evolutionarily conserved ER membrane protein that, when overexpressed, drives accumulation of TAG-rich LDs, and when absent, leads to fewer or aberrant LDs[65]. Mammals have FIT1 and FIT2 (FIT2 is ubiquitous, FIT1 in muscle), whereas yeast have two FIT2 homologs (Scs3 and Yft2). FIT2 has been shown to bind DAG and TAG and is thought to facilitate partitioning of newly made TAG from the ER bilayer into the droplet, perhaps by acting as a lipid transport or lipid-binding protein at the ER-LD interface[65]. Consistently, cells

lacking FIT2 function accumulate excess DAG in ER membranes and show aberrant LD morphology. Intriguingly, FIT2 was recently identified as an enzyme (an acyl-CoA diphosphatase) that might help detoxify or channel acyl-CoA at LD formation sites[66]. In any case, FIT2 appears to prevent toxic build-up of precursor lipids and ensures efficient flow into TAG and LDs. Proteins that shape the ER, such as reticulons and atlastins, have been implicated in providing the proper membrane geometry for droplet emergence[67]. Additionally, certain tethering factors like VAP27 (vesicle-associated membrane protein-associated protein) in plants have been linked to LD formation, possibly by bridging the ER with other structures or recruiting necessary enzymes[40]. In plants, a protein called LDIP (LD-associated protein interacting protein) was recently found to regulate LD size and abundance, potentially acting at ER-LD contact sites similar to the Seipin-LDAF1 complex in animals[68].

Degradation of lipid droplets

It is crucial for organisms to efficiently break down stored energy when needed. In the context of this study, our team published a cross-kingdom review about LD degradation in different organisms: "Lipid droplets degradation mechanisms from microalgae to mammals, a comparative overview"[69] published in **Biochimie** in 2024, which can be found at the end of this chapter. This review provides an in-depth overview of LD consumption, and the main key points are summarized hereafter.

There are two canonical pathways for breakdown of LDs: lipolysis (enzymatic hydrolysis of lipids) and lipophagy (autophagic consumption of LDs). In lipolysis, neutral lipid molecules (TAGs and steryl esters) are hydrolyzed by specific lipases to release fatty acids (and glycerol, in the case of TAG). Mammals have a well-characterized cascade of TAG lipases: adipose triglyceride lipase (ATGL) initiates the first step, converting TAG to diacylglycerol; hormone-sensitive lipase (HSL) then often takes the next step, converting diacylglycerol to monoacylglycerol; and finally monoglyceride lipase (MGL) frees the last fatty acid[70]. These lipases are regulated by proteins on the LD surface, notably perilipins. In adipocytes, for example, ATGL is co-activated by a cofactor (CGI-58) that is sequestered by Plin1 on LDs; upon β-adrenergic stimulation, Plin1 phosphorylation releases CGI-58 to activate ATGL[71]. HSL relocates from the cytosol to LDs when phosphorylated. The coordinated action of these enzymes leads to quick lipid mobilization during fasting or exercise, supplying fatty acids to mitochondria for energy. In non-adipose cells, ATGL (also called PNPLA2 in humans) is still a key TAG lipase, and there are additional patatin-domain lipases (PNPLA family) that act on LDs for basal lipid turnover[72]. Yeast, which lack close homologs of ATGL or HSL, employ their own set of enzymes: yeast TAG lipases include Tgl3, Tgl4, and Tgl5, which break down TAG stored in LDs, and Tgl1 which primarily hydrolyzes steryl esters[73]. These lipases are active especially upon glucose or nutrient depletion, when the cell needs to tap into energy

stores. Yeast mutants lacking these lipases accumulate excess neutral lipids and are slow to utilize storage fat, underscoring their importance. Plant seeds utilize a major TAG lipase called SUGAR-DEPENDENT1 (SDP1), a patatin-like lipase that localizes to oil bodies and initiates lipolysis during germination[74]. Other plant lipases (e.g., SDP1-like and various lipase/hydrolase family proteins) also contribute, particularly in vegetative tissues or under stress, but SDP1 is a key player in many species[40].

In addition to cytosolic lipases, cells can break down LDs through autophagy – a process termed lipophagy when targeted at LDs. In lipophagy, LDs are delivered to lysosomes (or the vacuole in yeast and plants) where lipases within these organelles complete the breakdown. Mammalian cells primarily use macroautophagy: portions of LDs or whole small LDs are engulfed by autophagosomes, which then fuse with lysosomes for content degradation[75]. Starvation conditions upregulate this pathway; for instance, liver cells during fasting show increased LD-lysosome interactions, and pharmacological or genetic inhibition of autophagy can cause excessive TAG accumulation in hepatocytes[75]. Notably, research demonstrated that in liver, stimulation of autophagy (via AMPK activation or other signals) promotes LD clearance (fasting-induced lipophagy) and provides fatty acids for mitochondrial oxidation[39]. In yeast, microautophagy appears to be the dominant mode: the vacuole membrane directly sequesters LDs by invaginating and pinching off LD-containing vesicles into the vacuole lumen[76]. Yeast mutants defective in core autophagy genes (Atg proteins) show impaired LD turnover, especially when shifted from nutrient-rich to carbon-starvation conditions, indicating lipophagy supplements yeast lipases in degrading LDs. Interestingly, yeast cells form specialized vacuole-LD contact sites involving the Vac8 protein and LD tether proteins (Ldo proteins) to initiate lipophagy, suggesting a selective mechanism for targeting LDs to the vacuole[77]. In plants, recent evidence suggests that LD turnover in vegetative tissues also involves autophagy. For example, during prolonged carbon starvation in *Arabidopsis* leaves (e.g., extended darkness), LDs are observed to associate with autophagosome markers and are delivered to the vacuole for degradation[40]. Genetic disruption of autophagy in plants leads to higher retention of TAG in leaves under stress, implying lipophagy contributes to lipid remobilization when β-oxidation alone is insufficient. However, the relative contribution of lipolysis vs. lipophagy can vary with conditions. In oil-rich seeds, lipolysis by cytosolic enzymes (SDP1) is the primary pathway for TAG mobilization post-germination. In contrast, during moderate stress in leaves or algal cells, a combination of partial lipolysis and autophagic turnover might occur[40].

It is important to note the interplay between these pathways. Often, lipophagy and lipolysis are not entirely independent. For instance, when lipases act on an LD, they may reduce its size to a point where autophagy can more easily engulf the shrunken LD. Conversely, autophagy can selectively remove LDs that are inaccessible or surplus, even when lipases are active. A balance exists: excess activation of lipophagy could lead to

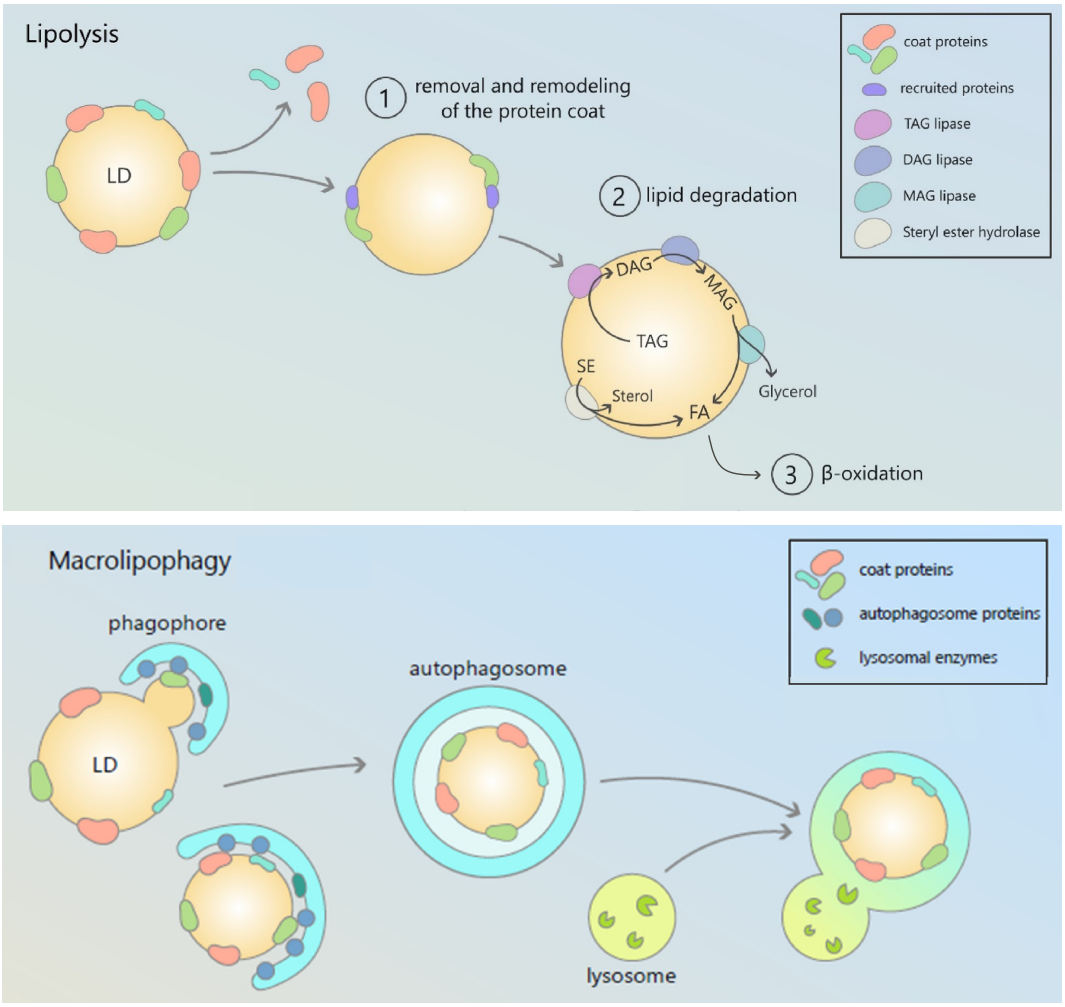

Figure 1.9: Schematic Illustration of the two main pathways for lipid droplet degradation: lipolysis and lipophagy. In lipolysis, cytosolic lipases (e.g., ATGL, HSL in mammals; Tgl3/4/5 in yeast; SDP1 in plants) hydrolyze TAGs into fatty acids and glycerol directly at the LD surface. In lipophagy, LDs are engulfed by autophagosomes (macroautophagy) or directly sequestered by lysosomes or vacuoles (microautophagy, not shown). Made by Marta Carletti in the review presented at the end of this chapter.

uncontrolled lipid release and oxidation, whereas too little could result in pathological fat accumulation. In mammalian cells, there is evidence that lipophagy is hormonally regulated (e.g., by glucagon in liver during fasting) alongside classical lipolysis regulated by catecholamines[75]. In yeast and plants, nutrient signals (like carbon/nitrogen status) modulate both lipase expression and autophagy activity for coordinated LD management[78]. Across eukaryotes, LD degradation mechanisms are thus dual-pronged and tightly regulated, ensuring that the stored lipids can be made available when needed but also safely sequestered when in excess[39].

In summary, eukaryotic cells have evolved robust mechanisms to both create LDs from excess lipids and to degrade LDs to release energy. The balance of these processes is crucial. Disruption in LD formation (e.g., seipin mutations leading to lipodystrophy)

or in LD breakdown (e.g., ATGL deficiency leading to neutral lipid storage disease) can cause or contribute to disease by either inability to store fats safely or inability to retrieve stored fats when needed[41]. The fundamental processes – ER-based biogenesis and lipase/autophagy-based degradation – are conserved, but each organism adapts the regulation of these processes to its environmental and developmental context.

3.4 Response to external stimuli

Lipid droplets are highly responsive to the metabolic and environmental state of the cell. Their formation and turnover are dynamically regulated by external stimuli such as nutrient availability, energy status, and stress conditions. A unifying theme is that LDs buffer the cell against fluctuations: they form when excess lipids need to be safely stored (or when stress signals trigger protective sequestration), and they are consumed when energy or building blocks are required.

Nutrient excess

In animals, nutrient excess (for instance, a high-fat diet or carbohydrate overfeeding) consistently induces LD formation. After a meal, insulin levels rise and stimulate adipose tissue and liver to take up glucose and lipids, converting excess carbohydrates into fatty acids and then into triglycerides that are stored in LDs[39]. Adipocytes respond by synthesizing and enlarging LDs, and hepatocytes package surplus fat into cytosolic LDs (hepatic steatosis if chronic). Thus, feeding signals an anabolic state: LDs act as sinks for the incoming energy to prevent lipotoxicity in other tissues[63]. On a cellular timescale, within hours of lipid influx, one can observe small nascent LDs budding from the ER and growing or fusing into larger droplets. In yeast or cultured cells supplied with excess fatty acids, LD biogenesis is likewise induced to esterify the fatty acids into TAG and SE for storage[41]. Notably, if phospholipid supply is insufficient during rapid LD expansion, abnormal LD coalescence can occur, again underscoring the need for balanced surfactant provision during nutrient-induced LD formation[46].

This response to the high-nutrient condition is coordinated by metabolic signaling pathways. In mammals, a major signaling regulator for LD biogenesis is the mTOR (mechanistic target of rapamycin) pathway, which acts as a nutrient sensor and promotes lipogenesis and LD formation when active.The mTOR complex 1 (mTORC1) is an evolutionarily conserved kinase that integrates nutrient (amino acid, glucose) availability and growth factor signals (e.g. insulin) to coordinate anabolic versus catabolic metabolism[79]. Under nutrient-replete conditions, active mTORC1 stimulates biosynthetic programs, including protein translation, nucleotide and lipid synthesis, leading to LD formation. Active mTORC1 enhances the maturation and nuclear localization of sterol regulatory element-binding proteins (SREBP1/2), leading to induction of genes for de novo fatty acid and triglyceride synthesis[79]. In particular, SREBP1 upregulates

canonical lipogenic enzymes and DGAT1/2, coupling mTORC1 signaling to triglyceride synthesis and LD biogenesis. Moreover, transcription factors like PPARs in mammals are activated by lipid accumulation and induce genes for storage (e.g., PPARγinduces DGAT and perilipin for adipogenesis[80]).

Nutrient deprivation

Most organisms regularly experience situations of organic carbon deficit: in heterotrophic cells, this results from absence or scarcity of glucose and other organic-carbon sources. In photosynthetic cells, darkness halts carbon fixation and similarly creates an organic carbon deprivation. In this situation, most organisms mobilize LDs to release stored energy. In animals, the canonical example is during an overnight fast or exercise: adipose tissue LDs undergo lipolysis driven by hormonal signaling (e.g., elevated glucagon or catecholamines). Fatty acids released from adipocyte LDs enter the bloodstream and are taken up by muscle and liver for oxidation. Within cells, nutrient-sensing pathways also modulate LD turnover: for instance, AMPK (AMP-activated protein kinase) acts as an energy sensor and promotes lipolysis and autophagy under energy stress[75]. Mammalian cells activate coordinated catabolic programs to mobilize lipid stores. Low ATP/high AMP ratios trigger the AMPK kinase (via LKB1/CaMKK2), while amino-acid depletion and loss of growth-factor signaling suppress mTORC1. Activated AMPK directly phosphorylates the autophagy-initiating ULK1 complex, whereas mTORC1 is concurrently inactivated (AMPK phosphorylates Raptor and TSC2 to shut off mTORC1)[81]. The result is a switch in ULK1 phosphorylation with a loss of inhibitory mTORC1 sites (e.g. Ser757) and a gain of AMPK active sites (e.g. Ser317, Ser777), thus initiating lipophagy. Nutrient sensing by the AMP/ATP ratio and amino-acid levels is therefore mediated by reciprocal AMPK-mTORC1 cross-talk to induce autophagosome formation around LDs. AMPK also promotes cytosolic lipolysis. Notably, AMPK phosphorylates the major triglyceride lipase ATGL (a.k.a. desnutrin) at Ser406, significantly increasing its TAG hydrolase activity[82]. This releases fatty acids for oxidation under energy deprivation. AMPK can likewise phosphorylate HSL to augment lipolysis in adipocytes. Thus, AMPK drives a two-pronged LD breakdown: activating the ULK1-autophagy pathway and the ATGL lipase. In parallel, mTORC1 inhibition relieves suppression of autophagy and alters LD coat proteins: for example, mTORC1-dependent phosphorylation of perilipin3 and AMPK-dependent phosphorylation of ORP8 recruit these factors to LDs to facilitate lipophagy[83]. Together, low-energy signals potentiate LD mobilization via both lipolysis and lipophagy. Similarly, yeasts use related but distinct LD-degradation strategies. In budding yeast, Snf1 (the AMPK ortholog) drives a microlipophagy behaviour under acute glucose starvation: AMPK activates the Atg14-containing PI3K complex at the vacuole to engulf LDs[84], leading to LD catabolism: stored TAG is hydrolyzed to sustain mitochondrial respiration on ethanol or glycerol, and steryl esters are mobilized for membrane synthesis when growth resumes[85].

However, a scarcity in other essential nutrients can have the opposite effect in some instances. If nitrogen is depleted while carbon is still available, yeast will instead accumulate LDs: this is because this starvation induces a halt in cellular division and yeast cells instead channel surplus carbon into storage lipids[49]. Then upon refeeding nitrogen, they quickly consume those LDs to build membranes for new cell growth. Similarly in plants and algae, nutrient starvation (especially nitrogen starvation) is a well-documented trigger for LD accumulation. Microalgae such as *Chlamydomonas reinhardtii* or *Nannochloropsis sp.* greatly increase their TAG content and LD number when starved of nitrogen, even though this halts cell growth[78]. Once nutrients are reintroduced, autophagy and lipases in algae help degrade the LDs to fuel cell division and synthesis of proteins/nucleic acids that were lacking under nitrogen starvation.

Environmental Stresses

Beyond nutrients, various environmental stresses influence LD dynamics. Oxidative stress is a prime example: when cells experience high levels of reactive oxygen species (ROS), they often accumulate LDs as a protective response[86]. Polyunsaturated fatty acids (PUFAs) are highly susceptible to peroxidation by ROS due to their high number of insaturations; by sequestering these fatty acids into neutral TAG in LDs, cells can reduce lipid peroxidation damage to membranes. Additionally, certain toxic lipid oxidation products can be stored in or on LDs away from sensitive organelles[87]. Consistently, treatments that cause oxidative stress (for example with hydrogen peroxide exposure) are observed to stimulate LD formation in mammalian cells, accompanied by upregulation of genes in lipid synthesis pathways[88]. Some organisms use LDs in defense against pathogens: during infections, immune cells like macrophages accumulate LDs both as energy sources and as sites for assembling inflammatory mediators (as mentioned, LDs host eicosanoid synthesis). Interestingly, pathogens themselves can induce host LD formation: certain bacteria and viruses reprogram host metabolism to generate more LDs, which they then exploit for their replication or immune evasion[89]. For example, hepatitis C virus alters host lipid metabolism so that LDs (coated with viral proteins) become platforms for assembling viral particles[90]. Cells, in turn, can target these LD-associated viral components for degradation via lipophagy as an antiviral response. Thus, LDs can play a role in both host-pathogen interactions and innate immunity.

In plants, abiotic stresses such as drought, extreme temperatures, and high salinity have been linked to changes in LD prevalence. Under drought or high salinity, plants accumulate abscisic acid, a stress hormone that can trigger mobilization of membrane lipids and sometimes an increase in TAG in leaves: this is possibly as a way to remove harmful membrane fatty acids and store them until conditions normalize[91]. Cold stress in some plants leads to LD accumulation in cells (especially in chilling-sensitive plants) because membrane rearrangements may produce excess fatty acids that are routed into

LDs[92]. When normal temperatures return, those stored lipids can be reintegrated into membranes. There is also evidence that LDs in plants contribute to stress signaling: e.g., during pathogen attack, LDs in plant cells can move to the site of infection and deliver antifungal compounds or precursor lipids for defense signals[93].

We observe here a notable contrast on how heterotrophic and photosynthetic organisms use LDs. Both organisms typically store lipids during times of organic carbon excess (feasting or light exposure) and utilize it otherwise (fasting or under darkness). However, autotrophic cells such as microalgae and plant tissues accumulate TAG and LDs specifically during abiotic stresses (e.g., nutrient starvation) and might not accumulate as much during high-nutrient growth[78]. This difference reflects distinct life strategies: animals can move and seek food, so they store energy when food is abundant and tap it when needed; non-motile organisms like most microalgae or plants cannot anticipate when nutrients will return, so during nutrient stress they conserve what they have by converting it to stable storage (TAG in LDs)[78]. The adaptive plasticity of LDs is observed across species, though the specific triggers and responses are tuned to each organism's ecology and lifestyle.

3.5 Biotechnological and biomedical relevance

Given their central role in lipid metabolism and energy homeostasis, lipid droplets have significant biotechnological and biomedical relevance. From engineering microbes for biofuel production to developing therapies for metabolic diseases, LDs are increasingly seen as important targets and tools in biotechnology and synthetic biology.

One major area of interest is using LDs for renewable energy, specifically the production of lipid-based biofuels. TAGs stored in LDs can be converted to biodiesel via transesterification, so organisms that accumulate high levels of TAGs are viewed as potential biofuel sources. Microalgae are a prime example: certain algae can accumulate up to 50-60% of their biomass as TAG under stress conditions[94], far exceeding the oil content of most oilseed crops. They also grow quickly (doubling in a day or less) and can be cultivated in large photobioreactors, making them attractive for sustainable biofuel production. Synthetic biology and metabolic engineering efforts are underway to enhance lipid accumulation in microalgae by tweaking regulatory networks and enzyme levels[95]. Strategies include overexpressing key rate-limiting enzymes of fatty acid and TAG synthesis, knocking out competing pathways (like starch synthesis, so that more carbon goes into TAG), and modifying LD-associated proteins to enable larger or more stable LDs in algal cells[96]. For example, researchers have experimented with overexpressing DGAT or blocking β-oxidation in algae to boost TAG reserves. There is also interest in engineering oleaginous yeast (yeast that naturally accumulate lipids, such as *Yarrowia lipolytica*) or even *S. cerevisiae* to produce high TAG yields. Such yeast can serve as microbial factories that turn sugars or waste carbon (like glycerol or agricultural residues) into oils

stored in LDs[97]. Through metabolic engineering, yields of TAG in these microbes have been improved, and some strains can accumulate 50% of their dry mass as lipids. An interesting twist is using LD dynamics to improve production of other valuable lipids: for instance, one study coupled metabolic engineering with induced LD turnover to enhance production of vitamin A (a hydrophobic product) in yeast[98]. By engineering the yeast to transiently store an intermediate in LDs and then stimulating LD degradation at a certain time, the process achieved higher yields of the desired product. This highlights how controlling LD formation and breakdown can be a tool in biotechnology to manage the flux of hydrophobic compounds.

Plants are also being engineered for modified LD content for both nutritional and industrial purposes. Oilseed crops (like soybean, canola) are bred or engineered to increase oil content in seeds or to produce tailored fatty acid compositions. Understanding LD formation in seeds (e.g., the role of oleosins and seipin) helps in manipulating seed oil density. There is emerging interest in inducing higher TAG accumulation in vegetative tissues of plants (which normally have low lipid content)[99]. Synthetic biology approaches, such as introducing algal DGAT enzymes or knocking down lipases, have shown some success in creating oily leaves, although issues of plant fitness remain. Nonetheless, as global interest in bioenergy continues, LD-centric metabolic engineering in both microbes and plants stands as a promising avenue for producing renewable lipids.

Lipid droplets themselves can be considered natural micro-compartments for specialized metabolism, and synthetic biologists are looking at ways to exploit or modify them. One approach is to target non-native enzymes to LDs to perform specific reactions in a hydrophobic environment. For example, certain biochemical reactions (like production of carotenoids, sterols, or other lipophilic compounds) could potentially be enhanced if their enzymes are sequestered to LDs along with their hydrophobic substrates[100]. By engineering a protein with LD-targeting sequences (such as a hydrophobic hairpin that embeds in the LD monolayer), one can create designer LDs that carry out new functions. There have been attempts to use LDs as storage depots for engineered products, for instance to produce ω3 fatty acids or unusual biofuels in yeast and storing them in LDs until extraction. Using synthetic biology tools, one can recreate artificial LDs in vitro: these liposome-like structures can be loaded with neutral lipids to mimic LDs, which could serve as delivery vehicles for hydrophobic drugs or as models to study LD behavior in a controlled setting[100].

Moreover, lipid droplets are directly implicated in many metabolic diseases, making them a target for pharmacological intervention. In conditions like obesity and type 2 diabetes, excess LD accumulation in tissues (such as liver and muscle) is associated with insulin resistance and organ dysfunction. Conversely, in lipodystrophies, an inability to form normal adipocyte LDs leads to ectopic fat deposition and metabolic disorder. Researchers use cellular and animal models to study these conditions: for instance, mice

lacking ATGL have massive TAG-filled LDs in multiple tissues and develop insulin resistance, modeling neutral lipid storage disease[101]. By studying such models, scientists aim to unravel how altering LD dynamics contributes to disease.

From a therapeutic perspective, modulating LD formation or breakdown is an attractive strategy. One could envision promoting LD sequestration of toxic lipids to protect organs (e.g., enhancing LD formation in muscle to soak up fatty acids that would otherwise cause insulin resistance) or promoting LD breakdown in an over-lipidated liver to treat fatty liver disease. Drugs that activate adipose lipolysis (like β3-agonists) or hepatic autophagy (through AMPK activators) essentially act on LD pathways to improve metabolism. On the other hand, inhibitors of DGAT (which would reduce TAG synthesis) have been explored to treat obesity and NAFLD by preventing new LD formation in liver[102]. Caution is needed, however, as completely blocking LD formation can cause lipotoxic side effects (since excess fatty acids with nowhere to go wreak cellular damage). A more nuanced approach is targeting LD-associated proteins. For example, a drug enhancing ATGL activity in liver might reduce steatosis safely, or blocking perilipin interactions might increase lipase access in overfilled fat cells. Recent work suggests that certain natural compounds can influence LD metabolism; for instance, polyphenols or plant-derived molecules that downregulate Plin2 have been shown to reduce fatty liver in experimental models[72]. One study noted that donating hydrogen sulfide to cells caused a reduction in LD content by affecting Plin2 and stimulating lipid utilization, pointing to novel therapeutic leads[103].

In cancer, tumor cells often rewire metabolism to accumulate LDs, which serve as fuel for rapid growth and as buffers against oxidative stress in the tumor microenvironment[103]. Some aggressive cancers show heightened LD content (for example, clear cell cancers are literally clear due to abundant lipid droplets). Targeting this vulnerability is of interest drugs that force the cancer cell to burn through its LD stores or that prevent LD formation could starve cancer cells or make them more susceptible to oxidative damage. Indeed, researchers have found that blocking DGAT or ATGL in certain cancer models can impede tumor growth, suggesting LD turnover is critical for tumor metabolic flexibility.

Another biomedical angle is infectious disease. As mentioned, viruses like hepatitis C virus and some bacteria manipulate host LDs. Antiviral strategies are being explored that disrupt these virus-LD interactions[104]. For example, inhibiting a host enzyme that viruses co-opt to induce LD formation may reduce viral replication. Compounds that stabilize LDs or alter their protein composition could interfere with the assembly of viral replication complexes that often anchor on LDs.

Lastly, LDs are relevant in neurodegenerative and aging research. Neurons under stress sometimes accumulate LDs (especially in glial cells), and impairment in LD regulation has been linked to diseases like Alzheimer's (where certain brain regions show lipid

droplet buildup)[105]. While its still debated if these LDs are protective or pathogenic in such contexts, they are being used as markers and potential intervention points for brain metabolism under stress.

In summary, the study of lipid droplets is not only highlighting fundamental cell biology but is also being translated into diverse applications. In biotechnology, harnessing LDs can improve production of biofuels and valuable lipids by microorganisms and plants. In synthetic biology, LDs inspire new ways to compartmentalize and control metabolic pathways in cells. In medicine, LD-centric pathways are targets for treating metabolic disorders, combating certain cancers, and inhibiting pathogens. This organelle, once thought to be a simple and static fat storage, now appears as a multifaceted organelle at the interface of basic biology and real-world applications.

4 PhD objectives

The methodological approaches described in the first part of this chapter have demonstrated how powerful perturbative tools can be for probing organelle biology, including lipid droplets. Yet, each existing perturbative method comes with specific constraints and limitations. This highlights the continued need to develop new strategies that enable direct, reversible, and spatially controlled manipulations of organelles. The global aim of this PhD is to contribute to this field of cellular synthetic perturbation by designing an innovative tool dedicated to lipid droplets.

The main objective is to engineer an artificial compartment capable of physically isolating LDs from the rest of the cell (figure 1.10). The rationale is that such sequestration will allow LDs to be studied in specific ways, both by changing their accessibility and by probing their interactions with other organelles. To achieve this, the project relies on protein engineering: artificial scaffolds will be created by combining domains with the ability to self-assemble with domains that specifically target the LD surface. The resulting synthetic proteins are expected to form a protein meshwork localized around

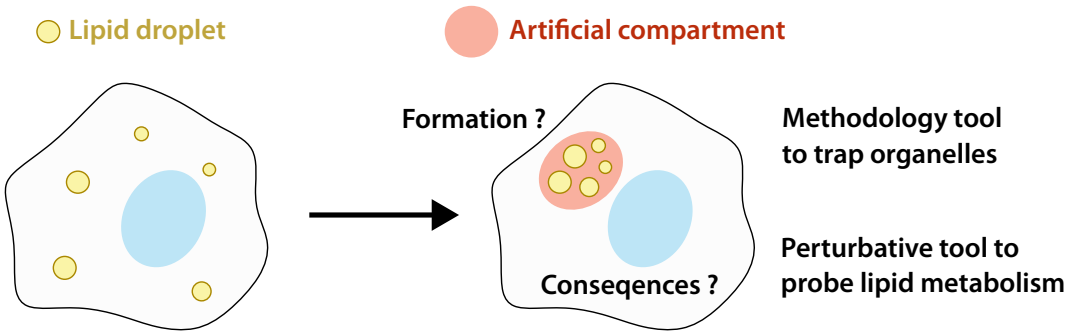

Figure 1.10: PhD general concept. The main objective of this PhD is to engineer an artificial compartment able to isolate lipid droplets from the rest of the cell.

LDs, thereby forming a controllable encapsulation system. A first objective is thus to design, express, and characterize these artificial condensates, both from a biophysical perspective (morphology, dynamics, reversibility).

As an initial step, the system will be implemented in human immortalized cells, which provide a robust mammalian model and facilitate experimentation. Beyond this proof of concept, the project also seeks to adapt the strategy to the model microalgae *Phaeodactylum tricornutum*, where LDs play key roles in photosynthetic lipid metabolism, opening perspectives for comparative cell biology.

Once the synthetic encapsulation system is established, a second objective will be to exploit it as a research tool to address fundamental questions in LD biology. By reversibly trapping and releasing LDs, the tool will make it possible to dissect the dynamics of lipid storage and mobilization under changing nutrient conditions, as well as to evaluate the consequences of LD isolation on organelle crosstalk, in particular with mitochondria and the endoplasmic reticulum.

This PhD project seeks to go beyond descriptive approaches and introduce a programmable perturbative platform directed to lipid droplets. By engineering an artificial LD-compartment, the study aims both to generate new mechanistic insights into LD biology and to establish a methodological framework that could be generalized in the future.

Biochimie 227 (2024) 19–34

Contents lists available at ScienceDirect

Biochimie

journal homepage: www.elsevier.com/locate/biochi

Lipid droplets degradation mechanisms from microalgae to mammals, a comparative overview

Chems Amari [a, b], Marta Carletti [a], Siqi Yan [a], Morgane Michaud [a], Juliette Salvaing [a, *]

[a] Laboratoire de Physiologie Cellulaire et Végétale, Université Grenoble Alpes, Institut National de Recherche pour l'Agriculture, l'Alimentation et l'Environnement, Centre National de la Recherche Scientifique, Commissariat à l'Energie Atomique et Aux Energies Alternatives, IRIG, CEA-Grenoble, 17 Rue des Martyrs, 38000, Grenoble, France

[b] Department of Chemistry, École Normale Supérieure, PSL University, Sorbonne Université, CNRS, Paris, France

ARTICLE INFO

Article history:
Received 1 July 2024
Received in revised form
15 August 2024
Accepted 16 September 2024
Available online 17 September 2024

Handling editor: C. Forest

Keywords:
Lipid droplets
Lipolysis
Lipophagy

ABSTRACT

Lipid droplets (LDs) are organelles composed of a hydrophobic core (mostly triacylglycerols and steryl esters) delineated by a lipid monolayer and found throughout the tree of life. LDs were seen for a long time as simple energy storage organelles but recent works highlighted their versatile roles in several fundamental cellular processes, particularly during stress response. LDs biogenesis occurs in the ER and their number and size can be dynamically regulated depending on their function, *e.g.* during development or stress. Understanding their biogenesis and degradation mechanisms is thus essential to better apprehend their roles. LDs degradation can occur in the cytosol by lipolysis or after their internalization into lytic compartments (*e.g.* vacuoles or lysosomes) using diverse mechanisms that depend on the considered organism, tissue, developmental stage or environmental condition. In this review, we summarize our current knowledge on the different LDs degradation pathways in several main phyla of model organisms, unicellular or pluricellular, photosynthetic or not (budding yeast, mammals, land plants and microalgae). We highlight the conservation of the main degradation pathways throughout evolution, but also the differences between organisms, or inside an organism between different organs. Finally, we discuss how this comparison can help to shed light on relationships between LDs degradation pathways and LDs functions.

© 2024 The Authors. Published by Elsevier B.V. This is an open access article under the CC BY license (http://creativecommons.org/licenses/by/4.0/).

Contents

1. Introduction 20
2. LD degradation through lipolysis 20
   2.1. Steryl esters degradation 20
   2.2. TAG degradation 20
      2.2.1. Canonical TAG degradation 20
      2.2.2. Alternative enzymes and tissue specificities 22
3. Lipolysis control mechanisms 23
   3.1. Removal or remodeling of the lipid coat 23
   3.2. Regulation of lipolytic enzymes activity 23
      3.2.1. In unicellular organisms 23
      3.2.2. In multicellular organisms 23
   3.3. Interactions with mitochondria and/or peroxisome and subsequent fate of FA 24

Abbreviations: AMPK, Adenosine monophosphate-activated protein kinase (AMPK); CE, cholesteryl ester; CMA, chaperone-mediated autophagy; DAG, diacylglycerol; ER, endoplasmic reticulum; ESCRT, endosomal sorting complex required for transport; FA, fatty acid; LD, Lipid droplet; MAG, monoacylglycerol; mTOR, mechanistic target of rapamycin; PtdIns(3)P, phosphatidylinositol 3-phosphate; PtdIns(4)P, phosphatidylinositol 4-phosphate; PRKA, protein kinase AMP-activated; TAG, triacylglycerol; SE, sterol ester; vCLIP, vacuole-LD contact site.

* Corresponding author.
E-mail address: juliette.salvaing@cea.fr (J. Salvaing).

https://doi.org/10.1016/j.biochi.2024.09.006
0300-9084/© 2024 The Authors. Published by Elsevier B.V. This is an open access article under the CC BY license (http://creativecommons.org/licenses/by/4.0/).

4. Lipophagy 24
4.1. Macrolipophagy in mammals 24
4.2. Microlipophagy in mammals and yeast 25
4.3. Microlipophagy-like processes in plants and algae 27
5. Conclusion 28
Funding 29
CRediT authorship contribution statement 29
Declaration of competing interest 29
References 29

1. Introduction

Lipid droplets (LDs) are found throughout the tree of life [1–3]. They contain a hydrophobic core, mostly composed of triacylglycerols (TAG) and steryl esters (SE), surrounded by a monolayer of membrane glycerolipids. Many proteins are found at their surface, either embedded in the lipid monolayer or associated through protein-lipid or protein-protein interactions [4,5]. For a long time, LDs were seen as simple storage organelles, used to absorb the excess of energy uptake (*e.g.* adipose tissues) or to provide energy to sustain developmental programs (*e.g.* plant seeds germination) [6,7]. This view has been progressively expanded to account for their central role in lipid metabolism and actual knowledge highlights the wide diversity of LD functions. In particular, LDs appear as essential in response to a multiple variety of stresses, of both abiotic and biotic origin, in algae and plants as well as in mammals and yeast [8–11]. However, these functions can vary greatly depending on the considered organism, tissue, environmental condition or even between LDs within the same cell.

In order to better understand LDs functions it is essential to apprehend their life cycle, from biogenesis to degradation. LDs biogenesis starts with the accumulation of neutral lipids between the two leaflets of the endoplasmic reticulum (ER) membrane; when their concentration increases, these neutral lipids coalesce into lenses and eventually bud from the ER, a process that can occur spontaneously but is promoted by proteins, in particular Seipin (reviewed in Refs. [12,13]). The Seipin protein functions, controlling the ER-LD junction and the TAG flux from ER to LDs, appear conserved in all eukaryotic cells (reviewed in Ref. [14]). Yet interactions of Seipin with other proteins emerge as potential important factors to modulate its activity and the composition of newly formed LDs [14,15].

Following their biogenesis, LDs fate can vary greatly. In oleaginous dry seeds, and to a lesser extent in adipocytes, which serve as storage, LDs are relatively stable organelles. By contrast, in unicellular organisms, and in most tissues from plants and animals, LDs can be very dynamic, and their number and size can quickly vary to respond to environmental cues (*e.g.* stress) or to developmental programs that trigger their formation or responsive remobilization. To answer these rapid LDs turnovers and their specific functions, two main degradation pathways have evolved in all eukaryotic groups: lipolysis and lipophagy [8,16–19]. The relative contributions of these pathways are difficult to estimate as they can vary depending on organism, tissue and condition considered. Moreover, while lipolysis has been studied for a long time, lipophagy studies are more recent, which may skew our understanding of LDs degradation. We will aim in the present review not to be exhaustive but to describe the different degradation pathways, highlighting their conservation throughout evolution, but also the differences between organisms, or inside an organism between different organs. Finally we will reflect on how LDs degradation relates to the functions of LDs. To this aim, we will focus on very different model organisms: the budding yeast *Saccharomyces cerevisiae*, mammals for animal models, angiosperms with the major model *Arabidopsis thaliana* and finally microalgae with two very different groups, green algae, in particular *Chlamydomonas reinhardtii*, and stramenopiles, with a focus on diatoms, in particular *Phaeodactylum tricornutum*.

2. LD degradation through lipolysis

The first way to degrade LDs is to degrade their hydrophobic core, mainly composed of TAG and SE, through lipolysis [17]. Three main steps can be distinguished (Fig. 1): 1) removal or remodeling of the LDs protein coat, 2) lipid degradation (lipolysis *sensu stricto*) and 3) subsequent degradation of released fatty acids (FA) in the peroxisome and/or mitochondria. In this section, we will focus on the central step, that is SE and TAG hydrolysis, while the other steps will be discussed in section 3.

2.1. Steryl esters degradation

Several enzymes involved in SE degradation have been identified in yeast, namely Tgl1, Yeh1, and Yeh2, but their study suggests that SE degradation is mainly important for sterol homeostasis with little impact on the global dynamics of LDs ([20–23], reviewed in Ref. [24]). Enzymes involved in the breakdown of plant SE are still unknown, although the LD-ASSOCIATED LIPASE (LIDL) 1 and 2, identified by quantitative proteomic analysis of LD-enriched fractions derived from *A. thaliana* seedlings, are homologs of Tgl1 and have been hypothesized to function as sterol esterases [25]. In mammals, SE exist as cholesteryl-esters (CE) and specific enzymes involved in their breakdown have been identified. Ghosh et al. [26] described a neutral cholesteryl ester hydrolase (CEH) in human macrophages named CES1, that is located at the surface of LDs and mobilizes LD-contained CE [27]. CES1 overexpression results in an increased rate of cholesterol efflux to ApoA1, HDL (high density lipoproteins) and serum [28], suggesting that CES1 can regulate both the CE content of LDs and the cholesterol efflux. KIAA1363/NCEH1/AADACL1 has also been identified as a CE hydrolase as its knock-out (KO) in mice results in a decreased CE activity [29], while its overexpression in macrophages markedly decreases the CE content [30]. However, its implication in macrophage CE metabolism is debated, and other yet unidentified CEH may exist [31]. In general, the importance of CE hydrolases in LDs degradation remains controversial (reviewed in Ref. [17]).

2.2. TAG degradation

2.2.1. Canonical TAG degradation

Three main lipolysis steps are required for TAG degradation: to diacylglycerol (DAG), monoacylglycerol (MAG) and finally glycerol, with fatty acids (FA) released at each step (Fig. 1).

In mammals, the primary step of TAG hydrolysis to DAG is

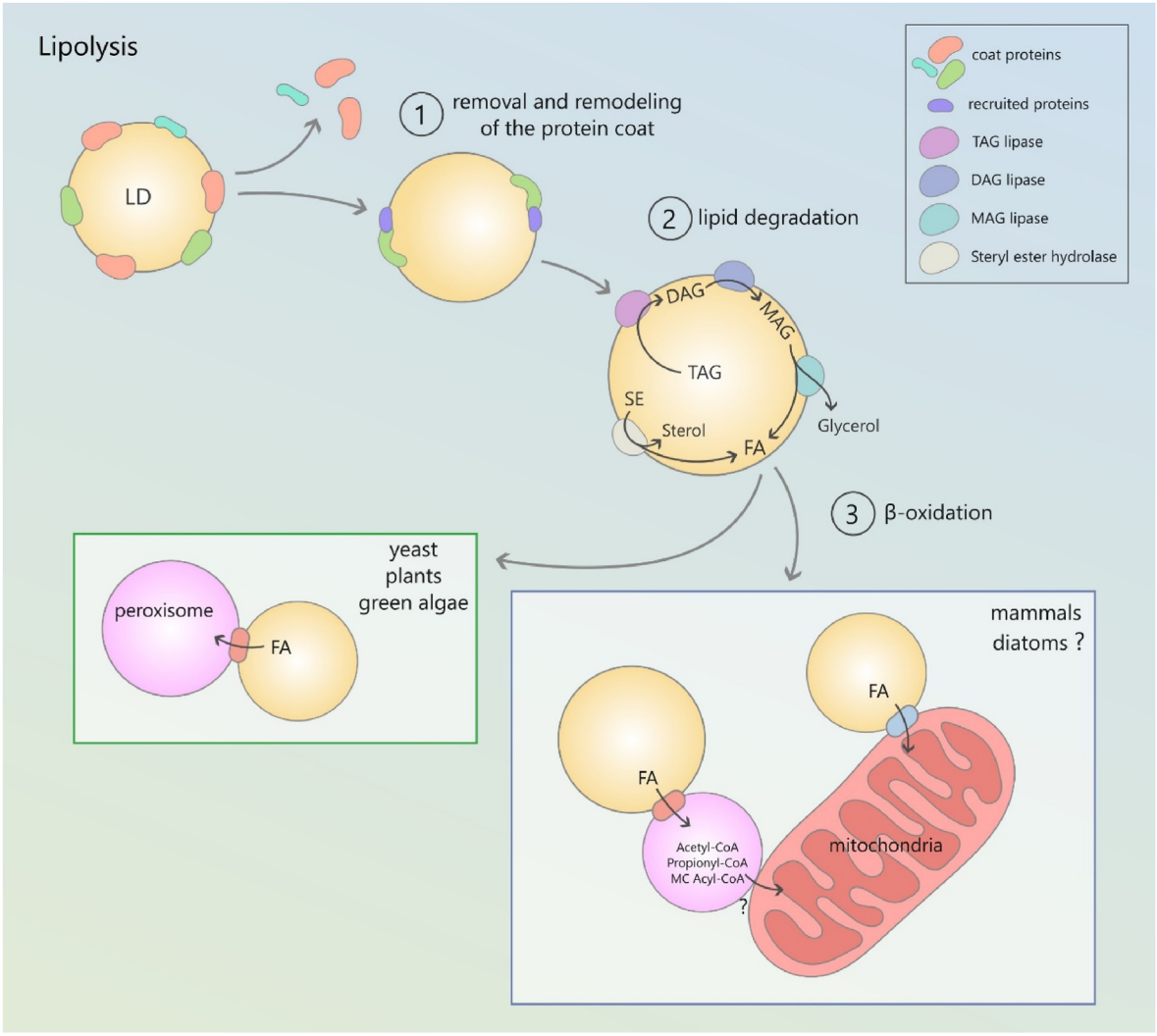

Fig. 1. Schematic representation of lipolysis mechanism. 1) Remodeling of the protein coat surrounding the LD that can include removal of proteins (*e.g.* oleosins in seeds, Perilipin2 and 3 in mammals) or post-translational modifications (*e.g.* Perilipin1 and 5 in mammals). This remodeling can induce recruitment of additional factors to the LDs; 2) Degradation of triacylglycerol (TAG) into diacylglycerol (DAG) and then monoacylglycerol (MAG) by membrane-localized enzymes, eventually leads to the release of glycerol and fatty acids (FA). A minor contribution is given by the degradation of steryl esters (SE). 3) FA can subsequently be degraded by β-oxidation, which can occur in the peroxisome, mitochondria or both depending on the considered organism.

catalyzed by the adipose triglyceride lipase (ATGL) [32], encoded by the *PNPLA2* (*patatin-like phospholipase domain-containing protein 2*) gene in humans (Table 1). KO of ATGL in mice results in a drastic decrease of lipolysis both in whole-body and specific adipocytes [33]. Accordingly, human mutations that disrupt ATGL activity are associated with decreased rates of glycerol and FA formation in response to lipolytic agents as well as with neutral lipid storage disease and myopathy [34]. Homologs of ATGL in other organisms have been widely identified and their function as major TAG lipases has also been demonstrated (Table 1). TGL4 is identified as the yeast ATGL homolog [35], but other patatin domain containing lipases have been identified. The major TAG lipase activity is ensured by TGL3, which shows unspecific activity towards TAG or even DAG [36]. TGL4 on the other hand shows a preference for TAG containing C14 and C16 acyl-chains, while a third enzyme, TGL5, is involved in the breakdown of TAG containing very long chain fatty acids C26 [35]. Both TGL3 and TGL5 also exhibit acyl-transferase activities, respectively towards lyso-phosphatidylethanolamine (LPE) and lyso-phosphatidic acid (LPA) [37]. In plants, the patatin-like lipase SUGAR DEPENDENT1 (SDP1) was identified in *Arabidopsis thaliana* as the major lipase involved in TAG mobilization during seed germination [38], and a second homolog named SDP1-LIKE (SDP1L) was later identified [39,40]. Together, SDP1 and SDP1L contribute to over 95 % of TAG hydrolysis activity during seed germination [39], and SDP1 also appears to be important for LD turnover in vegetative tissues, in particular roots and stems [41]. Identification of lipases in microalgae is more recent. LiSDP1 was identified in the LD proteome of the green alga *Lobosphera incisa* [42]. More recently, LIP4 was identified in the green alga *Chlamydomonas reinhardtii* as a homolog of SDP1, with which it shares 44 % amino acid identity; LIP4 is involved in TAG remobilization during nitrogen starvation recovery as well as in TAG global homeostasis [43]. Similarly, SDP1 homologs have been identified in secondary endosymbionts, but appear to have different importance in TAG breakdown. Indeed, while in the diatom *Phaeodactylum tricornutum,* TGL1 seems to play a major role, similar to ATGL or SDP1 [44], its role seems much more limited in *Fistulifera solaris* [45]; additionally, study of NoTGL1 and NoTGL2 in *Nannochloropsis oceanica* shows that these ER-localized enzymes modulate TAG synthesis at the ER by degrading *de novo* synthesized TAG [46].

Table 1
Summary of the proteins shown to play a role in lipid droplet degradation by lipolysis in *Homo sapiens*, *Saccharomyces cerevisiae*, *Arabidopsis thaliana*, *Chlamydomonas reinhardtii* and *Phaeodactylum tricornutum*.

	Name	Function	References
Lipases			
H. sapiens	ATGL	TAG lipase	[32]
	HSL	Hormone-sensitive lipase recruited at LDs surface upon cAMP stimulation, degrades preferentially DAG and cholesterol esters	[47]
	PNLPA3	TAG and DAG lipase	[48]
	MGL	MAG lipase	[49]
	CES1	TAG lipase and cholesteryl-esterase activities	[26,27]
S. cerevisiae	TGL4	TAG lipase	[35]
	TGL3	TAG and MAG lipase + acyltransferase (LPE)	[36]
	TGL5	TAG lipase + acyltransferase (LPA)	[35]
	Ldh1	TAG lipase, global lipid homeostasis	[50,51]
	Ayr1	TAG lipase	[52]
	Yju3	MAG lipase	[53]
	Yeh1 and 2	Sterol-esters hydrolases	[20]
	Tgl1	Sterol-esters hydrolases	[20,54]
A. thaliana	SDP1	TAG lipase, essential for seed germination	[41]
	SDP1-LIKE (SDP1L)	TAG lipase; overlapping function with SDP1 during seed germination, specific in the roots and leaves of mature plants	[39]
	AtOBL1	TAG, DAG and MAG lipase located at LDs surface; important for pollen tube growth	[55]
	MAGL8	MAG lipase associated with LDs in germinating seeds and in leaves	[56]
	At4g18550/ATDSEL	DAG and MAG lipase; involved in the regulation of storage oil mobilization and the establishment of early seedlings	[57]
	LIDL1 and LIDL2	Putative sterol-esters hydrolases; located at LDs	[25]
C. reinhardtii	LIP4	TAG lipase	[43]
	LIP1	DAG lipase	[58]
P. tricornutum	TGL1	TAG lipase	[44]
Coat proteins and coat proteins remodeling			
H. sapiens	PLIN1	LD coat protein removed through phosphorylation upon induction of LDs degradation	[59]
	PLIN2-3	LD coat proteins degraded through chaperone-mediated autophagy upon induction of LDs degradation	[60]
A. thaliana	OLE1-5	Oleosins, need to be removed for TAG degradation	[61,62]
	MIEL1, PUX10 and CDC48A	Oleosins degradation	[63–65]
C. reinhardtii	MLDP	LD coat protein, possible role in control of lypolysis	[66]
P. tricornutum	StLDP	LD coat protein, possible role in control of lypolysis	[67]
Lipolysis regulators			
H. Sapiens	CGI-58	ATGL activator	[68]
S. cerevisiae	Lct1	CGI-58 homolog	[69]
	Tld1	Negative regulator of Tgl3	[70]
A. thaliana	VPS29, PEX11e and FREE1	Regulate the translocation of SDP1 from peroxisomes to LDs through peroxisomal tubular extensions	[71,72]
	CGI-58	Regulates TAG breakdown; interacts with PXA1 at peroxisome surface	[73]
C. reinhardtii	CHT7	Major regulator of TAG remobilization during quiescence exit upon nitrogen resupply	[74]
	DTH1	regulator of TAG degradation, located at the LD	[75]
	LACS3	regulator of TAG degradation, located at the peroxisome	[76]
P. tricornutum	CGI-58	Located to mitochondria and promotes *de novo* fatty acid synthesis and TAG degradation through mitochondrial β-oxidation	[77]

Subsequent steps including DAG hydrolysis to MAG and MAG hydrolysis to glycerol and FA have been less well characterized. In mammals, the hormone-sensitive lipase (HSL, encoded by the *LIPE* gene) is the major DAG lipase but it also has a high activity in the hydrolysis of CE, and a lower one towards TAG, MAG, retinyl esters and short-chain acyl esters ([78], reviewed in Ref. [79]). Consistently, whole-body deficiency in HSL leads to DAG accumulation in the adipose tissue as well as decreased lipolysis in mice [80] and human [81]. Monoglyceride lipase (MGL) then catalyzes the hydrolysis of MAG, and can use both *sn*-1 MAG and *sn*-2 MAG, in which FA are esterified to the terminal or middle hydroxyl group of the glycerol backbone, respectively, as substrates [82,83]. In yeast, Yju3 has been identified as the functional ortholog of MGL [53]. In higher plants, several enzymes with DAG/MAG lipase activities have been identified, with different specificities [55–57,84]. In particular, in *A. thaliana,* a cytosolic member of the DAD1-like acylhydrolase family encoded by At4g18550 demonstrates a specific ability to hydrolyze DAG and MAG at the *sn*-1 position and is crucial in the establishment of early seedlings [57]. The MAG lipase AtMAGL8 plays an important role in seeds and exhibits a notable substrate preference for MAG containing C20:1 fatty acids [56]. Finally in microalgae, few reports of DAG or MAG lipases exist, apart from the non-selective DAG lipase CrLIP1 in *C. reinhardtii* [58]. The development of bioinformatics tools has however allowed the identification of many new potential lipases that remain to be investigated [85,86].

2.2.2. Alternative enzymes and tissue specificities

In multicellular organisms, the role of lipases can vary from one tissue to another. In land plants, studies on LDs were primarily

focused on seeds germination but such interest has since expanded to other tissues, in particular the pollen tube, where LDs are essential, and leaves, where LDs play roles in response to various abiotic and biotic stresses (for review: [9,87]). Oil body lipase 1 (AtOBL1 in *A. thaliana*) has been identified as a TAG lipase, but can also degrade DAG and MAG with no obvious substrate specificity. Its role in seeds is very minor, but it is essential in pollen tubes [55]. Alternatively to lipases, a LD-specific lipoxygenase (LOX)-dependent pathway for lipid mobilization during the early stages of seed germination has been proposed in various plant species, such as *Arabidopsis*, watermelon, cucumber, wheat, barley, potato, tomato, sunflower and tobacco. This pathway allows direct oxygenation of linoleate residues directly on TAG and the coupling of TAG degradation with the generation of oxylipins, involved in signaling, or phytoalexins [88,89]. In mammals, the canonical pathway through ATGL and HSL accounts for over 90 % of TAG degradation in adipocytes [90,90]. Many other lipases have been identified, but their importance even in other tissues remains poorly evaluated (reviewed in Ref. [17]). For instance, PNLPA3, a close relative of ATGL that can hydrolyze TAG and DAG [48], is expressed in both white and brown adipose tissue in mice, is highly abundant in human hepatocytes and is associated with liver diseases; however, PNLPA3 KO has little impact and deleterious effects are observed as results of dominant negative mutations that increase its association with comparative gene identification 58 (CGI-58) to the detriment of ATGL association and activation [91–93] (cf. sections 3.1 and 3.2.2).

3. Lipolysis control mechanisms

Lipolysis requires tight control to ensure that LDs breakdown answers to the cell/organism needs at a given time and/or in response to external or internal cues. As shown on Fig. 1, lipolysis involves three main steps, all of which are regulated through different mechanisms.

3.1. Removal or remodeling of the lipid coat

In plant seeds, LDs are very important to ensure proper germination and the establishment of the developing seedling, thus regulating the precise timing and sequence of LDs degradation is of high importance. Plant seed LDs are covered by specific proteins called Oleosins [7,94], which can protect stored TAG from lipolytic enzymes [61,62] and are absent from LDs in vegetative tissues. The removal of Oleosins is tightly regulated through initial ubiquitination and subsequent proteasome degradation [95,96]. It involves the sequential recruitment of MYB30-interacting E3 ligase 1 (MIEL1), plant ubiquitin regulatory X (UBX) domain-containing protein10 (PUX10) and cell division cycle 48A (CDC48A) ATPase [63–65] (Table 1). However, protection of TAG by Oleosins is not tight-proofed [97] and additional mechanisms are required to regulate lipolysis.

Similarly to Oleosins, Perilipins (PLIN), the major proteins found at the surface of LDs [98] in mammals, participate in lipolysis regulation ([99], reviewed in Ref. [100]). PLIN2 and 3 are degraded by another mechanism called chaperone-mediated autophagy (CMA): *in vivo* studies revealed that CMA degradation of both proteins is increased during starvation, and that their degradation enhances LDs degradation through lipolysis, but also through macroautophagy (see section 4) [60] (Table 1).

Yet, protein coat removal is not a general rule. PLIN1, the major coat protein in white adipocytes, can be phosphorylated by protein kinase A (PKA), which is activated by cyclic Adenosyl MonoPhosphate (cAMP) signaling in response to β-adrenergic stimulation (reviewed in Ref. [59]). This phosphorylation triggers the dissociation of PLIN1 and the major ATGL activator CGI-58 ([68] reviewed in Ref. [101]). A similar mechanism has been shown for PLIN5, which is important in oxidative tissues (heart, skeletal muscle, liver, brown adipose tissue) ([102–104], reviewed in Ref. [100]). In land plants, Lipid droplet associated protein (LDAP) and LDAP-interacting protein (LDIP) are the major LDs proteins in vegetative tissues, where they play important roles for LDs homeostasis [105–107] but their potential involvement in LDs degradation remains to investigate. Finally, in the diatom *Phaeodactylum tricornutum*, Stramenopile Lipid Droplet (StLDP) protein, which is the main coat protein [108–110], seems required for proper LDs degradation [67], although the mechanism remains unknown.

3.2. Regulation of lipolytic enzymes activity

3.2.1. In unicellular organisms

In unicellular organisms, cell cycle appears as a major regulator of metabolism and particularly of lipolysis. Indeed, in budding yeast, the TAG synthesis enzyme Pah1 is inhibited [111,112] while the TAG lipase TGL4 is activated [113] by Cdk1/Cdc28 during log phase. This regulation is consistent with the central role of TAG in lipid metabolism, as a source of building blocks for membrane lipids [114]. In photosynthetic microorganisms, light is another essential growth factor and circadian rhythms play important roles in the regulation of the cell cycle and of energy metabolism. This has been well shown in the diatom *P. tricornutum* [115–118], where LDs form during the day and are degraded during the night, when cell division occurs. Yet this coordination does not imply direct regulation of TAG degradation by cell-cycle dependent mechanisms. Such regulation has only been shown so far in the green alga *Chlamydomonas reinhardtii*, in which the regulatory protein COMPROMISED IN TAG HYDROLYSIS7 (CHT7) [74], involved in the exit of quiescence following nitrogen resupply, appears as a major regulator of TAG remobilization, linking the resumption of cell cycle and TAG hydrolysis.

This last examples also shows the importance of lipolysis following nutrient replenishment in microalgae. Another protein, Delayed in Triacylglycerol Hydrolysis (DTH1), which has only been identified in Chlorophyceae, localizes to the LDs and is a major player in lipolysis following nitrogen resupply in *C. reinhardtii*; however, although it is associated with the early steps of LDs degradation, upstream of β-oxidation, its exact function remains elusive [75].

Finally, finer regulation can also occur in unicellular organisms, for example to degrade specific LD subtypes. In budding yeast, it has recently been shown that the TG-associated LD protein 1 (Tld1) protein localizes specifically to LDs containing TAG but not SE and can specifically inhibit their degradation by TGL3 [70].

3.2.2. In multicellular organisms

In mammals, hormonal signals control LDs lipolysis through different mechanisms (reviewed in Ref. [17]). Both ATGL and HSL are regulated at the transcriptional level and can be upregulated in response to endocrine, paracrine or autocrine factors including hormones, cytokines and neurotransmitters. Peroxisome proliferator-activated receptor γ (PPARγ) in particular can promote lipase expression in response to starvation [119,120]. HSL expression can also be activated by sterol regulatory element binding proteins (SREBPs) [121]. In addition to this transcriptional regulation, the activity of lipases is regulated post-translationally, both directly and indirectly through cyclic Adenosyl MonoPhosphate (cAMP) signaling. Indeed, protein kinase A (PKA), which is activated by cAMP in response to β-adrenergic stimulation, can phosphorylate HSL in addition to PLIN1 (cf. section 3.1). This phosphorylation

triggers the relocation of HSL to LDs as well as activation of ATGL by CGI-58, that follows CGI-58 and PLIN1 dissociation ([68] reviewed in Ref. [101]). But ATGL can also be regulated by intracellular glucose levels through polyubiquitination, as glucose depletion leads to decreased assembly of the Golgi-located E3-ligase complex $CUL7^{FBXW8}$, reducing ATGL polyubiquitination, which increases its stability and enhances lipolysis [122].

In plant seeds, the main lipase SDP1 is initially localized on peroxisomes. Its relocalization to LDs requires the formation of peroxisomal tubulations called peroxules [71,123]. Recent advances have shown involvement of the endosomal sorting complex required for transport (ESCRT) machinery and PEROXIN 11e (PEX11e) in the formation of these tubules [72] but the triggering mechanisms remain elusive. Germination defects in SDP1 mutants can be rescued by providing sugar, hence the protein's name [38], but, like in mammals, sugar levels can modulate SDP1 activity, although the mechanism is very different. Indeed, sucrose supplementation inhibits the interactions between peroxisome and LDs, and thus the lipolytic activity of SDP1 [123].

3.3. Interactions with mitochondria and/or peroxisome and subsequent fate of FA

The peroxisomal localization of SDP1 in higher plants provides a direct link between lipolysis *sensu stricto* and further degradation of FA by β-oxidation, which occurs in the peroxisome in most organisms, but also in mitochondria in animals and diatoms (Fig. 1). Direct interactions between LDs and FA degradation organelles appear as an important way to regulate the fate of FA released through lipolysis.

In mammals, mitochondrial β-oxidation appears as the major pathway, feeding ATP-synthesis [124], while the peroxisome is responsible for the degradation of very-long chain fatty acids (VLCFA) and participate in cellular thermogenesis [125]. Many proteins participating in contact sites between LDs and these 2 organelles have been described (for review: [126]). In particular, both PLIN 2 [127] and PLIN5 [128] have recently been shown to participate in the tethering of LDs and mitochondria to promote FA β-oxidation following energy deprivation. Another LD protein, Spastin, participates in the tethering of LDs and peroxisome; as for SDP1 relocalization, this association involves ESCRT components [129]. A direct link between lipolysis and peroxisome is also provided by the role of PEX5 in recruiting ATGL to LDs upon fasting [130]. As these different systems have been investigated and shown in different cell types, it remains to investigate whether they can act in synergy or reflect different strategies allowing to fulfill specific needs of cells.

Proteins tethering LDs and β-oxidation organelles are not known in microalgae. Yet, some proteins linking lipolysis and β-oxidation have been identified. We have previously mentioned the importance of CGI-58 in regulating ATGL in mammals (see sections 3.1 and 3.2.2). CGI-58 homologs have been identified in *A. thaliana* [131], yeast [69] and microalgae [77,132] but their localizations and functions differ. Ict1, the yeast homolog of CGI-58, was originally described as an Acyl-CoA-dependent lysophosphatidic acid acyltransferase [133]. In *A. thaliana,* CGI-58 function in TAG breakdown is conserved [39,131] but unlike its mammalian counterparts, it localizes to peroxisome and interacts with the peroxisomal ABC transporter (PXA1) [73]. Plant CGI-58 seems to play only a minor role in seeds LDs breakdown, but its loss causes a major effect in plant leaves [131]. In diatoms, CGI-58 functions seem to diverge. Indeed, while reduction of CGI-58 homolog levels in the diatom *Thalassiosira pseudonana* has the expected effect of reducing TAG hydrolysis [132], the overexpression of the *P. tricornutum* homolog also leads to an overaccumulation of TAG; moreover, CGI-58 is reported to be localized to mitochondria and the authors suggest that it plays a role in promoting *de novo* fatty acids synthesis as well as TAG degradation through mitochondrial β-oxidation [77]. The localization and function of CGI-58 homologs in plants and diatoms suggests that these proteins could participate in tethering LDs and respectively peroxisome and mitochondria, though such role remains to be investigated.

Finally, in the green alga *C. reinhardtii*, the long chain acyl-coA synthetase 3 (LACS3), which is located in the peroxisome and links TAG degradation and peroxisomal FA β-oxidation could be an interesting candidate for tethering of LDs and peroxisome [76].

4. Lipophagy

Autophagy is a general process to target the degradation of specific organelles or compounds (for review: [134,135]). Initially described in yeast and mammals, autophagy core components are well conserved in plants (for reviews, see Refs. [136–138]) and algae (for review [139]). In plants, autophagy plays an important role in response to biotic and abiotic stresses. In agreement, plants having a decrease in autophagy flux usually present a higher sensitivity to many stresses including heat, drought and nutrient stresses, likely due to the role of this process in cell compounds recycling and damaged or unwanted organelles removal under harsh environments (for reviews, see Refs. [137,140]). The link between autophagy and LDs is complex as autophagy can be involved in both LDs biogenesis and degradation and LDs can also play a role in autophagy by providing lipids for autophagosome biogenesis (for review: [141]). Here we will focus on the role of autophagy in LDs degradation.

Regulation of lipid metabolism through autophagy, also known as lipophagy, has only been shown quite recently [142,143]. Several autophagy, and subsequently lipophagy, pathways can be distinguished. Macro- and micro-autophagy were initially described based on electronic microscopy observations (for review: [144]). Macroautophagy has been known for a long time [145]. It involves membrane elongation and the formation of an autophagosome, that will engulf the targeted organelle, and fuse with lysosomes in mammals, or vacuoles in other organisms, to direct their degradation. By contrast, microautophagy involves direct contact of the targeted organelle with lysosomes or lytic vacuoles and their subsequent engulfment in these lytic compartments. The use of these two pathways for LDs degradation differs between organisms. While macrolipophagy seems to be a major process in mammalian cells, LDs degradation by different microlipophagy processes has been described in yeast, plants and microalgae. It should be however noted that lipophagy processes only start to be studied in some organisms and that the current view is probably still very partial.

4.1. Macrolipophagy in mammals

In mammals, macrolipophagy, also known as lysosome-mediated acid lipolysis, has been well described in the liver, where it is important to control intracellular lipid storage, free lipids and energy homeostasis (Fig. 2A) (for review: [146]). It involves the Lysosomal acid lipase (LAL) [147], encoded by the *Lipa* gene. While LAL is ubiquitously expressed, its highest expression is in macrophages and hepatocytes. LAL can degrade most components of LDs, including TAG and DAG but also steryl and retinyl esters ([148–150] reviewed in Ref. [17]). LDs degradation by LAL follows targeting of LDs to lysosomes through the classical macroautophagy route, that relies on the evolutionarily conserved autophagy-related genes Atg [151]. It is triggered in response to starvation *via* several signaling pathways, including repression of

the mTOR (mechanistic target of rapamycin kinase) complex 1 (MTORC1) [152,153], and activation of protein kinase AMP-activated catalytic subunit (PRKA)/adenosine monophosphate-activated protein kinase (AMPK) [154,155]. These in turn activate the ULK1/Atg1 (unc-51 like autophagy activating kinase 1) kinase complex [156,157], leading to the formation of a phagophore, which will evolve in forming the nascent autophagosome [158]. Specifically, the ULK1 complex phosphorylates and activates the class III phosphatidylinositol 3-kinase (PtdIns3K) complex, composed of Beclin-1/Vps30/Atg6, PIK3R4/VPS15, Atg14, PIK3C3/VPS34, AMBRA1 and NRBF2 [159]. Recruitment of this complex and production of a pool of phosphatidylinositol 3-phosphate (PtdIns(3)P) at ER extensions called omegasomes promotes the recruitment of PtdIns3P-binding proteins, such as ZFYVE1/DFCP1 (zinc finger FYVE-type containing 1/double FYVE domain – containing protein 1) [160] and WIPI2 (WD repeat domain, phosphoinositide interacting) protein [161]. WIPI2/Atg18 will then recruit and promote the assembly of the Atgl12-5-16L1 complex [162] which acts as an E3-like ligase and recruits the E2-like protein Atg3 for the conjugation of the members of the MAP1LC3/LC3 (microtubule associated protein 1 light chain 3), also called Atg8, protein family to phosphatidylethanolamine (PE) [163]. LC3 proteins are important for autophagic cargo selection, phagophore elongation and closure. Last, autophagosomes appear to traffic along microtubules in higher eukaryotes, eventually targeting and fusing with lysosomes following a SNARE mechanism [164].

Several proteins involved in the recognition of LDs for macrolipophagy degradation have been identified (Table 2) but most of them are known as selective autophagy receptors, not specific of lipophagy. This is the case of the adaptator SQSTM1/p62 [165], as well as NBR1 and Optineurin [166]. In addition to these, some lipophagy-specific cargo recognition proteins have been identified in different tissues and conditions. The LD protein ancient ubiquitous protein 1 (AUP1) associates with a E2-ubiquitin ligase and can trigger LDs aggregation [167,168], potentially forming aggresomes to promote lipophagy [166] Moreover, AUP1 acts as a lipophagy cargo recognition protein following viral infection [169] and has been suggested as a potential target for therapeutic treatment of COVID-19 [170]. ORP8, which is involved in LDs biogenesis at mitochondria-associated ER membrane subdomains [171], can be phosphorylated by AMPK, promoting its role as a lipophagy cargo protein [172]. Finally, two proteins, whose mutants cause hereditary spastic paraplegia diseases, have been shown to act as cargo recognition proteins in lipophagy in the brain: DDH2 [173] and Spartin [174]. The identification of specific lipophagy cargo recognition proteins is of particular interest to understand the regulation of LDs degradation by lipophagy, and in particular the targeting of specific LD populations.

As in lipolysis, PLIN proteins are modified and or degraded to allow lipophagy. PLIN 2 protects LDs from lipophagy [175] and the degradation of PLIN2 and 3 by chaperone mediated autophagy can promote both association of ATGL (as described in section 3) and LC3 proteins at the surface of LDs [60,176]. Moreover, in addition to its above mentioned role, Spartin acts as an adaptator for PLIN2 ubiquitination [177]. PLIN1 colocalizes with p62 [165] and its phosphorylation is necessary to allow Rab7 docking [178], that participates in autophagosome maturation [179], together with other members of the Rab GTPase family like Rab10, 25 and 32 (reviewed in Ref. [146]) (Table 2).

4.2. Microlipophagy in mammals and yeast

The prevalence of macrolipophagy appears specific to mammals as in all other organisms, lipophagy mainly occurs through pathways related to microautophagy.

Microlipophagy was thought to be absent from mammalian cells, but some recent evidence have shown that this pathway plays a significant role in LDs degradation in mammal liver hepatocytes [180]. Indeed, in those cells LDs and lysosomes can form transient contacts that usually last 30–60 s and that do not depend on the canonical macroautophagic machinery pathway, both in presence or absence of nutrients.

In budding yeast, actors and mechanisms involved depend on the condition or stress promoting microlipophagy (Table 2). Microlipophagy was observed in response 1) to nutrients starvation triggered by cell entry into stationary phase or by acute nitrogen or glucose depletion [181–185]; 2) to ER stress mediated by lipid imbalance in a strain with a deficiency in phosphatidylcholine (PC) synthesis, or by the addition of dithiothreitol (DTT) or tunicamycin (TUN), an inhibitor of ER protein glycosylation [186–188] or 3) to diauxic shift triggered by yeast transfer from a fermentative to a respiratory media [189].

Microlipophagy requires the targeting of LDs and attachment to the vacuole membrane, followed by the engulfment of the LDs by an inward invagination of the vacuolar membrane in the lumen (Figs. 2B–1). After scission of the vacuole membrane, the LD is released in the vacuole lumen surrounded by the vacuolar membrane and is then degraded [190,191].

During microlipophagy induced by nutrient starvation, LDs were shown to be recruited at specific microdomains formed in the vacuolar membrane, the liquid-ordered (L_o) microdomains, before their inward budding to promote LD internalization. L_o domain formation is essential for efficient internalization of LDs into vacuoles under nutrient stress and lipid imbalance (Figs. 2B–3) [185,187]. Many proteins required for the formation of these microdomains were identified and their deletion negatively impacts microlipophagy (Table 2) [181,185,192,193]. L_o microdomains are enriched in sterols, contain sphingolipids, that are important for their formation [185,187,193–195] and also PtdIns(3)P and phosphatidylinositol-4-phosphate (PtdIns(4)P) located in the cytosolic leaflet [183,196]. Vacuolar membrane are usually poorly enriched in sterols and sphingolipids implying that these lipids have to be transported to the vacuole membrane when required to form L_o microdomains [194,197]. Several lipid sources and transport mechanisms were proposed: 1) transport from the lumen of sterols coming from the degradation of intraluminal vesicles (ILV) originating from the fusion of sterol-enriched multivesicular bodies (MVB) or from the degradation of LDs after their internalization by two vacuolar sterol transporters, Npc2 and Ncr1 [183,187,198]; 2) transport through non-vesicular pathway, as exemplified by Lam6, a sterol transporter located at the nucleo-vacuolar junction and involved in L_o microdomains formation [192]; 3) transport to the vacuole by autophagy, as autophagosomes that fuse with the vacuole membrane could be a source of sphingolipids and sterols [182,184,185,197]. The involved mechanisms depend on the condition used to induce microlipophagy. Recently, the LD surface proteins Ldo16 and Ldo45, also named LDOs for LD organization, were shown to interact with the vacuolar protein Vac8 and to promote vacuole-LD contact site (vCLIP) formation [199,200]. LDOs are also involved in LD biogenesis as they are associated to the Seipin complex during logarithmic phase [201] and their progressive dephosphorylation when yeasts enter the stationary phase promotes vCLIP formation and lipophagy induction [200]. Therefore, LDOs localization and function could be regulated by phosphorylation dependent on the metabolic status of the cells, connecting LD synthesis to LD degradation.

The mechanisms involved in microlipophagy during ER stress under induction by DTT or TUN present significant differences compared to the ones occurring under nutrient stress. First of all, neither the core autophagy components nor the formation of L_o

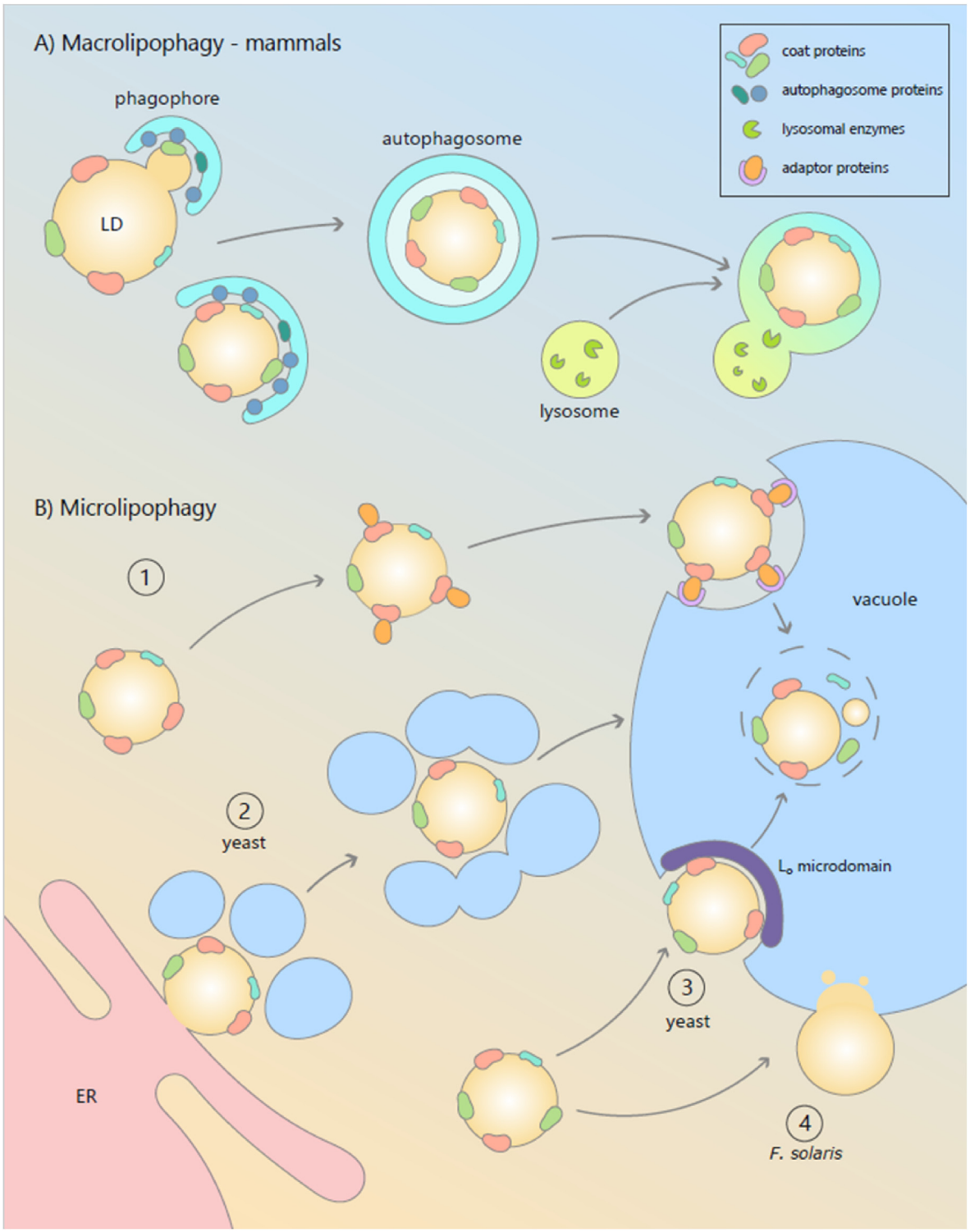

Fig. 2. Overview of lipophagy mechanisms in differents organisms. A) Macrolipophagy has been described in mammals: after the formation of the phagophore, the autophagosome completely surrounds the LDs and eventually fuses with lysosomes. B) Microlipophagy has been observed in several eukaryotic organisms, however several mechanisms have been described 1) Specific proteins bind to the LD coat proteins and direct it to the lytic compartment where it is recognized by specific receptors. This broad and simple description matches what has been described in *A. thaliana,* where the coat protein CLO1 appears to regulate addressing to the vacuole, possibly interacting with Atg8, and in yeast, where the LD proteins Ldo16 and Ldo45 can directly bind to the vacuolar protein Vac8 to trigger microlipophagy. 2) In yeast, in response to endoplasmic reticulum (ER) stress, the vacuole fragments into smaller vesicles that organize around the LDs, envelope them and form invagination which release the LDs into the vacuolar lumen following membrane scission; 3) In yeast, during nutrient starvation, LDs can be recruited to the vacuole thanks to specific microdomains (L_O microdomains) for efficient internalization. 4) In *Fistulifera solaris*, a direct fusion of vacuoles and LDs have been observed without the complete absorption of the LD, suggesting a novel type of microlipophagy.

Table 2
Summary of the proteins shown to play a role in lipid droplet degradation by lipophagy in *Homo sapiens*, *Saccharomyces cerevisiae*, *Arabidopsis thaliana, Chlamydomonas reinhardtii* and *Phaeodactylum tricornutum*.

	Name	Function	References
S. cerevisiae	Ncr1 and Npc2	Formation and expansion of L_o microdomains in vacuole membrane by transferring sterols from the vacuole lumen to the vacuolar membrane	[183,188]
	Pik4 and Stt4	PtdIns(4) kinases required for local synthesis of PtdIns(4)P into vacuolar L_o microdomains and lipophagy under nitrogen starvation	[196]
	Lam6	Sterol transporter located at nucleo-vacuolar junction andpromoting L_o microdomain formation	[192]
	Fab1	Phopshatidylinositides biosynthesis, required for L_o microdomains formation	[185,193]
	Nem	Phospholipid biosynthesis, required for L_o microdomains formation	[185,193]
	Vps4	AAA-ATPase, component of ESCRT complex involved in MVB synthesis, required for L_o microdomains formation	[181,185,188,193]
	Sec18	Involved in vesicular trafficking, required for Lo microdomains formation	[193]
	Pep4	Vacuolar protease, required for L_o microdomains formation	[181,185,188]
	Are1/2	Synthesis of ergosteryl esters, required for L_o domain formation	[185]
	ATG15	Vacuolar TAG lipase, degradation of LD TAG in the vacuole after internalization, required for L_o microdomains formation	[166,181]
	Snf1/4	Subunits of the AMP-activated protein kinase complex, activate lipophagy during accute glucose reduction by assisting the relocalization of Atg14 to the vacuolar membrane	[182]
	Atg6/14	Part of the phosphatidyl-inositol 3-kinase complex I that produces PtdIns(3)P. Could play a role in production or tageting of PtdIns(3)P to the vacuole for the formation of L_o microdomains	[181,182,202]
	ESCRT complex	Might assist LDs internalization by promoting vacuole membrane invagination and membrane scission in lipophagy induced by diauxic shift from glcolysis to respiration or ER stress.	[186,188,189]
	Ldo16, Ldo45 and Vac8	Triggers LDs attachment to vacuole *via* interaction of the LD protein Ldo45 and Ldo16 with the vacuolar membrane protein Vac8	[199,200]
	Core autophagy proteins	Important for LDs internalization into vacuole and for vacuole microdomain maintenance under nutrient starvation	[181–185]
	ATG39/ESM1	Involved in lipophagy under ER-stress triggers by PC imbalance	[188]
	Vam3, Ypt7 and Vps33	Proteins involved in vacuolar membrane fusion and playing a role in lipophagy during ER-stress induced by DTT	[186]
A. thaliana	ATG2/ATG5/ATG7	Involved in microautophagy to promote TAG degradation under starvation induced by extended darkness	[203]
		Regulation of lipid homeostasis in dark-induced senescence	[204]
		TAG degradation under carbon starvation in etiolated seedlings	[205]
	CLO1	LD coat protein interacting with ATG8f to promote LDs internalization into vacuole during lipophagy in germinating seeds	[206]
H. sapiens	SQSTM1/p62, NBR1, optineurin	General selective autophagy receptors, involved in lipophagy	[165,166] +
	Rab7, Rab10, Rab25 and Rab32	LDs targeting to autophagosomes	[146,179]
	Spartin	LDs ubiquitination and recognition for macroautophagy	[174,177]
	AUP1	LDs aggregation and recognition for macrolipophagy following viral infection	[167,169]
	DDH2	LDs recognition for macrolipophagy in the brain	[173]
	ORP8	LDs recognition for macrolipophagy	[172]
	Core autophagy components	Target LDs into vacuole by macrolipophagy	[151]
	LC3	Autophagic cargo selection, phagophore elongation and closure	[207]
	mTOR	Regulator of autophagy, is activated in presence of nutrients	[153]
	PRKA/AMPK	Regulator of autophagy	[146]
	Atg1	Initiator of the phagophore formation	[157]
	LAL/Lipa	Lysozomal lipase involved in LD lipids degradation after internalization by lipophagy	[148–150]
C. reinhardtii.	Core autophagy components	Promote TAG accumulation or LDs formation upon nitrogen or phosphate starvation	[208]
	ATG8	LDs degradation by microautophagy during nitrogen resupply	[209]
P. tricornutum.	StLDP	Putative interaction with Atg8	[67,108]
	ACBP	Regulation of *Atg5*?	[210]

microdomains are required [187,188]. In addition, both stresses trigger vacuolar membrane fragmentation; LD internalization is then mediated by the remodeling of membrane vacuoles that organize around LDs, envelop them and form invaginations that release LDs in the vacuolar lumen after membrane scission (Fig. 2B–) [186]. The formation of invaginations and the release of LDs in this situation was proposed to be facilitated respectively by the action of the ESCRT complex and of proteins involved in vacuole fusion rather than by the property of the L_o microdomains as demonstrated under nutrient stress [185–187]. An intermediate situation is observed during lipid imbalance as both the ESCRT complex and the L_o microdomains formation mediated by Npc2 and Ncr1 are required [187], demonstrating the co-existence of different pathways mediating LD microlipophagy.

Once in the vacuoles, degradation of LD proteins and lipids could involve the Pep4 protease and the Atg15 lipase, that are located in the vacuole lumen and play a role in microlipophagy under both nutrient starvation and ER stress [166,182,188]. More recently, as for PLIN2 and PLIN3 in mammals (see section 3), autophagy was shown to be required for the removal of LD surface proteins prior to their internalization into vacuole under nutrient stress [181], shedding light on the poorly understood role of general autophagy in microautophagy. However, protein removal is not a pre-requisite for LD entry in the vacuole suggesting that LD protein removal and LD entry in the vacuole for lipolysis are two independent processes [181].

4.3. Microlipophagy-like processes in plants and algae

In plants, the number of studies investigating the involvement

of autophagy core components in LD degradation is limited and results are variable depending on the species, the developmental stage, the tissue and/or the stress analyzed. During seed germination, TAG are mainly degraded by the cytosolic TAG lipases SDP1 and SDPL1 that are essential for seed germination in absence of carbon source in the media (see section 2). However, degradation of LDs by a process similar to microlipophagy was also observed in *A. thaliana* where a subset of LDs were located in the vacuoles 36–48h after germination [206,211]. In addition, autophagy inhibition by concanamycin A negatively impacts seedling growth after germination and leads to a high accumulation of LDs in cotyledons, likely due to a lower level of degradation compared to WT seedlings [206]. LDs accumulation into vacuoles was also observed in other plant tissues including in tapetum cells during pollen development in rice as well as under dark-induced starvation in *A. thaliana* leaves [203,212], suggesting that microlipophagy could be an important process involved in plant development and stress response. Microlipophagy in plants involves core components of the autophagy machinery as the absence of ATG7 in rice, or ATG2 and ATG5 in *A. thaliana* significantly reduces the accumulation of LDs into vacuoles [203,212]. In addition, ATG8e and b, key autophagy proteins involved in cargo selection and autophagosome biogenesis, were co-localized with LDs in leaves under dark stress and seedlings during germination, respectively [203,206]. During germination, the seed specific LD coat protein of the caleosin family CLO1 is also a key player in microlipophagy as CLO1 seems to regulate the entry of LDs into the vacuole during germination, but the exact mechanism remains to be investigated [206,211]. CLO1 could regulate LD-vacuole interactions and/or promote membrane fusion. In other plant tissues or stress conditions, mutations of autophagy core components can lead to a reduction of TAG and/or LD degradation. This is the case in tobacco pollen and maize leaves, as well as in *A. thaliana* seedlings under carbon starvation or leaves under dark-induced senescence [203,205,213,214]. However, the involvement of lipophagy in plants is not limited to lipids degradation but seems to play a more central role in lipid metabolism and homeostasis. Indeed, in leaves upon dark-induced senescence, ATG proteins were also shown to be involved in TAG synthesis and the authors propose that autophagy promotes TAG synthesis from membrane lipid turnover in specific tissues or developmental stages, while it is involved in TAG degradation in other tissues, such as pollen or seedlings, or under different stresses [203,204]. A similar view has been proposed in the green alga *Chlamydomonas reinhardtii,* where inhibition of the autophagic flux prevents TAG accumulation and LD formation upon nitrogen or phosphate starvation [208].

Studies of lipophagy in microalgae are only emerging, but more and more evidence of a role of this process in LD degradation are reported in the literature. Inclusion of LDs in vacuoles were initially observed in the green alga *Auxenochlorella protothecoides*, during heterotrophy to autotrophy transition [215]. Similarly, LDs are found in the vacuolar lumen of *Parachlorella kessleri* following salt stress [216] and in *C. reinhardtii,* microphagy-like interactions of LDs and vacuoles were observed during nitrogen resupply following starvation [217]. Like in plants, ATG8 is involved in lipophagy processes in *C. reinhardtii*. Indeed, LDs directly interact with ATG8-labeled structure under nitrogen starvation [218] and TAG degradation during nitrogen resupply is delayed in CrATG8 mutants [209,219]. While most lipophagy mechanisms in green microalgae are described as “microphagy-like”, the involvement of ATG8, a protein involved in autophagosome formation, and the description of autophagosome-like vesicles in both *C. reinhardtii* [218] and *Micrasterias denticulata* [220] suggest that macroautophagy processes can also be involved. The articulation between micro- and macro-autophagy processes remains unclear. Microphagy-like degradation of LDs and involvement of ATG8 are also observed in Stramenopiles. In *Nannochloropsis oceanica*, microphagy-like degradation of LDs during nitrogen resupply and interactions between NoATG8 and NoLSDP, the major LD protein in *N. oceanica*, have been observed [221]. An ATG8-interacting motif has also been identified in the Stramenopile lipid droplet protein (StLDP), the major protein at the surface of LDs in the diatom *P. tricornutum* [108,110], whose mutants show an overaccumulation of TAG and impaired LD degradation following nitrogen replenishment [67]. Similarly, a recent study has highlighted the importance of an acyl-binding protein (ACBP) in LD degradation and showed that impaired LD degradation in the ACBP KO could be linked to autophagy defects as *atg5* expression was repressed in these mutants [210]. Yet, the exact role of ACBP remains elusive and the role of lipophagy in LD degradation in *P. tricornutum* remains hypothetical. However, lipophagy has been shown to play a role in lipid degradation in another diatom, *Fistulifera solaris* [222]. Electron microscopy images suggested that in *F. solaris*, LD monolayer could directly fuse with the vacuole membrane, leading to the delivery of their lipid content directly in the vacuole lumen without complete LD internalization (Figs. 2B–4), suggesting that a microlipophagy pathway, different from what is described in yeast, could also exist in algae [222].

5. Conclusion

The degradation of LDs follows similar general pathways in all organisms considered in this review, and some key core components, involved in the initial steps of LD degradation, appear conserved. This is the case for the main TAG lipases, that orchestrate hydrolysis of TAG to DAG (Table 1) and for the general autophagy machinery. However, the following steps show a great diversity, depending on organisms but also tissue/organ within the same organism, and subsequent fate of released fatty acids. CGI-58 is an interesting example in the lipolysis process. Indeed, while the protein is conserved at the sequence level and has been identified in all considered phyla, its localization and function vary (cf. section 3.3). In plants, CGI-58 is localized at the surface at peroxisomes and interacts with PXA1 [73], likely to regulate FA entry into β-oxidation following TAG degradation (see Fig. 1) and the subsequent use of these FA as hormone precursors of the jasmonate and auxin biosynthetic pathways, particularly in vegetative tissues [73]. By contrast, localization at the surface of LD in mammals allows a wider range of fates of released FA [101], and association of CGI-58 with mitochondria in microalgae can serve to balance the fate of FA between degradation and recycling [77].

Lipophagy, and in particular microlipophagy, shows an even broader diversity of routes and players (Fig. 2 and Table 2), suggesting that it has evolved differently in the considered phyla. However, it is important to note that knowledge regarding lipophagy is only recent and partial, as illustrated by the recent discovery of microlipophagy in human [180]. Our vision may thus be biased by research focus that differs between phyla. Indeed, in mammals, defects in LD formation or degradation are associated with many diseases, including metabolic diseases but also central nervous system diseases (for review [223]). Metabolic diseases and the associated tissues (adipose tissue and liver) have consequently been a major focus of LD research. In plants, studies have for a long time focused on oleaginous seeds and germination, leaving aside other tissues or processes where LDs seem much less prominent but play essential roles. Finally, in microalgae, a lot of research is turned towards the increase or alteration of TAG content for biotechnological applications. It is therefore possible that the differences in lipophagy, and more generally LD degradation pathways relate to the physiology and/or functions of studied LDs in the

considered tissue/condition of one organism. An interesting example of lipophagy-specific function has been shown in response to ER stress in yeast, where microlipophagy was suggested to contribute to ER quality control promoting cell survival through the removal of damaged proteins from the ER, as well as through the removal of lipid excess observed during lipid imbalance [186,188]. Indeed, several cargo proteins, some being polyubiquitinated, are associated to LDs under stress and are internalized into vacuole with LDs for degradation, demonstrating the role of microlipophagy in proteostasis under ER stress [186,188]. Investigating similar mechanisms in other organisms would be very interesting, especially in other unicellular organism as some very interesting common points can be drawn. We have highlighted in part 3.2.1 the relationship between cell cycle and LD degradation in unicellular organisms, that relates to their life cycle. Another very interesting feature is the close link between LD biogenesis and degradation that seems to exist within these organisms. Indeed, while in mammals and plants, described functions of LD coat proteins are related to protection against LD degradation (cf. part 3), the major LD proteins of two distant stramenopiles, *N. oceanica* and *P. tricornutum,* are involved in LD degradation, probably through lipophagy (cf. part 4, [67,221]). In yeast, the LDO proteins are both involved in the Seipin complex and in LD degradation through microlipophagy (cf. part 4, [199,200]). Thus, in these organisms, that need to quickly respond to environmental changes, LDs seem to be primed for degradation during their biogenesis. This could also be the case in some tissues of pluricellular organisms. In plant leaves, the LD coat protein LDIP also interacts with Seipin and seems to be functionally homologous to LDO45 [224], while mammalian ORP8 seems involved in both LD biogenesis and lipophagy [171,172](cf. section 4.1).

Finally, in the present work we have presented lipolysis and lipophagy separately, but the degradation of large LDs highlights the integration of both main routes, and its possible conservation. In the green microalga *Auxenochlorella protothecoides,* it has been suggested that large LDs are first broken down by lipolysis to reduce their size, which allows their subsequent degradation by lipophagy [215]. Observations of LDs dynamics following nitrogen replenishment in *P. tricornutum* suggest that a similar mechanism could be at play, as two phases are observed: a first one during which the number of LDs increases while their size decreases, and a second where the number and size of LDs decrease [225]. The existence of non-essential lipophagy to degrade LDs in plant seeds [206,211] and adipocytes [178], as well as the involvement of ATGL [226,227] and other patatin-like lipases (reviewed in Ref. [228]) in lipophagy in the liver and brown adipose tissue, suggest that similar cooperation of lipolysis and lipophagy could facilitate the degradation of large LDs in these tissues.

Funding

All authors are supported by the French National Research Agency (GRAL Labex ANR-10-LABEX-04, EUR CBS ANR-17-EURE-0003, PEPR Algadvance A-22-PEBB-0002), CA is supported by a grant from the Ecole Normale Supérieure (ENS) of Paris, SY is supported by the French National Research Agency in the framework of the "Investissements d'avenir" program (ANR-15-IDEX-02). CA and JS are supported by the French National Research Agency (ANR-22-CE44-0036-02 CONTROLD) and MC and JS are supported by IDEX Université Grenoble-Alpes (DefiCO2 Cross-disciplinary Program Grant ANR-15-IDEX-02) and INRAE BAP division (S-PHAEO project).

CRediT authorship contribution statement

Chems Amari: Writing – review & editing, Writing – original draft, Conceptualization. **Marta Carletti:** Writing – review & editing, Writing – original draft, Visualization, Conceptualization. **Siqi Yan:** Writing – review & editing, Writing – original draft, Conceptualization. **Morgane Michaud:** Writing – review & editing, Writing – original draft, Data curation, Conceptualization. **Juliette Salvaing:** Writing – review & editing, Writing – original draft, Supervision, Funding acquisition, Conceptualization.

Declaration of competing interest

The authors declare that they have no conflict of interest.

References

[1] P.K. Lundquist, K.-K. Shivaiah, R. Espinoza-Corral, Lipid droplets throughout the evolutionary tree, Prog. Lipid Res. 78 (2020) 101029, https://doi.org/10.1016/j.plipres.2020.101029.
[2] J. Lupette, E. Maréchal, The puzzling conservation and diversification of lipid droplets from bacteria to eukaryotes, in: M. Kloc (Ed.), Symbiosis: Cellular, Molecular, Medical and Evolutionary Aspects, Springer International Publishing, Cham, 2020, pp. 281–334, https://doi.org/10.1007/978-3-030-51849-3_11.
[3] D.J. Murphy, The dynamic roles of intracellular lipid droplets: from archaea to mammals, Protoplasma 249 (2012) 541–585, https://doi.org/10.1007/s00709-011-0329-7.
[4] T. Fujimoto, R.G. Parton, Not just fat: the structure and function of the lipid droplet, Cold Spring Harb Perspect Biol 3 (2011) a004838, https://doi.org/10.1101/cshperspect.a004838.
[5] K. Tauchi-Sato, S. Ozeki, T. Houjou, R. Taguchi, T. Fujimoto, The surface of lipid droplets is a phospholipid monolayer with a unique fatty acid composition, J. Biol. Chem. 277 (2002) 44507–44512, https://doi.org/10.1074/jbc.M207712200.
[6] I.A. Graham, Seed storage oil mobilization, Annu. Rev. Plant Biol. 59 (2008) 115–142, https://doi.org/10.1146/annurev.arplant.59.032607.092938.
[7] A.H.C. Huang, Oil bodies and oleosins in seeds, Annu. Rev. Plant Physiol. Plant Mol. Biol. 43 (1992) 177–200, https://doi.org/10.1146/annurev.pp.43.060192.001141.
[8] A. Guzha, P. Whitehead, T. Ischebeck, K.D. Chapman, Lipid droplets: packing hydrophobic molecules within the aqueous cytoplasm, Annu. Rev. Plant Biol. 74 (2023) 195–223, https://doi.org/10.1146/annurev-arplant-070122-021752.
[9] D. Le Moigne, N. Guéguen, J. Salvaing, Lipid droplets in plants: more than a simple fat storage, in: Lipids in Plants and Algae: from Fundamental Science to Industrial Applications, Academic Press, 2022, pp. 191–223, https://doi.org/10.1016/bs.abr.2021.07.004.
[10] A.J. Mathiowetz, J.A. Olzmann, Lipid droplets and cellular lipid flux, Nat. Cell Biol. 26 (2024) 331–345, https://doi.org/10.1038/s41556-024-01364-4.
[11] J.A. Olzmann, P. Carvalho, Dynamics and functions of lipid droplets, Nat. Rev. Mol. Cell Biol. 20 (2019) 137–155, https://doi.org/10.1038/s41580-018-0085-z.
[12] A.R. Thiam, E. Ikonen, Lipid droplet nucleation, Trends Cell Biol. 31 (2021) 108–118, https://doi.org/10.1016/j.tcb.2020.11.006.
[13] T.C. Walther, J. Chung, R.V. Farese, Lipid droplet biogenesis, Annu. Rev. Cell Dev. Biol. 33 (2017) 491–510, https://doi.org/10.1146/annurev-cellbio-100616060608.
[14] Y.A. Klug, J.V. Ferreira, P. Carvalho, A unifying mechanism for seipin-mediated lipid droplet formation, FEBS (Fed. Eur. Biochem. Soc.) Lett. 598 (2024) 1116–1126, https://doi.org/10.1002/1873-3468.14825.
[15] M.S. Greer, Y. Cai, S.K. Gidda, N. Esnay, F.K. Kretzschmar, D. Seay, E. McClinchie, T. Ischebeck, R.T. Mullen, J.M. Dyer, K.D. Chapman, SEIPIN isoforms interact with the membrane-tethering protein VAP27-1 for lipid droplet formation, Plant Cell 32 (2020) 2932–2950, https://doi.org/10.1105/tpc.19.00771.
[16] Y. Filali-Mouncef, C. Hunter, F. Roccio, S. Zagkou, N. Dupont, C. Primard, T. Proikas-Cezanne, F. Reggiori, The menage a trois of autophagy, lipid droplets and liver disease, Autophagy 18 (2022) 50–72, https://doi.org/10.1080/15548627.2021.1895658.
[17] G.F. Grabner, H. Xie, M. Schweiger, R. Zechner, Lipolysis: cellular mechanisms for lipid mobilization from fat stores, Nat. Metab. 3 (2021) 1445–1465, https://doi.org/10.1038/s42255-021-00493-6.
[18] Y. Li-Beisson, F. Kong, P. Wang, Y. Lee, B.-H. Kang, The disassembly of lipid droplets in Chlamydomonas, New Phytol. 231 (2021) 1359–1364, https://doi.org/10.1111/nph.17505.
[19] J. Schepers, C. Behl, Lipid droplets and autophagy—links and regulations

from yeast to humans, J of Cellular Biochemistry 122 (2021) 602–611, https://doi.org/10.1002/jcb.29889.
[20] R. Köffel, R. Tiwari, L. Falquet, R. Schneiter, The Saccharomyces cerevisiae yll012/YEH1, ylr020/YEH2, and TGL1 genes encode a novel family of membrane-anchored lipases that are required for steryl ester hydrolysis, Mol. Cell Biol. 25 (2005) 1655, https://doi.org/10.1128/MCB.25.5.1655-1668.2005.
[21] R. Köffel, R. Schneiter, Yeh1 Constitutes the major steryl ester hydrolase under Heme-Deficient conditions in Saccharomyces cerevisiae, Eukaryot. Cell 5 (2006) 1018–1025, https://doi.org/10.1128/ec.00002-06.
[22] H. Müllner, G. Deutsch, E. Leitner, E. Ingolic, G. Daum, *YEH2/YLR020c* encodes a novel steryl ester hydrolase of the yeast *Saccharomyces cerevisiae*, J. Biol. Chem. 280 (2005) 13321–13328, https://doi.org/10.1074/jbc.M409914200.
[23] A. Wagner, K. Grillitsch, E. Leitner, G. Daum, Mobilization of steryl esters from lipid particles of the yeast *Saccharomyces cerevisiae*, Biochim. Biophys. Acta Mol. Cell Biol. Lipids 1791 (2009) 118–124, https://doi.org/10.1016/j.bbalip.2008.11.004.
[24] C.-W. Wang, Lipid droplet dynamics in budding yeast, Cell. Mol. Life Sci. 72 (2015) 2677–2695, https://doi.org/10.1007/s00018-015-1903-5.
[25] F.K. Kretzschmar, N.M. Doner, H.E. Krawczyk, P. Scholz, K. Schmitt, O. Valerius, G.H. Braus, R.T. Mullen, T. Ischebeck, Identification of Low-Abundance lipid droplet proteins in seeds and seedlings, Plant Physiology 182 (2020) 1326–1345, https://doi.org/10.1104/pp.19.01255.
[26] S. Ghosh, R.W. St Clair, L.L. Rudel, Mobilization of cytoplasmic CE droplets by overexpression of human macrophage cholesteryl ester hydrolase, JLR (J. Lipid Res.) 44 (2003) 1833–1840, https://doi.org/10.1194/jlr.M300162-JLR200.
[27] B. Zhao, B.J. Fisher, R.W.St Clair, L.L. Rudel, S. Ghosh, Redistribution of macrophage cholesteryl ester hydrolase from cytoplasm to lipid droplets upon lipid loading1, JLR (J. Lipid Res.) 46 (2005) 2114–2121, https://doi.org/10.1194/jlr.M500207-JLR200.
[28] B. Zhao, J. Song, W.N. Chow, R.W.S. Clair, L.L. Rudel, S. Ghosh, Macrophage-specific transgenic expression of cholesteryl ester hydrolase significantly reduces atherosclerosis and lesion necrosis in $Ldlr^{-/-}$ mice, J. Clin. Invest. 117 (2007) 2983–2992, https://doi.org/10.1172/JCI30485.
[29] M. Sekiya, J. Osuga, S. Nagashima, T. Ohshiro, M. Igarashi, H. Okazaki, M. Takahashi, F. Tazoe, T. Wada, K. Ohta, M. Takanashi, M. Kumagai, M. Nishi, S. Takase, N. Yahagi, H. Yagyu, K. Ohashi, R. Nagai, T. Kadowaki, Y. Furukawa, S. Ishibashi, Ablation of neutral cholesterol ester hydrolase 1 accelerates atherosclerosis, Cell Metabol. 10 (2009) 219–228, https://doi.org/10.1016/j.cmet.2009.08.004.
[30] M. Igarashi, J. Osuga, H. Uozaki, M. Sekiya, S. Nagashima, M. Takahashi, S. Takase, M. Takanashi, Y. Li, K. Ohta, M. Kumagai, M. Nishi, M. Hosokawa, C. Fledelius, P. Jacobsen, H. Yagyu, M. Fukayama, R. Nagai, T. Kadowaki, K. Ohashi, S. Ishibashi, The critical role of neutral cholesterol ester hydrolase 1 in cholesterol removal from human macrophages, Circ. Res. 107 (2010) 1387–1395, https://doi.org/10.1161/CIRCRESAHA.110.226613.
[31] M. Buchebner, T. Pfeifer, N. Rathke, P.G. Chandak, A. Lass, R. Schreiber, A. Kratzer, R. Zimmermann, W. Sattler, H. Koefeler, E. Fröhlich, G.M. Kostner, R. Birner-Gruenberger, K.P. Chiang, G. Haemmerle, R. Zechner, S. Levak-Frank, B. Cravatt, D. Kratky, Cholesteryl ester hydrolase activity is abolished in HSL-/- macrophages but unchanged in macrophages lacking KIAA1363, J. Lipid Res. 51 (2010) 2896–2908, https://doi.org/10.1194/jlr.M004259.
[32] R. Zimmermann, J.G. Strauss, G. Haemmerle, G. Schoiswohl, R. Birner-Gruenberger, M. Riederer, A. Lass, G. Neuberger, F. Eisenhaber, A. Hermetter, R. Zechner, Fat mobilization in adipose tissue is promoted by adipose triglyceride lipase, Science 306 (2004) 1383–1386, https://doi.org/10.1126/science.1100747.
[33] G. Haemmerle, A. Lass, R. Zimmermann, G. Gorkiewicz, C. Meyer, J. Rozman, G. Heldmaier, R. Maier, C. Theussl, S. Eder, D. Kratky, E.F. Wagner, M. Klingenspor, G. Hoefler, R. Zechner, Defective lipolysis and altered energy metabolism in mice lacking adipose triglyceride lipase, Science 312 (2006) 734–737, https://doi.org/10.1126/science.1123965.
[34] J. Fischer, C. Lefèvre, E. Morava, J.-M. Mussini, P. Laforêt, A. Negre-Salvayre, M. Lathrop, R. Salvayre, The gene encoding adipose triglyceride lipase (PNPLA2) is mutated in neutral lipid storage disease with myopathy, Nat. Genet. 39 (2007) 28–30, https://doi.org/10.1038/ng1951.
[35] K. Athenstaedt, G. Daum, Tgl4p and Tgl5p, two triacylglycerol lipases of the yeast Saccharomyces cerevisiae are localized to lipid particles, J. Biol. Chem. 280 (2005) 37301–37309.
[36] K. Athenstaedt, G. Daum, YMR313c/TGL3 encodes a novel triacylglycerol lipase located in lipid particles of Saccharomyces cerevisiae, J. Biol. Chem. 278 (2003) 23317–23323.
[37] S. Rajakumari, G. Daum, Janus-faced enzymes yeast Tgl3p and Tgl5p catalyze lipase and acyltransferase Reactions, Mol. Biol. Cell 21 (2010) 501–510, https://doi.org/10.1091/mbc.E09-09-0775.
[38] P.J. Eastmond, *SUGAR-DEPENDENT1* encodes a patatin domain triacylglycerol lipase that Initiates storage oil breakdown in germinating *Arabidopsis* seeds, Plant Cell 18 (2006) 665–675, https://doi.org/10.1105/tpc.105.040543.
[39] A.A. Kelly, A.-L. Quettier, E. Shaw, P.J. Eastmond, Seed storage oil mobilization is important but not essential for germination or seedling establishment in Arabidopsis, Plant Physiology 157 (2011) 866–875, https://doi.org/10.1104/pp.111.181784.
[40] G.F.E. Scherer, S.B. Ryu, X. Wang, A.R. Matos, T. Heitz, Patatin-related phospholipase A: nomenclature, subfamilies and functions in plants, Trends Plant Sci. 15 (2010) 693–700, https://doi.org/10.1016/j.tplants.2010.09.005.
[41] A.A. Kelly, H. van Erp, A.-L. Quettier, E. Shaw, G. Menard, S. Kurup, P.J. Eastmond, The SUGAR-DEPENDENT1 lipase limits triacylglycerol accumulation in vegetative tissues of Arabidopsis1, Plant Physiol 162 (2013) 1282–1289, https://doi.org/10.1104/pp.113.219840.
[42] H. Siegler, O. Valerius, T. Ischebeck, J. Popko, N.J. Tourasse, O. Vallon, I. Khozin-Goldberg, G.H. Braus, I. Feussner, Analysis of the lipid body proteome of the oleaginous alga Lobosphaera incisa, BMC Plant Biol. 17 (2017) 98, https://doi.org/10.1186/s12870-017-1042-2.
[43] J. Warakanont, Y. Li-Beisson, C. Benning, LIP4 is involved in triacylglycerol degradation in Chlamydomonas reinhardtii, Plant Cell Physiol. 60 (2019) 1250–1259, https://doi.org/10.1093/pcp/pcz037.
[44] F. Barka, M. Angstenberger, T. Ahrendt, W. Lorenzen, H.B. Bode, C. Büchel, Identification of a triacylglycerol lipase in the diatom Phaeodactylum tricornutum, Biochim. Biophys. Acta Mol. Cell Biol. Lipids 1861 (2016) 239–248, https://doi.org/10.1016/j.bbalip.2015.12.023.
[45] Y. Maeda, K. Watanabe, M. Kaha, Y. Yabu, T. Yoshino, M. Matsumoto, T. Tanaka, Assessment on the oil accumulation by knockdown of triacylglycerol lipase in the oleaginous diatom Fistulifera solaris, Sci. Rep. 11 (2021) 20905, https://doi.org/10.1038/s41598-021-00453-w.
[46] T. Nobusawa, K. Yamakawa-Ayukawa, F. Saito, S. Nomura, A. Takami, H. Ohta, A homolog of Arabidopsis SDP1 lipase in Nannochloropsis is involved in degradation of de novo-synthesized triacylglycerols in the endoplasmic reticulum, Biochim. Biophys. Acta Mol. Cell Biol. Lipids 1864 (2019) 1185–1193, https://doi.org/10.1016/j.bbalip.2019.05.013.
[47] O. Strand, M. Vaughan, D. Steinberg, Rat adipose tissue lipases - hormone-sensitive lipase activity against triglycerides compared with activity against lower glycerides, J. Lipid Res. 5 (1964) 554.
[48] S. He, C. McPhaul, J.Z. Li, R. Garuti, L. Kinch, N.V. Grishin, J.C. Cohen, H.H. Hobbs, A sequence variation (I148M) in PNPLA3 associated with nonalcoholic fatty liver disease disrupts triglyceride hydrolysis, J. Biol. Chem. 285 (2010) 6706–6715, https://doi.org/10.1074/jbc.M109.064501.
[49] S.-H. Chon, Y.X. Zhou, J.L. Dixon, J. Storch, Intestinal monoacylglycerol metabolism: developmental and nutritional regulation of monoacylglycerol lipase and monoacylglycerol acyltransferase, J. Biol. Chem. 282 (2007) 33346–33357, https://doi.org/10.1074/jbc.M706994200.
[50] M.O. Debelyy, S. Thoms, M. Connerth, G. Daum, R. Erdmann, Involvement of the Saccharomyces cerevisiae hydrolase Ldh1p in lipid homeostasis, Eukaryot. Cell 10 (2011) 776–781, https://doi.org/10.1128/ec.05040-11.
[51] S. Thoms, M.O. Debelyy, M. Connerth, G. Daum, R. Erdmann, The putative Saccharomyces cerevisiae hydrolase Ldh1p is localized to lipid droplets, Eukaryot. Cell (2011), https://doi.org/10.1128/ec.05038-11.
[52] B. Ploier, M. Scharwey, B. Koch, C. Schmidt, J. Schatte, G. Rechberger, M. Kollroser, A. Hermetter, G. Daum, Screening for hydrolytic enzymes reveals Ayr1p as a novel triacylglycerol lipase in Saccharomyces cerevisiae, J. Biol. Chem. 288 (2013) 36061–36072, https://doi.org/10.1074/jbc.M113.509927.
[53] C. Heier, U. Taschler, S. Rengachari, M. Oberer, H. Wolinski, K. Natter, S.D. Kohlwein, R. Leber, R. Zimmermann, Identification of Yju3p as functional orthologue of mammalian monoglyceride lipase in the yeast Saccharomycescerevisiae, Biochim. Biophys. Acta 1801 (2010) 1063–1071, https://doi.org/10.1016/j.bbalip.2010.06.001.
[54] A. Jandrositz, J. Petschnigg, R. Zimmermann, K. Natter, H. Scholze, A. Hermetter, S.D. Kohlwein, R. Leber, The lipid droplet enzyme Tgl1p hydrolyzes both steryl esters and triglycerides in the yeast, *Saccharomyces cerevisiae*, Biochim. Biophys. Acta Mol. Cell Biol. Lipids 1735 (2005) 50–58, https://doi.org/10.1016/j.bbalip.2005.04.005.
[55] A.O. Müller, T. Ischebeck, Characterization of the enzymatic activity and physiological function of the lipid droplet-associated triacylglycerol lipase AtOBL1, New Phytol. 217 (2018) 1062–1076, https://doi.org/10.1111/nph.14902.
[56] R.J. Kim, H.J. Kim, D. Shim, M.C. Suh, Molecular and biochemical characterizations of the monoacylglycerol lipase gene family of Arabidopsis thaliana, Plant J. 85 (2016) 758–771, https://doi.org/10.1111/tpj.13146.
[57] E.Y. Kim, Y.S. Seo, W.T. Kim, AtDSEL, an *Arabidopsis* cytosolic DAD1-like acylhydrolase, is involved in negative regulation of storage oil mobilization during seedling establishment, J. Plant Physiol. 168 (2011) 1705–1709, https://doi.org/10.1016/j.jplph.2011.03.004.
[58] X. Li, C. Benning, M.-H. Kuo, Rapid triacylglycerol turnover in Chlamydomonas reinhardtii requires a lipase with broad substrate specificity, Eukaryot. Cell 11 (2012) 1451–1462, https://doi.org/10.1128/EC.00268-12.
[59] A.R. Kimmel, C. Sztalryd, The perilipins: major cytosolic lipid droplet–associated proteins and their roles in cellular lipid storage, mobilization, and systemic homeostasis, Annu. Rev. Nutr. 36 (2016) 471–509, https://doi.org/10.1146/annurev-nutr-071813-105410.
[60] S. Kaushik, A.M. Cuervo, Degradation of lipid droplet-associated proteins by chaperone-mediated autophagy facilitates lipolysis, Nat. Cell Biol. 17 (2015) 759, https://doi.org/10.1038/ncb3166.
[61] N. Jacquier, S. Mishra, V. Choudhary, R. Schneiter, Expression of oleosin and perilipins in yeast promotes formation of lipid droplets from the endoplasmic reticulum, J. Cell Sci. 126 (2013) 5198–5209, https://doi.org/10.1242/jcs.131896.
[62] S. Winichayakul, R.W. Scott, M. Roldan, J.-H.B. Hatier, S. Livingston, R. Cookson, A.C. Curran, N.J. Roberts, In vivo packaging of triacylglycerols enhances Arabidopsis leaf biomass and energy density, Plant Physiology 162

(2013) 626–639, https://doi.org/10.1104/pp.113.216820.
[63] M.S. Traver, B. Bartel, The ubiquitin-protein ligase MIEL1 localizes to peroxisomes to promote seedling oleosin degradation and lipid droplet mobilization, Proc. Natl. Acad. Sci. U.S.A. 120 (2023) e2304870120, https://doi.org/10.1073/pnas.2304870120.
[64] C. Deruyffelaere, Z. Purkrtova, I. Bouchez, B. Collet, J.-L. Cacas, T. Chardot, J.-L. Gallois, S. D'Andrea, PUX10 is a CDC48A adaptor protein that regulates the extraction of ubiquitinated oleosins from seed lipid droplets in Arabidopsis, Plant Cell 30 (2018) 2116–2136, https://doi.org/10.1105/tpc.18.00275.
[65] F.K. Kretzschmar, L.A. Mengel, A.O. Müller, K. Schmitt, K.F. Blersch, O. Valerius, G.H. Braus, T. Ischebeck, PUX10 is a lipid droplet-localized scaffold protein that interacts with CELL DIVISION CYCLE48 and is involved in the degradation of lipid droplet proteins, Plant Cell 30 (2018) 2137–2160, https://doi.org/10.1105/tpc.18.00276.
[66] E.R. Moellering, C. Benning, RNA interference silencing of a major lipid droplet protein affects lipid droplet size in Chlamydomonas reinhardtii, Eukaryot. Cell 9 (2010) 97–106, https://doi.org/10.1128/EC.00203-09.
[67] Y. Taparia, A.K. Dolui, S. Boussiba, I. Khozin-Goldberg, Multiplexed genome editing via an RNA polymerase II promoter-driven sgRNA array in the diatom Phaeodactylum tricornutum: insights into the role of StLDP, Front. Plant Sci. 12 (2022) 784780, https://doi.org/10.3389/fpls.2021.784780.
[68] A. Lass, R. Zimmermann, G. Haemmerle, M. Riederer, G. Schoiswohl, M. Schweiger, P. Kienesberger, J.G. Strauss, G. Gorkiewicz, R. Zechner, Adipose triglyceride lipase-mediated lipolysis of cellular fat stores is activated by CGI-58 and defective in Chanarin-Dorfman Syndrome, Cell Metabol. 3 (2006) 309–319, https://doi.org/10.1016/j.cmet.2006.03.005.
[69] A.K. Ghosh, G. Ramakrishnan, C. Chandramohan, R. Rajasekharan, CGI-58, the causative gene for Chanarin-Dorfman syndrome, mediates acylation of lysophosphatidic acid, J. Biol. Chem. 283 (2008) 24525–24533, https://doi.org/10.1074/jbc.M801783200.
[70] N.O. Speer, R.J. Braun, E.G. Reynolds, A. Brudnicka, J.M.J. Swanson, W.M. Henne, Tld1 is a regulator of triglyceride lipolysis that demarcates a lipid droplet subpopulation, J. Cell Biol. 223 (2023) e202303026, https://doi.org/10.1083/jcb.202303026.
[71] N. Thazar-Poulot, M. Miquel, I. Fobis-Loisy, T. Gaude, Peroxisome extensions deliver the Arabidopsis SDP1 lipase to oil bodies, Proc. Natl. Acad. Sci. USA 112 (2015) 4158–4163, https://doi.org/10.1073/pnas.1403322112.
[72] S. Huang, Z. Liu, W. Cao, H. Li, W. Zhang, Y. Cui, S. Hu, M. Luo, Y. Zhu, Q. Zhao, L. Xie, C. Gao, S. Xiao, L. Jiang, The plant ESCRT component FREE1 regulates peroxisome-mediated turnover of lipid droplets in germinating Arabidopsis seedlings, Plant Cell (2022) koac195, https://doi.org/10.1093/plcell/koac195.
[73] S. Park, S.K. Gidda, C.N. James, P.J. Horn, N. Khuu, D.C. Seay, J. Keereetaweep, K.D. Chapman, R.T. Mullen, J.M. Dyer, The α/β hydrolase CGI-58 and peroxisomal transport protein PXA1 coregulate lipid homeostasis and signaling in Arabidopsis, Plant Cell 25 (2013) 1726–1739, https://doi.org/10.1105/tpc.113.111898.
[74] C.H. Tsai, J. Warakanont, T. Takeuchi, B.B. Sears, E.R. Moellering, C. Benning, The protein Compromised Hydrolysis of Triacylglycerols 7 (CHT7) acts as a repressor of cellular quiescence in Chlamydomonas, Proceedings of the National Academy of Sciences of the United States of America 111 (2014) 15833–15838, https://doi.org/10.1073/pnas.1414567111.
[75] J. Lee, Y. Yamaoka, F. Kong, C. Cagnon, A. Beyly-Adriano, S. Jang, P. Gao, B.-H. Kang, Y. Li-Beisson, Y. Lee, The phosphatidylethanolamine-binding protein DTH1 mediates degradation of lipid droplets in *Chlamydomonas reinhardtii*, Proc. Natl. Acad. Sci. U.S.A. 117 (2020) 23131–23139, https://doi.org/10.1073/pnas.2005600117.
[76] F. Bai, L. Yu, J. Shi, Y. Li-Beisson, J. Liu, Long-chain acyl-CoA synthetases activate fatty acids for lipid synthesis, remodeling and energy production in Chlamydomonas, New Phytol. 233 (2022) 823–837, https://doi.org/10.1111/nph.17813.
[77] Q. Shu, Y. Pan, H. Hu, CGI-58 protein acts as a positive regulator of triacylglycerol accumulation in Phaeodactylum tricornutum, J. Microbiol. Biotechnol. 33 (2023) 242–250, https://doi.org/10.4014/jmb.2209.09029.
[78] M. Vaughan, J. Berger, D. Steinberg, HORMONE-SENSITIVE lipase + monoglyceride lipase activities in adipose tissue, J. Biol. Chem. 239 (1964), 401-+.
[79] E. Recazens, E. Mouisel, D. Langin, Hormone-sensitive lipase: sixty years later - ScienceDirect, Prog. Lipid Res. 82 (2021), https://doi.org/10.1016/j.plipres.2020.101084.
[80] G. Haemmerle, R. Zimmermann, M. Hayn, C. Theussl, G. Waeg, E. Wagner, W. Sattler, T.M. Magin, E.F. Wagner, R. Zechner, Hormone-sensitive lipase deficiency in mice causes diglyceride accumulation in adipose tissue, muscle, and testis, J. Biol. Chem. 277 (2002) 4806–4815, https://doi.org/10.1074/jbc.M110355200.
[81] V. Bezaire, A. Mairal, C. Ribet, C. Lefort, A. Girousse, J. Jocken, J. Laurencikiene, R. Anesia, A.-M. Rodriguez, M. Ryden, B.M. Stenson, C. Dani, G. Ailhaud, P. Arner, D. Langin, Contribution of adipose triglyceride lipase and hormone-sensitive lipase to lipolysis in hMADS adipocytes, J. Biol. Chem. 284 (2009) 18282–18291, https://doi.org/10.1074/jbc.M109.008631.
[82] G. Fredrikson, H. Tornqvist, P. Belfrage, Hormone-sensitive lipase and monoacylglycerol lipase are both required for complete degradation of adipocyte triacylglycerol, Biochim. Biophys. Acta Lipids Lipid. Metabol. 876 (1986) 288–293, https://doi.org/10.1016/0005-2760(86)90286-9.
[83] H. Tornqvist, P. Belfrage, Purification and some properties of a monoacylglycerol-hydrolyzing enzyme of rat adipose-tissue, J. Biol. Chem. 251 (1976) 813–819.
[84] L. Yu, W. Shen, J. Fan, S.K. Sah, I. Mavraganis, L. Wang, P. Gao, J. Gao, Q. Zheng, D. Meesapyodsuk, H. Yang, Q. Li, J. Zou, C. Xu, A chloroplast diacylglycerol lipase modulates glycerolipid pathway balance in Arabidopsis, Plant J. 115 (2023) 335–350, https://doi.org/10.1111/tpj.16228.
[85] S. Ali, X. Liu, L. Sen, D. Lan, J. Wang, MdI. Hassan, Y. Wang, Sequence and structure-based method to predict diacylglycerol lipases in protein sequence, Int. J. Biol. Macromol. 182 (2021) 455–463, https://doi.org/10.1016/j.ijbiomac.2021.04.011.
[86] V. Murison, J. Hérault, B. Schoefs, J. Marchand, L. Ulmann, Bioinformatics-based screening approach for the identification and characterization of lipolytic enzymes from the marine diatom Phaeodactylum tricornutum, Mar. Drugs 21 (2023), https://doi.org/10.3390/md21020125.
[87] I. Bouchnak, D. Coulon, V. Salis, S. D'Andréa, C. Bréhélin, Lipid droplets are versatile organelles involved in plant development and plant response to environmental changes, Front. Plant Sci. 14 (2023) 1193905, https://doi.org/10.3389/fpls.2023.1193905.
[88] I. Feussner, H. Kühn, C. Wasternack, Lipoxygenase-dependent degradation of storage lipids, Trends Plant Sci. 6 (2001) 268–273, https://doi.org/10.1016/S1360-1385(01)01950-1.
[89] K.K. Viswanath, P. Varakumar, R.R. Pamuru, S.J. Basha, S. Mehta, A.D. Rao, Plant lipoxygenases and their role in plant physiology, J. Plant Biol. 63 (2020) 83–95, https://doi.org/10.1007/s12374-020-09241-x.
[90] M. Schweiger, R. Schreiber, G. Haemmerle, A. Lass, C. Fledelius, P. Jacobsen, H. Tornqvist, R. Zechner, R. Zimmermann, Adipose triglyceride lipase and hormone-sensitive lipase are the major enzymes in adipose tissue triacylglycerol catabolism, J. Biol. Chem. 281 (2006) 40236–40241, https://doi.org/10.1074/jbc.M608048200.
[91] X.C. Dong, PNPLA3—a potential therapeutic target for personalized treatment of chronic liver disease, Front. Med. 6 (2019), https://doi.org/10.3389/fmed.2019.00304.
[92] S. McHenry, N.O. Davidson, Missense mutant PNPLA3 alters lipid droplet turnover in partnership with CGI-58, Hepatology 69 (2019) 2323–2325, https://doi.org/10.1002/hep.30620.
[93] P.A. Wilson, S.D. Gardner, N.M. Lambie, S.A. Commans, D.J. Crowther, Characterization of the human patatin-like phospholipase familys, JLR (J. Lipid Res.) 47 (2006) 1940–1949, https://doi.org/10.1194/jlr.M600185-JLR200.
[94] P. Jolivet, E. Roux, S. D'Andrea, M. Davanture, L. Negroni, M. Zivy, T. Chardot, Protein composition of oil bodies in Arabidopsis thaliana ecotype WS, Plant Physiol. Biochem. : PPB (Plant Physiol. Biochem.) 42 (2004) 501–509, https://doi.org/10.1016/j.plaphy.2004.04.006.
[95] C. Deruyffelaere, I. Bouchez, H. Morin, A. Guillot, M. Miquel, M. Froissard, T. Chardot, S. D'Andrea, Ubiquitin-mediated proteasomal degradation of oleosins is involved in oil body mobilization during post-germinative seedling growth in Arabidopsis, Plant Cell Physiol. 56 (2015) 1374–1387, https://doi.org/10.1093/pcp/pcv056.
[96] B. Sharma, D. Joshi, P.K. Yadav, A.K. Gupta, T.K. Bhatt, Role of ubiquitin-mediated degradation system in plant biology, Front. Plant Sci. 7 (2016), https://doi.org/10.3389/fpls.2016.00806.
[97] F. Beisson, N. Ferté, S. Bruley, R. Voultoury, R. Verger, V. Arondel, Oil-bodies as substrates for lipolytic enzymes, Biochim. Biophys. Acta Mol. Cell Biol. Lipids 1531 (2001) 47–58, https://doi.org/10.1016/S1388-1981(01)00086-5.
[98] C. Londos, D.L. Brasaemle, C.J. Schultz, J.P. Segrest, A.R. Kimmel, Perilipins, ADRP, and other proteins that associate with intracellular neutral lipid droplets in animal cells, Semin. Cell Dev. Biol. 10 (1999) 51–58, https://doi.org/10.1006/scdb.1998.0275.
[99] D.L. Brasaemle, B. Rubin, I.A. Harten, J. Gruia-Gray, A.R. Kimmel, C. Londos, Perilipin A increases triacylglycerol storage by decreasing the rate of triacylglycerol hydrolysis, J. Biol. Chem. 275 (2000) 38486–38493, https://doi.org/10.1074/jbc.M007322200.
[100] E. Griseti, A.A. Bello, E. Bieth, B. Sabbagh, J.S. Iacovoni, J. Bigay, H. Laurell, A. Čopič, Molecular mechanisms of perilipin protein function in lipid droplet metabolism, FEBS (Fed. Eur. Biochem. Soc.) Lett. 598 (2024) 1170–1198, https://doi.org/10.1002/1873-3468.14792.
[101] L. Yu, Y. Li, A. Grisé, H. Wang, CGI-58: versatile regulator of intracellular lipid droplet homeostasis, in: X.-C. Jiang (Ed.), Lipid Transfer in Lipoprotein Metabolism and Cardiovascular Disease, Springer, Singapore, 2020, pp. 197–222, https://doi.org/10.1007/978-981-15-6082-8_13.
[102] J.G. Granneman, H.-P.H. Moore, E.P. Mottillo, Z. Zhu, L. Zhou, Interactions of perilipin-5 (Plin5) with adipose triglyceride lipase, J. Biol. Chem. 286 (2011) 5126–5135, https://doi.org/10.1074/jbc.M110.180711.
[103] S.N. Keenan, W. De Nardo, J. Lou, R.B. Schittenhelm, M.K. Montgomery, J.G. Granneman, E. Hinde, M.J. Watt, Perilipin 5 S155 phosphorylation by PKA is required for the control of hepatic lipid metabolism and glycemic control, JLR (J. Lipid Res.) 62 (2021) 100016, https://doi.org/10.1194/jlr.RA120001126.
[104] N.M. Pollak, D. Jaeger, S. Kolleritsch, R. Zimmermann, R. Zechner, A. Lass, G. Haemmerle, The interplay of protein kinase A and perilipin 5 regulates cardiac lipolysis, J. Biol. Chem. 290 (2015) 1295–1306, https://doi.org/10.1074/jbc.M114.604744.
[105] S.K. Gidda, S. Park, M. Pyc, O. Yurchenko, Y. Cai, P. Wu, D.W. Andrews, K.D. Chapman, J.M. Dyer, R.T. Mullen, Lipid droplet-associated proteins (LDAPs) are required for the dynamic regulation of neutral lipid compartmentation in plant cells, Plant Physiology 170 (2016) 2052–2071, https://doi.org/10.1104/pp.15.01977.
[106] S.K. Gidda, S.C. Watt, J. Collins-Silva, A. Kilaru, V. Arondel, O. Yurchenko,

P.J. Horn, C.N. James, D. Shintani, J.B. Ohlrogge, K.D. Chapman, R.T. Mullen, J.M. Dyer, Lipid droplet-associated proteins (LDAPs) are involved in the compartmentalization of lipophilic compounds in plant cells, Plant Signal. Behav. 8 (2013) e27141, https://doi.org/10.4161/psb.27141.
[107] M. Pyc, Y. Cai, S.K. Gidda, O. Yurchenko, S. Park, F.K. Kretzschmar, T. Ischebeck, O. Valerius, G.H. Braus, K.D. Chapman, J.M. Dyer, R.T. Mullen, Arabidopsis lipid droplet-associated protein (LDAP) - interacting protein (LDIP) influences lipid droplet size and neutral lipid homeostasis in both leaves and seeds, Plant J. : For Cell and Molecular Biology 92 (2017) 1182–1201, https://doi.org/10.1111/tpj.13754.
[108] B. Leyland, A. Zarka, S. Didi-Cohen, S. Boussiba, I. Khozin-Goldberg, High resolution proteome of lipid droplets isolated from the pennate diatom *Phaeodactylum tricornutum* (*bacillariophyceae*) strain pt4 provides mechanistic insights into complex intracellular coordination during nitrogen deprivation, J. Phycol. 56 (2020) 1642–1663, https://doi.org/10.1111/jpy.13063.
[109] J. Lupette, A. Jaussaud, K. Seddiki, C. Morabito, S. Brugière, H. Schaller, M. Kuntz, J.-L. Putaux, P.-H. Jouneau, F. Rébeillé, D. Falconet, Y. Couté, J. Jouhet, M. Tardif, J. Salvaing, E. Maréchal, The architecture of lipid droplets in the diatom Phaeodactylum tricornutum, Algal Res. 38 (2019) 101415, https://doi.org/10.1016/j.algal.2019.101415.
[110] K. Yoneda, M. Yoshida, I. Suzuki, M.M. Watanabe, Identification of a major lipid droplet protein in a marine diatom *Phaeodactylum tricornutum*, Plant Cell Physiol. 57 (2016) 397–406, https://doi.org/10.1093/pcp/pcv204.
[111] L. O'Hara, G.-S. Han, P.-C. Sew, N. Grimsey, G.M. Carman, S. Siniossoglou, Control of phospholipid synthesis by phosphorylation of the yeast lipin Pah1p/Smp2p Mg2+-dependent phosphatidate phosphatase, J. Biol. Chem. 281 (2006) 34537–34548, https://doi.org/10.1074/jbc.M606654200.
[112] H. Santos-Rosa, J. Leung, N. Grimsey, S. Peak-Chew, S. Siniossoglou, The yeast lipin Smp2 couples phospholipid biosynthesis to nuclear membrane growth, EMBO J. 24 (2005) 1931–1941, https://doi.org/10.1038/sj.emboj.7600672.
[113] C.F. Kurat, H. Wolinski, J. Petschnigg, S. Kaluarachchi, B. Andrews, K. Natter, S.D. Kohlwein, Cdk1/Cdc28-Dependent activation of the major triacylglycerol lipase Tgl4 in yeast links lipolysis to cell-cycle progression, Mol. Cell 33 (2009) 53–63, https://doi.org/10.1016/j.molcel.2008.12.019.
[114] S. Rajakumari, R. Rajasekharan, G. Daum, Triacylglycerol lipolysis is linked to sphingolipid and phospholipid metabolism of the yeast *Saccharomyces cerevisiae*, Biochim. Biophys. Acta Mol. Cell Biol. Lipids 1801 (2010) 1314–1322, https://doi.org/10.1016/j.bbalip.2010.08.004.
[115] M.S. Chauton, P. Winge, T. Brembu, O. Vadstein, A.M. Bones, Gene regulation of carbon fixation, storage, and utilization in the diatom Phaeodactylum tricornutum acclimated to light/dark Cycles1, Plant Physiol 161 (2013) 1034–1048, https://doi.org/10.1104/pp.112.206177.
[116] M.J. Huysman, A. Tanaka, C. Bowler, W. Vyverman, L. De Veylder, Functional characterization of the diatom cyclin-dependent kinase A2 as a mitotic regulator reveals plant-like properties in a non-green lineage, BMC Plant Biol. 15 (2015) 86, https://doi.org/10.1186/s12870-015-0469-6.
[117] M.J.J. Huysman, A.E. Fortunato, M. Matthijs, B.S. Costa, R. Vanderhaeghen, H. Van den Daele, M. Sachse, D. Inzé, C. Bowler, P.G. Kroth, C. Wilhelm, A. Falciatore, W. Vyverman, L. De Veylder, AUREOCHROME1a-Mediated induction of the diatom-specific cyclin dsCYC2 controls the onset of cell division in diatoms (Phaeodactylum tricornutum), Plant Cell 25 (2013) 215–228, https://doi.org/10.1105/tpc.112.106377.
[118] T. Zhang, J. Huang, Z. Zhang, J. Lv, D. Zhang, R. Qing, L. Lan, Flow cytometry and 5-ethynyl-2′-deoxyuridine (EdU) labeling to detect the cell cycle dynamics of Phaeodactylum tricornutum under light, J. Phycol. 58 (2022) 555–567, https://doi.org/10.1111/jpy.13250.
[119] D. Roy, K.T. Farabaugh, J. Wu, A. Charrier, C. Smas, M. Hatzoglou, K. Thirumurugan, D.A. Buchner, Coordinated transcriptional control of adipocyte triglyceride lipase (*Atgl*) by transcription factors Sp1 and peroxisome proliferator–activated receptor γ (PPARγ) during adipocyte differentiation, J. Biol. Chem. 292 (2017) 14827–14835, https://doi.org/10.1074/jbc.M117.783043.
[120] S. Yogosawa, S. Mizutani, Y. Ogawa, T. Izumi, Activin receptor-like kinase 7 suppresses lipolysis to accumulate fat in obesity through downregulation of peroxisome proliferator–activated receptor g and C/EBPa, Diabetes 62 (2013) 115–123.
[121] Y. Gambo, M. Matsumura, K. Fujimori, Triiodothyronine enhances accumulation of intracellular lipids in adipocytes through thyroid hormone receptor α via direct and indirect mechanisms, Mol. Cell. Endocrinol. 431 (2016) 1–11, https://doi.org/10.1016/j.mce.2016.04.023.
[122] L. Ding, F. Huwyler, F. Long, W. Yang, J. Binz, K. Wernlé, M. Pfister, M. Klug, M. Balaz, B. Ukropcova, J. Ukropec, C. Wu, T. Wang, M. Gao, P.-A. Clavien, P. Dutkowski, M.W. Tibbitt, C. Wolfrum, Glucose controls lipolysis through Golgi PtdIns4P-mediated regulation of ATGL, Nat. Cell Biol. 26 (2024) 552–566, https://doi.org/10.1038/s41556-024-01386-y.
[123] S. Cui, Y. Hayashi, M. Otomo, S. Mano, K. Oikawa, M. Hayashi, M. Nishimura, Sucrose production mediated by lipid metabolism suppresses the physical interaction of peroxisomes and oil bodies during germination of Arabidopsis thaliana, J. Biol. Chem. 291 (2016) 19734–19745, https://doi.org/10.1074/jbc.M116.748814.
[124] M.M. Adeva-Andany, N. Carneiro-Freire, M. Seco-Filgueira, C. Fernández-Fernández, D. Mouriño-Bayolo, Mitochondrial β-oxidation of saturated fatty acids in humans, Mitochondrion 46 (2019) 73–90, https://doi.org/10.1016/j.mito.2018.02.009.
[125] M. Tahri-Joutey, P. Andreoletti, S. Surapureddi, B. Nasser, M. Cherkaoui-Malki, N. Latruffe, Mechanisms mediating the regulation of peroxisomal fatty acid beta-oxidation by PPARα, Int. J. Mol. Sci. 22 (2021) 8969, https://doi.org/10.3390/ijms22168969.
[126] P.-C. Liao, E.J. Yang, T. Borgman, I.R. Boldogh, C.N. Sing, T.C. Swayne, L.A. Pon, Touch and go: membrane contact sites between lipid droplets and other organelles, Front. Cell Dev. Biol. 10 (2022) 852021, https://doi.org/10.3389/fcell.2022.852021.
[127] Y. Meng, D. Guo, L. Lin, H. Zhao, W. Xu, S. Luo, X. Jiang, S. Li, X. He, R. Zhu, R. Shi, L. Xiao, Q. Wu, H. He, J. Tao, H. Jiang, Z. Wang, P. Yao, D. Xu, Z. Lu, Glycolytic enzyme PFKL governs lipolysis by promoting lipid droplet–mitochondria tethering to enhance β-oxidation and tumor cell proliferation, Nat. Metab. 6 (2024) 1092–1107, https://doi.org/10.1038/s42255-024-01047-2.
[128] G.E. Miner, C.M. So, W. Edwards, J.V. Ragusa, J.T. Wine, D. Wong Gutierrez, M.V. Airola, L.E. Herring, R.A. Coleman, E.L. Klett, S. Cohen, PLIN5 interacts with FATP4 at membrane contact sites to promote lipid droplet-to-mitochondria fatty acid transport, Dev. Cell 58 (2023) 1250–1265.e6, https://doi.org/10.1016/j.devcel.2023.05.006.
[129] C.-L. Chang, A.V. Weigel, M.S. Ioannou, H.A. Pasolli, C.S. Xu, D.R. Peale, G. Shtengel, M. Freeman, H.F. Hess, C. Blackstone, J. Lippincott-Schwartz, Spastin tethers lipid droplets to peroxisomes and directs fatty acid trafficking through ESCRT-III, J. Cell Biol. 218 (2019) 2583–2599, https://doi.org/10.1083/jcb.201902061.
[130] J. Kong, Y. Ji, Y.G. Jeon, J.S. Han, K.H. Han, J.H. Lee, G. Lee, H. Jang, S.S. Choe, M. Baes, J.B. Kim, Spatiotemporal contact between peroxisomes and lipid droplets regulates fasting-induced lipolysis via PEX5, Nat. Commun. 11 (2020) 578, https://doi.org/10.1038/s41467-019-14176-0.
[131] C.N. James, P.J. Horn, C.R. Case, S.K. Gidda, D. Zhang, R.T. Mullen, J.M. Dyer, R.G. Anderson, K.D. Chapman, Disruption of the Arabidopsis CGI-58 homologue produces Chanarin-Dorfman-like lipid droplet accumulation in plants, Proceedings of the National Academy of Sciences of the United States of America 107 (2010) 17833–17838, https://doi.org/10.1073/pnas.0911359107.
[132] E.M. Trentacoste, R.P. Shrestha, S.R. Smith, C. Glé, A.C. Hartmann, M. Hildebrand, W.H. Gerwick, Metabolic engineering of lipid catabolism increases microalgal lipid accumulation without compromising growth, Proc. Natl. Acad. Sci. USA 110 (2013) 19748–19753, https://doi.org/10.1073/pnas.1309299110.
[133] A.K. Ghosh, G. Ramakrishnan, R. Rajasekharan, YLR099C (ICT1) encodes a soluble Acyl-CoA-dependent lysophosphatidic acid acyltransferase responsible for enhanced phospholipid synthesis on organic solvent stress in Saccharomyces cerevisiae, J. Biol. Chem. 283 (2008) 9768–9775, https://doi.org/10.1074/jbc.M708418200.
[134] D. Gatica, V. Lahiri, D.J. Klionsky, Cargo recognition and degradation by selective autophagy, Nat. Cell Biol. 20 (2018) 233–242, https://doi.org/10.1038/s41556-018-0037-z.
[135] N. Mizushima, A brief history of autophagy from cell biology to physiology and disease, Nat. Cell Biol. 20 (2018) 521–527, https://doi.org/10.1038/s41556-018-0092-5.
[136] T. Avin-Wittenberg, A. Honig, G. Galili, Variations on a theme: plant autophagy in comparison to yeast and mammals, Protoplasma 249 (2012) 285–299, https://doi.org/10.1007/s00709-011-0296-z.
[137] R.E. Gomez, J. Lupette, C. Chambaud, J. Castets, A. Ducloy, J.-L. Cacas, C. Masclaux-Daubresse, A. Bernard, How lipids contribute to autophagosome biogenesis, a critical process in plant responses to stresses, Cells 10 (2021) 1272, https://doi.org/10.3390/cells10061272.
[138] F.-C. Lin, H.-B. Shi, X.-H. Liu, Similarities and differences of autophagy in mammals, plants, and microbes, in: Z. Xie (Ed.), Autophagy: Biology and Diseases, Springer Singapore, Singapore, 2021, pp. 99–114, https://doi.org/10.1007/978-981-16-2830-6_7.
[139] M.E. Pérez-Pérez, S.D. Lemaire, J.L. Crespo, The ATG4 protease integrates redox and stress signals to regulate autophagy, J. Exp. Bot. 72 (2021) 3340–3351, https://doi.org/10.1093/jxb/erab063.
[140] M. Yagyu, K. Yoshimoto, New insights into plant autophagy: molecular mechanisms and roles in development and stress responses, J. Exp. Bot. (2023) erad459, https://doi.org/10.1093/jxb/erad459.
[141] C. Xu, J. Fan, Links between autophagy and lipid droplet dynamics, J. Exp. Bot. 73 (2022) 2848–2858, https://doi.org/10.1093/jxb/erac003.
[142] K. Liu, M.J. Czaja, Regulation of lipid stores and metabolism by lipophagy, Cell Death Differ. 20 (2013) 3–11, https://doi.org/10.1038/cdd.2012.63.
[143] R. Singh, S. Kaushik, Y. Wang, Y. Xiang, I. Novak, M. Komatsu, K. Tanaka, A.M. Cuervo, M.J. Czaja, Autophagy regulates lipid metabolism, Nature 458 (2009) 1131–1135, https://doi.org/10.1038/nature07976.
[144] H. Yamamoto, T. Matsui, Molecular mechanisms of macroautophagy, microautophagy, and chaperone-mediated autophagy, J. Nippon Med. Sch. 91 (2024) 2–9, https://doi.org/10.1272/jnms.JNMS.2024_91-102.
[145] C. de Duve, R. Wattiaux, Functions of lysosomes, Annu. Rev. Physiol. 28 (1966) 435–492, https://doi.org/10.1146/annurev.ph.28.030166.002251.
[146] S. Feng, Z. Sun, X. Jia, L. Li, Y. Wu, C. Wu, L. Lin, J. Liu, B. Zeng, Lipophagy: molecular mechanisms and implications in hepatic lipid metabolism, FBL 28 (2023) 6, https://doi.org/10.31083/j.fbl2801006.
[147] S. Mahadevan, A. Tappel, Lysosomal lipases of rat liver and kidney, J. Biol. Chem. 243 (1968), 2849-+.
[148] L. Grumet, T.O. Eichmann, U. Taschler, K.A. Zierler, C. Leopold, T. Moustafa,

B. Radovic, M. Romauch, C. Yan, H. Du, G. Haemmerle, R. Zechner, P. Fickert, D. Kratky, R. Zimmermann, A. Lass, Lysosomal acid lipase hydrolyzes retinyl ester and affects retinoid turnover, J. Biol. Chem. 291 (2016) 17977–17987, https://doi.org/10.1074/jbc.M116.724054.
[149] S. Sheriff, H. Du, G. Grabowski, Characterization of lysosomal acid lipase by site-directed mutagenesis and heterologous expression, J. Biol. Chem. 270 (1995) 27766–27772, https://doi.org/10.1074/jbc.270.46.27766.
[150] T. Warner, L. Dambach, J. Shin, J. Obrien, Purification of the lysosomal acid lipase from human-liver and its role in lysosomal lipid hydrolysis, J. Biol. Chem. 256 (1981) 2952–2957.
[151] N. Mizushima, T. Yoshimori, Y. Ohsumi, The role of atg proteins in autophagosome formation, Annu. Rev. Cell Dev. Biol. 27 (2011) 107–132, https://doi.org/10.1146/annurev-cellbio-092910-154005.
[152] N. Hosokawa, T. Hara, T. Kaizuka, C. Kishi, A. Takamura, Y. Miura, S. Iemura, T. Natsume, K. Takehana, N. Yamada, J.-L. Guan, N. Oshiro, N. Mizushima, Nutrient-dependent mTORC1 association with the ULK1–atg13–fip200 complex required for autophagy, MBoC 20 (2009) 1981–1991, https://doi.org/10.1091/mbc.e08-12-1248.
[153] A. Soto-Avellaneda, B.E. Morrison, Signaling and other functions of lipids in autophagy: a review, Lipids Health Dis. 19 (2020) 214, https://doi.org/10.1186/s12944-020-01389-2.
[154] I. Tamargo-Gómez, G. Mariño, AMPK: regulation of metabolic dynamics in the context of autophagy, Int. J. Mol. Sci. 19 (2018), https://doi.org/10.3390/ijms19123812.
[155] H. Zhu, M. Foretz, Z. Xie, M. Zhang, Z. Zhu, J. Xing, J. Leclerc, M. Gaudry, B. Viollet, M.-H. Zou, PRKAA1/AMPKα1 is required for autophagy-dependent mitochondrial clearance during erythrocyte maturation, Autophagy 10 (2014) 1522–1534, https://doi.org/10.4161/auto.29197.
[156] C.H. Jung, C.B. Jun, S.-H. Ro, Y.-M. Kim, N.M. Otto, J. Cao, M. Kundu, D.-H. Kim, ULK-Atg13-FIP200 complexes mediate mTOR signaling to the autophagy machinery, MBoC 20 (2009) 1992–2003, https://doi.org/10.1091/mbc.e08-12-1249.
[157] P.-M. Wong, C. Puente, I.G. Ganley, X. Jiang, The ULK1 complex: sensing nutrient signals for autophagy activation, Autophagy 9 (2013) 124–137, https://doi.org/10.4161/auto.23323.
[158] R. Roberts, N.T. Ktistakis, Omegasomes: PI3P platforms that manufacture autophagosomes, Essays Biochem. 55 (2013) 17–27, https://doi.org/10.1042/bse0550017.
[159] C. He, B. Levine, The Beclin 1 interactome, Curr. Opin. Cell Biol. 22 (2010) 140–149, https://doi.org/10.1016/j.ceb.2010.01.001.
[160] E.L. Axe, S.A. Walker, M. Manifava, P. Chandra, H.L. Roderick, A. Habermann, G. Griffiths, N.T. Ktistakis, Autophagosome formation from membrane compartments enriched in phosphatidylinositol 3-phosphate and dynamically connected to the endoplasmic reticulum, JCB (J. Cell Biol.) 182 (2008) 685–701, https://doi.org/10.1083/jcb.200803137.
[161] H.E.J. Polson, J. de Lartigue, D.J. Rigden, M. Reedijk, S. Urbé, M.J. Clague, S.A. Tooze, Mammalian Atg18 (WIPI2) localizes to omegasome-anchored phagophores and positively regulates LC3 lipidation, Autophagy 6 (2010) 506–522, https://doi.org/10.4161/auto.6.4.11863.
[162] H.C. Dooley, M. Razi, H.E.J. Polson, S.E. Girardin, M.I. Wilson, S.A. Tooze, WIPI2 links LC3 conjugation with PI3P, autophagosome formation, and pathogen clearance by recruiting atg12-5-16l1, Mol. Cell 55 (2014) 238–252, https://doi.org/10.1016/j.molcel.2014.05.021.
[163] M. Sakoh-Nakatogawa, K. Matoba, E. Asai, H. Kirisako, J. Ishii, N.N. Noda, F. Inagaki, H. Nakatogawa, Y. Ohsumi, Atg12–Atg5 conjugate enhances E2 activity of Atg3 by rearranging its catalytic site, Nat. Struct. Mol. Biol. 20 (2013) 433–439, https://doi.org/10.1038/nsmb.2527.
[164] U. Nair, A. Jotwani, J. Geng, N. Gammoh, D. Richerson, W.-L. Yen, J. Griffith, S. Nag, K. Wang, T. Moss, M. Baba, J.A. McNew, X. Jiang, F. Reggiori, T.J. Melia, D.J. Klionsky, SNARE proteins are required for macroautophagy, Cell 146 (2011) 290–302, https://doi.org/10.1016/j.cell.2011.06.022.
[165] L. Wang, J. Zhou, S. Yan, G. Lei, C.-H. Lee, X.-M. Yin, Ethanol-triggered lipophagy requires SQSTM1 in AML12 hepatic cells, Sci. Rep. 7 (2017) 12307, https://doi.org/10.1038/s41598-017-12485-2.
[166] S. Robichaud, G. Fairman, V. Vijithakumar, E. Mak, D.P. Cook, A.R. Pelletier, S. Huard, B.C. Vanderhyden, D. Figeys, M. Lavallée-Adam, K. Baetz, M. Ouimet, Identification of novel lipid droplet factors that regulate lipophagy and cholesterol efflux in macrophage foam cells, Autophagy 17 (2021) 3671–3689, https://doi.org/10.1080/15548627.2021.1886839.
[167] D. Lohmann, J. Spandl, A. Stevanovic, M. Schoene, J. Philippou-Massier, C. Thiele, Monoubiquitination of ancient ubiquitous protein 1 promotes lipid droplet clustering, PLoS One 8 (2013) e72453, https://doi.org/10.1371/journal.pone.0072453.
[168] J. Spandl, D. Lohmann, L. Kuerschner, C. Moessinger, C. Thiele, Ancient ubiquitous protein 1 (AUP1) localizes to lipid droplets and binds the E2 ubiquitin conjugase G2 (Ube2g2) via its G2 binding region, J. Biol. Chem. 286 (2011) 5599–5606, https://doi.org/10.1074/jbc.M110.190785.
[169] J. Zhang, Y. Lan, M.Y. Li, M.M. Lamers, M. Fusade-Boyer, E. Klemm, C. Thiele, J. Ashour, S. Sanyal, Flaviviruses exploit the lipid droplet protein AUP1 to trigger lipophagy and drive virus production, Cell Host Microbe 23 (2018) 819–831, https://doi.org/10.1016/j.chom.2018.05.005, e5.
[170] Y. Wu, Z. Wu, Q. Jin, J. Liu, P. Xu, Identification and analysis of biomarkers associated with lipophagy and therapeutic agents for COVID-19, Viruses 16 (2024) 923, https://doi.org/10.3390/v16060923.
[171] V. Guyard, V.F. Monteiro-Cardoso, M. Omrane, C. Sauvanet, A. Houcine, C. Boulogne, K. Ben Mbarek, N. Vitale, O. Faklaris, N. El Khallouki, A.R. Thiam, F. Giordano, ORP5 and ORP8 orchestrate lipid droplet biogenesis and maintenance at ER–mitochondria contact sites, JCB (J. Cell Biol.) 221 (2022) e202112107, https://doi.org/10.1083/jcb.202112107.
[172] M. Pu, W. Zheng, H. Zhang, W. Wan, C. Peng, X. Chen, X. Liu, Z. Xu, T. Zhou, Q. Sun, D. Neculai, W. Liu, ORP8 acts as a lipophagy receptor to mediate lipid droplet turnover, Protein Cell 14 (2023) 653–667, https://doi.org/10.1093/procel/pwac063.
[173] F. Jia, X. Wang, Y. Fu, S.-M. Zhao, B. Lu, C. Wang, DDHD2, whose mutations cause spastic paraplegia type 54, enhances lipophagy via engaging ATG8 family proteins, Cell Death Differ. 31 (2024) 348–359, https://doi.org/10.1038/s41418-024-01261-1.
[174] J. Chung, J. Park, Z.W. Lai, T.J. Lambert, R.C. Richards, J. Zhang, T.C. Walther, R.V. Farese, The Troyer syndrome protein spartin mediates selective autophagy of lipid droplets, Nat. Cell Biol. 25 (2023) 1101–1110, https://doi.org/10.1038/s41556-023-01178-w.
[175] T.-H. Tsai, E. Chen, L. Li, P. Saha, H.-J. Lee, L.-S. Huang, G.S. Shelness, L. Chan, B.H.-J. Chang, The constitutive lipid droplet protein PLIN2 regulates autophagy in liver, Autophagy 13 (2017) 1130–1144, https://doi.org/10.1080/15548627.2017.1319544.
[176] C. Sztalryd, D.L. Brasaemle, The perilipin family of lipid droplet proteins: gatekeepers of intracellular lipolysis, Biochim. Biophys. Acta 1862 (2017) 1221–1232, https://doi.org/10.1016/j.bbalip.2017.07.009.
[177] C. Hooper, S.S. Puttamadappa, Z. Loring, A. Shekhtman, J.C. Bakowska, Spartin activates atrophin-1-interacting protein 4 (AIP4) E3 ubiquitin ligase and promotes ubiquitination of adipophilin on lipid droplets, BMC Biol. 8 (2010) 72, https://doi.org/10.1186/1741-7007-8-72.
[178] A. Lizaso, K.-T. Tan, Y.-H. Lee, β-adrenergic receptor-stimulated lipolysis requires the RAB7-mediated autolysosomal lipid degradation, Autophagy 9 (2013) 1228–1243, https://doi.org/10.4161/auto.24893.
[179] B. Schroeder, R.J. Schulze, S.G. Weller, A.C. Sletten, C.A. Casey, M.A. McNiven, The small GTPase Rab7 as a central regulator of hepatocellular lipophagy, Hepatology 61 (2015) 1896–1907, https://doi.org/10.1002/hep.27667.
[180] R.J. Schulze, E.W. Krueger, S.G. Weller, K.M. Johnson, C.A. Casey, M.B. Schott, M.A. McNiven, Direct lysosome-based autophagy of lipid droplets in hepatocytes, Proc. Natl. Acad. Sci. U. S. A. 117 (2020) 32443–32452, https://doi.org/10.1073/pnas.2011442117.
[181] N. Kang, J. Tan, S. Yan, L. Lin, Q. Gao, General autophagy-dependent and -independent lipophagic processes collaborate to regulate the overall level of lipophagy in yeast, Autophagy (2024), https://doi.org/10.1080/15548627.2024.2325297.
[182] A.Y. Seo, P.-W. Lau, D. Feliciano, P. Sengupta, M.A.L. Gros, B. Cinquin, C.A. Larabell, J. Lippincott-Schwartz, AMPK and vacuole-associated Atg14p orchestrate μ-lipophagy for energy production and long-term survival under glucose starvation, Elife 6 (2017) e21690, https://doi.org/10.7554/eLife.21690.
[183] T. Tsuji, M. Fujimoto, T. Tatematsu, J. Cheng, M. Orii, S. Takatori, T. Fujimoto, Niemann-Pick type C proteins promote microautophagy by expanding raft-like membrane domains in the yeast vacuole, Elife 6 (2017) e25960, https://doi.org/10.7554/eLife.25960.
[184] T. van Zutphen, V. Todde, R. de Boer, M. Kreim, H.F. Hofbauer, H. Wolinski, M. Veenhuis, I.J. van der Klei, S.D. Kohlwein, Lipid droplet autophagy in the yeast *Saccharomyces cerevisiae*, MBoC 25 (2014) 290–301, https://doi.org/10.1091/mbc.e13-08-0448.
[185] C.-W. Wang, Y.-H. Miao, Y.-S. Chang, A sterol-enriched vacuolar microdomain mediates stationary phase lipophagy in budding yeast, J. Cell Biol. 206 (2014) 357–366, https://doi.org/10.1083/jcb.201404115.
[186] E.J. Garcia, P.-C. Liao, G. Tan, J.D. Vevea, C.N. Sing, C.A. Tsang, J.M. McCaffery, I.R. Boldogh, L.A. Pon, Membrane dynamics and protein targets of lipid droplet microautophagy during ER stress-induced proteostasis in the budding yeast, Saccharomyces cerevisiae, Autophagy 17 (2021) 2363–2383, https://doi.org/10.1080/15548627.2020.1826691.
[187] P.-C. Liao, E.J. Garcia, G. Tan, C.A. Tsang, L.A. Pon, Roles for L o microdomains and ESCRT in ER stress-induced lipid droplet microautophagy in budding yeast, Mol. Biol. Cell 32 (2021) br12, https://doi.org/10.1091/mbc.E21-04-0179.
[188] J.D. Vevea, E.J. Garcia, R.B. Chan, B. Zhou, M. Schultz, G. Di Paolo, J.M. McCaffery, L.A. Pon, Role for lipid droplet biogenesis and microlipophagy in adaptation to lipid imbalance in yeast, Dev. Cell 35 (2015) 584–599, https://doi.org/10.1016/j.devcel.2015.11.010.
[189] M. Oku, Y. Maeda, Y. Kagohashi, T. Kondo, M. Yamada, T. Fujimoto, Y. Sakai, Evidence for ESCRT- and clathrin-dependent microautophagy, J. Cell Biol. 216 (2017) 3263–3274, https://doi.org/10.1083/jcb.201611029.
[190] G. Fairman, M. Ouimet, Lipophagy pathways in yeast are controlled by their distinct modes of induction, Yeast 39 (2022) 429–439, https://doi.org/10.1002/yea.3705.
[191] P.-C. Liao, L.A. Pon, Lipid droplets in stress protection: distinct mechanisms of lipid droplet microautophagy, Autophagy Rep 1 (2022) 197–200, https://doi.org/10.1080/27694127.2022.2067643.
[192] A. Murley, R.D. Sarsam, A. Toulmay, J. Yamada, W.A. Prinz, J. Nunnari, Ltc1 is an ER-localized sterol transporter and a component of ER–mitochondria and ER–vacuole contacts, JCB (J. Cell Biol.) 209 (2015) 539–548, https://doi.org/10.1083/jcb.201502033.
[193] A. Toulmay, W.A. Prinz, Direct imaging reveals stable, micrometer-scale lipid domains that segregate proteins in live cells, J. Cell Biol. 202 (2013) 35–44,

https://doi.org/10.1083/jcb.201301039.
[194] H. Kim, I. Budin, Intracellular sphingolipid sorting drives membrane phase separation in the yeast vacuole, J. Biol. Chem. 300 (2024) 105496, https://doi.org/10.1016/j.jbc.2023.105496.
[195] D. Lingwood, K. Simons, Lipid rafts as a membrane-organizing principle, Science 327 (2010) 46–50, https://doi.org/10.1126/science.1174621.
[196] Y. Kurokawa, R. Konishi, A. Yoshida, K. Tomioku, K. Tanabe, A. Fujita, Microautophagy in the yeast vacuole depends on the activities of phosphatidylinositol 4-kinases, Stt4p and Pik1p, Biochim. Biophys. Acta Biomembr. 1862 (2020) 183416, https://doi.org/10.1016/j.bbamem.2020.183416.
[197] T. Tsuji, T. Fujimoto, Lipids and lipid domains of the yeast vacuole, Biochem. Soc. Trans. 46 (2018) 1047–1054, https://doi.org/10.1042/BST20180120.
[198] M.B.L. Winkler, R.T. Kidmose, M. Szomek, K. Thaysen, S. Rawson, S.P. Muench, D. Wüstner, B.P. Pedersen, Structural insight into eukaryotic sterol transport through niemann-pick type C proteins, Cell 179 (2019) 485–497.e18, https://doi.org/10.1016/j.cell.2019.08.038.
[199] I. Álvarez-Guerra, E. Block, F. Broeskamp, S. Gabrijelčič, T. Infant, A. de Ory, L. Habernig, C. Andréasson, T.P. Levine, J.L. Höög, S. Büttner, LDO proteins and Vac8 form a vacuole-lipid droplet contact site to enable starvation-induced lipophagy in yeast, Dev. Cell 59 (2024) 759–775.e5, https://doi.org/10.1016/j.devcel.2024.01.014.
[200] D.T.V. Diep, J. Collado, M. Hugenroth, R.M. Fausten, L. Percifull, M. Wälte, C. Schuberth, O. Schmidt, R. Fernández-Busnadiego, M. Bohnert, A metabolically controlled contact site between vacuoles and lipid droplets in yeast, Dev. Cell 59 (2024) 740–758, https://doi.org/10.1016/j.devcel.2024.01.016, e10.
[201] V. Teixeira, L. Johnsen, F. Martínez-Montañés, A. Grippa, L. Buxó, F.-Z. Idrissi, C.S. Ejsing, P. Carvalho, Regulation of lipid droplets by metabolically controlled Ldo isoforms, JCB (J. Cell Biol.) 217 (2018) 127–138, https://doi.org/10.1083/jcb.201704115.
[202] Y. Maeda, M. Oku, Y. Sakai, A defect of the vacuolar putative lipase Atg15 accelerates degradation of lipid droplets through lipolysis, Autophagy 11 (2015) 1247–1258, https://doi.org/10.1080/15548627.2015.1056969.
[203] J. Fan, L. Yu, C. Xu, Dual role for autophagy in lipid metabolism in Arabidopsis, Plant Cell 31 (2019) 1598–1613, https://doi.org/10.1105/tpc.19.00170.
[204] J.A.S. Barros, S. Magen, T. Lapidot-Cohen, L. Rosental, Y. Brotman, W.L. Araújo, T. Avin-Wittenberg, Autophagy is required for lipid homeostasis during dark-induced senescence, Plant Physiology 185 (2021) 1542–1558, https://doi.org/10.1093/plphys/kiaa120.
[205] T. Avin-Wittenberg, K. Bajdzienko, G. Wittenberg, S. Alseekh, T. Tohge, R. Bock, P. Giavalisco, A.R. Fernie, Global analysis of the role of autophagy in cellular metabolism and energy homeostasis in Arabidopsis seedlings under carbon starvation, Plant Cell 27 (2015) 306–322, https://doi.org/10.1105/tpc.114.134205.
[206] M. Miklaszewska, K. Zienkiewicz, E. Klugier-Borowska, M. Rygielski, I. Feussner, A. Zienkiewicz, CALEOSIN 1 interaction with AUTOPHAGY-RELATED PROTEIN 8 facilitates lipid droplet microautophagy in seedlings, Plant Physiol 193 (2023) 2361–2380, https://doi.org/10.1093/plphys/kiad471.
[207] M.B.E. Schaaf, T.G. Keulers, M.A. Vooijs, K.M.A. Rouschop, LC3/GABARAP family proteins: autophagy-(un)related functions, FASEB J 30 (2016) 3961–3978, https://doi.org/10.1096/fj.201600698R.
[208] I. Couso, M.E. Perez-Perez, E. Martinez-Force, H.S. Kim, Y. He, J.G. Umen, J.L. Crespo, Autophagic flux is required for the synthesis of triacylglycerols and ribosomal protein turnover in Chlamydomonas, J. Exp. Bot. 69 (2018) 1355–1367, https://doi.org/10.1093/jxb/erx372.
[209] M. Kajikawa, M. Yamauchi, H. Shinkawa, M. Tanaka, K. Hatano, Y. Nishimura, M. Kato, H. Fukuzawa, Isolation and characterization of *Chlamydomonas* autophagy-related mutants in nutrient-deficient conditions, Plant Cell Physiol. 60 (2019) 126–138, https://doi.org/10.1093/pcp/pcy193.
[210] B. Leyland, E. Novichkova, A.K. Dolui, D. Jallet, F. Daboussi, B. Légeret, Z. Li, Y. Li-Beisson, S. Boussiba, I. Khozin-Goldberg, Acyl-CoA binding protein is required for lipid droplet degradation in the diatom Phaeodactylum tricornutum, Plant Physiology | Oxford Academic 194 (2024) 958–981.
[211] M. Poxleitner, S.W. Rogers, A. Lacey Samuels, J. Browse, J.C. Rogers, A role for caleosin in degradation of oil-body storage lipid during seed germination, Plant J. 47 (2006) 917–933, https://doi.org/10.1111/j.1365-313X.2006.02845.x.
[212] T. Kurusu, T. Koyano, S. Hanamata, T. Kubo, Y. Noguchi, C. Yagi, N. Nagata, T. Yamamoto, T. Ohnishi, Y. Okazaki, N. Kitahata, D. Ando, M. Ishikawa, S. Wada, A. Miyao, H. Hirochika, H. Shimada, A. Makino, K. Saito, H. Ishida, T. Kinoshita, N. Kurata, K. Kuchitsu, OsATG7 is required for autophagy-dependent lipid metabolism in rice postmeiotic anther development, Autophagy 10 (2014) 878–888, https://doi.org/10.4161/auto.28279.
[213] F. McLoughlin, R.S. Marshall, X. Ding, E.C. Chatt, L.D. Kirkpatrick, R.C. Augustine, F. Li, M.S. Otegui, R.D. Vierstra, Autophagy plays prominent roles in amino acid, nucleotide, and carbohydrate metabolism during fixed-carbon starvation in maize, Plant Cell 32 (2020) 2699–2724, https://doi.org/10.1105/tpc.20.00226.
[214] D. Zhao, T. Li, Z. Li, J. Sun, J. Tao, Characteristics of Paeonia ostii seed oil body and OLE17.5 determining oil body morphology, Food Chem. 319 (2020) 126548, https://doi.org/10.1016/j.foodchem.2020.126548.
[215] L. Zhao, J. Dai, Q. Wu, Autophagy-like processes are involved in lipid droplet degradation in Auxenochlorella protothecoides during the heterotrophy-autotrophy transition, Front. Plant Sci. 5 (2014), https://doi.org/10.3389/fpls.2014.00400.
[216] Z. You, Q. Zhang, Z. Peng, X. Miao, Lipid droplets mediate salt stress tolerance in *Parachlorella kessleri* 1, Plant Physiology 181 (2019) 510–526, https://doi.org/10.1104/pp.19.00666.
[217] C.-H. Tsai, S. Uygun, R. Roston, S.-H. Shiu, C. Benning, Recovery from N Deprivation is a transcriptionally and functionally distinct state in *Chlamydomonas*, Plant Physiol 176 (2018) 2007–2023, https://doi.org/10.1104/pp.17.01546.
[218] Q.-G. Tran, H.R. Yoon, K. Cho, S.-J. Lee, J.L. Crespo, R. Ramanan, H.-S. Kim, Dynamic interactions between autophagosomes and lipid droplets in Chlamydomonas reinhardtii, Cells 8 (2019) 992, https://doi.org/10.3390/cells8090992.
[219] M. Kajikawa, H. Fukuzawa, Algal autophagy is necessary for the regulation of carbon metabolism under nutrient deficiency, Front. Plant Sci. 11 (2020) 36, https://doi.org/10.3389/fpls.2020.00036.
[220] V. Schwarz, A. Andosch, A. Geretschläger, M. Affenzeller, U. Lütz-Meindl, Carbon starvation induces lipid degradation via autophagy in the model alga Micrasterias, J. Plant Physiol. 208 (2017) 115–127, https://doi.org/10.1016/j.jplph.2016.11.008.
[221] A. Zienkiewicz, K. Zienkiewicz, E. Poliner, J.A. Pulman, Z.-Y. Du, G. Stefano, C.-H. Tsai, P. Horn, I. Feussner, E.M. Farre, K.L. Childs, F. Brandizzi, C. Benning, The microalga *Nannochloropsis* during transition from quiescence to autotrophy in response to nitrogen availability, Plant Physiol 182 (2020) 819–839, https://doi.org/10.1104/pp.19.00854.
[222] T. Tanaka, S. Moriya, T. Nonoyama, Y. Maeda, M. Kaha, T. Yoshino, M. Matsumoto, C. Bowler, Lipid droplets-vacuoles interaction promotes lipophagy in the oleaginous diatom Fistulifera solaris, Algal Res. 79 (2024) 103481, https://doi.org/10.1016/j.algal.2024.103481.
[223] A. Zadoorian, X. Du, H. Yang, Lipid droplet biogenesis and functions in health and disease, Nat. Rev. Endocrinol. (2023) 1–17, https://doi.org/10.1038/s41574-023-00845-0.
[224] M. Pyc, S.K. Gidda, D. Seay, N. Esnay, F.K. Kretzschmar, Y. Cai, N.M. Doner, M.S. Greer, J.J. Hull, D. Coulon, C. Bréhélin, O. Yurchenko, J. de Vries, O. Valerius, G.H. Braus, T. Ischebeck, K.D. Chapman, J.M. Dyer, R.T. Mullen, LDIP cooperates with SEIPIN and LDAP to facilitate lipid droplet biogenesis in Arabidopsis, Plant Cell (2021) koab179, https://doi.org/10.1093/plcell/koab179.
[225] V. Murison, J. Hérault, M. Côme, S. Guinio, A. Lebon, C. Chamot, M. Bénard, L. Galas, B. Schoefs, J. Marchand, M. Bardor, L. Ulmann, Comparison of two Phaeodactylum tricornutum ecotypes under nitrogen starvation and resupply reveals distinct lipid accumulation strategies but a common degradation process, Front. Plant Sci. 14 (2023), https://doi.org/10.3389/fpls.2023.1257500.
[226] N. Martinez-Lopez, M. Garcia-Macia, S. Sahu, D. Athonvarangkul, E. Liebling, P. Merlo, F. Cecconi, G.J. Schwartz, R. Singh, Autophagy in the CNS and periphery coordinate lipophagy and lipolysis in the brown adipose tissue and liver, Cell Metab 23 (2016) 113–127, https://doi.org/10.1016/j.cmet.2015.10.008.
[227] A. Sathyanarayan, M.T. Mashek, D.G. Mashek, ATGL promotes autophagy/lipophagy via SIRT1 to control hepatic lipid droplet catabolism, Cell Rep. 19 (2017) 1–9, https://doi.org/10.1016/j.celrep.2017.03.026.
[228] D.W. Shin, Lipophagy: molecular mechanisms and implications in metabolic disorders, Mol Cells 43 (2020) 686–693, https://doi.org/10.14348/molcells.2020.0046.

Chapter 2

Designing artificial condensates to entrap lipid droplets

Objectives

This chapter details the design and validation of **ControLD**, an engineered liquid-liquid phase-separating scaffold targeted to lipid droplets and able to build a tunable, reversible protein meshwork at the LD surface. We establish design rules, deploy in mammalian cells, and demonstrate formation reversibility, then quantify condensate dynamics and biophysical properties. We then use ControLD to probe LD physiology by measuring effects on lipid metabolism and inter-organelle communication.

Contents

1 Liquid-liquid phase separation in synthetic biology **56**
1.1 Physical Principles governing Liquid-Liquid Phase Separation (LLPS) 56
1.2 Quick overview of endogenous biological LLPS 59
2 Mimicking biological LLPS through protein engineering **61**
3 Using synthetic condensates to control lipid droplet dynamics **69**
4 Main findings **70**
5 Main article: Controlling lipid droplet dynamics via tether condensates **73**
6 Conclusion and transition **92**

1 Liquid-liquid phase separation in synthetic biology

Over the past decade, **liquid-liquid phase separation (LLPS)** has emerged as a unifying principle to explain the formation of membraneless compartments (or biomolecular condensates) in cell. During a LLPS, molecules demix into a concentrated *dense phase* (a droplet) coexisting with a *dilute phase*, without any membrane enclosing the dense phase. Modern studies have revitalized interest by connecting intracellular droplets to classical phase transition physics. A landmark example was the discovery that **P granules** in *C. elegans* germ cells behave like liquid droplets: they fuse, drip, wet surfaces, and can reversibly dissolve or condense in response to cellular conditions. Brangwynne *et al.* showed that P granules exhibit such *liquid-like behaviors*[106] in 2009, indicating a *classic phase transition* underlies their assembly. This finding provided direct evidence that cells can organize some components via LLPS, inspiring research into the physical parameters that govern condensate formation and properties.

1.1 Physical Principles governing Liquid-Liquid Phase Separation (LLPS)

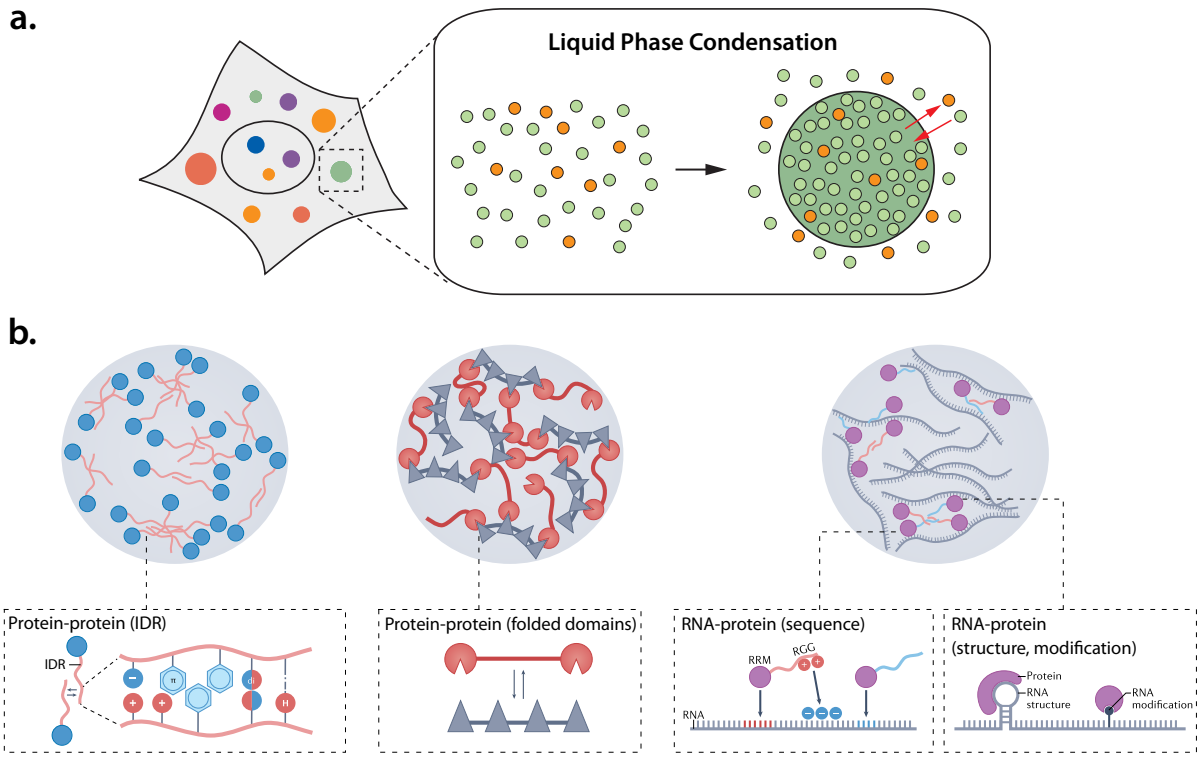

Figure 2.1: General principles of liquid-liquid phase separation. **a.** LLPS scaffolds are in equilibrium between a condensed phase and a diffuse phase. Adapted from [Shin et al. 2017]. **b.** Intermolecular scaffold interactions are either driven by IDP or folded protein domains, and involve either protein-protein or protein-RNA interactions. IDP, intrinsically disordered domains. Adapted from [Hirose et al. 2023]

.

LLPS is a physico-chemical phenomenon influenced by multiple physical and biochemical factors. The following key parameters are crucial for understanding how and why LLPS occurs in biological systems:

Affinity and valency: Two key molecular factors determine whether and how phase separation occurs: the strength of intermolecular interactions (the *affinity*) and the number of interaction sites per molecule (the *valency*). Theoretical and experimental studies show that the *critical point* (or threshold conditions) for phase separation depends strongly on these properties[109]. In essence, a molecule must have sufficient binding opportunities and binding strength to overcome mixing entropy leading to uniform solubilization. *Valency* refers to how many distinct connections a molecule can form – for example, a protein with multiple domains or motifs that can each bind a partner is multivalent. A sufficiently high valency is needed for LLPS because it enables the formation of an extended interaction network or "polymer" of molecules. Indeed, the minimum concentration needed for phase separation is inversely related to valency: increasing the number of binding sites per molecule allows droplets to form at lower concentration[110].*Affinity*, the strength of each interaction (often quantified by a binding energy or dissociation constant), also crucially influences LLPS. Stronger attractive interactions make phase separation more thermodynamically favorable by lowering the energy cost of clustering molecules. In practice, higher affinities drive more robust phase separation, and the extent of phase-separated clustering increases with interaction affinity. However, there is a delicate balance: if interactions are too strong or irreversible, the system can turn into an aggregate or gel rather than a fluid droplet. Biological phase separation generally operates in a regime of *weak-to-moderate affinity* interactions, so that molecules can bind and unbind on short timescales.

Avidity and cooperative binding: The combination of high valency and intermediate affinity leads to *avidity*, which is the cooperative enhancement of overall binding strength through multiple simultaneous interactions. Once a few interactions form between two molecules, those molecules are held in proximity, raising the *local concentration* of additional binding sites and making further interactions more likely[111]. This *cooperative binding* means the propensity to phase-separate can rise nonlinearly with concentration: below a certain point, molecules mostly remain unbound, but beyond that point, binding creates more binding, rapidly condensing molecules into a droplet. Cooperativity (*avidity*) thus underlies the switch-like assembly of condensates when reaching certain conditions.

Critical concentration (or saturation concentration): An essential hallmark of LLPS is the existence of a *critical concentration threshold* for phase separation. Below this, the system remains mixed; above it, thermodynamics favor separation into two phases, as shown in figure 2.1a. At equilibrium, the dilute phase concentration is fixed at the saturation value, with the remainder partitioned into the dense phase. The solubility of a protein or RNA (its phase separation threshold) depends on temperature, salt, pH,

and the molecular parameters presented above. As stated before, higher valency and intermocular affinity lower the critical concentration. Many systems exhibit a sharp onset: condensates appear only when core scaffolding components exceed a threshold and dissolve when dilution brings the concentration below it.

Molecular interactions driving LLPS range from lock-and-key contacts between folded protein domains, to interactions between enangled disordereds regions. Folded interactions, such as domain-motif pairings or short linear motifs (SLiMs), confer selectivity and regulation, allowing condensates to recruit defined partners and respond to modifications like phosphorylation[112, 113]. Interactions from IDR are often described as resulting in bulkier structures: these multivalent contacts can alone drive phase separation, as shown for proteins with anisotropic surface charge distributions[114]. Most biological condensates exploit a **combination**: disordered interactions concentrate molecules locally, while specific interactions stabilize selected partners. This synergy provides both robustness and compositional control, ensuring condensates remain dynamic yet functionally precise[115]. These different intermolecular interactions are illustrated in figure 2.1b.

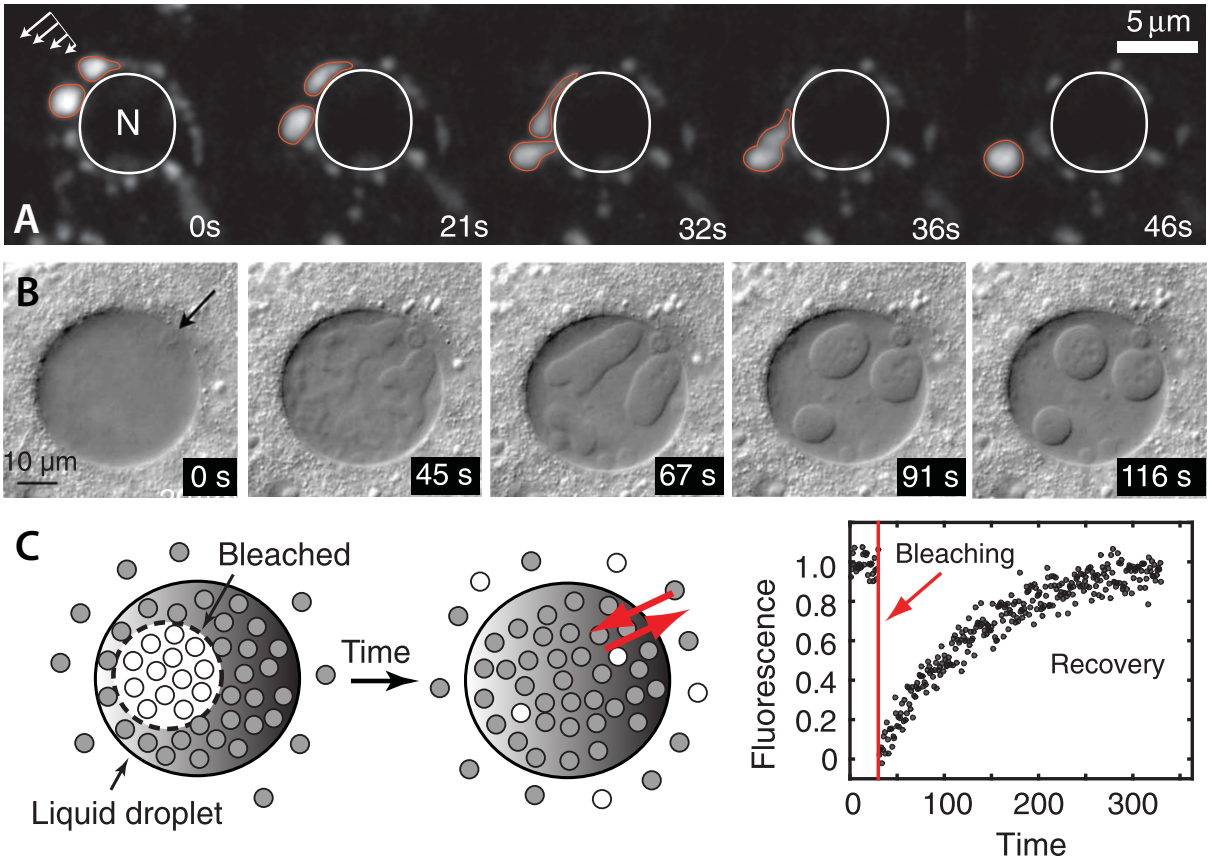

Figure 2.2: Examples of dynamic properties of LLPS condensates illustrated in **P granules**. (A) P Granules flow, coalesce, and drip off the surface of a nucleus in response to shear. (B) Liquid-like nuclear bodies induced to nucleate and grow in the nucleus of a Drosophila oocyte. (C) Molecules within a liquid phase exhibit dynamic reorganization, which can be probed with FRAP. Adapted from [Shin et al. 2017]

.

Dynamic properties displayed by liquid-like condensates are a major hallmark of LLPS. Condensates are not static structures; unlike irreversible aggregates, LLPS condensates maintain rapid molecular exchange between the dense and dilute phases, with constituents diffusing in and out on timescales of seconds to minutes. Such dynamics can be quantified using fluorescence recovery after photobleaching (FRAP) experiments, which consistently show partial and fast recovery of fluorescence within droplets[116]. This mobility reflects the weak and reversible nature of the underlying interactions, allowing condensates to remain liquid-like and adaptive. Internal rearrangements enable droplets to fuse, relax into spherical shapes, and respond rapidly to cellular signals by dissolving or reassembling. Moreover, modulation of post-translational modifications or environmental conditions (such as salt or temperature) can tune exchange rates and material properties, shifting condensates along a spectrum from liquid-like to gel-like states[117]. These dynamic properties are essential for their biological functions, ensuring that condensates are neither static depots nor rigid aggregates but responsive, transient hubs of biochemical activity.

1.2 Quick overview of endogenous biological LLPS

Since the discovery of Brangwynne in 2009, a variety of biomolecular condensates (also called membraneless organelles or MLOs) that form via LLPS were found in eukaryotic cells. These structures lack a lipid boundary yet remain distinct compartments, assembling and disassembling in response to cellular conditions. Below we present a brief overview of some of the most well-characterized endogenous condensates, highlighting their and biological functions. For a more comprehensive overview, we refer the reader to the recent review by Hirose et al.[108].

Among the best-characterized membraneless organelles, the **nucleolus** stands out as the earliest known and most prominent. Forming around clusters of ribosomal DNA, it acts as a self-organizing factory for ribosome production, concentrating rRNA transcripts, ribosomal proteins, and processing factors into distinct but fluid subcompartments. Its liquid-like nature, established through phase separation, allows rapid exchange with the surrounding nucleoplasm. Beyond its central role in ribosome biogenesis, the nucleolus also functions as a stress sensor, sequestering regulatory proteins and thus linking growth and metabolism to cellular stress states.

In the cytoplasm, **stress granules** emerge under adverse conditions such as oxidative stress or nutrient deprivation. Composed of untranslated mRNAs, RNA-binding proteins like G3BP1, and translation initiation factors, these condensates temporarily halt protein synthesis by storing and protecting mRNAs. Their dynamic assembly and dissolution enable the cell to redirect resources towards stress survival while preventing degradation of key transcripts. Stress granules also influence signaling pathways by clustering or sequestering regulatory proteins, thereby integrating proteostasis and stress response

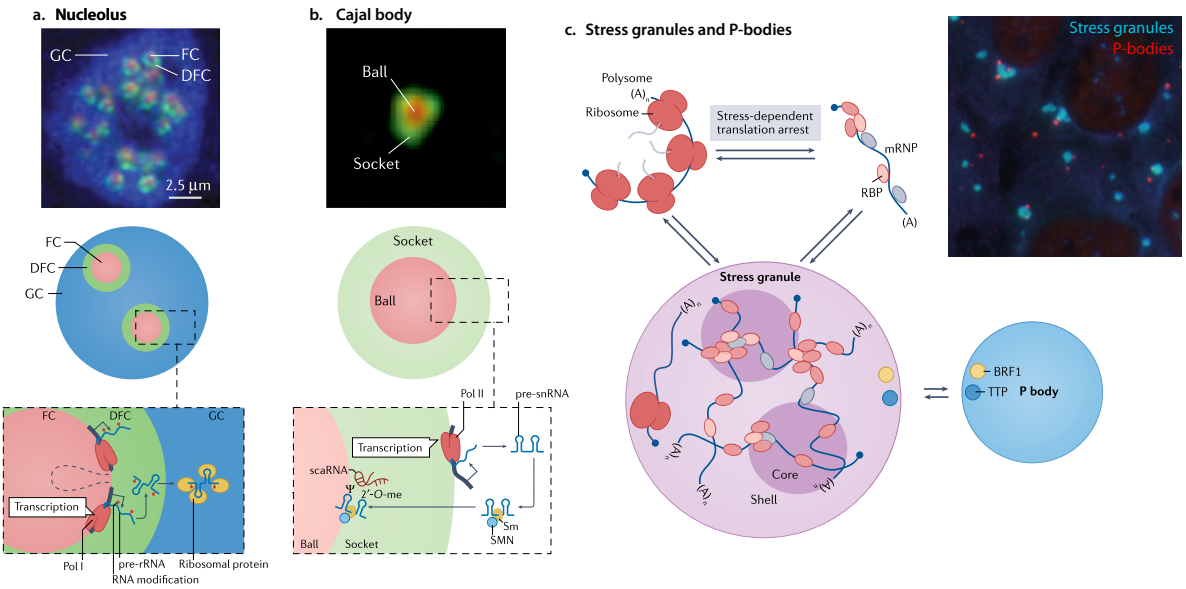

Figure 2.3: Microscopy images of four representative biomolecular condensates, schematics of their internal structure and physiological functions. **a.** The nucleolus is organized into three domains: the fibrillar center (FC), the dense fibrillar component (DFC) and the granular component (GC). At the border between the FC and the DFC, rDNA is transcribed by RNA polymerase I (Pol I), and in the DFC the transcribed pre-rRNAs are processed and modified. **b.** Cajal body with a ball-and-socket-like structure. The transcribed snRNAs are exported to the cytoplasm, where together with an Sm-ring (Sm) protein they form core small nuclear RNPs (snRNPs) and are then imported back to the nucleus and into the Cajal bodies. **c.** Stress granule formation in the cytoplasm is induced by global translation arrest in stress conditions, resulting in the accumulation of mRNPs comprising RBPs associated with ribosome-unbound mRNAs, which subsequently condense to form stress granules. Two dense cores are shown (dark purple circles). Stress granules communicate with the processing body (P body) by exchanging their respective components. Recently, translation was shown to routinely occur in stress granules. Pol II, RNA polymerase II. Adapted from [Hirose et al. 2023]

.

mechanisms.

Closely related in function but distinct in composition are **processing bodies** (P-bodies). Present even in unstressed cells, P-bodies concentrate enzymes involved in mRNA decapping and decay, along with silencing factors from the microRNA pathway. They serve as hubs for mRNA turnover and storage, offering cells a flexible way to modulate gene expression post-transcriptionally. Like stress granules, P-bodies exchange components rapidly with the cytoplasm, ensuring that transcripts can be degraded or returned to translation depending on physiological needs.

Within the nucleus, **Cajal bodies** highlight the role of phase separation in RNA maturation. These condensates gather newly transcribed snRNAs, coilin, and associated factors, facilitating the modification and assembly of spliceosomal RNPs. By acting as organizational centers, Cajal bodies accelerate the maturation of RNA-protein complexes

essential for splicing and other nuclear processes. Their dynamic liquid-like state ensures that RNA processing adapts swiftly to transcriptional demands.

Beyond these examples, cells harbor additional phase-separated condensates that illustrate the diversity of the phenomenon. **Paraspeckles**, built around the long noncoding RNA NEAT1, regulate gene expression by retaining specific mRNAs in the nucleus. **PML nuclear bodies** contribute to DNA damage responses, antiviral defense, and senescence. Other condensates, such as **germ granules** in reproductive cells, nuclear stress bodies induced by heat shock, or **amyloid-like stress assemblies**, further demonstrate how cells exploit phase separation to compartmentalize biochemical functions without membranes.

These organelles exemplify how liquid-liquid phase separation complements membrane-bound compartments by providing flexible, reversible, and rapidly tunable microenvironments. By concentrating nucleic acids, enzymes, and regulatory proteins, they enable cells to control gene expression, protein quality, and stress responses with remarkable spatial and temporal precision.

2 Mimicking biological LLPS through protein engineering

The concept of compartmentalization through phase separation is an idea older than the emergence of molecular biology as a discipline. In the early 20th century, Alexander I. Oparin proposed a revolutionary view of life's origin that continues to resonate in modern cell biology. In his 1924 publication The Origin of Life[118], Oparin described coacervate droplets—phase-separated colloidal mixtures of polymers as potential precursors to living cells. These droplets could form spontaneously from organic molecules in the prebiotic environment, selectively concentrating reactants and enabling chemical reactions that might lead to the emergence of life. Although lacking a molecular understanding of the forces driving droplet formation, Oparin's idea anticipated the concept of biomolecular condensates, now recognized as a widespread organizing principle in modern cells.

The latter half of the 20th century brought more controlled and reproducible examples of engineered phase separation. A notable advance came in the 1990s with **elastin-like polypeptides** (ELPs), designed and studied by Meyer, Chilkoti, et al.[119]. ELPs are synthetic polypeptide repeats based on motifs from human tropoelastin that undergo a reversible phase transition at a characteristic temperature, aggregating into coacervates when the temperature exceeds this threshold. While primarily intended for applications such as protein purification and drug delivery, ELPs represented an early instance of deliberately engineered LLPS *in vitro*, showing that protein sequence design could control phase behavior. Although these systems did not initially aim to mimic biological condensates or function in living cells, they can be considered a first effort to engineer LLPS as

a cellular control mechanism.

A true paradigm shift arrived when Li et al., developed the first intentional engineering of protein-based condensates in living cells using defined molecular interaction rules[110]. This work focused on the **SH3-PRM** system: the SRC homology 3 (SH3) domain binds specifically to its associated proline-rich motifs (PRMs) with weak non-covalent interactions. By genetically fusing multiple copies of these domains or motifs in tandem, the authors created multivalent interaction scaffolds. The increase in valency from a single binding site to arrays of five or more strongly enhanced the likelihood of forming an extended interaction meshwork. At a critical concentration, these networks undergo a liquid-like phase separation, yielding micron-scale liquid droplets both *in vitro* and *in vivo*, as depicted in figure 2.4. Technically, the authors combined biophysical measurements of phase diagrams with live-cell imaging and fluorescence recovery after photobleaching (FRAP) to confirm liquid-like dynamics. In cells, co-expression of SH3-array and PRM-array proteins led to dynamic puncta that fused, flowed, and exchanged components rapidly. Importantly, Li et al. also demonstrated that clustering an actin nucleation-promoting factor (N-WASP) via SH3-PRM droplets amplified actin polymerization, thereby linking condensate formation to functional biochemical output. This was a decisive moment: LLPS could now be programmed into the cellular environment to control biochemical processes.

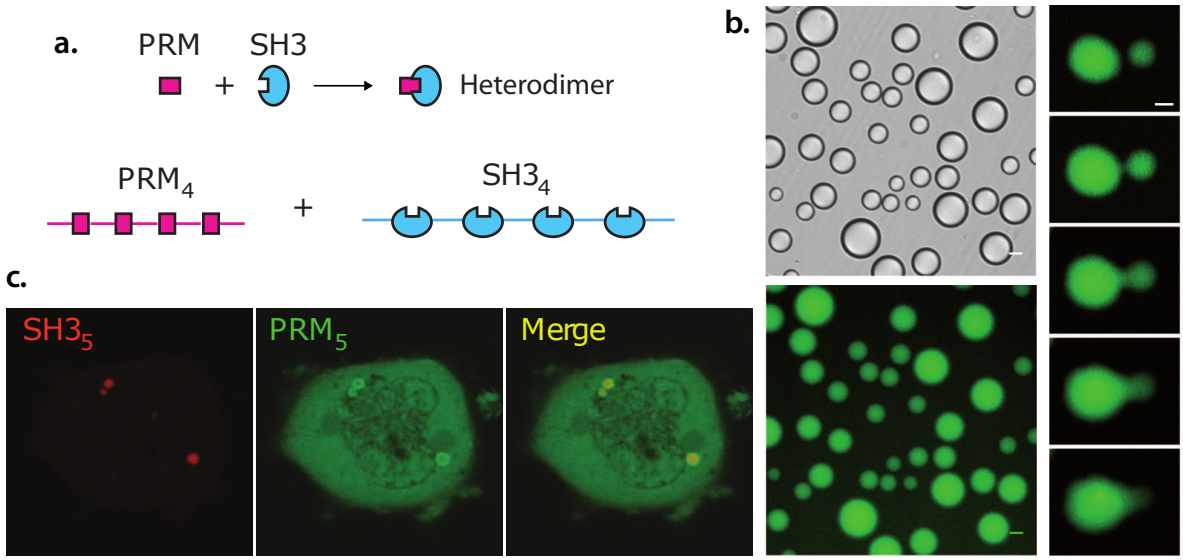

Figure 2.4: **a.** SH3-PRM engineered LLPS scaffolds. **b.** Condensates observed by differential interference contrast microscopy and fluorescence microscopy when SH34, PRM4 and OG-SH34 were mixed **c.** Time-lapse imaging of merging droplets that were formed as in b. **d.** Co-expression of $SH3_4$ and PRM_4 in HeLa cells leading to condensate formation. Adapted from [Li et al. 2012].

The **SUMO-SIM** scaffold system introduced by Banani et al. expanded the LLPS design space beyond SH3-PRM chemistry. SUMO (Small Ubiquitin-like Modifier) domains

and their cognate SUMO-interacting motifs (SIMs) form specific but weak interactions, ideal for phase separation when arranged multivalently. By varying the number of repeats and relative concentrations, Banani et al. could tune droplet composition, demonstrating selective recruitment or exclusion of client proteins fused to interaction motifs. The SUMO-SIM platform validated multivalency as a generalizable engineering principle and highlighted that condensates could be compositionally programmable, not merely structural features.

While SH3-PRM and SUMO-SIM systems established how to build synthetic condensates, their assembly was constitutive—forming wherever and whenever the interacting partners were expressed. The next leap was to integrate spatiotemporal control, enabling condensates to be turned on or off at will. This was achieved by Shin et al.[120] with the **optoDroplet** system. Here, an intrinsically disordered region (IDR) from an LLPS-prone protein such as FUS was fused to the blue-light-sensitive oligomerization domain CRY2. In the dark, the fusion protein remained dispersed; upon blue-light illumination, CRY2 underwent rapid oligomerization, concentrating the attached IDRs and triggering phase separation. The transition was fully reversible: switching off the light led to droplet dissolution. figure 2.5 depicts this illumination-induced condensate nucleation. OptoDroplets offered millisecond-to-minute timescale control over condensate formation in specific cellular regions, enabling experiments probing the kinetics, thresholds, and reversibility of LLPS in vivo. The authors further discovered that prolonged droplet existence promoted maturation into less dynamic, more solid-like states—paralleling pathogenic aggregation in neurodegenerative disease—making optoDroplets a powerful disease-modeling tool.

Building on the optogenetic principle, Bracha et al. introduced **Corelets**[121], a modular two-component optogenetic condensate system. The "core" was a ferritin nanocage functionalized with an iLID domain, while the "shell" was an IDR fused to SspB, which binds iLID under blue light. Activation brought many SspB-IDR units to the ferritin surface, locally concentrating IDRs to trigger LLPS. Corelets allowed systematic mapping of intracellular phase diagrams by varying core-to-shell ratios and illumination patterns, thereby quantifying how scaffold stoichiometry and local concentration govern droplet nucleation.

At the same time, Shin et al. developed **CasDrop**[122], which brought spatial precision to a new level by combining LLPS scaffolds with CRISPR/dCas9 targeting. A multivalent scaffold fused to dCas9 and guided by a specific sgRNA could nucleate condensates directly at a chosen genomic locus. This demonstrated not only targeted condensate assembly but also that LLPS structures could physically reorganize nuclear architecture by excluding surrounding chromatin or clustering distant loci. In parallel, Dine et al.[123] introduced PixELLs, a light-controlled "off-switch" for LLPS. Based on PixD/PixE proteins from cyanobacteria that form oligomers in the dark and dissociate under blue light, PixELLs formed droplets in darkness and dissolved upon illumination. This complemented

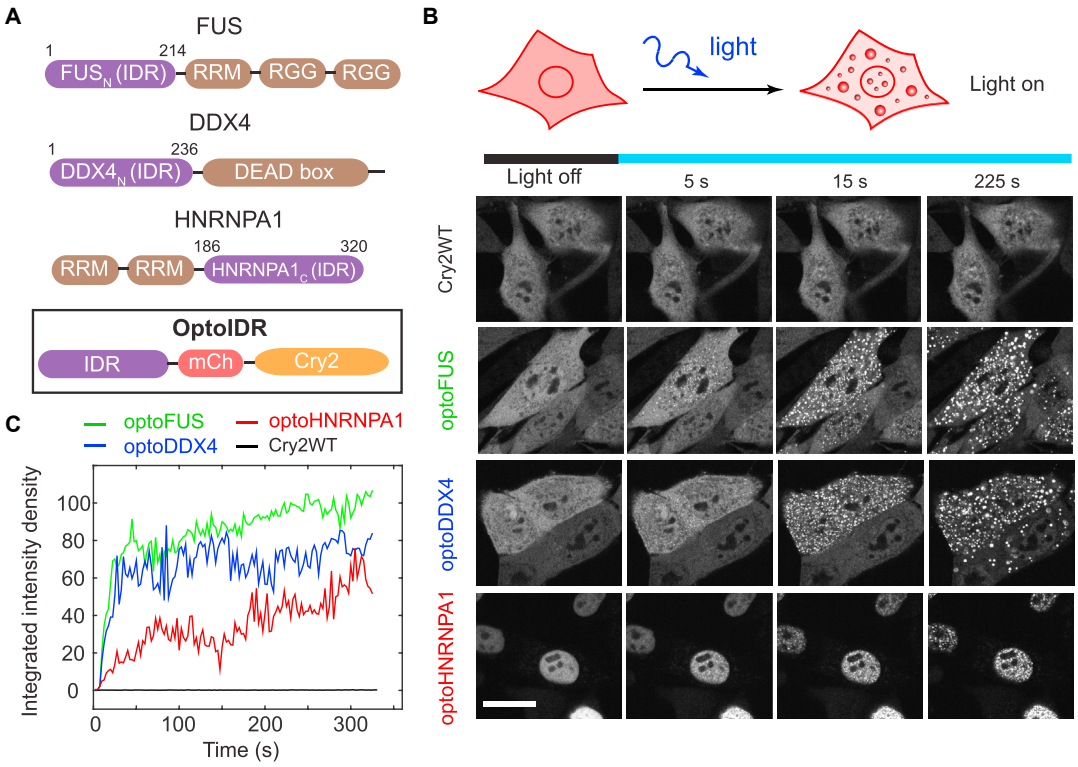

Figure 2.5: **A.** Schematic diagram of the optogenetic platform. Three IDR-containing RNA binding proteins are used in this study: FUS, DDX4, and HNRNPA1. The "optoIDR" construct consists of the N-terminal IDR fused to mCherry fluorescent protein and the Cry2PHR domain. **B.** Blue light activation of optoIDRs leads to rapid clustering in living cells. Representative fluorescence images of light-activated assembly of Cry2WT, optoFUS, optoDDX4, and optoHNRNPA1. All cells here are at similar expression levels and activated under identical conditions. Scale bar, 20 µm. **C.** Temporal evolutions of integrated fluorescence intensity density of cytoplasmic (except optoHNRNPA1 that predominantly localized in nucleus) clusters for cells shown in B. Figure from [Shin et al. 2017].

optoDroplets, enabling reciprocal control strategies.

While optogenetics offered precise temporal control, some applications required robust, sustained condensate formation or chemical triggering. **iPOLYMER**[124] addressed this need using the chemically inducible dimerization system FKBP-FRB with rapamycin. Two engineered proteins—one containing multiple FKBP domains and another with multiple FRB domains—remained dispersed until rapamycin addition, which cross-linked the domains, forming an extensive network that phase-separated into a hydrogel-like compartment inside cells. The design allowed tunable cross-link density by adjusting the number of repeats, and the compartments exhibited selective permeability, mimicking nuclear pore-like filtering. Later iterations, such as iPOLYMER-LI, incorporated photocleavable linkers or reversible CID systems to introduce control over dissolution, making iPOLYMER a versatile chemical complement to optogenetic LLPS platforms.

In the last few years, the field has shifted from proof-of-concept systems toward plat-

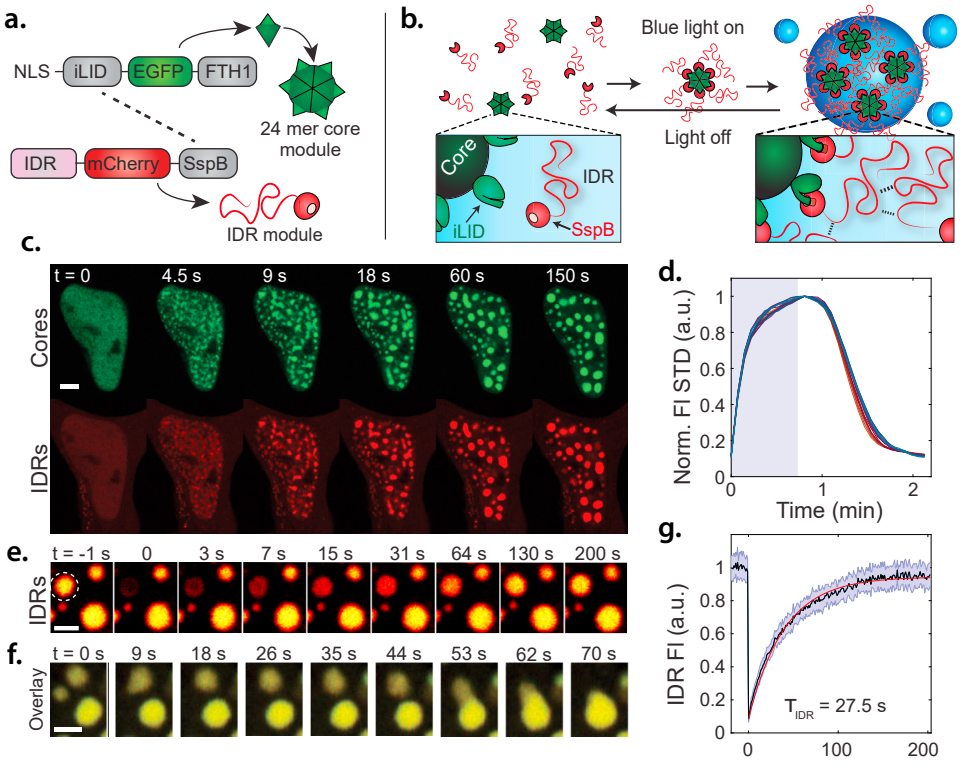

Figure 2.6: **a.** Corelets consists of two modules: a nuclear targeted, GFP-tagged ferritin core functionalized by 24 photoactivatable iLID domains, and iLID's partner's SspB, mCherry-tagged and conjugated to a self-interacting protein domain, such as the N-terminal IDR of FUS. Dashed lines designate photo-inducible heterodimerizing units. **b.** Upon global blue-light illumination, up to 24 IDR modules are captured by each Core, which subsequently phase separate by multivalent IDR interactions in a reversible manner. **c.** Time-lapse confocal imaging of photo-activated FUSN Corelet-expressing HEK293 cells. **d.** Condensates completely disassemble within 0.5-2 min after blue-light removal. **e.** FUSN Corelet condensates exhibit liquid-like properties as inferred by FRAP of FUSN IDR. **f.** Quantified FRAP curves from e. (mean and SD). **g.** Corelet condensates rapidly fuse and coarsen. Adapted from [Bracha et al. 2018].

forms with programmable material properties, orthogonality, and targeted biological applications. Below we integrate two of the most impactful recent examples, which illustrate this transition. Dai et al. presented a rational engineering strategy to design synthetic protein condensates with programmable properties and functions[125]. Using intrinsically disordered protein (IDP) sequence design, the authors created modular scaffolds whose phase-separation propensity and material characteristics could be tuned by altering sequence composition and sticker–spacer patterning. The design rules linked scaffold composition to droplet dynamics, such as fusion behavior, permeability, and client recruitment capacity. In *E. coli*, engineered condensates were used to sequester plasmid DNA, effectively silencing gene expression through physical compartmentalization. In mammalian cells, synthetic condensates were applied to modulate a protein signaling circuit, illustrating the versatility of the platform across domains of life. This work establishes a generalizable approach for constructing condensates to regulate DNA, transcription, or

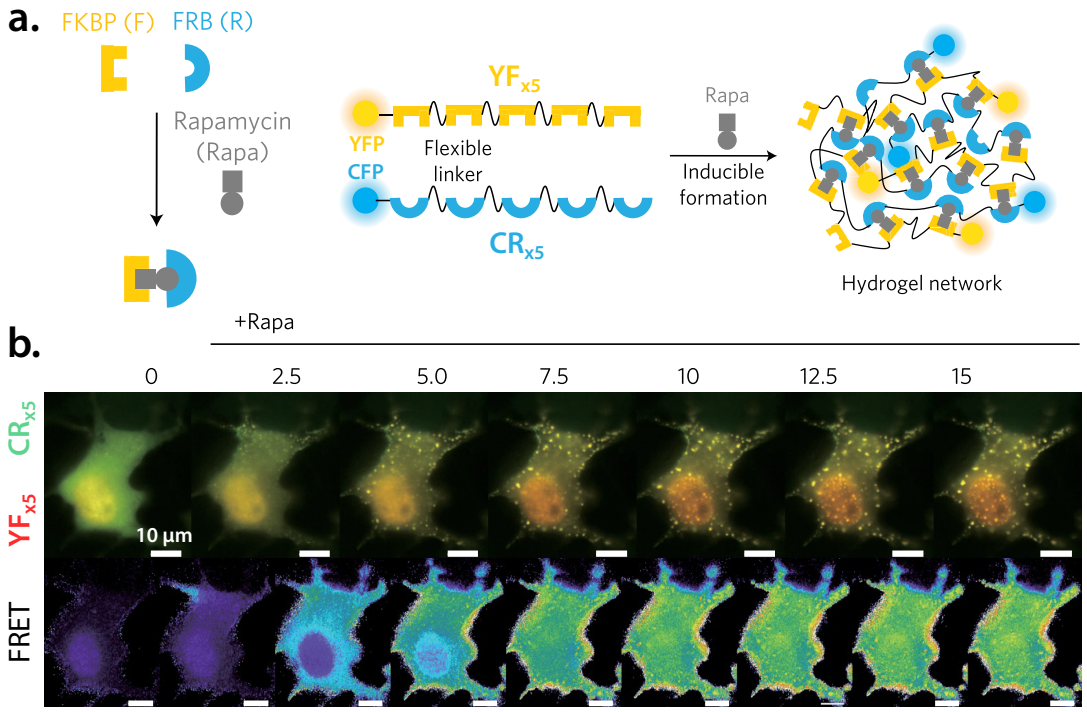

Figure 2.7: **a.** Rapamycin induces rapid, stable and specific binding between FKBP and FRB molecules. Two multivalent proteins, YFx5 and CRx5, were engineered to track their expression in cells: a yellow fluorescent protein (YFP) on five tandem repeats of an FKBP domain and a cyan fluorescent protein (CFP) on five tandem repeats on an FRB. **b.** Time-lapse imaging of fluorescent puncta formation in COS-7 cells following the addition of rapamycin. Punctate structures enriched with CFP, YFP, and FRET signals start to emerge within 5 min. Adapted from [Nakamura et al. 2018].

protein signaling with biophysical properties optimized for the desired function, both in eucaryotic and procaryotic cells.

Ramšak et al. engineered condensates using *de novo* designed coiled-coil (CC) domains as building blocks[126]. Unlike IDR-based systems, CCs are small, well-folded oligomerization motifs with tunable specificity. By concatenating multiple CC dimer motifs separated by flexible linkers, the authors created synthetic proteins that phase-separated predictably in living cells. The modular design allowed control over the number and type of CC pairs, enabling programming of phase-separation thresholds and dynamics. A key achievement was the generation of multiple coexisting condensates within the same cell using orthogonal CC pairs. These compartments remained immiscible and independently recruited their cognate clients, enabling parallel, non-interfering biochemical processes. Incorporation of drug-binding domains permitted chemical dissolution of the condensates, adding another layer of regulation. By varying multivalency and linker properties, the authors could bias the material state toward purely liquid or more solid-like droplets. This work provides a versatile platform for orthogonal, chemically controllable compartmentalization, complementing IDR-based systems and expanding the synthetic biology toolbox for organizing intracellular space.

More recently was developed an elegant and polyvalent LLPS system, which couples an oligomeric ferritin scaffold with the F36M mutated FKBP protein (FKBP-F36M or Fm), known to form weak homodimers. In this design, Fm domains are arrayed on the surface of a self-assembling 24-mer ferritin nanocage, providing up to 24 weak intermolecular contacts per particle. Above a critical cytosolic concentration, these multivalent particles undergo rapid liquid-liquid phase separation in living cells, nucleating a few micron-sized droplets that grow and coalesce over time (figure 2.8a-b) The Fm-Ft scaffold is highly modular - additional client domains can be fused without disrupting self-assembly. For example, Garcia-Jove Navarro et al. attached an mRNA-binding Pumilio homology domain to create an ArtiGranule that recruits specific mRNAs from the cytoplasm (figure 2.8c). The enriched RNA seeds condensate formation at lower protein concentrations and tunes the material properties: with RNA, more numerous but smaller granules form, and P-body proteins specifically concentrate at condensate interfaces (while unrelated RNP components remain excluded) (figure 2.8d). Thus, Fm-Ft condensates can be functionalized to mimic biological RNP granules and to probe how recruited biomolecules (like RNAs) modulate phase-separation behavior in cells.

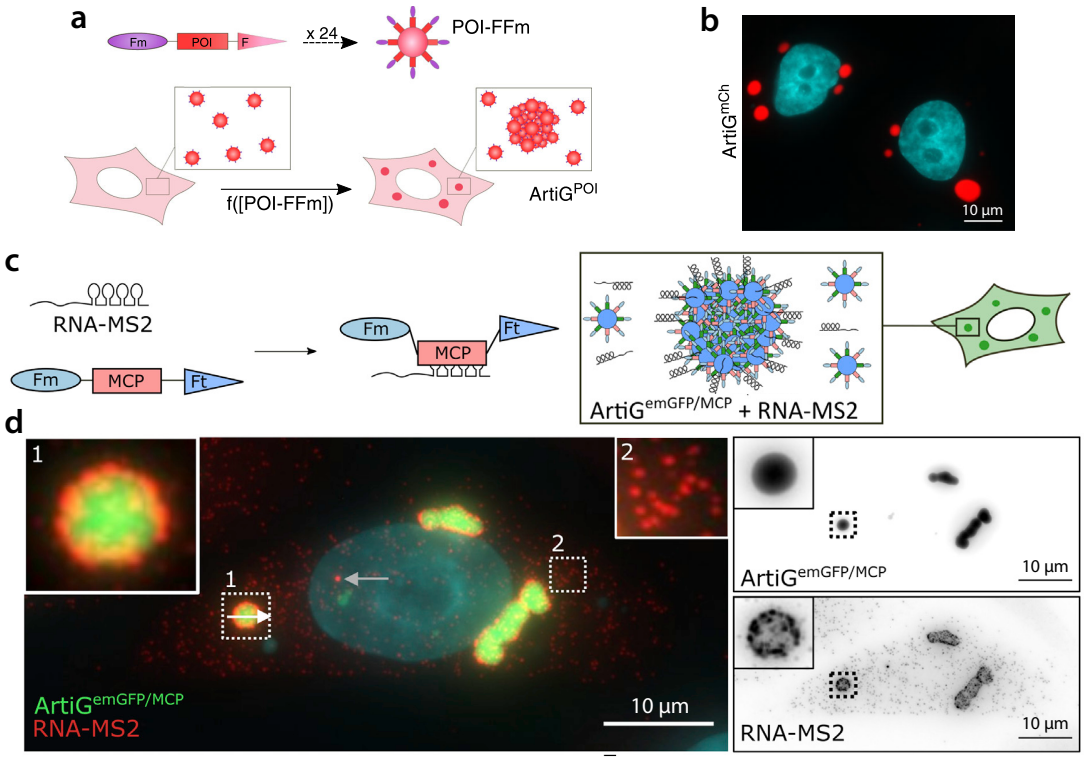

Figure 2.8: **a.** Schematic of **Fm-Ft** multivalent scaffold. Engineered ferritin subunits assemble into condensates via phase separation (Fm: F36M-FKBP, POI: protein of interest, Ft: Ferritin). **b.** Confocal image of HeLa cells expressing **Fm-mCherry-Ft**, showing cytosolic condensates (red) distinct from nucleus (blue). **c.** Adding MCP as a protein of interest allow condensates to recruit RNA at their surface. **d.** Epifluorescence imaging of Fm-Ft/MCP condensates (green) and RNA-MS2 (red), showing effective RNA enrichment at condensates surface. Adapted from [Garcia-Jove Navarro et al. 2019] and [Cochard et al. 2022].

A complementary engineered LLPS system is 5Fm, a single-chain scaffold containing five tandem Fm domains. This pentavalent design is composed of a repetition of Fm domains, each able to homodimerize. The 5Fm scaffold protein generates weak multivalent interactions that drive phase separation above a threshold concentration, forming intracellular condensates (figure 2.9a-c.). Components still exchange with the scaffolds solubilized in the cytoplasm, and the assemblies can be rapidly dissolved by adding the small-molecule FK506 to competitively disrupt the F36M-FKBP interactions. Taking advantage of this synthetic platform, researchers have targeted 5Fm condensates to specific processes. Coupling 5Fm to the aggregation-prone protein α-synuclein has been used to study neurodegenerative disease mechanisms. Strikingly, when exogenous α-synuclein fibrils are introduced, the 5Fm-α-syn condensates rapidly transition into solid, amyloid-like assemblies with needle-shaped inclusions (figure 2.9d.), mimicking pathological aggregation seen in Parkinson's disease. The 5Fm has also been used to relocate biomolecules: functionalizing 5Fm scaffolds with molecular motors (KIF1A/KIF5B), condensates are transported to the cell periphery. Equipping 5Fm with MCP creates motor/MCP condensates that specifically recruit MS2-tagged RNAs and control RNA localization, delocalizing it away from centrosomes.

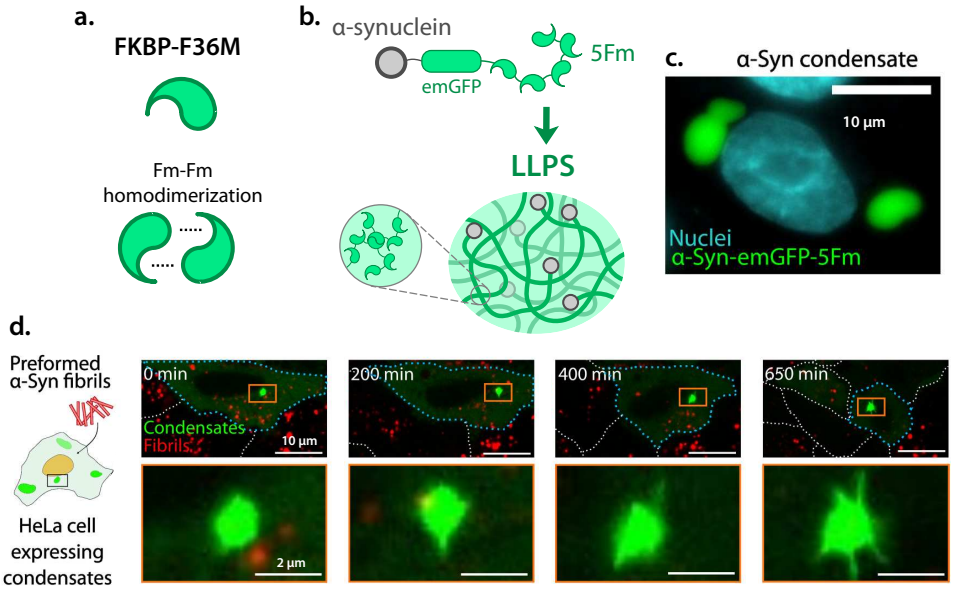

Figure 2.9: **a.** The F36M mutant of the protein FKBP (Fm) is able to homodimerize. **b.** Proteins containing five repeats of the Fm domain undergo a concentration-dependent LLPS. A protein of interest (here, α-Synuclein) can be added to the scaffold, and is integrated in the phase-separated condensate. **c.** Representative epifluorescence images of a HeLa cell expressing α-Syn-functionalized 5Fm condensates. **d.** Live confocal microscopy frames depicting HeLa cells expressing α-Syn condensates (green) changing morphology upon exposure to preformed α-Synuclein fibrils (red), mimicking pathological protein aggregation. Adapted from [Piroska et al. 2023]

From Oparin's coacervates to modern programmable, multi-functional condensate frameworks, the trajectory of engineered LLPS biocondensates reflects an increasing so-

phistication in both design principles and functional ambitions. Early work established that multivalency and weak interactions can drive LLPS; subsequent innovations layered on spatial, temporal, and chemical control; and the latest systems integrate predictive design, orthogonal compartmentalization, and functional output ranging from metabolism to computation. Together, these developments position engineered condensates as a central toolkit in synthetic and cell biology, with the potential to reshape how we manipulate and understand cellular organization.

3 Using synthetic condensates to control lipid droplet dynamics

The global aim of this PhD is to build a new lipid droplet research methodology tool to restrict surface accessibility to LDs, and use it to gain a causal understanding in LD physiology. To to so, we aim to engineer an artificial, protein-based meshwork that assembles directly at LD surfaces in living cells and transiently traps them into a controllable compartment. Such a tool would let us impose, synchronize, and reverse LD surface availability on demand. Practically, this means creating a platform that can be targeted with organelle specificity, and tune their material properties so that LDs can be selectively captured and then released without disrupting cellular homeostasis.

This is where synthetic biomolecular condensates offer an opportunity. The principles of liquid-liquid phase separation make it possible to engineer protein-based compartments that assemble in living cells under defined conditions, at chosen locations, and with tunable material properties. By linking multivalent scaffolds to specific targeting domains, condensates can be made to nucleate at organelle surfaces; by incorporating reversible interaction domains, they can be dissolved on demand. These features align precisely with the unmet needs of LD research: specificity, controllability, and reversibility.

The central motivation of the first part of this PhD is to harness these principles to create a tool, capable of selectively encapsulating LDs in living cells. This tool, called **ControLD** for Controlled Trapping of LDs, is based on a bifunctionnal scaffold containing a LLPS domain and a targeting domain. To build the LLPS meshwork, we chose to use the 5Fm scaffold described above, which has been shown to form liquid-like condensates in mammalian cells. As presented in the previous section, the 5Fm scaffold is based on five repeats of the FKBP12-F36M domain, which self-associates into a dense phase through multivalent interactions. The targeting domain consists of a lipid droplet-binding protein from the perilipin family, such as Plin1, Plin2, or Plin3. These proteins are known to associate with LDs and can be fused to the 5Fm scaffold to direct condensate formation specifically at LD surfaces.

The objectives of this part of the PhD are therefore twofold. First, to establish Con-

troLD as a robust and versatile tool for mammalian LD biology, by optimizing scaffold design, targeting specificity, and condensate stability. Second, to use ControLD to investigate how physical sequestration alters LD metabolism in mammalian cells, including lipid storage and mobilization under nutrient-rich and nutrient-deprived conditions, and to assess its impact on LD-mitochondria contact site dynamics.

By achieving these goals, this work will provide the first platform for acute, reversible, and selective manipulation of LD functions in living mammalian cells. Beyond its immediate applications, it will serve as a proof of principle for using engineered LLPS compartments as programmable regulators of organelle behavior, a strategy with potential to reshape how we probe dynamic processes in cell biology.

4 Main findings

The main findings of this study are grouped in the article *Controlling lipid droplet dynamics via tether condensates*[130] published in **Nature Chemical Biology** in 2025. The article is available in full at the end of this chapter, and a graphical abstract (figure 2.10), as well as the main findings of the article, are presented here.

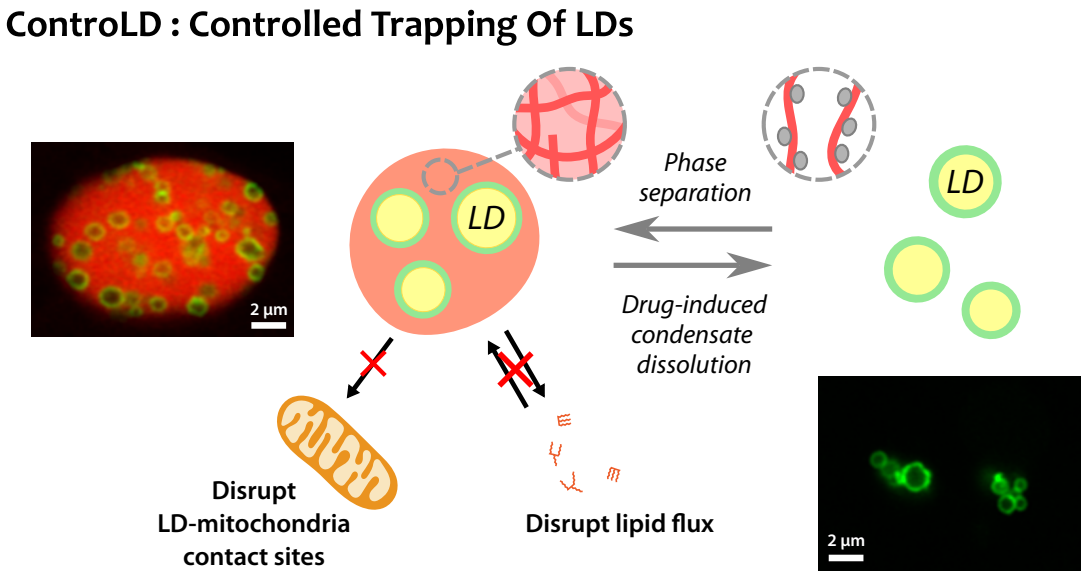

Figure 2.10: Graphical abstract of the ControLD framework.

Concept of the ControLD approach

We developed Controlled Trapping of LDs (ControLD), a synthetic biology tool that employs engineered LLPS condensates to physically sequester LDs in a reversible manner. The system is based on:

- An LLPS scaffold (5Fm, containing five FKBP12-F36M repeats) that self-associates into condensates and can be dissolved by the small molecule FK506.

- A fluorescent protein tag (emGFP or mCherry) fused to the scaffold for visualization.
- A targeting module, consisting of a lipid droplet-binding protein from the perilipin family, Plin2.

Nucleation and growth of LD-Condensates

When expressed in cells, the fusion protein binds LD surfaces and nucleates condensates around them, forming micrometer-sized compartments. Live-cell imaging demonstrated that LD-condensates form in a two-step process. First, the targeting domain anchors the scaffold to the LD surface, creating a two-dimensional protein layer. Second, local nucleation of condensates occurs, followed by growth and coalescence into larger bodies. This process is concentration-dependent and begins once cytosolic scaffold levels exceed a critical threshold. Fluorescence recovery after photobleaching (FRAP) revealed that proteins bound to the LD surface were less dynamic than those within the 3D condensate phase, indicating differential molecular mobility.

Versatility across perilipin variants

We demonstrated that ControLD is versatile and can be adapted to different LD-binding proteins. The system was tested with three perilipin family members: Plin1, Plin2, and Plin3, each with distinct affinities for LDs. Each perilipin variant produced condensates with different properties:

- Plin1 (high LD affinity) produced stable condensates and showed the lowest protein mobility at the LD surface.
- Plin2 (intermediate affinity) generated robust condensates with moderate dynamics.
- Plin3 (low affinity) required higher expression levels to effectively trap LDs and often positioned LDs at the condensate periphery.

Competition experiments showed that overexpression of a higher-affinity perilipin could prevent a lower-affinity one from recruiting LLPS scaffolds to LDs, preventing the engulfment of LDs by condensates.

Effect on lipid trafficking

LD confinement inside condensates blocked the exchange of fatty acids between droplets. Pre-existing LDs trapped within condensates retained fluorescently labeled fatty acids (BODIPY-C12) and did not transfer them to newly formed LDs. When condensates were dissolved with FK506, lipid exchange resumed, demonstrating that ControLD can temporarily arrest and then restore LD trafficking.

Protection against starvation-induced LD consumption

Starvation experiments revealed that unconfined LDs were almost completely degraded under nutrient deprivation, while LDs inside condensates were largely preserved. This protective effect was consistent across condensates formed with Plin1, Plin2, and Plin3, and was attributed to restricted access of lipases and other catabolic machinery to the LD surface.

Reversible modulation of LD-Mitochondria contacts

LD-mitochondria contact sites are key hubs for lipid metabolism. In the model adipocyte HuH7 cells, ControLD reduced LD-mitochondria colocalization up to threefold (most strongly with Plin1 scaffolds) and electron microscopy confirmed the physical exclusion of mitochondria from condensates. Upon condensate dissolution, LD-mitochondria contacts were restored, both in normal and starvation conditions, demonstrating that this interaction is dynamically and reversibly controlled.

nature chemical biology

Article

https://doi.org/10.1038/s41589-025-01915-2

Controlling lipid droplet dynamics via tether condensates

Received: 23 June 2024

Accepted: 18 April 2025

Published online: 21 May 2025

Check for updates

Chems Amari[1,2], Damien Simon[1,3], Emma Pasquier[1], Theodore Bellon[1], Marie-Aude Plamont[1], Sylvie Souquere[4], Gérard Pierron[5], Juliette Salvaing[2], Abdou Rachid Thiam[3] ✉ & Zoher Gueroui[1] ✉

Lipid droplets (LDs) are dynamic cellular organelles that regulate lipid metabolism and various cellular processes. Their functionality relies on a dynamic proteome and precise spatiotemporal interactions with other organelles, making LD biology highly complex. Tools that enable the sequestration and release of LDs within their intracellular environment could synchronize their behavior, providing deeper insights into their functions. To address this need, we developed Controlled Trapping of LDs (ControLD), a new method for manipulating LD dynamics. This approach uses engineered condensates to reversibly sequester LDs, temporarily halting their activity. Upon release, the LDs resume their normal functions. ControLD effectively disrupts LD remobilization during metabolic demands and prevents the formation of LD–mitochondria contact sites, which are re-established upon condensate dissociation. ControLD represents a powerful tool for advancing the study of LD biology and opens avenues for investigating and manipulating other cellular organelles.

Lipid droplets (LDs) are unique organelles at the nexus of cellular lipid metabolism. They consist of a neutral lipid core (mainly triacylglycerol, TG, and cholesterol ester) covered by a lipid monolayer embedded with proteins[1]. They have a substantial role in diverse biological functions, primarily to balance cellular energy fluxes—storing excess energy and delivering lipids during scarcities for making membranes or generating ATP[2,3]. In humans, dysregulation of LD formation and dynamics is related to several metabolic diseases linked to obesity, such as type II diabetes, liver or cardiac diseases, or lipodystrophies and neuronal disorders[2,4]. LDs interact with nearly all other cell organelles to perform their biological processes, for example, the endoplasmic reticulum (ER), mitochondria, autophagosomes, lysosomes, or peroxisomes, for anabolic or catabolic processes[5,6]. For instance, during metabolic shifts towards energy expenditure, LDs recruit at their surface enzymes such as lipases, for example, adipose triglyceride lipase and hormone-sensitive lipase, for lipid breakdown and use microtubules to associate with mitochondria, to which they deliver the fatty acid products for β-oxidation[7]. This exemplifies the importance of LD communication with organelles to fulfill cellular needs[8,9].

LD dynamics and functions are partially regulated by proteins recruited to the LD surface[10,11]. Most of these proteins come either from the cytosol, often associating with LDs by amphipathic helices, or from the ER membrane, associating with LDs with monotopic domains[10,11]. How LDs form and how proteins control their dynamics and function have been studied from cell biology, in vitro reconstitution experiments or biochemically perspectives[12–14], identifying key steps leading to LD nucleation, growth and maturation[15–19]. Yet, how LD biogenesis and functions are spatiotemporally controlled to coordinate response to metabolic fluctuations remains poorly understood[20].

Developing methodologies to probe and perturb LDs directly in cells could be instrumental in answering these questions[21]. To achieve this goal, we devised a strategy to create intracellular compartments programmed to selectively confine LDs, capitalizing on our ability to create biomolecular assemblies. This approach could enable the

[1]CPCV, Department of Chemistry, ENS, PSL University, Sorbonne Université, CNRS, Paris, France. [2]LPCV, Université Grenoble-Alpes, CEA, CNRS, INRAE, Grenoble, France. [3]Department of Physics, ENS, PSL University, Sorbonne Université, CNRS, Université Paris Cité, Paris, France. [4]AMMICA UMS-3655, Institut Gustave Roussy, Université Paris-Saclay, Villejuif, France. [5]CNRS UMR-9196, Institut Gustave Roussy, Villejuif, France. ✉e-mail: thiam@phys.ens.fr; zoher.gueroui@ens.psl.eu

physical sequestration of selected intracellular structures, potentially allowing for the modification of their biological functions. Our method, termed Controlled Trapping of LDs (ControLD), focuses on targeting and confining LDs in cells in a controllable and reversible manner. ControLD employs engineered condensates as artificial compartments designed to target specifically LDs to reorganize and sequester them in cells.

ControLD is based on the design of a chimeric protein scaffold, composed of a part that is prone to phase-separate in cells and a second one, composed of an LD targeting protein, for example, here validated for Perilipin 2 (Plin2). When produced in cells, our scaffolds eventually condensed at the surface of LDs to form micrometric condensates, entrapping all LDs. These LD-containing condensates displayed the hallmarks of phase-separated condensates, including localized nucleation, growth and coalescence of the condensed phases. Furthermore, we could trigger the release of LDs within a minute time scale by dissociating the condensates. LD-condensates robustly formed with three different LD-associated proteins, Plin1, Plin2 and Plin3, indicating that the LD-anchoring proteins could be used for a broad range of protein–LD affinities. LDs entrapped within condensates had their activity temporarily paused, which resumed upon release from confinement. This reversible process disrupted LD remobilization during metabolic demands and prevented LD–mitochondria contact sites, which re-established after the LDs were released.

Results

An engineered condensate designed to bind to lipid droplets

To promote the interactions between LDs and engineered condensates, we developed a protein scaffold with two specific properties—the ability to undergo phase separation in the cytoplasm and the capability to interact with the surface of LDs (Fig. 1a). We selected a protein scaffold (hereafter called 5Fm) consisting of five consecutive repeats of FKBP12-F36M, a protein domain able to form weak and specific homodimers. Due to its self-interacting multivalency, this scaffold undergoes a concentration-dependent phase separation, forming liquid-like condensates in cells. Furthermore, the condensates that can be reversibly dissociated by the small molecule FK506 (refs. 22,23). As the LD protein-targeting component, we opted for Plin2, a member of the perilipin family known to target LD surface in most human cells[24,25]. As anticipated, the expression of 5Fm scaffolds lacking the LD surface protein (Plin2) for 24 h in HeLa cells resulted in micrometric mCherry condensates scattered throughout the cytoplasm (Fig. 1b). These condensates did not interact with emGFP-Plin2-coated LDs and stained with LipidTOX, indicating the absence of nonspecific interactions between Plin2-coated LDs and the 5Fm-based condensates (Fig. 1b). In contrast, when 5Fm-emGFP-Plin2 was coexpressed with mCherry-5Fm for 24 h in cells, it led to the formation of large structures comprising LDs embedded within condensates (Fig. 1c,d). Typically, we observed approximately two to six large compartments per cell with a diameter of about 2–6 µm, encompassing tens of LDs (Fig. 1e). Nearly all LDs present in the HeLa cells were consistently trapped within the condensates (Fig. 1e). On closer examination, we observed that the 3D condensed phase typically separates individual LDs from each other (Extended Data Fig. 1a,b). A second pattern of LD organization was observed when the stoichiometry of cotransfected emGFP-5Fm-Plin2/5Fm plasmids was increased from 1:20 to 1:4, that is, an increase in the levels of emGFP-5Fm-Plin2 quantity. Under these conditions, LDs were predominantly densely packed in a beads-on-a-string arrangement (Fig. 1g). While 5Fm-emGFP-Plin2 scaffolds were homogeneously localized around LDs, the mCherry-5Fm signal was enriched at the contacts between adjacent LDs, potentially forming optically unresolved condensates (Extended Data Fig. 1c–e).

Overall, our data demonstrate that bioengineered condensates designed to target the LD surface can trap and confine LDs.

LD surface triggers localized condensate formation

Next, we conducted live imaging to determine the timing and location of condensate formation within the intracellular space. At early stages of protein expression, the 5Fm-emGFP-Plin2 signal localized at the surface of LDs, suggesting a 2D anchoring mechanism (Fig. 2a and Supplementary Video 1). Subsequently, the mCherry-5Fm signal was recruited to the LD surface through Fm intermolecular interactions (Fig. 2a and Supplementary Video 1). The condensates eventually nucleated on the LD surface for both 5Fm-emGFP-Plin2 and mCherry-5Fm scaffolds, indicating that LD surfaces played a role in seeding their nucleation. These LD-nucleated condensates tended to coalesce into larger structures (Fig. 2b), as commonly observed with classical liquid condensates. The typical time scale for the relaxation towards spherical bodies was approximately 30 minutes for a 5 µm-sized LD-condensate. Furthermore, we noted that LDs, initially in contact, moved apart during condensate growth (Fig. 2a and Supplementary Video 1). Fluorescence recovery after photobleaching (FRAP) revealed distinct dynamic properties of Plin2 within condensates depending on their localization. Specifically, approximately 60% of Plin2 within 3D condensate phase exhibited dynamic reorganization, occurring on a time scale of about one minute, while most Plin2 proteins were static when they were located at the LD surface (Fig. 2c).

Simultaneously with the initiation of LD-condensate formation, we observed a strong slowdown of the increase of the cytosolic fluorescence intensity, regarding both emGFP-5Fm-Plin2 and mCherry-5Fm. In contrast, the total cytoplasmic fluorescence intensity (cytosolic + condensates) kept increasing at a regular rate (Fig. 2d (left) and Extended Data Fig. 2). This suggests that the nucleation of LD-condensates occurs when a critical concentration of freely diffusing scaffolds is reached, driven by both homotypic and heterotypic interactions, with heterotypic interactions making a smaller but still significant contribution in determining the condensate location, that is, around LDs. Overall, these results imply a sequential process in which the initial formation of a 2D scaffold layer takes place on the LD surface (as depicted in Fig. 2a), followed by the localized nucleation, growth and coarsening of condensates, ultimately leading to the entrapment of LDs.

We next assessed whether the condensates could be disassembled by treating cells with FK506 (2.5 µM). This competitive binder disrupts Fm–Fm interactions (Fig. 3a). Upon addition of FK506, we observed the rapid dissociation of the condensates, followed by the release of LDs, allowing them to move freely within the cytosol (Fig. 3b and Supplementary Video 2). This demonstrates the potential for targeted manipulation, entrapment and synchronous release of LDs, thereby expanding the range of possibilities for druggable applications.

The Plin-binding affinity to LDs impacts LD-condensates

Plin2 belongs to the perilipin family of LD-associated proteins, known for their role in stabilizing LDs and regulating their surface accessibility[26]. To investigate the possibility of entrapping LDs using engineered condensates targeting alternative LD surface proteins, we focused on Plin1 and Plin3, which interact with stronger and weaker affinities, respectively, than Plin2 to the LD surface (Extended Data Fig. 3a,b)[27,28]. When coexpressing 5Fm-emGFP-Plin1 with mCherry-5Fm, we observed LD-condensates that exhibited a similar pattern to those observed for Plin2–LD-condensates (Fig. 4a). Specifically, LDs were embedded within condensates composed of 5Fm-emGFP-Plin1 and mCherry-5Fm. Plin3-condensates were equally observed but only when we used a larger concentration of 5Fm-emGFP-Plin3 scaffolds (Fig. 4b). Together, these findings indicate the robust formation of LD-condensates with different LD-associated proteins characterized by distinct protein–LD affinities.

LD surface binding competition affects condensate formation

Because LD proteome is regulated by protein binding competitions occurring at the LD monolayer surface[29], we probed the impact of protein competition on condensate formation. Knowing that Plin1 exhibits

https://doi.org/10.1038/s41589-025-01915-2

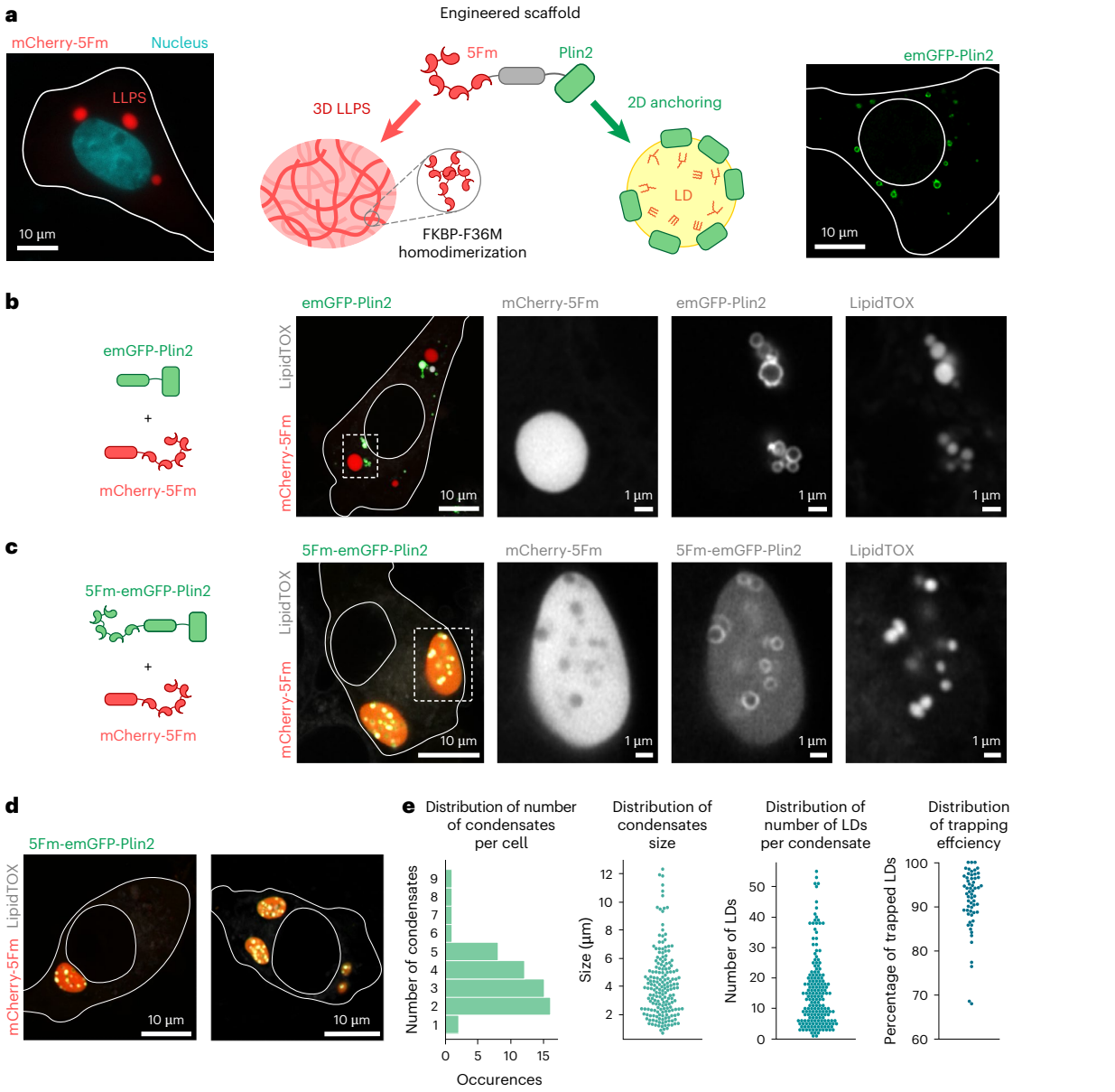

Fig. 1 | ControLD using bioengineered condensates programmed to interact with LDs. a, Schematic of the LD-targeting protein scaffold enabling phase separation. The scaffold is made of a repetition of homodimerization domains, and an LD-binding protein was used for LD surface recognition (Fm and Plin2). Left, HeLa cell expressing mCherry-5Fm condensates. Right, HeLa cell expressing Plin2 localized at LD surface. **b**, Confocal imaging of mCherry-5Fm condensates and Plin2-coated LDs in HeLa cells. **c**, Confocal imaging of HeLa cells expressing Plin2-functionalized LLPS scaffolds. **d**, Cells expressing Plin2-functionalized 5Fm scaffolds. The experiments in **b**–**d** were repeated independently three times with similar results. **e**, From left to right, distribution of the number of condensates per cell; size distribution of the condensates (Feret's diameter); distribution of the number of LDs per condensate; percentage of total LDs trapped within condensates per cell ($n = 60$ cells, two independent experiments). For all panels, cells were fixed 24 h after transfection, and LDs were revealed using LipidTOX. Scale bars = 10 µm for full cell images and 1 µm for zooms. Fm, FKBP12-F36M.

a stronger affinity with LDs than Plin2 (refs. 27,28), we assessed the effect of such competition on LD-condensate formation by cotransfecting Plin2 condensate scaffolds (5Fm-mCherry-Plin2 and 5Fm) with emGFP-Plin1. Whereas emGFP-Plin1 strongly labeled LD surface as expected, Plin2-condensates were devoid of LDs (Fig. 4d). This behavior was also observed when cotransfecting Plin3 condensate scaffolds with mCherry-Plin2, for which we found that mCherry-Plin2 were labeling all LDs and Plin3-condensates formed without trapping any LDs (Fig. 4e). The saturation of the LD surface with a higher-affinity protein could prevent the targeting of LD-functionalized LLPS scaffolds and consequently the entrapping of LDs. Therefore, the overexpression of Plin of stronger affinity, which binds preferentially to the LD surface, resulted in the formation of condensates of Plin of weaker affinities devoid of LDs.

Next, we assessed the impact of the condensates' properties depending on the Plin type. First, we noticed differences in the proteins' enrichment at the LD surface and within the condensates. We observed a tenfold difference in the intensity ratio of Plin proteins at the LD surface compared to within the condensates between Plin1 and Plin3 (Fig. 4c). Interestingly, this result aligns with the previously reported tenfold difference in LD affinity between Plin1 and Plin3 (ref. 27). The intensity ratio for Plin2 showed an intermediate distribution, consistent with its intermediate affinity for the LD surface. This trend

https://doi.org/10.1038/s41589-025-01915-2

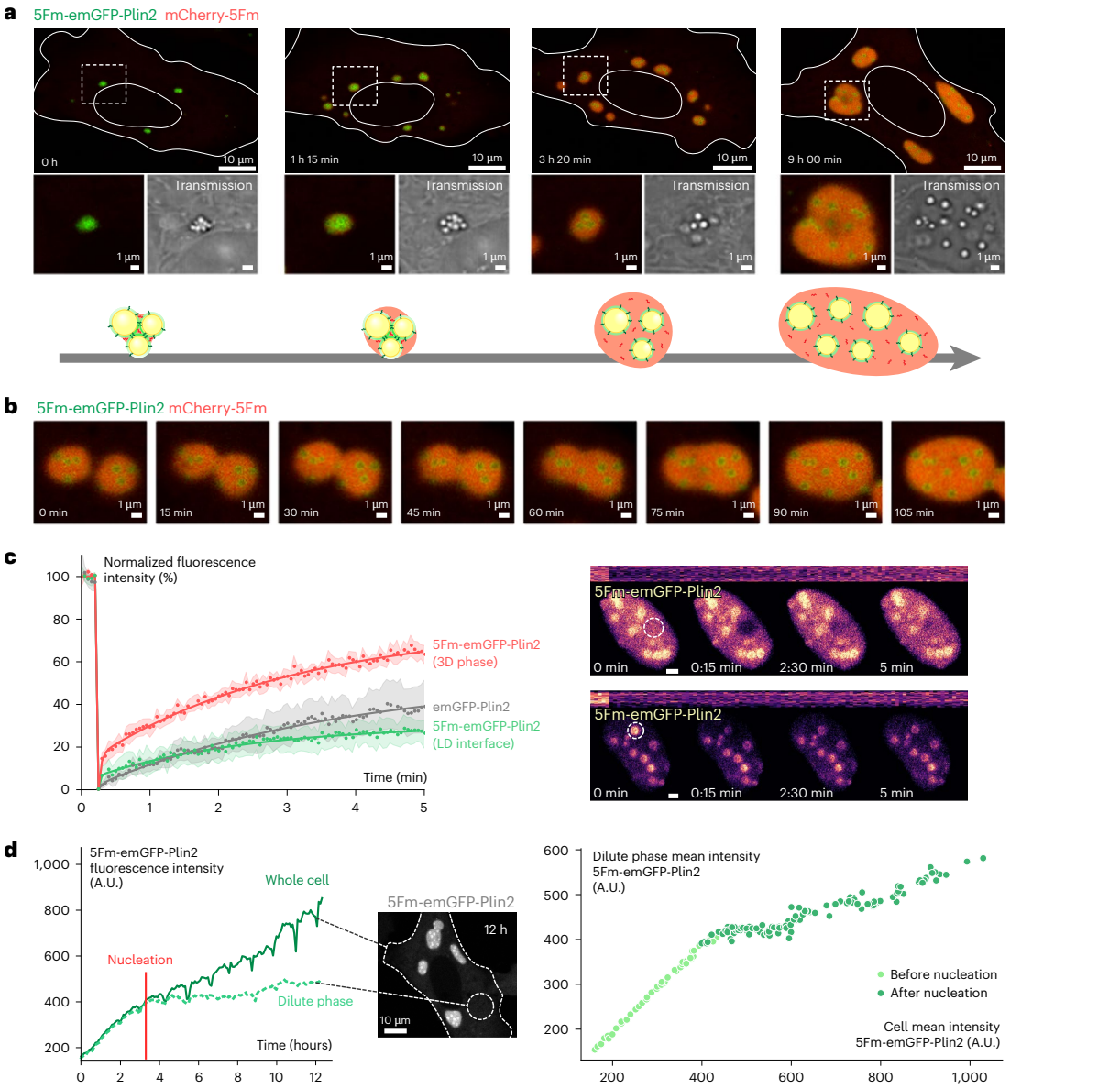

Fig. 2 | Dynamics of formation of LD-condensates. a, Time-lapse confocal imaging of the formation of LD-condensates in HeLa cells. Cells were transfected 6 h before the start of the time lapse. **b**, Time-lapse confocal imaging showing the coalescence of two LD-condensates in HeLa cells. **c**, Left, fluorescence recovery after photobleaching performed on 5Fm-emGFP-Plin2 within the 3D condensate phase (red curve, 13 cells) and at the LD surface (green curve, 8 cells). Control experiments were performed on unconfined Plin2-labeled LDs (gray curve, 13 cells). Solid line represents the mean value, and the colored area represents 95% confidence interval. Right, two representative FRAP experiments associated with the kymograph of intensity recovery extracted on the region of interest (dash circle). **d**, Left, plot of the temporal evolution of the GFP mean fluorescence intensities during the formation of LD-condensates in a HeLa cell, looking at the entire cell area ('whole cell') and at areas without LD-condensates ('dilute phase'). Right, evolution of solubilized 5Fm-emGFP-Plin2 fluorescence compared to total fluorescence, before and after condensates nucleation. The experiments in **d** were repeated independently two times with similar results. Scale bars = 10 µm for full cell images and 1 µm for zooms.

was further confirmed using FRAP, with Plin1 exhibiting weak and slow fluorescence recovery, consistent with its strong binding to the LD surface (Extended Data Fig. 4a). In contrast, Plin3 recovered approximately 80% of its fluorescence within 20 s, reflecting its strong enrichment in the condensed phase and low affinity for the LD surface (Extended Data Fig. 4b). Plin2 showed an intermediate behavior, with roughly 50% fluorescence recovering within one to two minutes (Fig. 2c).

Condensates halt lipid fluxes across LDs

Condensates physically isolate LDs, prompting us to investigate whether this isolation could block or modulate LD functions. To assess this, we examined the ability of sequestered LDs to store and exchange lipids by tracking lipid flux into LDs. This was achieved by visualizing the localization of the fluorescently labeled fatty acid BODIPY-C12 supplied with oleate. Without LD-confinement in condensates, all LDs were BODIPY-positive, following the fatty acid supply, indicating their ability to store newly synthesized lipids (Extended Data Fig. 5a). In contrast, when we added the fatty acids to the cells for a limited time before the condensate formation (during 4 h post-transfection), the formed condensates contained two distinct but co-existing populations of LDs (Fig. 5a). BODIPY-labeled LD population was primarily located at the condensate center, and an unstained LD population

https://doi.org/10.1038/s41589-025-01915-2

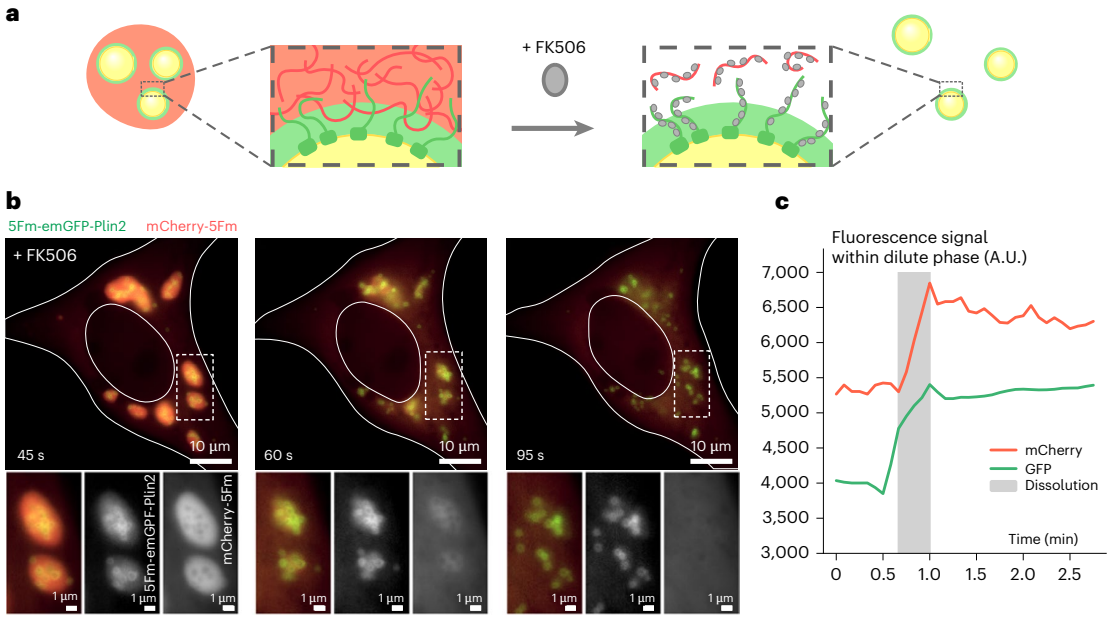

Fig. 3 | Drug-induced dissociation of LD-condensates. a, Schematic of FK506-induced dissolution of LD-condensates. **b**, Time-lapse epifluorescence imaging of the drug-induced dissolution of LD-trapping condensates in HeLa cells. Cells were transfected 24 h before observation with 5Fm-emGFP-Plin2, mCherry-5Fm and 5Fm (plasmid ratio = 1:5:14). Dissolution is induced upon the addition of FK506 (2.5 µM) at the start of the time lapse. The experiment was independently repeated three times with similar results. Scale bars = 10 µm for full cell images and 1 µm for zooms. **c**, Evolution of fluorescence in the dilute phase during the condensate dissolution of the cell shown in **b**, for 5Fm-GFP-Plin2 and mCherry-5Fm. The gray area represents the timing of dissolution of condensates.

was positioned at the condensate periphery (Fig. 5a,c). This suggests that LDs that incorporated BODIPY-C12 fatty acids are trapped within the condensates and that their fatty acid content is no longer available for exchange. By contrast, LDs at the periphery were probably newly synthesized LDs produced when BODIPY-C12 was no longer available. We interpreted this phenotype as an LD age marking phenotype whereby the BODIPY-C12-positive LDs were made first and trapped before the second wave of unstained LDs were made. In agreement with this interpretation, when we supplemented the BODIPY-C12 after condensate formation, the newly formed BODIPY-C12 LDs were primarily found at the periphery of the condensates (Fig. 5b,c and Extended Data Fig. 5b). This data suggests that the centrally located LDs originated from pre-existing LDs, while the peripheral LDs formed de novo after condensate formation (Fig. 5d).

The spatial separation of LDs within condensates remained stable over several hours, likely due to the viscosity of the condensates, which restricts LD diffusion and interactions. The absence of labeled fatty acid transfer to unlabeled LDs indicates that condensates act as physical barriers, limiting lipid exchange. In contrast, when LDs were released by dissociating the condensates with FK506, all LDs became BODIPY-positive after 24 h (Extended Data Fig. 5c). Together, these data provide evidence of our ability to temporarily pause and resume LD dynamics through condensate dissolution.

LD confinement shields LDs during energy remobilization

Our data suggest that LDs embedded within condensates are physically isolated from the rest of the cell, disrupting their life cycle and dynamics, and potentially jeopardizing their capacity to supply fatty acids and be an energy source during nutrient fluctuations. To investigate this possibility, we studied the consumption of LDs, confined or not within Plin2–LD-condensates, during cell starvation. The induction of starvation was achieved by switching the cell culture medium to a nutrient-low culture Earle's balanced salt solution medium (EBSS). As expected, we observed that unconfined LDs, detected using LipidTOX, were entirely consumed when cells were placed in the nutrient-deprived media for 24 h, in contrast to cells placed in complete medium, as shown by Plin2-coated signals (Fig. 5e). Most interestingly, we observed a large number of LDs within condensates in the starved cells, indicating that they were protected from consumption by the confinement (Fig. 5f). To analyze the effect further, we quantified the total number of LDs in cells in an unconfined or confined situation, that is, either expressing nonfunctionalized condensates or LD-condensates, both with and without starvation induction (Fig. 5e,f). Following starvation, we found a sevenfold decrease in the mean of LD numbers in cells when LDs were unconfined. In comparison, this decrease was only about 1.2-fold for the cells containing LD-condensates. Plin1–LD-condensates and Plin3–LD-condensates were also found to protect LDs from being consumed during starvation (Extended Data Fig. 5d). Altogether, this reveals that condensates protect LDs from being consumed during cell starvation, most probably due to a restriction of LD surface accessibility.

Reversible disruption of LD–mitochondria contact sites

LD–mitochondria contact sites are hubs of cellular lipid metabolism, prompting us to investigate how ControLD can modulate these interactions. We used the human hepatocyte-derived HuH7 cell model, which is suitable for studying interorganelle communication. We first confirmed that LD-condensates form in HuH7 cells, exhibiting the same canonical morphologies observed in HeLa cells, thereby demonstrating the robustness of ControLD (Extended Data Fig. 6). Mitochondria, stained with MitoTracker Deep Red, and LDs were imaged in cells expressing both unfunctionalized and Plin-functionalized condensates. To analyze their proximity, we employed an automated image analysis pipeline based on organelle segmentation to quantify colocalization from spinning-disk microscopy acquisitions; moreover, we used electron microscopy to visualize contact sites.

Without LD confinement, colocalization between mitochondria and Plin1-coated LDs was more frequent compared to Plin2–LDs (Fig. 6a,g). Ultrastructural characterization using electron microscopy revealed that Plin1-coated LDs were indeed often in close contact

https://doi.org/10.1038/s41589-025-01915-2

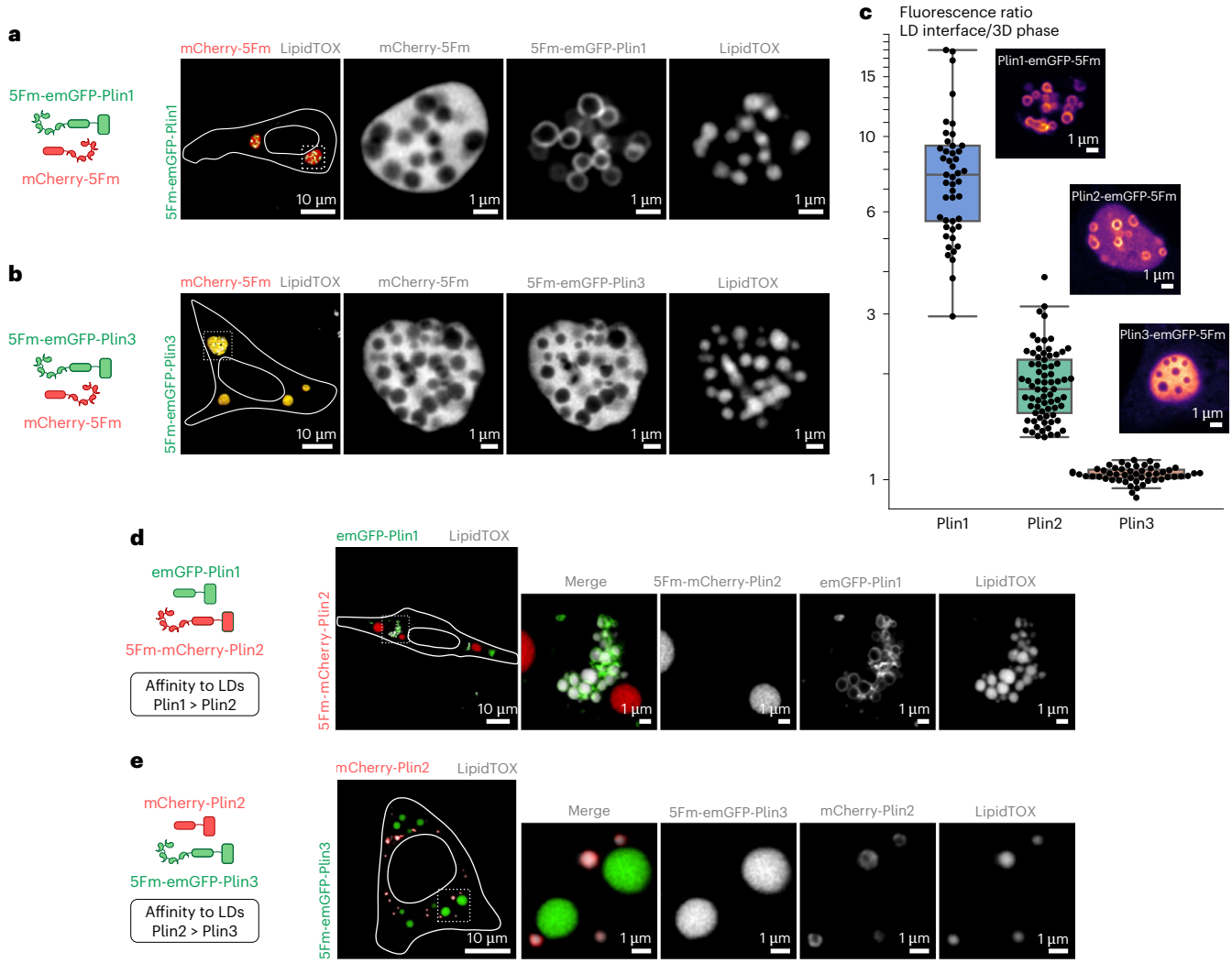

Fig. 4 | Formation of LD-condensates using Plin1 and Plin3 and protein binding competition. a, Confocal imaging of LD-condensates in HeLa cells using Plin1-functionalized LLPS scaffolds. **b**, Confocal imaging of LD-condensates in HeLa cells using Plin3-functionalized LLPS scaffolds. Cells were transfected with plasmids 5Fm-emGFP-Plin3, mCherry-5Fm and 5Fm. **c**, Quantification of the intensity ratio at the LD surface and within the condensates for Plin1, Plin2 and Plin3 (n = 46, 73, 61 cells, two independent experiments). Centerlines represent medians, boxes show IQR and whiskers represent 1.5× IQR. **d**, Protein binding competition and condensate formation with cells cotransfected with emGFP-Plin1, 5Fm-mCherry-Plin2 and 5Fm, showing no Plin2-coated LDs and no subsequent trapping. **e**, Protein binding competition and condensate formation with cells cotransfected with mCherry-Plin2, 5Fm-emGFP-Plin3 and 5Fm, showing no Plin3-coated LDs and no subsequent trapping. The experiments in **a**, **b**, **d** and **e** were repeated independently thrice with similar results. For **a**–**e**, LDs were marked using LipidTOX. Scale bars = 10 µm for full cell images and 1 µm for zooms. IQR, interquartile ranges.

with mitochondria, while noninteracting with nonfunctionalized condensates (Fig. 6b). Strikingly, upon Plin1–LD-confinement, we observed that mitochondrial structures were largely excluded from LDs (Fig. 6c,d) and spinning-disk microscopy analysis revealed that LD–mitochondria colocalization decreased approximately three-fold (Fig. 6g). Electron microscopy further confirmed the exclusion of mitochondria from Plin1–LD-condensates, with the majority of entrapped LDs showing no contact with mitochondria (Fig. 6d). These findings suggest that condensates effectively prevented the formation of LD–mitochondria contact sites. Similar disruptions were observed with Plin2–LD-condensates, although to a lesser extent (Fig. 6e–g).

To determine whether the disrupted contacts could re-form, we monitored LD–mitochondria colocalization after dissociating the condensates. Remarkably, the colocalization percentage was restored, demonstrating the dynamic reassembly of LD–mitochondria contact sites (Fig. 6g).

Next, we examined changes in LD–mitochondria contacts during nutrient deprivation, when fatty acids are transferred from LDs to mitochondria for β-oxidation. We found that Plin1-mediated LD confinement prevented the formation of LD–mitochondria contact sites (Fig. 6h), similar to what was observed in complete media. These findings indicate that condensates effectively shield LDs from mitochondria even during acute starvation, as confirmed by electron microscopy (Extended Data Fig. 7). Similarly, LD–mitochondria contact sites were inhibited by Plin2 condensates (Fig. 6h). Finally, we observed the re-establishment of LD–mitochondria contacts upon the release of LDs from condensates under nutrient-deprived conditions (Fig. 6h).

These findings collectively suggest that tethering condensates effectively prevents LD–mitochondria interactions, and that these contacts can re-form upon condensate dissociation, highlighting the dynamic and plasticity of these interactions.

https://doi.org/10.1038/s41589-025-01915-2

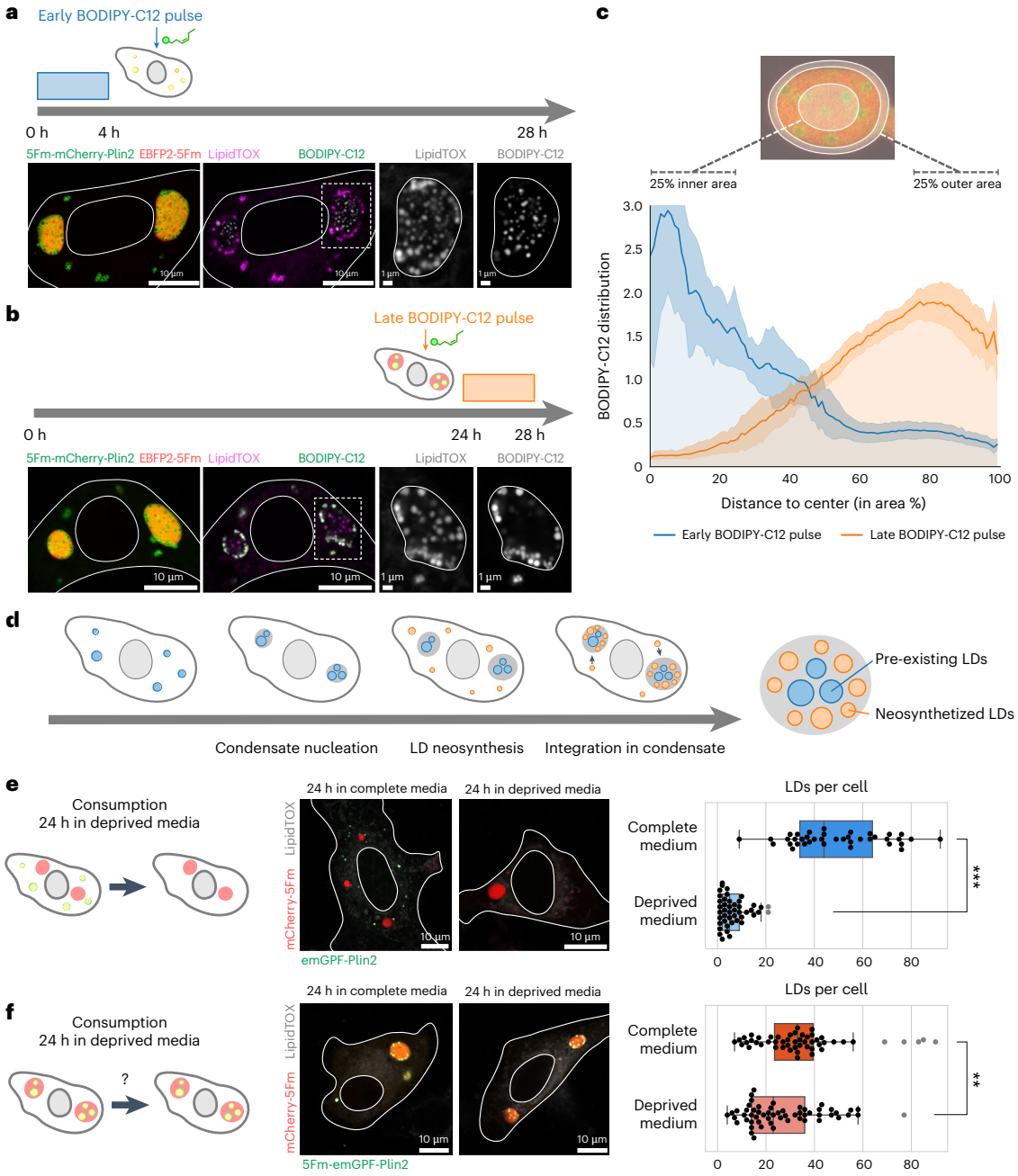

Fig. 5 | LD-trapping condensates restrict trafficking between LDs and protect LDs during starvation. a, Schematic showing incorporation of fluorescent fatty acid analogs (BODIPY-C12) before condensate formation in HeLa cells expressing LD-condensates. HeLa cells were fixed 28 h post-transfection and cultured in oleic acid-enriched medium. Bottom, imaging of LDs within Plin2-condensates. **b**, Schematic showing incorporation of BODIPY-C12 after condensate formation. Bottom, imaging of LDs within Plin2-condensates. Cells were fixed 28 h post-transfection. The experiments in **a** and **b** were repeated independently three times with similar results. **c**, Quantification of radial distribution of BODIPY-labeled LDs within condensates. Solid line represents the mean value, and colored area represents 95% confidence interval. **d**, Schematic illustrating condensate formation from pre-existing LDs, followed by peripheral incorporation of new lipids. **e**,**f**, Starvation effect on unconfined and confined LDs. Left, epifluorescence imaging of Plin2-coated LDs and 5Fm-mCherry condensates (**e**) and LDs confined in condensates (**f**) 48 h post-transfection. Media changed 24 h before fixation to complete or low-nutrient media (EBSS + 1% BSA). Right, mean LD number per cell expressing ≥1 condensate (5Fm or LD-condensate), ±starvation; unconfined LDs ($P = 8 \times 10^{-15}$), confined LDs ($P = 4.3 \times 10^{-3}$). For **e** and **f** box plots, centerlines represent medians, boxes show IQR and whiskers represent 1.5× IQR. ***$P < 10^{-3}$, **$P < 10^{-2}$. Scale bars, 10 µm for full cell images and 1 µm for zooms.

Discussion

We developed ControLD, a versatile method to trap and confine LDs within engineered condensates. To demonstrate its effectiveness, ControLD was tested using Perilipin-functionalized phase-separating scaffolds. These scaffolds specifically target the surface of LDs, nucleating a condensed protein meshwork that effectively isolates LDs from the surrounding intracellular environment. Importantly, the trapping of LDs is reversible, as they can be synchronously released

https://doi.org/10.1038/s41589-025-01915-2

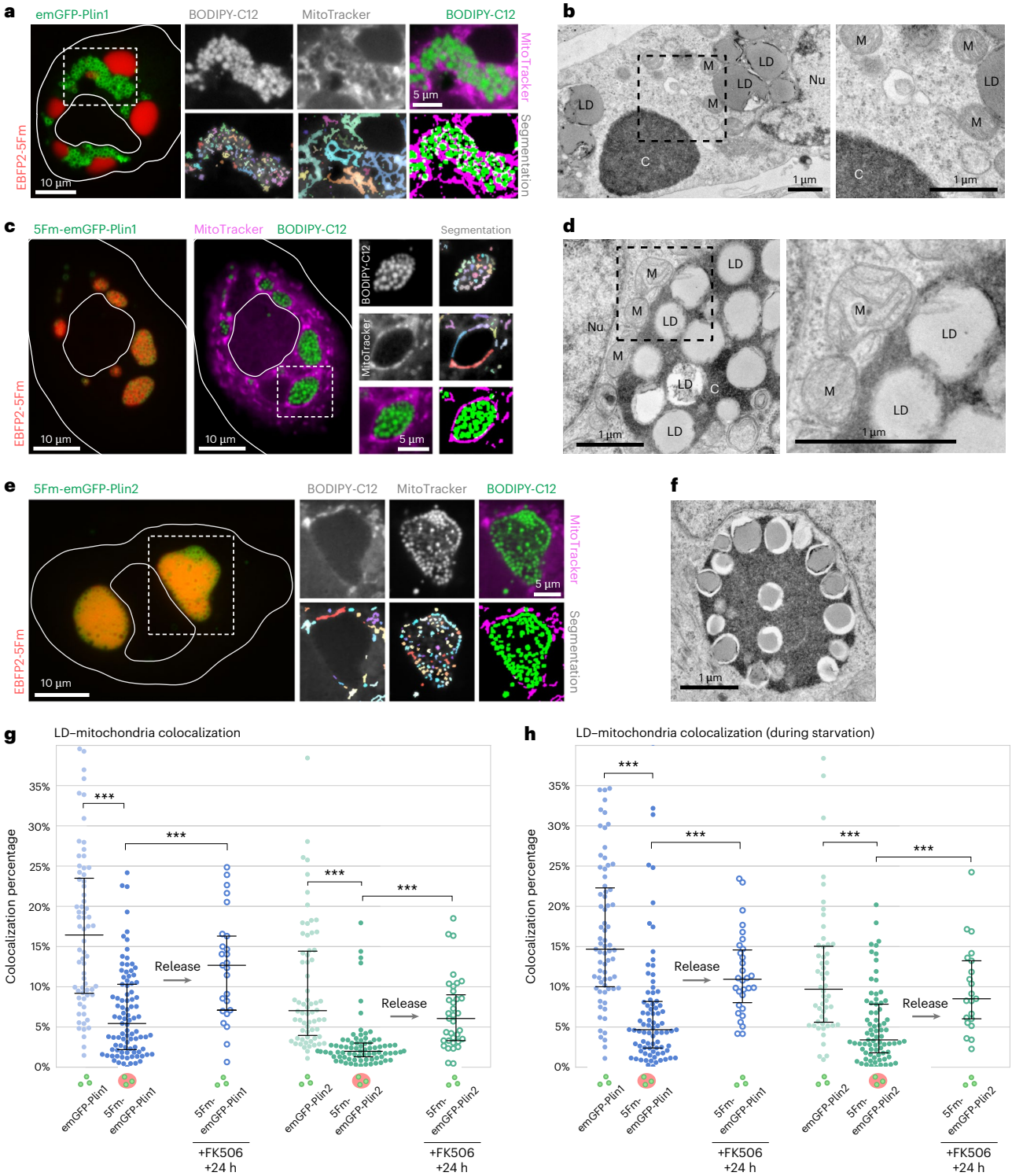

Fig. 6 | Reversible disruption of LD–mitochondria contacts. a, Spinning-disk imaging of Plin1-coated LDs in HuH7 expressing for 24 h emGFP-Plin1, BFP-5Fm and 5Fm with BODIPY-C12 red and MitoTracker Deep Red. **b**, Ultrastructural characterization of nonfunctionalized condensate, LDs and mitochondria in HuH7 cells (C, M and Nu). **c**, Spinning-disk imaging of Plin1–LD-condensates in HuH7 expressing for 24 h emGFP-5Fm-mCherry-Plin1, BFP-5Fm and 5Fm with BODIPY-C12 and MitoTracker Deep Red. **d**, TEM image of LDs trapped into a large Plin1-condensate from which mitochondria are excluded. **e**, Imaging of Plin2–LD-condensates in HuH7 expressing for 24 h 5Fm-mCherry-Plin2, BFP-5Fm and 5Fm with BODIPY-C12 and MitoTracker Deep Red. **f**, TEM image of Plin2 condensates with entrapped LDs. The experiments in **a**, **c**, **e**, **b**, **d** and **f** were independently repeated three and two times, respectively, with similar results. **g**, Quantification of LD–mitochondria colocalization in complete media conditions for HuH7 cells expressing LD-condensates (confined LDs) or Plin-coated LDs (unconfined LDs). Displayed $P = 10^{-12}, 10^{-9}, 10^{-16}$ and 10^{-15}. **h**, Quantification of LD–mitochondria colocalization during starvation. Displayed $P = 10^{-13}, 10^{-11}, 10^{-8}$ and 10^{-7}. ***$P < 10^{-3}$. In **g** and **h**, middle line represents medians, and error bars show IQR. Scale bars = 10 µm for full cell images, 5 µm for zooms and 1 µm for TEM images. C, condensate; M, mitochondria; Nu, nucleus.

within a minute by triggering the disassembly of the condensates. Remarkably, ControLD enables temporary arrest of LD dynamics and restoration of their activity upon release. We demonstrated that physically isolating LDs from the cytosol protects them from consumption during metabolic demands. Additionally, condensate formation substantially reduces LD–mitochondria contacts across the three assessed Perilipin types, with Plin1-based condensates having the greatest impact, probably due to the implication of Plin1 safeguarding the surface of LDs and controlling metabolic processes. Notably, LD–mitochondria contact sites reform upon condensate disassembly, highlighting the dynamic and reversible nature of this approach. Thus, our tool provides temporal control over LD dynamics, offering a powerful approach to studying LD biology.

The life cycle and dynamics of LDs are central to the metabolic roles they play, and such processes are tightly linked to specific biochemical mechanisms occurring at LDs' surface and LD–organelle contact sites. How does entrapping LDs within condensates result in arresting such LD dynamics? We could envision distinct but not exclusive mechanisms. Firstly, condensates may act as a diffusion barrier, preventing enzymes such as lipases from targeting the LD surface. Secondly, the condensate physical barrier could limit the initiation of the degradation machinery of LDs, for example, mediated by lipophagy[30]. Thirdly, contact sites between LDs and other organelles could be strongly perturbed, leading to altered communication between organelles. This perturbation of LD dynamics is, indeed, in agreement with the loss of LD–mitochondria contacts upon condensate entrapping (Fig. 6).

All these mechanisms could play collectively, enabling ControLD to manipulate LD metabolism and interactions with organelles reversibly.

Beyond its technical characteristics, ControLD opens up avenues for exploring the significance of condensates in regulating LD biology. While mounting evidence shows an interplay between membrane-bound organelles, for example, ER, Golgi, plasma membrane, mitochondria and condensates, no conclusive evidence exists that LDs might interact with condensates. Only Cidec, mediating LD–LD material transfer, has been recently suggested to undergo 2D phase separation, leading to the formation of a 2D plate between LDs[31]. Yet, a description of the interplay between LD dynamics and protein phase separation could provide a fresh perspective on regulatory mechanisms to tune the LD life cycle. Our characterization offers a new framework describing the interplay between LD dynamics and protein phase separation.

In our study, we found that the nucleation of condensates occurred on LDs by a step-wise formation process with the recruitment of LLPS scaffolds at the LD surface, followed by their localized condensation (Fig. 2 and Supplementary Video 1). LD surface provides numerous anchoring sites for disordered motifs such as amphipathic helices[32]. Therefore, LDs may favorably recruit LLPS scaffolds and restrict their mobility on 2D compared to freely diffusing in the cytosol. This restriction in scaffold diffusion could reduce the concentration threshold for condensation, as proposed for the regulation of phase-separated condensates by membranes[33]. As LD phospholipid monolayers show more packing voids than bilayer membranes[34], it is perfectly plausible that the LD surface facilitates more LLPS nucleation events.

Our observations of condensate nucleation triggered at the LD surface are also consistent with in vitro experiments using the histidine-modified FUS low-complexity domain interacting with NTA(Ni)-phospholipids[35]. In our system, the mechanism of recruitment of LLPS scaffolds to the LD surface is mediated by Plin proteins, which are LD-specific proteins. Other biomolecules than LD surface proteins are likely to bind to their surface, including RNA or RNA-binding proteins[36], which could act as putative linkers with endogenous condensates. Our data suggest that the surface of LD could drive the nucleation of condensates, which implies a general mechanism of regulation of phase separation that is based on both the biophysical and biochemical properties of lipid droplet/condensate interactions.

The affinity between Plin and LD surface controls several features of Plin-condensate organization and biophysical properties. For instance, Plin1-condensates were less dynamic than other Plin-condensates (Extended Data Fig. 4). Furthermore, the weaker affinity of Plin3 could drive the peripheral localization of LDs to the condensate interface rather than in condensates, as LD surface localization was more frequent for Plin3 than for other Plins. Physical considerations may also explain how LD organizations targeted with Plin-functionalized scaffolds could be remodeled through two main different patterns, either entrapped within large condensates or arranged into a string-like pattern (Fig. 1f,g). Two patterns depended on 5Fm-emGFP-Plin2 expressed in cells, with a lower quantity of 5Fm-emGFP-Plin2 favoring large 3D condensates. Our time-lapse imaging suggests that LDs-on-a-string arrangements formed through the irreversible adhesion between close LDs (Fig. 1g). In these conditions, large condensates on LD surface failed to grow. Because the cocondensation of mCherry-5Fm with 5Fm-emGFP-Plin2 at the LD surface is energetically more favorable than forming 3D condensates, this prevents independent nucleation elsewhere in the cell. These patterns were mainly observed when a larger amount of 5Fm-emGFP-Plin2 was transfected compared to the quantity used for forming LD-condensates (fivefold increase). This indicates that competition between adhesion strength, dependent on the 5Fm-emGFP-Plin2 surface density, and 3D phase separation dictates the balance between LDs-on-a-string arrangements and LD-condensates. This mechanism could potentially elucidate why, under physiological conditions, LDs often cluster resembling a grape-like structure, potentially facilitated by proteins prone to forming condensates, similar to Cidec[31]. When metabolic demands arise, these adhesion interactions may be disrupted by removing such proteins, allowing for LDs to disperse and fulfill their metabolic functions.

Several applications can be envisioned using ControLD as a tool to synchronize LD availability, enabling detailed investigations of specific molecular processes controlling LD dynamics. ControLD also facilitates the disruption and restoration of LD contact sites, making it a versatile method for studying these dynamic interactions. Its adaptability further supports its use in exploring other LD surface proteins in physiological contexts, such as in adipocyte cells. Given the increasing evidence of the pivotal roles of LD metabolism and contact sites in health and disease[5], understanding how LDs entrapped within condensates influence the progression of pathogen-infected or cancer cells represents an exciting direction for future research. Furthermore, we anticipate that the extension of the ControLD concept to control other cellular organelles will significantly broaden its potential applications.

Online content

Any methods, additional references, Nature Portfolio reporting summaries, source data, extended data, supplementary information, acknowledgements, peer review information; details of author contributions and competing interests; and statements of data and code availability are available at https://doi.org/10.1038/s41589-025-01915-2.

References

1. Welte, M. A. & Gould, A. P. Lipid droplet functions beyond energy storage. *Biochim. Biophys. Acta Mol. Cell Biol. Lipids* **1862**, 1260–1272 (2017).
2. Olzmann, J. A. & Carvalho, P. Dynamics and functions of lipid droplets. *Nat. Rev. Mol. Cell Biol.* **20**, 137–155 (2019).
3. Walther, T. C., Chung, J. & Farese, R. V. Lipid droplet biogenesis. *Annu. Rev. Cell Dev. Biol.* **33**, 491–510 (2017).
4. Ralhan, I., Chang, C.-L., Lippincott-Schwartz, J. & Ioannou, M. S. Lipid droplets in the nervous system. *J. Cell Biol.* **220**, e202102136 (2021).

5. Herker, E., Vieyres, G., Beller, M., Krahmer, N. & Bohnert, M. Lipid droplet contact sites in health and disease. *Trends Cell Biol.* **31**, 345–358 (2021).
6. Thiam, A. R. & Dugail, I. Lipid droplet-membrane contact sites—from protein binding to function. *J. Cell Sci.* **132**, jcs230169 (2019).
7. Herms, A. et al. AMPK activation promotes lipid droplet dispersion on detyrosinated microtubules to increase mitochondrial fatty acid oxidation. *Nat. Commun.* **6**, 7176 (2015).
8. Ugrankar, R. et al. Drosophila snazarus regulates a lipid droplet population at plasma membrane–droplet contacts in adipocytes. *Dev. Cell* **50**, 557–572 (2019).
9. Thiam, A. R. & Beller, M. The why, when and how of lipid droplet diversity. *J. Cell Sci.* **130**, 315–324 (2017).
10. Kory, N., Farese, R. V. & Walther, T. C. Targeting fat: mechanisms of protein localization to lipid droplets. *Trends Cell Biol.* **26**, 535–546 (2016).
11. Dhiman, R., Caesar, S., Thiam, A. R. & Schrul, B. Mechanisms of protein targeting to lipid droplets: a unified cell biological and biophysical perspective. *Semin. Cell Dev. Biol.* **108**, 4–13 (2020).
12. Santinho, A. et al. Membrane curvature catalyzes lipid droplet assembly. *Curr. Biol.* **30**, 2481–2494 (2020).
13. Ben M'barek, K. et al. ER membrane phospholipids and surface tension control cellular lipid droplet formation. *Dev. Cell* **41**, 591–604.e7 (2017).
14. Krahmer, N. et al. Phosphatidylcholine synthesis for lipid droplet expansion is mediated by localized activation of CTP:phosphocholine cytidylyltransferase. *Cell Metab.* **14**, 504–515 (2011).
15. Thiam, A. R. & Forêt, L. The physics of lipid droplet nucleation, growth and budding. *Biochim. Biophys. Acta* **1861**, 715–722 (2016).
16. Bersuker, K. et al. A proximity labeling strategy provides insights into the composition and dynamics of lipid droplet proteomes. *Dev. Cell* **44**, 97–112 (2018).
17. Krahmer, N. et al. Organellar proteomics and phospho-proteomics reveal subcellular reorganization in diet-induced hepatic steatosis. *Dev. Cell* **47**, 205–221 (2018).
18. Mejhert, N. et al. The lipid droplet knowledge portal: a resource for systematic analyses of lipid droplet biology. *Dev. Cell* **57**, 387–397 (2022).
19. John Peter, A. T., Petrungaro, C., Peter, M. & Kornmann, B. METALIC reveals interorganelle lipid flux in live cells by enzymatic mass tagging. *Nat. Cell Biol.* **24**, 996–1004 (2022).
20. Renne, M. F. & Hariri, H. Lipid droplet–organelle contact sites as hubs for fatty acid metabolism, trafficking, and metabolic channeling. *Front. Cell Dev. Biol.* **9**, 726261 (2021).
21. Shubeita, G. T. et al. Consequences of motor copy number on the intracellular transport of kinesin-1-driven lipid droplets. *Cell* **135**, 1098–1107 (2008).
22. Piroska, L. et al. α-Synuclein liquid condensates fuel fibrillar α-synuclein growth. *Sci. Adv.* **9**, eadg5663 (2023).
23. Cochard, A. et al. Condensate functionalization with microtubule motors directs their nucleation in space and allows manipulating RNA localization. *EMBO J.* **42**, e114106 (2023).
24. Griseti, E. et al. Molecular mechanisms of perilipin protein function in lipid droplet metabolism. *FEBS Lett.* **598**, 1170–1198 (2024).
25. Brasaemle, D. L. Thematic review series: adipocyte biology. The perilipin family of structural lipid droplet proteins: stabilization of lipid droplets and control of lipolysis. *J. Lipid Res.* **48**, 2547–2559 (2007).
26. Sztalryd, C. & Brasaemle, D. L. The perilipin family of lipid droplet proteins: gatekeepers of intracellular lipolysis. *Biochim. Biophys. Acta Mol. Cell Biol. Lipids* **1862**, 1221–1232 (2017).
27. Ajjaji, D. et al. Dual binding motifs underpin the hierarchical association of perilipins1–3 with lipid droplets. *Mol. Biol. Cell* **30**, 703–716 (2019).
28. Wolins, N. E., Brasaemle, D. L. & Bickel, P. E. A proposed model of fat packaging by exchangeable lipid droplet proteins. *FEBS Lett.* **580**, 5484–5491 (2006).
29. Damm, A. et al. Steric repulsion counteracts ER-to-lipid droplet protein movement. Preprint at *bioRxiv* https://doi.org/10.1101/2024.11.14.623598 (2024).
30. Schulze, R. J. et al. Direct lysosome-based autophagy of lipid droplets in hepatocytes. *Proc. Natl Acad. Sci. USA* **117**, 32443–32452 (2020).
31. Lyu, X. et al. A gel-like condensation of Cidec generates lipid-permeable plates for lipid droplet fusion. *Dev. Cell* **56**, 2592–2606 (2021).
32. Chorlay, A. & Thiam, A. R. Neutral lipids regulate amphipathic helix affinity for model lipid droplets. *J. Cell Biol.* **219**, e201907099 (2020).
33. Snead, W. T. & Gladfelter, A. S. The control centers of biomolecular phase separation: how membrane surfaces, PTMs, and active processes regulate condensation. *Mol. Cell* **76**, 295–305 (2019).
34. Chorlay, A., Forêt, L. & Thiam, A. R. Origin of gradients in lipid density and surface tension between connected lipid droplet and bilayer. *Biophys. J.* **120**, 5491–5503 (2021).
35. Kamatar, A. et al. Lipid droplets as substrates for protein phase separation. *Biophys. J.* **123**, 1494–1507 (2024).
36. Welte, M. A. Expanding roles for lipid droplets. *Curr. Biol.* **25**, R470–R481 (2015).

Publisher's note Springer Nature remains neutral with regard to jurisdictional claims in published maps and institutional affiliations.

Springer Nature or its licensor (e.g. a society or other partner) holds exclusive rights to this article under a publishing agreement with the author(s) or other rightsholder(s); author self-archiving of the accepted manuscript version of this article is solely governed by the terms of such publishing agreement and applicable law.

© The Author(s), under exclusive licence to Springer Nature America, Inc. 2025

Methods

Experimental model

Human epithelioid carcinoma HeLa cells (American Type Culture Collection, ccl-2) were kept in Dulbecco's modified Eagle's medium (with 4.5 g l^{-1} D-glucose, HyClone) with 10% FBS (Gibco) and 1% penicillin–streptomycin (Sigma, P4333), at 37 °C in a 5% CO_2-humidified atmosphere. Hepatocyte-derived carcinoma HuH7 cells (American Type Culture Collection) were kept in minimum essential medium with 10% FBS (Gibco), 1% penicillin–streptomycin (Sigma, P4333), 1% minimum essential medium nonessential amino acids (Gibco) and 1% sodium pyruvate (Gibco) at 37 °C in a 5% CO_2-humidified atmosphere. Tests for mycoplasma contamination were routinely carried out.

Plasmids

The plasmids used during this study are listed in Suplementary Table 1. The pcDNA3.1-5Fm and pcDNA3.1-mCherry-5Fm plasmids were obtained as described in ref. 23. The pcDNA3.1-emGFP-Plin2 plasmid was created by replacing the 5Fm coding sequence from the pcDNA3.1-emGFP-5Fm (between the Eco47III and XbaI restriction sites) with the mPlin2 coding sequence. The pcDNA3.1-5Fm-emGFP-Plin2 plasmid was created by inserting the mPlin2 coding sequence between the XbaI and AgeI restriction sites from the pcDNA3.1-5Fm-emGFP. The pcDNA3.1-5Fm-emGFP-Plin1 plasmid was created by replacing the Plin2 coding sequence from the pcDNA3.1-5Fm-emGFP-Plin2 (between the XbaI and AgeI restriction sites) with the mPlin1 coding sequence. The pcDNA3.1-5Fm-emGFP-Plin3 plasmid was created by replacing the mPlin2 coding sequence from the pcDNA3.1-5Fm-emGFP-Plin2 (between the XbaI and AgeI restriction sites) with the mPlin3 coding sequence. The pcDNA3.1-emGFP-Plin1 plasmid was created by replacing the mPlin2 coding sequence from the pcDNA3.1-emGFP-Plin2 (between the AfeI and XbaI restriction sites) with the mPlin1 coding sequence. The pcDNA3.1-5Fm-mCherry-Plin2 plasmid was created by replacing the emGFP coding sequence from the pcDNA3.1-5Fm-emGFP-Plin2 (between the SacII and XbaI restriction sites) with the mCherry coding sequence. The pcDNA3.1-mCherry-Plin2 plasmid was created by replacing the 5Fm coding sequence from the pcDNA3.1-mCherry-5Fm (between the Eco47III and XbaI restriction sites) with the Plin2 coding sequence. The pcDNA3.1-emGFP-Plin3 plasmid was created by replacing the 5Fm coding sequence from the pcDNA3.1-emGFP-5Fm (between the Eco47III and XbaI restriction sites) with the mPlin3 coding sequence.

Transfection

For imaging after cell transfection and fixation, HeLa cells were cultured on 22 × 22 mm glass coverslips (VWR) in six-well plates (Falcon, 3.5×10^5 cells per well). For live imaging, HeLa cells were seeded on 35-mm dishes with a polymer coverslip bottom (Ibidi, 1.5×10^5 cells per dish). In both cases, adhesion surfaces were treated with a solution of 0.002% poly-L-lysine (Sigma) for 30 min. Cells were transfected with Lipofectamine 2000 (Invitrogen) 24 h after seeding. In every case, cells were incubated at 37 °C under a 5% CO_2 atmosphere.

For fixed samples, a total quantity of 2 µg of DNA was used for every well. Unless stated otherwise, when Plin1-related and Plin2-related proteins are transfected, 0.1 µg of plasmid was used. When plin3-related proteins were used, 0.5 µg of plasmid was used. When 5Fm-related proteins are transfected, 0.5 µg of mCherry-5Fm + 1.4 µg of 5Fm plasmids were used. For every condition, when the total mass of coding DNA was lower than 2 µg, an empty pcDNA3.1 plasmid was added to reach 2 µg. For live imaging, a total quantity of 0.85 µg of DNA was used, and quantities described above were scaled accordingly.

Fixation

To prepare fixed samples, cells were washed twice with PBS, and then incubated 20 min in a solution of 4% paraformaldehyde (Thermo Fisher Scientific) in PBS. Cells were washed again twice with PBS, and mounted on slides (VWR) using Vectashield mounting medium (Vector Laboratories, H-1200).

Fluorescent staining

To stain LDs with a fluorescent reporter, a solution of LipidTOX HCS Deep Red (Thermo Fisher Scientific, H34477) diluted at 1:1,000 in PBS was used. Fixed samples were exposed 30 min to this solution, then mounted on slides without washes. To reveal mitochondria, MitoTracker (Thermo Fisher Scientific, 17531655) was used following the manufacturer's protocol.

Fluorescent fatty acid assays

To feed cells with the fluorescent fatty acids BODIPY-C12 green (Fig. 5a–d), culture medium was supplemented with 200 µM of oleic acid (complexed with BSA, ratio 8:1) during the 28 h following the transfection. During the 4 h BODIPY-C12 pulse, culture medium was also supplemented with 2 µM of BODIPY-C12 green. To label cells with fluorescent BODIPY-C12 red (Fig. 6), the medium was solely supplemented with 2 µM BODIPY-C12 red, without oleic acid supplementation.

Live dissolution assay

To induce the live dissolution of condensates (Fig. 3 and Supplementary Video 2), 1 µl of FK506 (Sigma, F4679) at 2.5 mM in DMSO was added to the medium at the edge of the culture plate, after the start of live acquisition. No mixing was performed to allow the slow diffusion of FK506 in the medium to reach a final concentration of 2.5 µM.

Delipidation assays

To induce the delipidation of cells, HeLa cells were first seeded and transfected 24 h later as previously described, on a 22 × 22 mm coverslip in a six-well plate. After another 24 h, cells were washed twice with preheated Dulbecco phosphate-buffered saline (Sigma) and placed in EBSS (Thermo Fisher Scientific) containing 1% BSA (Sigma) for 24 h. Control cells were instead placed again in the same culture medium as the first steps for 24 h. Cells were then fixed and observed as described above.

Imaging

For overnight live imaging (Fig. 2 and Supplementary Video 1), cells were imaged on a Zeiss LSM 710 confocal microscope using an ×63 oil-immersion objective (PlanApochromatic, numerical aperture (NA) 1.4), at 37 °C under a 5% CO_2 atmosphere. The acquisition was started 6 h after transfection for the formation of condensates. Microscope hardware and image acquisition were controlled with LSM Software Zen 2012. For the dissolution assay (Fig. 3 and Supplementary Video 2), cells were imaged on an Olympus IX81 microscope and ×60 oil-immersion objective (PlanApo, NA 1.42), equipped with a CMOS camera, Orca-Fusion and a LED system of illumination (Spectra X, Lumencor) at 37 °C. The acquisition was started 24 h after cell transfection. Microscope hardware and image acquisition were controlled using Micro-Manager. For Airyscan images, cells were imaged with Zeiss LSM 880 confocal microscope equipped with Airyscan detector using a ×60 oil-immersion objective (PlanApo, NA 1.42). Airyscan processing was performed automatically with Zeiss Zen software (v. 2.3).

FRAP

FRAP experiments on LD-condensates in live HeLa cells were performed starting approximately 24 h after transfection. Bleaching experiments were performed in a humidified chamber maintained at 37 °C and 5% CO_2, which was mounted on a Zeiss LSM 710 META laser scanning confocal microscope (using an ×63 (NA 1.4) oil-immersion objective) and operated with the LSM Zen 2012 software. Each region of interest was scanned five times to establish the average level of initial fluorescence, then bleached using 25 iterations at 100% 488-nm laser intensity. Subsequently, the fluorescence recovery was monitored using one

acquisition every 3 s for at least 300 s. FRAP data analysis and fitting of the recovery curves were performed with Python. Fluorescence of the bleached zone was normalized using the intensity of a nonbleached zone, as far as possible from the bleaching ROI. The presented FRAP curves were also normalized using the initial average fluorescence of the ROI before bleaching as the maximum value, and its fluorescence right after bleaching as the minimum value. Fitting was performed using a biexponential decay $f(t) = A \times \exp(-t/\text{tau}) + A_{\text{init}} \times \exp(-t/\text{tau}_{\text{init}})$, with tau_{init} constrained in [0 s;1 s] to reflect the freely diffusing species. To determine the spatiotemporal FRAP patterns, kymographs were generated by measuring fluorescence evolution as a function of time across a line of interest, using Fiji.

Transmission electron microscopy

Cells fixed in 2% glutaraldehyde in 0.1 M Sörensen phosphate buffer were postfixed with 2% osmium tetroxide and stained in bloc in 2% uranyl acetate in 30% methanol. Following dehydration through a graded ethanol series, cells were embedded in Epon 812. Ultrathin sections were stained with standard uranyl acetate and lead citrate and observed with a Tecnai 12 electron microscope (Thermo Fisher Scientific). Digital images were taken with a SIS MegaviewIII CCD camera.

Data analysis

To measure mean fluorescence signals in cells (Fig. 2c and Extended Data Fig. 2), cells were systematically segmented using Cellpose[37,38] using a pretrained model, which was fine-tuned on our data, across an overnight time-lapse movie. Fluorescence mean values were then computed using Python. To obtain the signal in the cytosol only, condensates were systematically thresholded using Otsu threshold[39] provided by the scikit-image Python package[40], and fluorescence mean values were computed on the remaining areas of the cell as before. Segmentation of organelles on fluorescence images (Fig. 6) has been performed using Nellie[41], an automated organelle segmentation plugin for Napari (https://zenodo.org/records/8115575). Colocalization was then computed using Mander's coefficient m1, defined as the percentage of LDs pixels that were also located on mitochondria pixels. Plotted fluorescence profiles (Extended Data Fig. 1) were generated using Fiji[42]. All plots were generated using the seaborn Python package[43].

Statistical analysis and reproducibility

All statistical analyses were performed using Python and plotted using Seaborn. To measure the distribution of condensate features (Fig. 1e), 60 cells expressing condensates from two independent experiments were imaged through blind acquisition. Imaging and analysis were performed using a 3D stack with a *Z*-step of 0.5 µm. Counting was done manually, and size measurement was performed using Fiji. To measure the ratio of intensities (Fig. 4c), 11 (Plin1), 18 (Plin2) and 14 (Plin3) different images of LD-condensates were used. For each of them, a fluorescence profile was measured in at least four different LD interfaces, obtaining a total of 46, 73 and 61 fluorescence profiles, respectively. Counting of LDs in cells during the starving experiments (Fig. 5e,f) was performed by blind 3D acquisitions of at least 35 cells expressing condensates for each condition, from two independent experiments, followed by manual counting of all LDs in the 3D stack using a *Z*-step of 0.5 µm. The number of cells for these plots were 39 (unconfined LDs and complete medium), 45 (unconfined LDs and starving medium), 52 (confined LDs and complete medium) and 57 (confined LDs and starving medium), and cells from two independent experiments were observed through blind acquisition by selecting every cell expressing a condensate. Cell numbers for Fig. 6g are as follows: $n = 68, 93, 25, 66, 77$ and 35 cells from two independent experiments. Cell numbers for Fig. 6h are as follows: $n = 50, 82, 30, 52, 77$ and 21 cells from two independent experiments. For all experiments displaying *P* values, the *P* value was calculated using a two-sided Wilcoxon–Mann–Whitney provided by the Scipy Python package[44].

Reporting summary

Further information on research design is available in the Nature Portfolio Reporting Summary linked to this article.

Data availability

All data needed to interpret and analyze the research in the article are present in the paper and/or the Supplementary Materials. Source data are provided with this paper.

References

37. Stringer, C., Wang, T., Michaelos, M. & Pachitariu, M. Cellpose: a generalist algorithm for cellular segmentation. *Nat. Methods* **18**, 100–106 (2021).
38. Pachitariu, M. & Stringer, C. Cellpose 2.0: how to train your own model. *Nat Methods* **19**, 1634–1641 (2022).
39. Otsu, N. A threshold selection method from gray-level histograms. In *Proc. IEEE Transactions on Systems, Man, and Cybernetics* Vol. 9 62–66 (IEEE, 1979).
40. Van der Walt, S. et al. scikit-image: image processing in Python. *PeerJ* **2**, e453 (2014).
41. Lefebvre, A. E. Y. T. et al. Nellie: automated organelle segmentation, tracking and hierarchical feature extraction in 2D/3D live-cell microscopy. *Nat. Methods* **22**, 751–763 (2025).
42. Rueden, C. T. et al. ImageJ2: ImageJ for the next generation of scientific image data. *BMC Bioinform.* **18**, 529 (2017).
43. Waskom, M. L. seaborn: statistical data visualization. *J. Open Source Softw.* **6**, 3021 (2021).
44. Virtanen, P. et al. SciPy 1.0: fundamental algorithms for scientific computing in Python. *Nat. Methods* **17**, 261–272 (2020).

Acknowledgements

We thank M. Omrane for his help with the project. C.A. was supported by a PhD fellowship from ENS. D.S. was supported by the Labex IPGG (ANR-10-IDEX-0001-02). This work was supported by the Centre National de la Recherche Scientifique, Ecole Normale Superieure and ANR (ANR-22-CE44-0036) to A.-R.T., J.S. and Z.G., and the foundation ARC (ARCPJA2023080007011) to Z.G.

Author contributions

C.A., A.-R.T. and Z.G. conceived and analyzed the experiments. Z.G. supervised the work. C.A., D.S., E.P. and T.B. carried out and analyzed the experiments. J.S. and M.-A.P. contributed to the design of the experiments. S.S. and G.P. performed and analyzed TEM experiments. All authors analyzed the data and commented on the paper. C.A., A.-R.T. and Z.G. wrote the paper.

Competing interests

The authors declare no competing interests.

Additional information

Extended data is available for this paper at https://doi.org/10.1038/s41589-025-01915-2.

Supplementary information The online version contains supplementary material available at https://doi.org/10.1038/s41589-025-01915-2.

Correspondence and requests for materials should be addressed to Abdou Rachid Thiam or Zoher Gueroui.

Peer review information *Nature Chemical Biology* thanks Ashutosh Chilkoti, Pingsheng Liu and the other, anonymous, reviewer(s) for their contribution to the peer review of this work.

Reprints and permissions information is available at www.nature.com/reprints.

https://doi.org/10.1038/s41589-025-01915-2

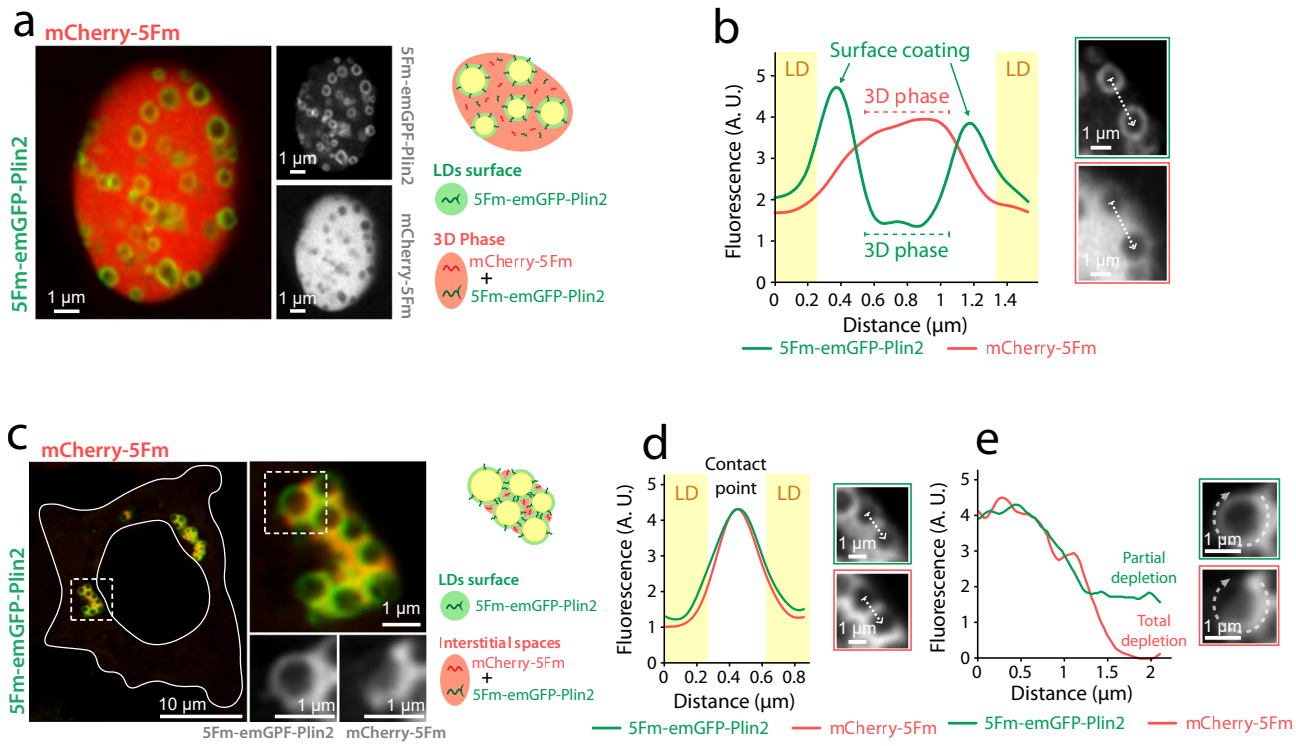

Extended Data Fig. 1 | Fluorescence profile in LD-condensates as a function of Plin2 stoichiometry. (**a**) Left, confocal imaging of LD-condensates in HeLa cells observed at low Plin2 stoichiometry. Right, schematic of the distribution of proteins composing LD-condensates. The protein corona depicted around LDs represents 5Fm-emGFP-Plin2, and the condensed phase symbolizes both protein scaffolds (5Fm-emGFP-Plin2 and mCherry-5Fm). (**b**) Plot profile of fluorescence signals across two LDs within LD-condensates. Dashed arrow shows the profile section. The fluorescence background was set to the cytosol fluorescence signal, and the intensity scale is arbitrary. Yellow rectangles indicate LDs. (**c**) Left, Confocal imaging shows patterns of LDs' beads-on-a-string arrangements of LDs in HeLa cells at high Plin2 stoichiometry. Cells were fixed 24 h after transfection with 5Fm-emGFP-Plin2, mCherry-5Fm, and 5Fm at high Plin2 stoichiometry (plasmid ratio = 5:5:10). Right, schematic of the distribution of protein scaffolds. (**d**) Plot profile of fluorescence signals between two LDs within LD-condensates. The dashed arrow shows the profile location. The fluorescence background was set to the cytosol fluorescence signal, and the scale is arbitrary. Yellow rectangles indicate LDs. (**e**) Plot profile of fluorescence signals around an LD. The experiments were independently repeated three times with the same results. For all panels, scale bars are 10 μm for full cell images and 0.5 μm for zooms.

https://doi.org/10.1038/s41589-025-01915-2

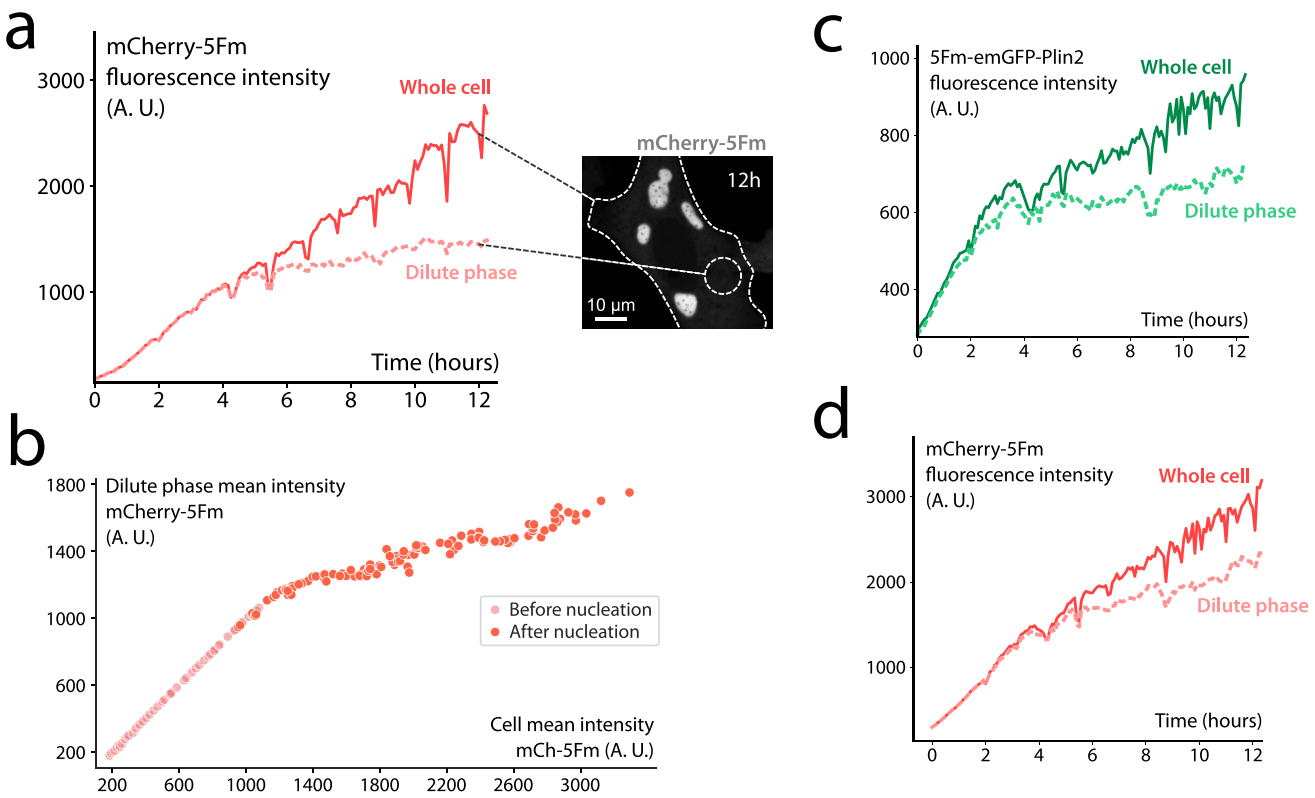

Extended Data Fig. 2 | Fluorescence intensities during LD-condensates formation. (**a**) mCherry mean fluorescence intensities during the formation of LD-condensates in the same HeLa cell as Fig. 2d. The whole-cell intensity comprises the entire cell area, whereas the dilute phase intensity corresponds to the mean intensity of the areas outside LD-condensates. The event of nucleation correlates with the slope break of the dilute phase intensity. Scale bar, 10 µm. (**b**) Evolution of solubilized mCherry-5Fm fluorescence compared to total fluorescence, before and after condensates nucleation. (**c**) GFP mean fluorescence intensities during the formation of LD-condensates in another HeLa cell. (**d**) mCherry mean fluorescence intensities during the formation of LD-condensates in the same HeLa cell as (**c**). The experiments in were independently repeated two times with similar results.

https://doi.org/10.1038/s41589-025-01915-2

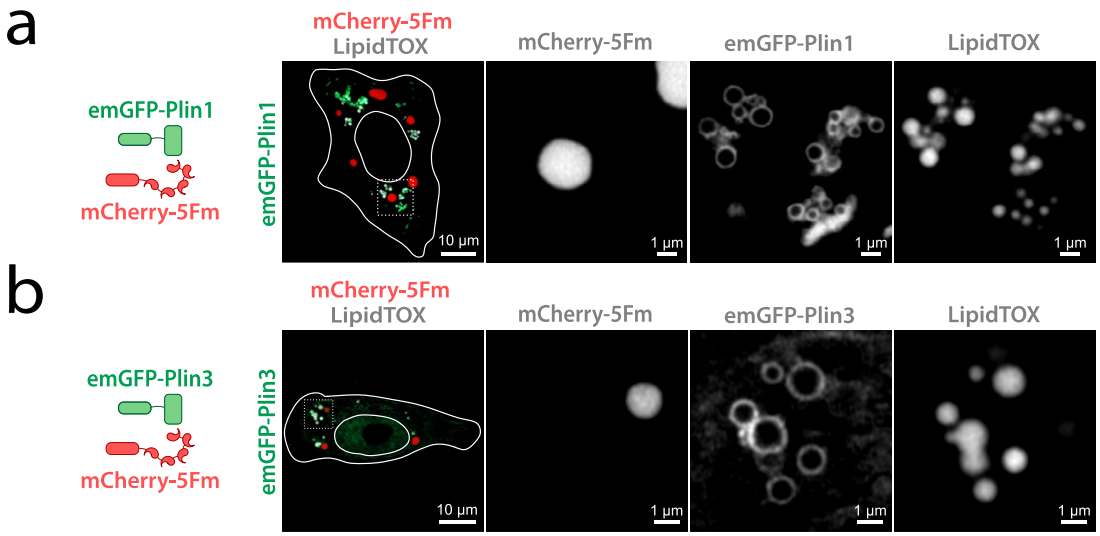

Extended Data Fig. 3 | Plin1 and Plin3 LDs with 5Fm condensates. (**a**) Confocal imaging of mCherry-5Fm condensates and Plin1-coated LDs in HeLa cells. Cells transfected with emGFP-Plin1, mCherry-5Fm, and 5Fm (plasmid ratio = 1:5:14). (**b**) Confocal imaging of mCherry-5Fm condensates and Plin3-coated LDs in HeLa cells. Cells were transfected with emGFP-Plin3, mCherry-5Fm, and 5Fm (plasmid ratio = 1:1:2). The experiments were independently repeated three times with similar results. For all panels, and LDs were marked using LipidTOX, and scale bars are 10 μm for full cell images and 1 μm for zooms.

https://doi.org/10.1038/s41589-025-01915-2

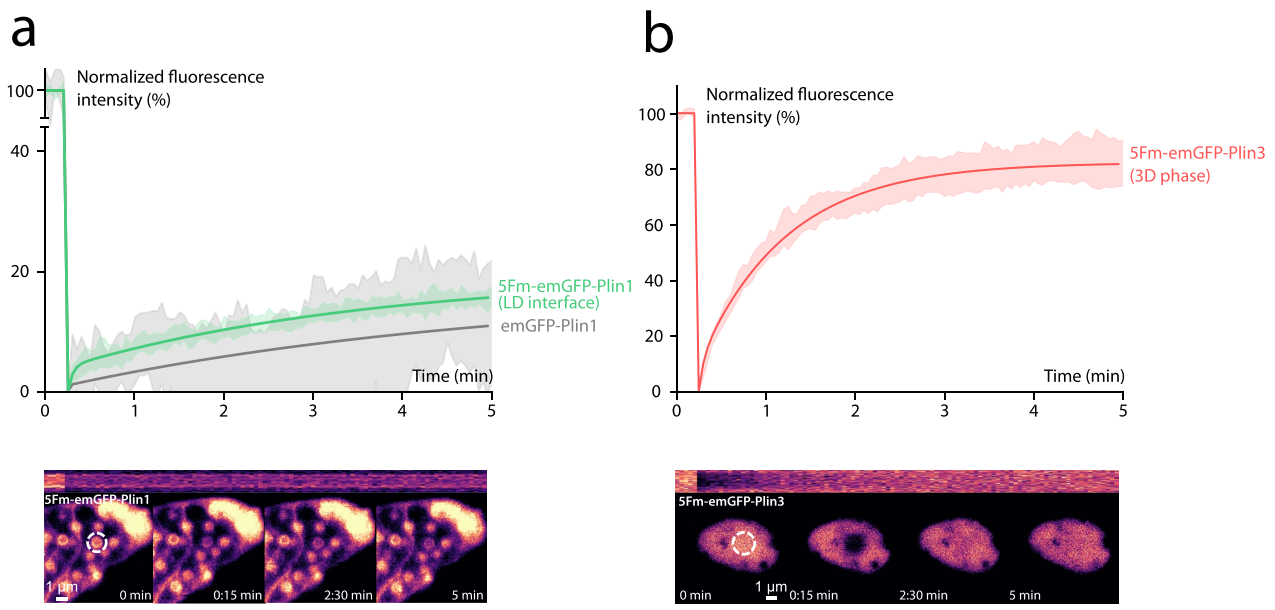

Extended Data Fig. 4 | Fluorescence recovery after photobleaching. (**a**) FRAP performed on 5Fm-emGFP-Plin1 within LD-condensates (green curve, 8 cells) and at LD surface (black curve, 12 cells); and (**b**) on 5Fm-emGFP-Plin3 within the 3D phase of LD-condensates (red curve, 9 cells). The experiments were independently repeated two times with similar results. Scale bar, 1 µm.

https://doi.org/10.1038/s41589-025-01915-2

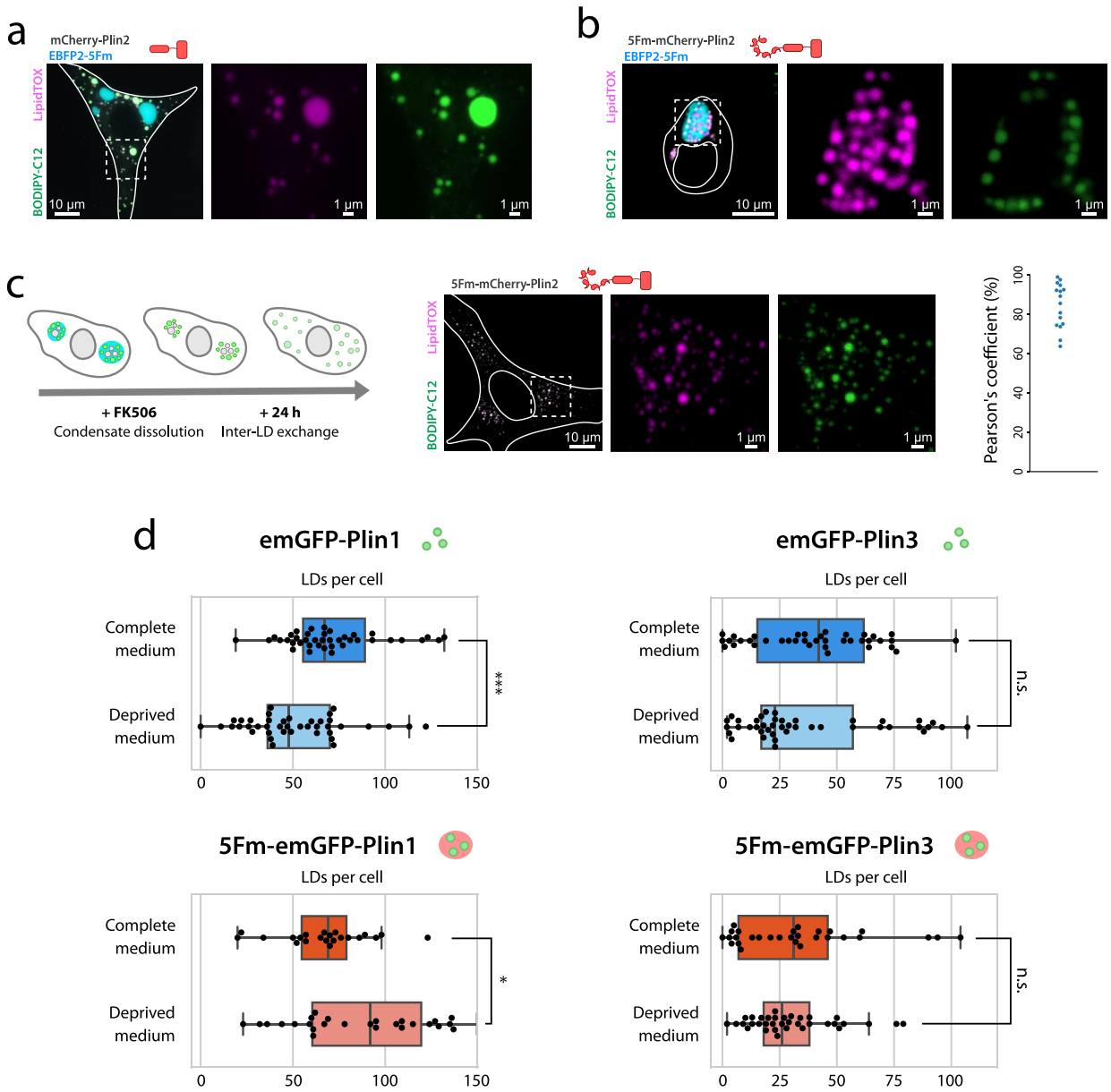

Extended Data Fig. 5 | Resuming LD dynamics through condensate dissociation. (**a**) Spinning-disk imaging of Plin2-coated LDs (LipidTOX and BODIPY-green staining) with non-functionalized condensates in HeLa cells (EBFP2-5Fm). Cells were transfected with plasmids mCherry-Plin2, EBFP2-5Fm, and 5Fm (plasmid ratio = 1:5:14). (**b**) Spinning-disk imaging of LDs confined into Plin2-condensates in HeLa cells. (**c**) Left, Schematic of the release of confined LDs containing BODIPY-labeled LDs. Right, spinning-disk imaging of released LDs, 24 h after condensate dissolution. Colocalization between BODIPY and LipidTOX was determined using Pearson's coefficient (10 cells). The experiments were repeated independently three times with similar results. (**d**) Effect of starvation on cells expressing unconfined and confined LDs. Mean number of LDs per cell, for cells expressing at least one LD-condensate, with and without starvation. Top left, unconfined LDs coated with emGFP-Plin1 (p-value: 5×10^{-4}). Bottom left, effect of starvation on confined LDs in Plin1-condensates (p-value: 7×10^{-2}). Top right, effect of starvation on unconfined LDs coated with emGFP-Plin3 (p-value: 4×10^{-1}). Bottom right, effect of starvation on confined LDs in Plin3-condensates (p-value: 9×10^{-1}). Two independent experiments were analyzed. For all panels, scale bars are 10 µm for full cell images and 1 µm for zooms.

https://doi.org/10.1038/s41589-025-01915-2

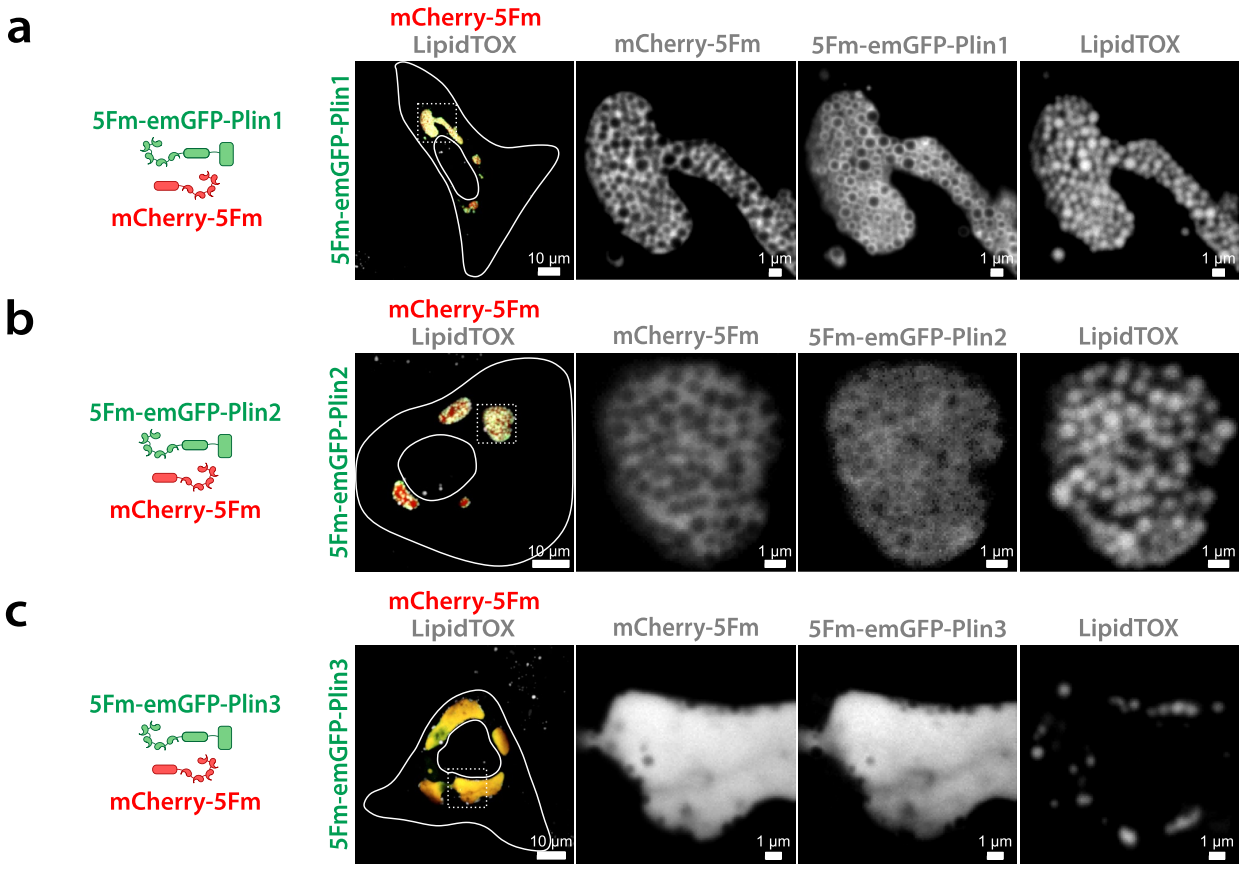

Extended Data Fig. 6 | Formation of LD-condensates in HuH7 cells. (**a**) Spinning-disk imaging of LD-condensates in HuH7 cells using Plin1 scaffolds. Cells were transfected with plasmids 5Fm-emGFP-Plin1, mCherry-5Fm, and 5Fm (plasmid ratio = 1:5:14). (**b**) Spinning-disk imaging of LD-condensates in HuH7 cells using Plin2 scaffolds. transfected with plasmids 5Fm-emGFP-Plin2, mCherry-5Fm, and 5Fm (plasmid ratio = 1:5:14). (**c**) Spinning-disk imaging of LD-condensates in HuH7 cells using Plin3 functionalized LLPS scaffolds. Cells were transfected with plasmids 5Fm-emGFP-Plin3, mCherry-5Fm, and 5Fm (plasmid ratio = 1:1:2). The experiments in were repeated independently three times with similar results. For all panels, scale bars are 10 µm for full cell images and 1 µm for zooms.

https://doi.org/10.1038/s41589-025-01915-2

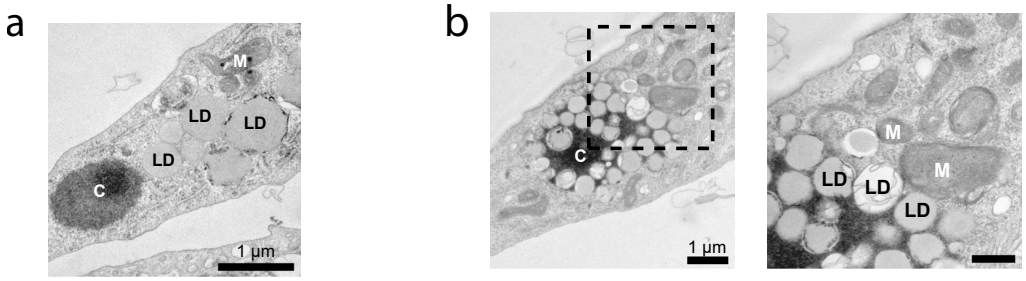

Extended Data Fig. 7 | Representative TEM of Plin1-coated LDs and LD-condensates in starvation condition. (**a**) Ultrastructural characterization of non-functionalized condensate, LDs and mitochondria of HuH7 expressing for 24 h emGFP-Plin1, mCherry-5Fm, and 5Fm (plasmid ratio = 1:5:14) (C: condensate, M: mitochondria, scale bar: 1 µm). (**b**) Representative TEM image of LDs-trapped into a large Plin1-condensate in starvation condition. The experiments were independently repeated two times with similar results. (Scale bar: 1 µm, 0.5 µm for the zoom).

6 Conclusion and transition

This work establishes **ControLD** as a general strategy to reversibly control lipid droplet surface accessibility in living cells. By functionally decoupling LD surface access from global lipid synthesis or degradation, ControLD provides causal control over LD trafficking and contact formation, and reveals how physical sequestration alone reshapes lipid exchange and organelle crosstalk. In mammalian cells, we showed that this system arrests inter-LD fatty-acid exchange, preserves LDs under starvation and transiently lowers LD-mitochondria contact frequency, with rapid restoration of fluxes and contacts upon dissolution.

Methodologically, ControLD provides a generalizable template for 'tether condensates' as programmable regulators of organelle interactions: modular in targeting, orthogonally switchable, and compatible with live-cell readouts of flux and contact dynamics. The approach complements genetic knockouts or pharmacology by isolating the contribution of geometry and access to organelle function, allowing systematic structure-function tests (e.g., scaffold valency, material state, dissolution kinetics) to map how crowding at a surface rewires downstream metabolism. As such, the article positions LLPS-based confinement as a versatile experimental method to causally probe LD physiology and organelle crosstalk.

Chapter 3

Design and application of LD-entrapment techniques to the microalga *Phaeodactylum tricornutum*

Objectives

In this chapter, we aim to deploy **ControLD** in the diatom *Phaeodactylum tricornutum*, establishing inducible expression and investigating whether different LLPS scaffolds are able to phase-separate in Pt. We then functionalize condensates with endogenous and heterologous LD-binding proteins and evaluate strategies to promote scaffold–LD interaction.

Contents

1 From mammalian cells to *Phaeodactylum tricornutum* **96**
2 Experimental strategies **102**
2.1 Adapting the ControLD scaffolds to *Phaeodactylum tricornutum* 102
2.2 Pt transformation 102
2.3 Choice of promoter 103
2.4 Introducing Fm-Ft as an alternative scaffold for phase separation 103
2.5 Development of a method for quantitative condensate localization and measurement 105
3 Expression of non-targeted condensates in Pt **108**
3.1 Description of artificial condensates in Pt 108
3.2 Quantitative analysis of condensate growth rate 110
3.3 Concentration buffering effect of condensate formation 111
3.4 Dynamic properties of condensates in Pt 113
3.5 Development of a live-imaging setup for Pt 115
3.6 Live dissolution of condensates in Pt 117
4 Functionalization of condensates for lipid droplets targeting **120**
4.1 Functionalization with endogenous LD-associated proteins 120
4.2 Optimization of LD-targeting strategies 125

4.3 Induction of bigger LDs to favor StLDP recruitment 129
5 Discussion and perspectives **131**
6 Material and methods **135**

1 From mammalian cells to *Phaeodactylum tricornutum*

In the previous chapter, this thesis has described how lipid droplets can be trapped and studied in mammalian cells. This work established both the possibility of engineering phase-separated scaffolds to confine LDs and the biological significance of such confinement for organelle dynamics and metabolic accessibility. The next step of our study is to test the confinement framework in a real unicellular organism: although the systems used in the previous chapter were immortalized cells lines, mammalian cells evolved in the context of multicellular organisms and rely on tissue-level interactions and systemic regulation. This would allow us to explore new biological questions in a fully autonomous biological system.

Moreover, we searched to broaden the biological scope and orient the study toward a phylogenetically distant system: to distinguish what is universal from what is context-dependent in our ControLD framework, it is essential to test our tools and questions in a fundamentally different type of eukaryotic cell. We sought a model that contrasts with mammalian cells in terms of energy acquisition, cellular architecture, and ecological niche, while still forming lipid droplets as a central organelle of metabolic regulation. These considerations motivate the choice of a microalgal model, the diatom *Phaeodactylum tricornutum* (Pt). With its unicellular nature, evolutionary distance, widespread use, and strong lipid accumulation response, Pt provides an ideal model. Applying our LD-trapping system in this context will allow us to evaluate the versatility of our method, identify conserved versus divergent phenomena, and situate LD regulation within the broader diversity of eukaryotic life.

Presentation of *Phaeodactylum tricornutum*

Phaeodactylum tricornutum is a unicellular marine diatom belonging to the Stramenopiles, a major eukaryotic lineage distinct from both plants and animals. With more than 100,000 estimated species, diatoms are major contributors in global carbon fixation despite their microscopic size.

Diatoms arose from a secondary endosymbiotic event, in which a heterotrophic eukaryote engulfed a red alga, giving rise to a complex photosynthetic lineage[134] (see figure 3.1). In particular, its plastid is surrounded by four membranes[135]: in Pt, the outermost membrane is continuous with the endoplasmic reticulum, forming a chloroplast-ER bundle that complexifies the topology of organelle interactions. This arrangement contrasts with mammalian cells, which lack plastids and whose organelle contact landscape is dominated by the endoplasmic reticulum. The architecture of Pt therefore provides a different platform for organelle communication, with LDs frequently juxtaposed to both chloroplasts and the ER.

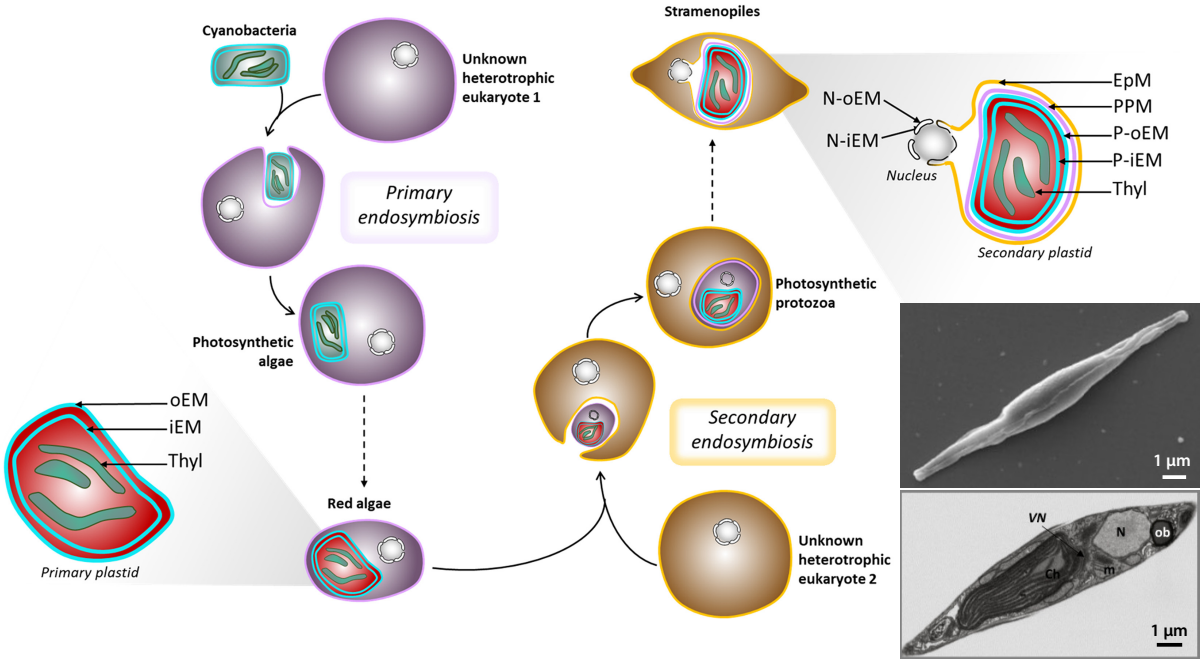

Figure 3.1: Schematic representation of primary and secondary endosymbiosis, and organelle architecture in evolution of *Phaeodactyum tricornutum*. EpM, epiplastidial membrane; PPM, periplastidial membrane; P-oEM and P-iEM, plastid outer and inner envelope membranes respectively; Thyl, thylakoids; N-oEM and P-iEM, nucleus outer and inner envelope membranes respectively. Adapted from [Guéguen et al. 2021]. Images from [Francius et al. 2008] and [Flori et al. 2016], VN, vesicular network; Ch, chloroplast; m, mitochondrion; N, nucleus; ob, oil body (a.k.a lipid droplet).

Structurally, Pt is a pennate diatom with axial symmetry. However, while most diatoms are encased in intricate silica frustules, Pt instead secretes extracellular polysaccharides and shows morphotype-dependent rigidity[135]. The cell wall is especially rigid in Pt: if the microalga *Microchloropsis* can deform upon lipid accumulation, Pt cell wall does not deform and instead constrains LD sizes. This intermediate behavior places Pt between highly silicified diatoms and other walled plant and algae cells.

Energy Metabolism: autotrophy versus heterotrophy

A major distinction between Pt and mammalian cells lies in their energy metabolism. Pt is a photoautotroph, meaning it can harness light energy to fix inorganic carbon (CO_2) into organic molecules. Through photosynthesis in its plastid, Pt produces biomolecules such as sugars from CO_2 and water, releasing O_2 as a byproduct. This mode of metabolism allows microalgae to contribute roughly 50% of global primary production in the biosphere[135], despite their microscopic size. Pt can grow in a simple seawater-based medium with light and a few inorganic nutrients (the most critical being nitrogen, phosphate and iron), synthesizing all the organic matter it needs. Mammalian cells, in contrast, are obligate heterotrophs – they must consume pre-formed organic compounds (like glucose, amino acids, lipids) in their environment to generate energy and build biomass.

They rely on mitochondrial respiration and glycolysis of external nutrients and have no ability to convert CO_2 into organic carbon.

Pt exemplifies the concept of a "metabolic mosaic." Its plastids carry plant-like pathways, including fatty acid synthesis, while its cytosol harbors a complete urea cycle, a pathway usually restricted to animals[135]. This unusual mixture, a legacy of endosymbiosis and horizontal gene transfer, equips Pt with a metabolic flexibility: depending on conditions, it can grow autotrophically but also mixotrophically using different carbon sources such as glucose, acetate, fructose, and glycerol[136, 137]

Lipid metabolism and lipid droplet biology in *P. tricornutum*

As explained in the previous chapters, lipid droplets are ancient and conserved organelles that serve as cytosolic depots for neutral lipids. Their presence in both Pt and mammalian cells suggests a common evolutionary origin, yet their different composition and regulation reflect the divergent ecological context of these organisms.

Lipid droplets in *Phaeodactylum tricornutum* share the universal eukaryotic architecture of a neutral lipid core surrounded by a glycerolipid monolayer, but their detailed composition reflects the unique physiology of diatoms. As in mammals, triacylglycerols (TAGs) represent the dominant neutral lipid, accounting for 99% of total lipids, with only trace amounts of polar lipids such as phosphatidylcholine (PC), the betaine lipid DGTA, and the chloroplast sulfolipid SQDG[131]. The presence of both ER-derived lipids (PC) and plastid-derived lipids (SQDG) in the LD monolayer suggests that diatom LDs are connected to the ER and the complex plastid. While membrane sterols (e.g. brassicasterol) can also be detected, TAG clearly dominates the storage function of diatom LDs, compared to the more diverse lipid distribution of mammalian LDs. In general, the main components of the fatty acid profile of Pt TAG are palmitic acid (C16:0) and palmitoleic acid (C16:1), which are favored for biodiesel production[138]. Interestingly, it includes substantial levels of long-chain polyunsaturated fatty acids (PUFAs), especially the health–beneficial ω3 eicosapentaenoic acid (C20:5)[138].

The surface of diatom LDs is stabilized and regulated by a set of specialized proteins. Notably, Pt and its stramenopile relatives do not possess homologs of the well-known LD-coating proteins of plants (oleosins and LDAP/LDIP) or animals (perilipins). Instead, they have evolved lineage-specific structural proteins that associate with the LD monolayer. The most prominent LD coat protein in *P. tricornutum* is the Stramenopile-type Lipid Droplet Protein (StLDP). StLDP was originally identified by proteomic analysis of isolated LDs as the most abundant LD-associated protein in this diatom[139]. It appears to be unique to stramenopiles, with no close analog in green algae or animals. StLDP is a relatively hydrophobic protein predicted to adopt an amphipathic hairpin structure that inserts into the LD monolayer[131]. Functionally, StLDP acts as a scaffold protein

that influences LD size and number. Loss-of-function studies have shown that deleting the StLDP gene leads to fewer but much larger lipid droplets per cell, without a change in total neutral lipid stored[140, 141]. This phenotype confirms that StLDP presence helps to maintain a higher number of smaller droplets, effectively modulating LD morphology. StLDP localizes specifically to the LD surface and intriguingly also to regions of the endoplasmic reticulum associated with the plastid[141]. Notably, StLDP has been proposed to participate in LD turnover as well; the protein contains a conserved autophagy interaction motif, hinting that it might target lipid droplets for macroautophagy[131].

A second LD-associated protein termed Pt Lipid Droplet Protein 1 (PtLDP1) has been noted in some studies – it shares some features with a *Fistulifera* diatom LD protein (DOAP1) and is predicted to form a β-barrel structure in the LD monolayer[142]. Like StLDP, PtLDP1 may contribute to regulate droplet size or stability, although its function is less characterized.

As in most eukaryotes, Pt expresses a conserved Seipin homolog, an ER membrane protein critical for LD formation[134]. In mammals, Seipin loss often results in aberrant LD morphology and impaired lipid storage in non-adipogenic cells[143], and in hypertrophic LDs in adipocytes[144]. Intriguingly, diatom PtSeipin knockouts display larger LDs and accumulate even more TAG, especially under light stress[134]. This suggests that while Seipin retains its ancestral role in organizing ER-LD junctions, its regulatory influence on lipid flux has evolved in diatoms.

More broadly, high-resolution proteomics of Pt LDs identified an unexpectedly diverse collection of proteins on the droplets. These include not only enzymes directly involved in lipid metabolism (such as acyltransferases for TAG synthesis and lipases for TAG catabolism) but also proteins related to vesicle trafficking, membrane fusion, and even components of the translation and degradation machinery.[145]

Stress responses and environmental adaptation

In Pt, LD formation is closely linked to stress adaptation. Nitrogen deprivation induces a redirection of carbon flux into triacylglycerol (TAG), producing abundant LDs that increase in size[146]. These LDs function as reservoirs of energy and carbon skeletons, allowing LDs to expand and store up to 20-30% of cell dry weight during starvation, buffering the cell until favorable conditions return[135]. This apparently surprising behavior is due to a physiological slowdown: cell division is halted but the photosynthetic machinery is still operational, leading to excess energy and lipid accumulation.

Beyond nutrient limitation, Pt encounters a wide range of abiotic stresses in its natural marine environment. Light fluctuations, temperature changes, and oxidative stress all modulate its physiology. Photosynthetic organisms must balance energy capture with protection against photodamage, and LDs have been implicated in sequestering fatty

acids and pigments that mitigate oxidative stress. Compared with mammalian cells, which operate in buffered tissue environments, Pt exemplifies the resilience required for survival in open oceans. This resilience is relevant to confinement studies: Pt's robustness makes it particularly suited for testing how artificial confinement alters LD dynamics, in ways that would be more difficult to observe in fragile mammalian cells.

P. tricornutum as a model organism

Historically, Pt was adopted as a laboratory model because of its unusual morphology and culture flexibility and over time, it has grown into a cornerstone of diatom genomics and synthetic biology. *Phaeodactylum tricornutum* is highly compatible with laboratory cultivation, with rapid asexual reproduction with no need for a sexual cycle (no sexual stage has ever been observed in this species)[147]. Cultures of *P. tricornutum* grow robustly in simple media, enabling convenient maintenance and experimental manipulation. Importantly, its entire genome has been sequenced and annotated[148] (along with the organellar genomes), providing extensive genetic information and curated databases for molecular analyses. Moreover, a collection of molecular techniques has been established to genetically probe and modify *P. tricornutum*. Stable nuclear transformation was initially achieved via biolistics (particle bombardment) methods, using the *shble* selectable marker to confer zeocin resistance[149]. This opened the door to routine insertion of foreign DNA and transgene expression in the diatom (e.g., introduction of reporter genes under native promoters). Subsequently, electroporation-based protocols were developed to facilitate DNA uptake with high efficiency, eliminating the requirement for a gene gun apparatus[150].

More recent innovations have further enhanced this diatom's genetic tractability. An autonomously replicating plasmid system has been created, allowing exogenous DNA to be maintained as an episome rather than integrating into the genome[151]. These episomal vectors (delivered, for example, by conjugation with *E. coli*) replicate stably in *P. tricornutum* and support high-throughput functional studies by avoiding the complications of random chromosomal integration. In parallel, genome editing via CRISPR/Cas9 has been successfully implemented. Pioneering work demonstrated that a diatom-codon-optimized Cas9 and guide RNA can induce precise, heritable gene knockouts in *P. tricornutum*[152]. Before this, targeted mutagenesis in Pt was performed using TALENs[153], but this new approach enabled considerably simpler reverse-genetic analyses. The ease of culturing and clonally propagating *P. tricornutum*, the availability of its fully sequenced genome, and the collection of genetic tools (from classical transformation with selectable markers to modern episomal expression and CRISPR editing) establish this diatom as an ideal model organism for genetic and cell biology research.

Biotechnological relevance

The applied interest in Pt stems from its ability to accumulate high levels of neutral lipids, pigments, and bioactive compounds. Under nitrogen starvation, Pt channels carbon into TAG, making it a candidate for biofuel feedstocks. It naturally produces omega-3 fatty acids such as EPA, which are essential for human health and widely used in nutraceuticals[134]. Additionally, Pt synthesizes the carotenoid fucoxanthin, a compound with antioxidant and pharmaceutical potential. Unlike terrestrial oil crops, Pt and other microalgae can be cultivated on non-arable land using seawater, sunlight, and CO_2, offering a sustainable path for lipid and pigment production. These features position Pt at the intersection of basic and applied research, making it both a model organism for understanding diatom biology and a useful model for metabolic engineering.

Positioning Pt for confinement studies

For the purposes of this study, Pt provides specific advantages for studying LD dynamics under engineered confinement. Its photoautotrophic growth reduces reliance on complex media, enabling long-term single-cell experiments in microdevices. Chlorophyll autofluorescence serves as an intrinsic marker of photosynthetic health, while neutral lipid dyes allow quantitative imaging of LDs in vivo. These optical properties, combined with its robust LD accumulation under stress, create an experimentally rich platform.

By applying our LD-trapping system to Pt, we can test whether the confinement strategy validated in mammalian cells generalizes to an autotrophic chassis. This comparative analysis will help parse conserved principles of LD biology from lineage-specific differences, while also demonstrating the versatility of the trapping approach.

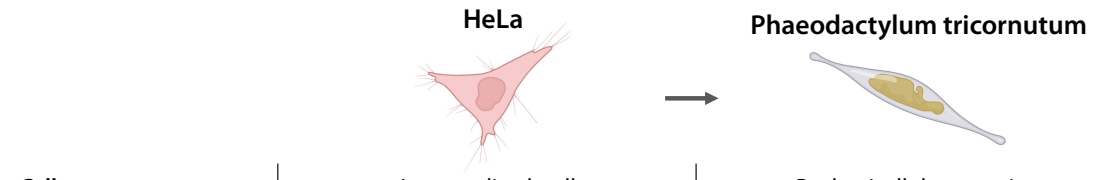

	HeLa	*Phaeodactylum tricornutum*
Cell category	Immortalized cells	Real unicellular organism
Energy source	Heterotroph	Photoautotroph
Transformation technique	Chemical transfection	Biolistic transformation
Transformation type	Transient expression	Inducible stable cell line
Transformation timeframe	1h (Chemical transfection)	8 weeks (biolistics / selection / screening)

Figure 3.2: Main experimental differences between the mammalian cell model used in the previous chapter and the diatom *Phaeodactylum tricornutum*.

2 Experimental strategies

2.1 Adapting the ControLD scaffolds to *Phaeodactylum tricornutum*

The first step in adapting the LD-trapping system to *Phaeodactylum tricornutum* was to redesign the protein scaffolds for expression in this new organism. The scaffolds used in mammalian cells were codon-optimized for human expression, but Pt has a similar codon usage and no optimization was necessary for our scaffolds. However, the scaffolds needed to be adapted to the specific molecular biology tools available for Pt. In particular, we sought to incorporate the StLDP protein as a LD-targeting domain, replacing the mammalian perilipin2 (Plin2) used previously. StLDP is the most abundant and well-characterized LD coat protein in Pt, and its inclusion would ensure proper LD localization in this diatom. In order to explore other LD-associated proteins, we also designed scaffolds using the PtLDP1 protein described above.

2.2 Pt transformation

We then aimed at expressing these new scaffolds in *Phaeodactylum tricornutum.* As stated above, one canonical and widespread way to produce proteins in algae and plants is to integrate exogenous DNA into cell genome to establish stable cell lines. This differs from the previously presented work in mammal cells, where the protein expression was transient. Biolistic transformation, also known as particle bombardment, is a physical method used to introduce foreign DNA, RNA, or proteins into cells. In this technique, microscopic particles (typically tungsten) are coated with nucleic acids and propelled at high velocity into target cells using a gene gun. Upon impact, some of these particles penetrate the cell wall and plasma membrane, delivering the genetic material directly into the cytoplasm or nucleus, where it can be expressed or integrated into the genome. This method is particularly useful for organisms that are resistant to other transformation techniques, such as microalgae, fungi, or plants with rigid cell walls. Biolistics allows stable transformation and is independent of host-vector compatibility. However, the integration of the transgene occurs largely at random, with little control over the insertion site or orientation, leading to variability in gene expression possibly disrupting endogenous genes. Furthermore, copy number is difficult to regulate, with multiple insertions frequently observed, sometimes resulting in gene silencing or instability of the transgene. These limitations are partially mitigated by generating multiple independent transformants, which can be screened for stable expression and desired phenotypes.

2.3 Choice of promoter

Selecting an appropriate promoter is crucial for transgene expression in *Phaeodactylum tricornutum*. One of the most canonical choice for transgene expression in Pt is the promoter of the fucoxanthin chlorophyll protein A (fcpA), a major component of the light-harvesting complex of Pt [149, 154]. This widespread promoter is light-inducible, leading to a constitutive expression of the transgenes under normal growth conditions. However, the continuous expression of transgenes during the lengthy selection phase may have introduced toxicity issues, as observed by a notably low success rate: only three colonies were obtained from eight biolistic transformations using **emGFP-5Fm**, **StLDP-emGFP-5Fm**, **Fm-emGFP-Ft**, and **StLDP-Fm-emGFP-Ft** scaffolds.

This low efficiency could result from prolonged scaffold-induced cytotoxicity or interference from premature condensate formation. Consequently, we shifted our strategy toward an inducible promoter, allowing precise control over the timing of protein expression, a valuable feature for our experimental approach.

Among several available inducible promoters responsive to environmental triggers, we selected the nitrate reductase promoter (*pNR*). Nitrogen is a key nutrient for diatoms like Pt, which metabolizes nitrogen as either nitrate (NO_3^-) or ammonium (NH_4^+) [155]. Importantly, the growth rate is not dependent on the used nitrogen source[156], allowing flexibility in culturing composition. Under nitrate availability, the nitrate reductase enzyme, controlled by *pNR*, is produced to reduce nitrate to nitrite. Moreover, this promoter was the first inducible promoter to be established in Pt and is nowadays considered a reliable choice. However, expression slowly cease after nitrate withdrawal [157] (see figure 3.3). As for every inducible protein expression, the produced protein may still be present for a prolonged period after the induction, depending on the protein half-life. Using only this induction therefore leads to a trapping system that is easily turned on, but not easily turned off. This is not a problem for our experiments, as we are interested in the physiological dynamics after trapping, but it is worth noting that this system is not suitable for experiments requiring a precise control of the protein expression level.

In order to avoid any protein expression during the transformation process, we routinely cultured Pt cells with ammonium, switching to nitrate only for experimental inductions, thereby avoiding potential toxicity during the selection phase and precisely controlling protein expression timing.

2.4 Introducing Fm-Ft as an alternative scaffold for phase separation

Every artificial condensate presented until now in this study has been engineered using the scaffold protein 5Fm, due to its robustness and its relative simplicity. However, another LLPS protein scaffold has been developed in our lab, hereafter called **Fm-Ft** [127]. In

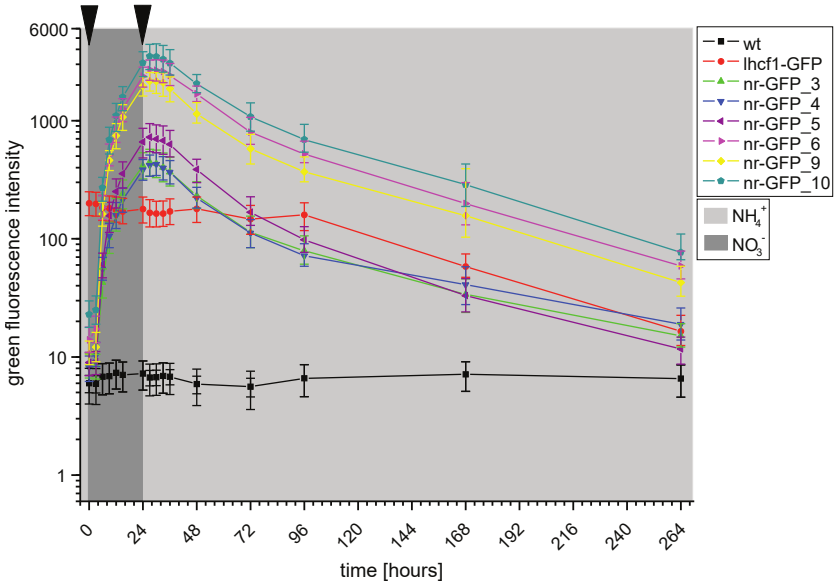

Figure 3.3: Schematic representation of the nitrate-inducible system used in *P. tricornutum*. Cells are maintained in ammonium to repress expression, and switching to nitrate medium triggers transgene induction within a few hours. Adapted from [Chu et al. 2016].

order to test experimental hypotheses using a different system, it is proposed to investigate the formation of **Fm-Ft** condensates in *P. tricornutum* alongside **5Fm** condensates.

This fusion protein is composed of two domains in this simplest form:

- A single Fm domain.
- An optional protein of interest (POI) domain.
- A human ferritin light-chain domain (Ft).

Human ferritin light-chain self-assembles into stable 24-subunit nanocages at sub-nanomolar protein concentrations[158]. These nanocages, presenting 24 Fm domains each, then interact through Fm-Fm interactions when concentration increases further, leading to the formation of a LLPS condensate.

Fm-Ft differs significantly from 5Fm:

- Thanks to its exceptionally high multivalency, **Fm-Ft** creates a LLPS at a much lower concentration than **5Fm**
- The **Fm-Ft** protein is shorter than 5Fm
- The **Fm-Ft** condensate formation mechanism is somewhat more complex that 5Fm and its straightforward nucleation step.
- In case of fusing this scaffold with other proteins of interest, the ferritin domain of **Fm-Ft** must be in C-terminal position of the protein, whereas **5Fm** is functional no matter its position.

	LLPS scaffold	LD protein	Promoter	Fluo.	Antibiotic selection	#Bltc.	#Scr.	#Pos.
1	5Fm	StLDP	*fcpB*	emGFP	Blasti.	2	4	0
2	5Fm	∅	*fcpB*	emGFP	Blasti.	2	8	0
3	Fm-Ft	StLDP	*fcpB*	emGFP	Blasti.	2	4	1
4	Fm-Ft	∅	*fcpB*	emGFP	Blasti.	2	4	0
5	5Fm	StLDP	pNR	emGFP	Blasti.	3	11	4
6	5Fm	∅	pNR	emGFP	Blasti.	2	15	3
7	Fm-Ft	StLDP	pNR	emGFP	Blasti.	2	18	2
8	Fm-Ft	∅	pNR	emGFP	Blasti.	2	14	8
9	5Fm	PtLDP1	pNR	emGFP	Blasti.	4	40	2
10	Fm-Ft	PtLDP1	pNR	emGFP	Blasti.	2	17	4
11	5Fm	∅	pNR	mOrange	Blasti.	-	-	-
12	Fm-Ft	∅	pNR	mOrange	Blasti.	-	-	-
13	∅	StLDP	pNR	emGFP	Blasti.	3	12	3
14	∅	PtLDP1	pNR	emGFP	Blasti.	1	7	4
15	5Fm	∅	pNR	mOrange	**Zeocin**	3	8	2
16	Fm-Ft	∅	pNR	mOrange	**Zeocin**	3	16	1
17	5Fm	StLDPΔNter	pNR	emGFP	Blasti.	3	13	2
18	∅	StLDPΔNter	pNR	emGFP	Blasti.	2	12	4
19	∅	HOGP	pNR	emGFP	Blasti.	2	8	1
20	5Fm	HOGP	pNR	emGFP	Blasti.	2	12	1
21	Fm-Ft	HOGP	pNR	emGFP	Blasti.	2	17	1

Table 3.1: Complete list of generated plasmids and Pt strains. Bltc.: number of biolistics performed; Scr.: number of screened colonies; Pos.: number of positive colonies showing fluorescence after nitrate induction. Blasti, blasticidine.

2.5 Development of a method for quantitative condensate localization and measurement

In order to study various properties of condensates, we aimed at developing a quantitative and reliable method to measure the size and number of condensates in each Pt cell. This task requires both an accurate cell outline detection, and a precise condensate spotting. Therefore, we opted for three-dimensional z-stack imaging to maximize information content and facilitate robust analyses.

A first analytical objective was to accurately detect the fluorescent spots corresponding to LLPS condensates in an automated workflow (figure 3.4a.). Automated detection of condensates is challenging due to substantial variability in fluorescence intensity and condensate size. Traditional thresholding approaches based solely on intensity or local maxima often resulted in false positives due to the relatively diffuse but detectable fluorescence in the plastid and cytosol.

To overcome these limitations, we employed a deep-learning approach. Most conventional deep-learning models, such as the widely used U-Net [159], are tailored for 2D

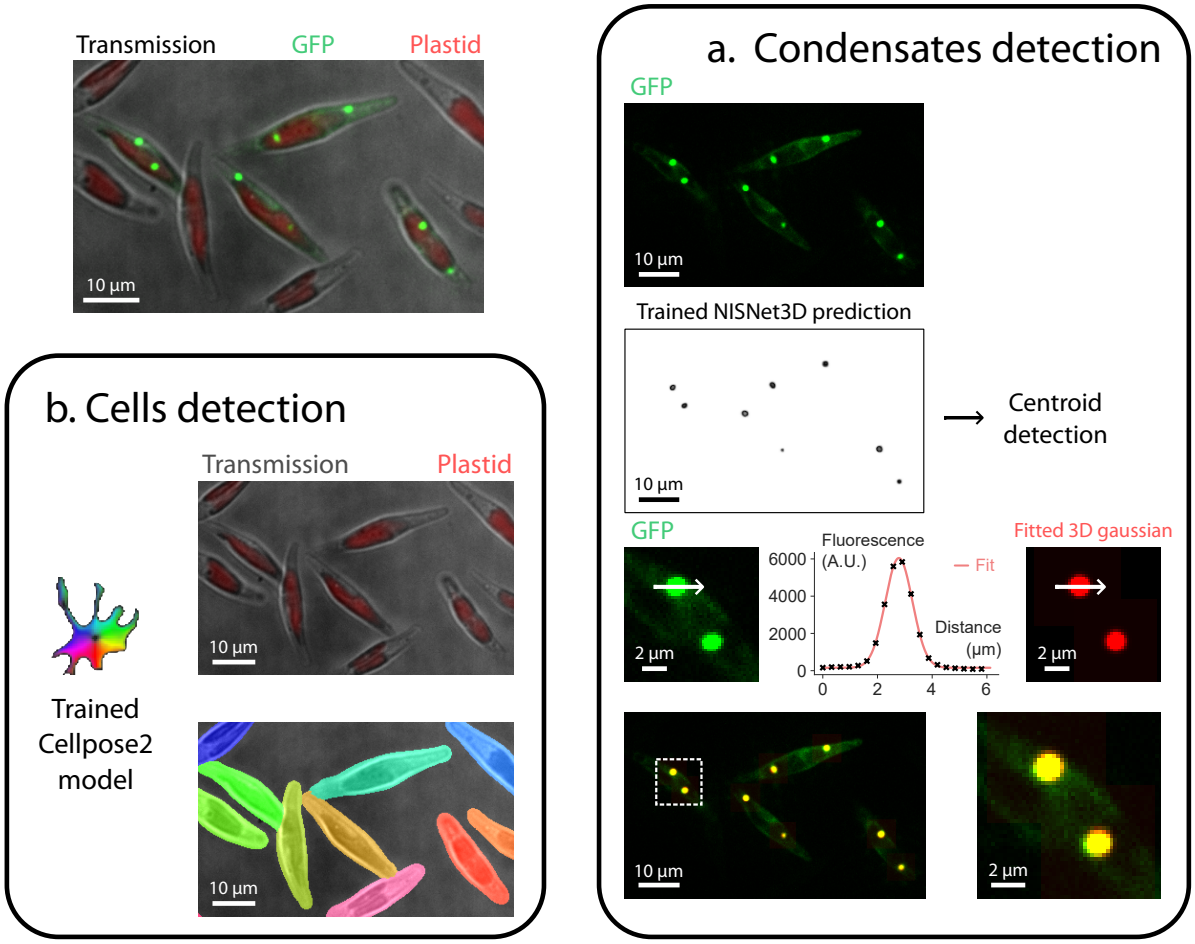

Figure 3.4: Analysis pipeline for automated detection and quantification of LLPS condensates in P. tricornutum. **a.** Trained NISNet3D deep-learning model finds condensate positions volumes from 3D z-stacks. Subsequent Gaussian fitting yields condensate size and location metrics for each cell. **b.** Cellpose trained model segments cell outlines using transmitted light and plastid autofluorescence.

images. For this study, we chose the NISNet3D convolutional neural network (CNN), a state-of-the-art model capable of direct 3D image processing [160]. Although 3D manual annotation is typically labor-intensive, the spherical morphology and distinct intensity profiles of condensates allowed effective model training with fewer annotated images compared to more complex cellular structures.

We trained a NISNet3D model using only 50 manually annotated cells presenting faint and large condensates, and no condensate at all. Once trained, the model showed a high accuracy at finding every kind of condensate, without giving false positive when processing diffuse signals. Using the NISNet3D predictions, it was then straightforward to isolate coordinates of the center of condensates, leading to an accurate count of condensates in the image.

Next, we sought to quantify condensate size accurately. Considering their submicrometer dimensions and proximity to the diffraction limit (approx. 500 nm), direct

measurement approaches were challenging. We therefore implemented a mathematical fitting approach, modeling each condensate intensity as a 3D Gaussian distribution:

$$f(x,y,z) = \sum_i A_i * \exp\left(-\frac{(x-x_i)^2 + (y-y_i)^2}{{\sigma_{xy,i}}^2} - \frac{(z-z_i)^2}{{\sigma_{z,i}}^2}\right) + B$$

Condensate coordinates, predicted by NISNet3D, served as initial estimates for the Gaussian fit. After optimization, the integrated intensity of each Gaussian function provided an indirect but reliable metric of condensate size, circumventing limitations imposed by diffraction. We chose to use the metric $I_{tot} = A * {\sigma_{xy}}^3$ as a proxy mesurement of the condensates size, assuming a spherical shape. This approach allowed us to compare condensate sizes across different images and conditions.

In parallel, to enable accurate single-cell analyses, we developed a method to detect Pt cell outlines (figure 3.4b.). We employed Cellpose [161] as in the previous chapter, training a custom model from 10 randomly selected, manually annotated cells. Using transmitted light images and plastid autofluorescence as inputs, this model precisely segmented individual cells in each z-plane. A final processing step combined segmented masks across z-planes and eliminated artifacts, ensuring robust single-cell quantification.

3 Expression of non-targeted condensates in Pt

To validate the adaptability of our LLPS scaffolds to *Phaeodactylum tricornutum*, we first assessed whether the expression of physiologically neutral, non-targeted scaffold proteins could form condensates in vivo. Inducible strains expressing **emGFP-5Fm** and **Fm-emGFP-Ft** were established using biolistic transformation (see table 3.1).

3.1 Description of artificial condensates in Pt

Since LLPS events are concentration-dependent and scaffold concentration is raising during nitrate induction, a first step was to define a standard nitrogen induction period which allows a reproducible observation of condensates. After preliminary kinetics experiments, we chose to observe the strains 3 days after changing the nitrogen source of the culture medium from ammonium to nitrate (hereafter this step will simply be called **nitrate induction**). This allows relatively high levels of scaffold proteins in the cells, and therefore a higher probability to observe condensate formations.

A first observation is that, after 3 days of induction, some of our strains were correctly presenting a fluorescent signal. Moreover, none of these strains were containing a detectable fluorescent signal (other than the endogenous signal of the plastid) before nitrate induction, validating the use of the pNR promoter as an inducible promoter with an appropriate time-frame.

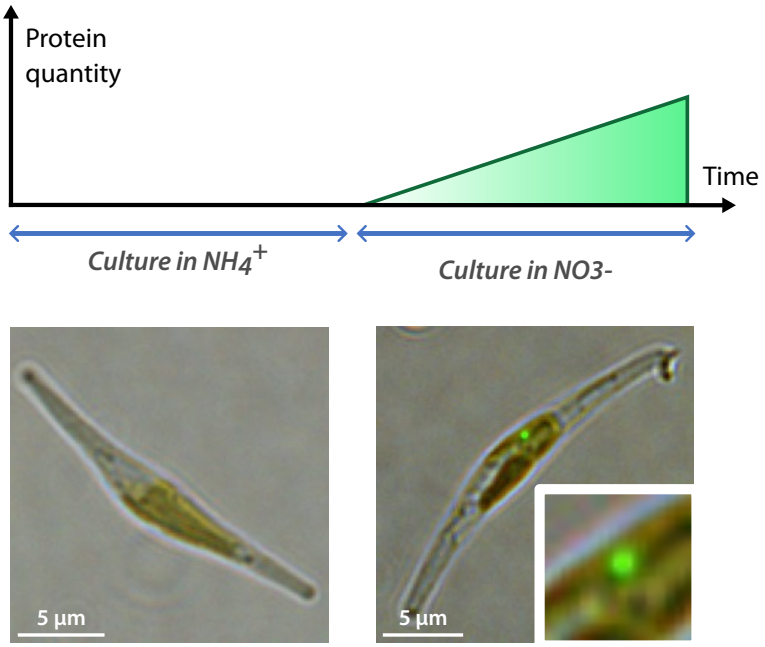

Figure 3.5: Validation of inducible GFP expression in engineered Pt strains. GFP signal is absent in ammonium-grown cells and appears only after 3 days of nitrate induction, using brightfield and epifluorescence microscopy.

We confirmed that inducible strains showed detectable fluorescence only post-induction (figure 3.5), validating the controlled expression via the *pNR* promoter. For each scaffold, colonies presenting the most satisfying fluorescence levels upon nitrate induction were selected for subsequent analyses unless otherwise specified.

Upon closer examination, one can observe micrometric and spherical fluorescent objects formed in the cytosol of the induced cells, for both **emGFP-5Fm** and **Fm-emGFP-Ft**, as depicted in figure 3.6. These structures are coherent in shape and size with what had been observed in previous studies for **5Fm** and **Fm-Ft** condensates. Most notably, these objects present a high sphericity possibly hinting at a surface tension effect, which is a hallmark of a phase-separation phenomenon. Hereafter, these objects will therefore be called "condensates" for the sake of conciseness, even though this observation enough is not sufficient to prove that these structures are indeed phase separated objects.

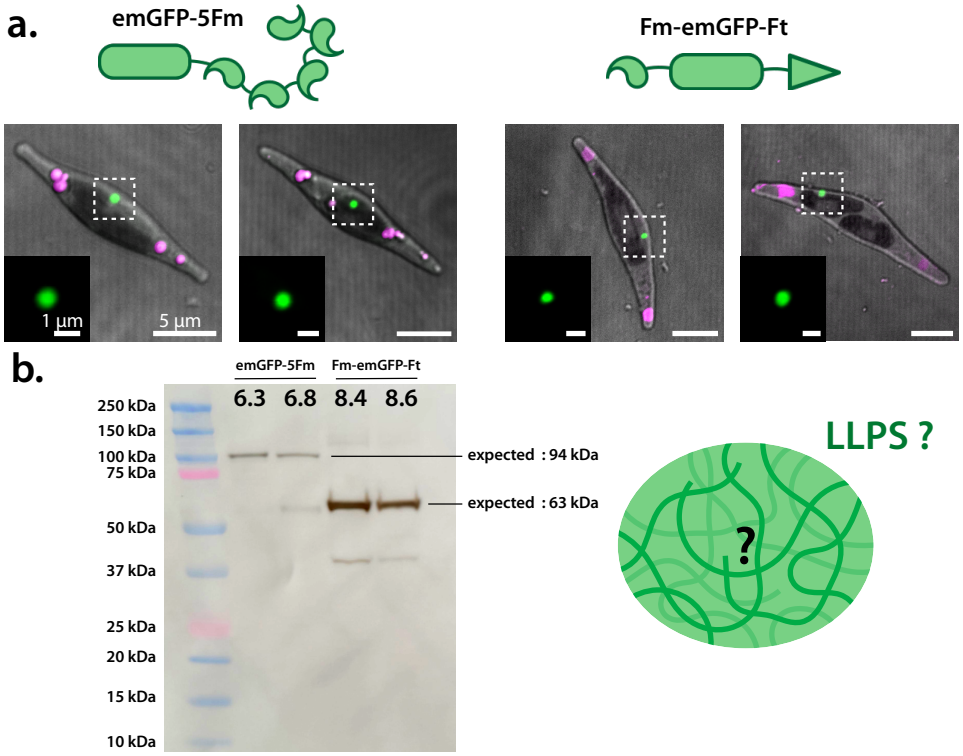

Figure 3.6: **a.** Representative confocal images of Pt strains expressing non-targeted **emGFP-5Fm** and **Fm-emGFP-Ft** condensates in Pt. **b.** Western blot probed with anti-GFP antibody shows expected molecular weights for both constructs.

Genomes of selected strains were sequenced and presented no truncation or mutation on the inserted coding sequence. Western blots have also been performed using anti-GFP staining, and showed that scaffolds expressed in the strains present the expected sizes. For the **Fm-emGFP-Ft** strains, another band is observed at 40 kDa, although much fainter than the expected band at 63 kDa. We therefore concluded that the observed GFP signals shown above does correspond to **emGFP-5Fm** and **Fm-emGFP-Ft** respectively.

Additionally, condensates showed no specific subcellular localization, with occurrences

both near and far from the plastid. In particular, no specific proximity seems to be present between condensates and the lipid droplets of Pt, indicating minimal nonspecific scaffold interactions.

In the majority of cell presenting condensates, a unique micrometric condensate is observed, but some cells with two or more condensates can also be observed (figure 3.7).

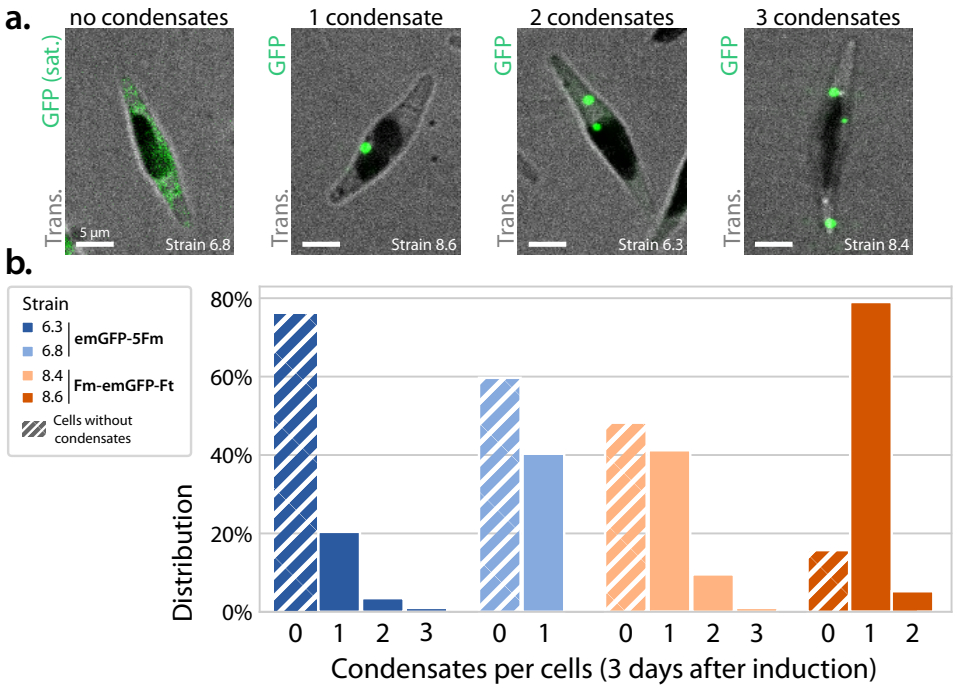

Figure 3.7: **a.** Examples of cells highlighting condensate number variability using spinning disk imaging. **b.** Distribution of the number of condensates per cell after 3 days of nitrate induction, for Pt strains expressing **5Fm-emGFP** and **Fm-emGFP-Ft**. (Preliminary data). Dashed bars represent cells without any condensates; in most cases, no fluorescence could be detected in those cells at all, and as such they were not included in the interpretation.

3.2 Quantitative analysis of condensate growth rate

Having established condensate formation, we next aimed at characterizing the temporal dynamics of their assembly. LLPS processes depend on the scaffold concentration reaching a critical threshold, and scaffold protein levels are expected to increase progressively after nitrate induction. Thus, we performed a systematic imaging of a large number of cells every day following nitrate induction, for two strains expressing **emGFP-5Fm** and two strains expressing **Fm-emGFP-Ft**. We then employed the high-throughput single-cell analysis pipeline presented in section 2.5 to quantify the number and size of condensates precisely at each time point.

Using both these analyses allowed us to extract an average number of condensates per cell, alongside an average condensate size, as shown in figure 3.8.

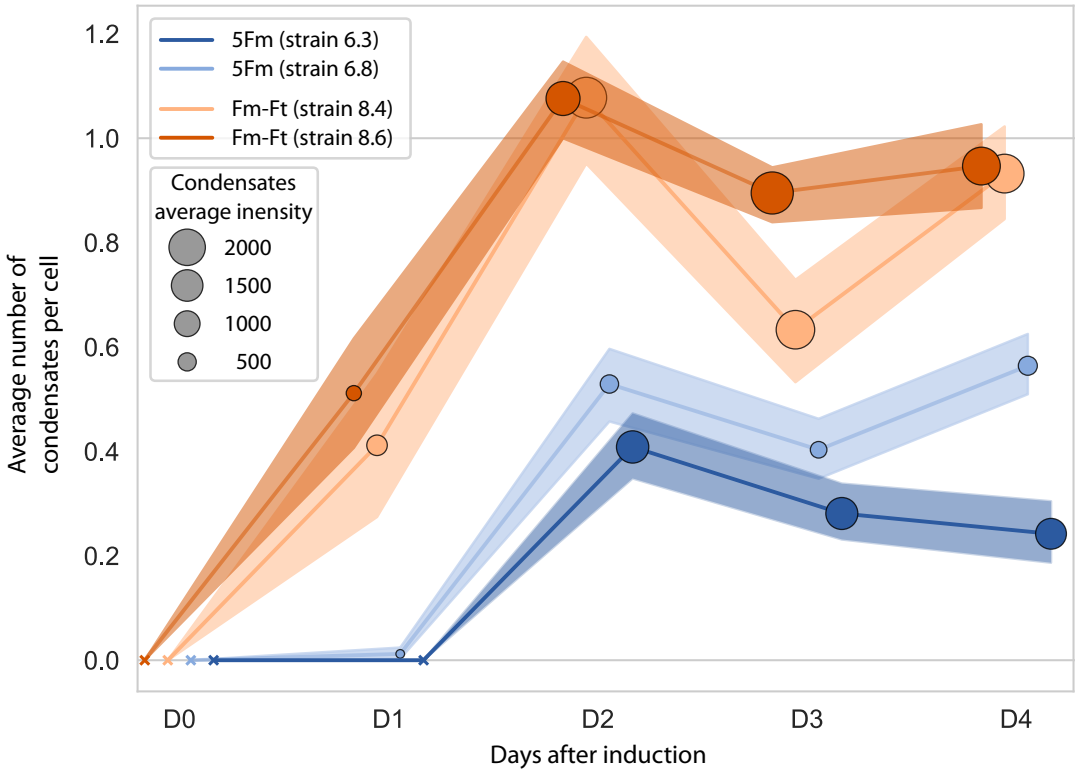

Figure 3.8: Temporal dynamics of condensate formation. Average number of condensates per cell (left axis) and mean condensate intensity plotted over days following nitrate induction for strains expressing **emGFP-5Fm** and **Fm-emGFP-Ft** (n > 200 cells per time point).

Over the course of days post-induction, both strains exhibited a progressive increase in the average number of condensates per cell, reaching a stable number by day 3. Concurrently, the mean condensate size, inferred from integrated fluorescence intensity, also increased steadily. Notably, the **Fm-emGFP-Ft** strains displayed a slightly earlier appearance of consensates, since some condensates are detected after only one day for those strains, potentially reflecting differences in nucleation dynamics due to scaffold properties. This progressive appearance of condensates is in line with a gradual increase in scaffold concentration following induction, eventually surpassing the critical threshold for LLPS.

3.3 Concentration buffering effect of condensate formation

As described in the previous chapter, a single-component LLPS presents the important hallmark of buffering the scaffold concentration in the dilute phase:

- Below a critical threshold, no condensates are able to form, resulting in a uniform diffuse fluorescence.
- Upon reaching this threshold, condensate nucleation occurs, maintaining a constant scaffold concentration in the dilute phase no matter the total protein concentration.

Moreover, this critical concentration threshold depends on the strength of interactions between scaffold proteins: a higher-affinity scaffold will be able to perform nucleation at a lower concentration. Since our LLPS components are multivalent (5 binding sites for the **5Fm** scaffold, and 24 binding sites for **Fm-Ft** particles), one has to consider the avidity of the scaffold, which is the collective effect of the individual **Fm-Fm** affinities as explained in the previous chapter. This avidity is therefore higher for the **Fm-Ft** LLPS compared to **5Fm** due to its higher valency, which should lead to a lower concentration in the dilute phase when condensates are formed.

To validate this, we imaged two **emGFP-5Fm** and two **Fm-emGFP-Ft** strains under conditions optimized for detecting weak cytosolic fluorescence three days after nitrate induction.

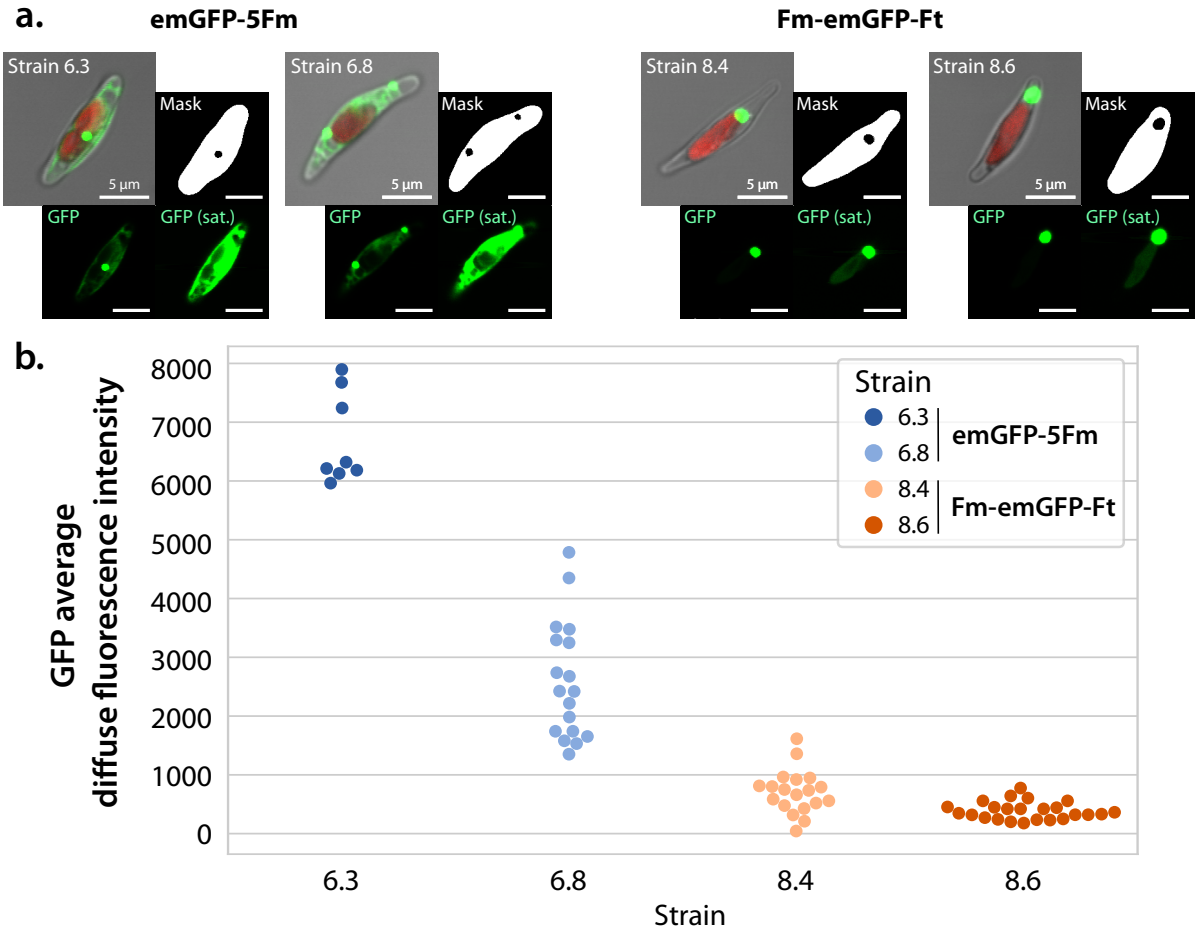

Figure 3.9: Comparison of cytosolic fluorescence between **5Fm-emGFP** and **Fm-emGFP-Ft** scaffolds. **a.** Confocal imaging displaying diffuse fluorescence in cytosol with image saturation. **b.** Measurement of average diffuse intensity measured in regions excluding condensates (as displayed in masks in **a.**)

With these acquisition parameters, one can observe a notable fluorescence in the cytosol for the two **GFP-5Fm** strains. On the other hand, strains expressing **Fm-GFP-Ft** were showing almost no cytosol signal with the same parameters, with only a faint detectable plastid autofluorescence.

To quantify the cytosol signal, cell masks were first predicted as before through Cellpose using both the transmission and far-red plastidial autofluorescence. On the other hand, condensates were thresholded using the Li thresholding algorithm [162]. The remaining area of the cell was used to obtain an average diffuse fluorescence signal. By comparing these value between strains, we observe a 10-fold (strain 5.3) and 6-fold (strain 5.8) respectively intensity difference between **5Fm** and **Fm-Ft** LLPS. Moreover, the diffuse fluorescence signals of Fm-Ft strains is due almost exclusively to the plastidial autofluorescence, and is to be considered the baseline fluorescence level of Pt.

The striking difference in the scaffold concentration in the dilute phase is coherent with the difference of avidity between **5Fm** and **Fm-Ft** leading to a specific concentration threshold to nucleate condensates for either scaffold. Surprisingly, the **5Fm** strains 5.3 and 5.8 present notably different cytosolic fluorescence levels, where the fluorescence level is expected to be the same for a given LLPS scaffold. This is possibly a measure artifact, and will be confirmed with replicates. Nonetheless, this result is a strong hint that the observed fluorescent objects are indeed LLPS-driven condensates, compared to the hypothesis of an irreversible aggregation or an accumulation in a vacuole.

3.4 Dynamic properties of condensates in Pt

Another important hallmark of a LLPS is its dynamic property: the weak Fm-Fm interactions driving the phase separation are constantly reorganized and reconfigured, giving the characteristic liquid-like behavior. In the previous chapter, we discussed that this property is the origin of a surface tension giving condensate a spherical shape, and that this dynamic equilibrium could be disrupted using the chemical Fm-Fm competitor FK506.

In order to assess that the objects described above are actual LLPS, we proposed to investigate condensate dissolution properties in *P. tricornutum*, using the strains expressing **emGFP-5Fm**. We used the same nitrate induction protocol as above, using Pt cells exposed to nitrate three days before the experiment and presenting fully formed condensates. A straightforward first test was to add FK506 to the cell culture medium during 1h, using the same concentration as the LLPS dissolution experiments on mammalian cells (2.5 µM). However, no phenotype change could be found, and cells were still containing condensates.

One of the key differences of Pt cells structures compared to mammals is the presence of a cell wall surrounding the cell membrane. Even if we previously established that FK506 permeates the mammalian plasma membrane, no data is available regarding this thicker and denser layer, and we hypothesized that this negative result indicates that FK506 is not able to permeate Pt cell wall.

To address this issue, we investigated another way to perturb the Fm-Fm interaction. DMSO is a solvent known for its efficient membrane penetration properties across a wide

variety of cells, including diatoms [163]. DMSO is also used in some imaging protocols for Pt, such as NileRed staining for fluorescent marking of LDs, and is therefore compatible with fluorescence observation while preserving Pt cell integrity.

Moreover, crystallographic studies reported that DMSO is able to form a weak complex with FKBP at the approximative same binding site as FK506[164](figure 3.10a.), theoretically allowing to use it to dissolve condensates at high concentrations. We therefore chose to test the effect of DMSO exposure on Pt cells expressing condensates, for different concentrations.

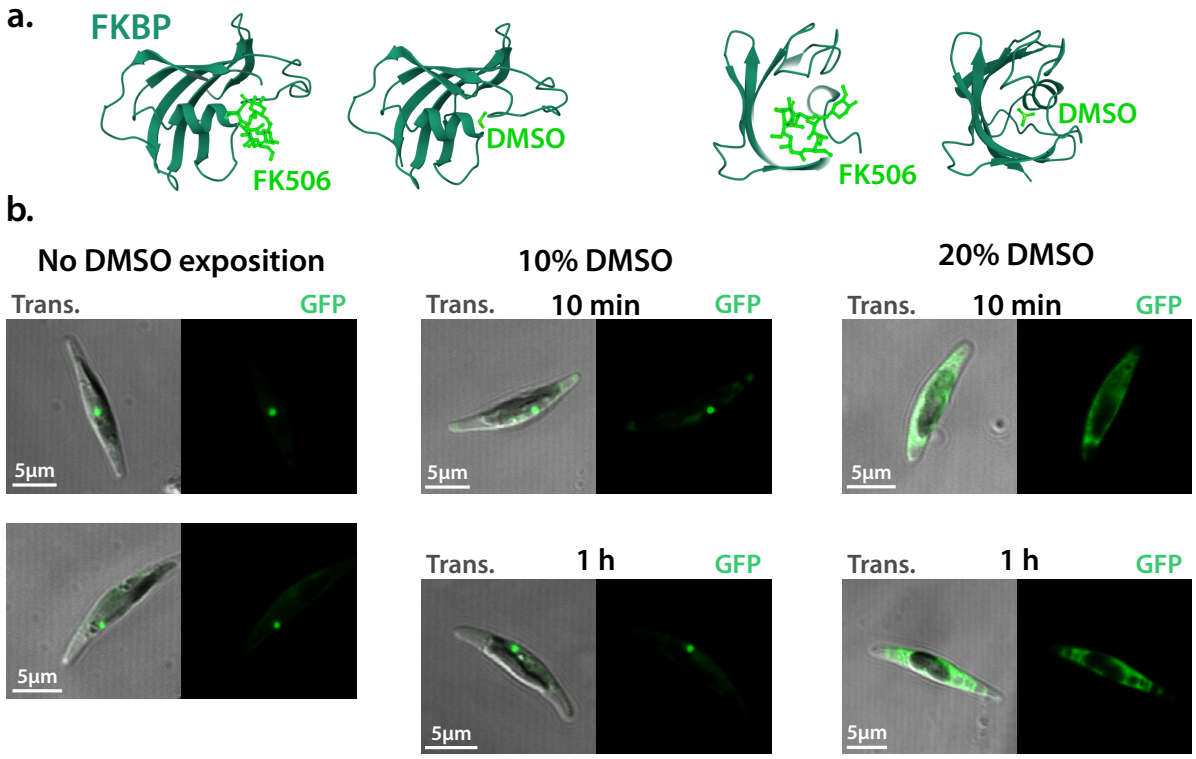

Figure 3.10: Effect of DMSO on **5Fm** condensates. **a.** structures of interaction between FKBP and respectively FK506 and DMSO (from [Burkhard et al. 2000]). **b.** Confocal imaging of Pt cells expressing **5Fm-emGFP** using different concentrations of DMSO. Cells were exposed to DMSO either 10 min or 1h before observation.

A clear and notable effect emerges here, as shown in figure 3.10b. At lower DMSO concentrations (2%, 5%, 10%), condensates remain unaffected, and no apparent phenotypic alterations occur. However, upon treatment with 20% DMSO, condensate-containing cells completely lose their distinct phenotype, replaced instead by uniform cytosolic fluorescence. Remarkably, this outcome is consistent across all cells, with no detectable condensates remaining under these conditions. Furthermore, identical observations at 10 min and 1 h post-exposure imply that prolonged incubation at 10% DMSO does not induce condensate dissolution, suggesting a equilibrium-driven phenomenon.

After this first observation, we hypothesized that the DMSO treatment could help FK506 to permeate inside Pt cells. However, we did not observe any change in the

condensate morphology after a 1h FK506 treatment at 2.5 µM, even after a 10% DMSO pre-treatment. This result suggests that DMSO is not able to facilitate FK506 permeation through the cell membrane.

The disappearance of condensates could indicate a disruption of the Fm-Fm interaction due to DMSO, and therefore hints toward a dynamic and reversible organization of the condensate. However, it is not possible to conclude with this observation whether the condensates really underwent a LLPS dissolution. DMSO is indeed reported to perturb a wide variety of sub-cellular organizations, and the disappearance of the localized fluorescent signal could also be the result of the disruption of an endogenous membrane, leading to a release of the scaffold in the cytosol. In order to have a definitive answer, one needs to investigate the time scale of this change of morphology.

3.5 Development of a live-imaging setup for Pt

We then aimed at elucidating the dynamics at LLPS-related events at a single-cell scale, to gain a better understanding of what mechanisms are involved. Classical observation of time-points during experiments has been proven useful, but we now aim to probe at time scale and chronology of events. Our next goal was to develop a method for live-imaging of Pt based on micropatterning. This approach would enable us to directly observe dynamic cellular behavior in real-time, particularly regarding condensate dynamics within individual Pt cells.

A straightforward approach would have been to immobilize Pt cells in low-melting agar, or deposit them directly on agar. However, our experimental design required spatial immobilization of cells while maintaining them in liquid medium, preserving routine culture conditions and allowing medium exchange during observation. To do so, we proposed to adapt a novel system of micropatterned microscopy wells, using biologically compatible and optically transparent materials [165]. Although these wells were initially developed in another team of our laboratory to visualize reconstituted biological processes, we planned to use these microwells as holders for live Pt in order to perform controlled live-imaging experiments.

Those microwells are built using a PDMS stamp generated from photolithographically produced molds, as depicted in figure 3.11. This stamp is applied onto a microscopy coverslip, and a photo-polymerizable resin (Norland Optical Adhesive 85S, NOA) is injected in between. Using UV exposition, NOA is photo-polymerized, and PDMS stamp is finally removed. These wells present different diameters ranging from 50 to 100 µm, and are 40 µm deep. The microwells are ready to use, and Pt cells are finally deposited in the wells.

Initially, we assessed whether this microwell system was compatible with Pt cell viability. Wild-type Pt cells in exponential growth phase were deposited into microwells and observed daily under routine culture conditions (controlled illumination, temperature,

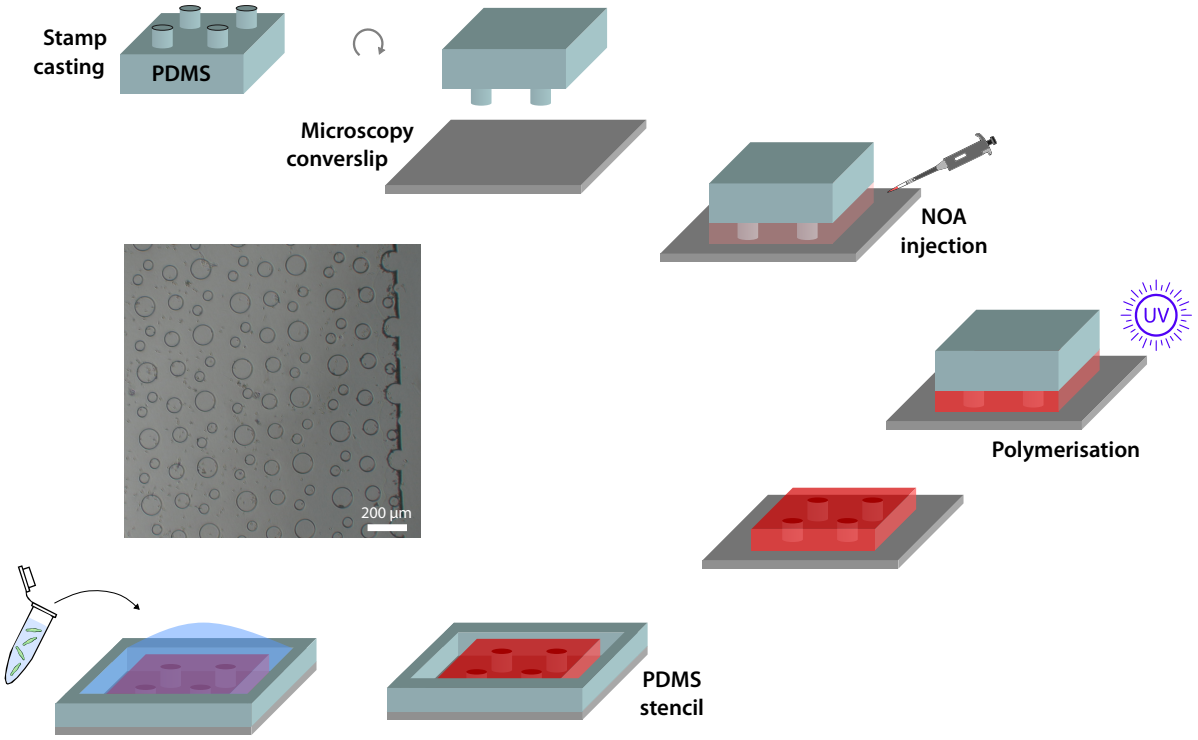

Figure 3.11: Procedure for micropatterned well fabrication. PDMS stamps cast from photo-patterned molds are used to imprint Norland Optical Adhesive (NOA) on coverslips. This process creates wells (50-100 µm diameter, 40 µm depth) to be used for spatially confined live imaging of Pt cells.

and humidity).

As shown in figure 3.12, we observed that, in some wells, several cell division happened after the first day, denoting no strong alteration of metabolic functions. Based on their position and the fact that the new cells are still partially attached, we assessed that these cells are the result of a cell division rather than cells that fell in the well between time-points. However, subsequent cell divisions were not detected after prolonged confinement, suggesting a limitation in nutrient or gaseous exchange in this format over longer time scales. Nevertheless, these microwells remained suitable for shorter-term (up to one day) live-cell imaging studies.

A next step was to use this setup during a live microscopy acquisition, to validate the feasibility of this system. After a few tests, we realized that simply patterning the microwells on coverslips dish was not sufficient to prevent drying, and we therefore decided to pattern the microwells on the bottom of ibidi dishes.

Live overnight acquisitions was then performed, using minimal brightfield and fluorescence illumination parameters. Using plastidial autofluorescence as a metabolic state reporter, we could assess that cells were not strongly stressed or damaged by this time-lapse imaging. However, alghtough some divisions were observed (figure 3.13), all of them happened during the first 6 hours of the overnight timelapse. We concluded that either

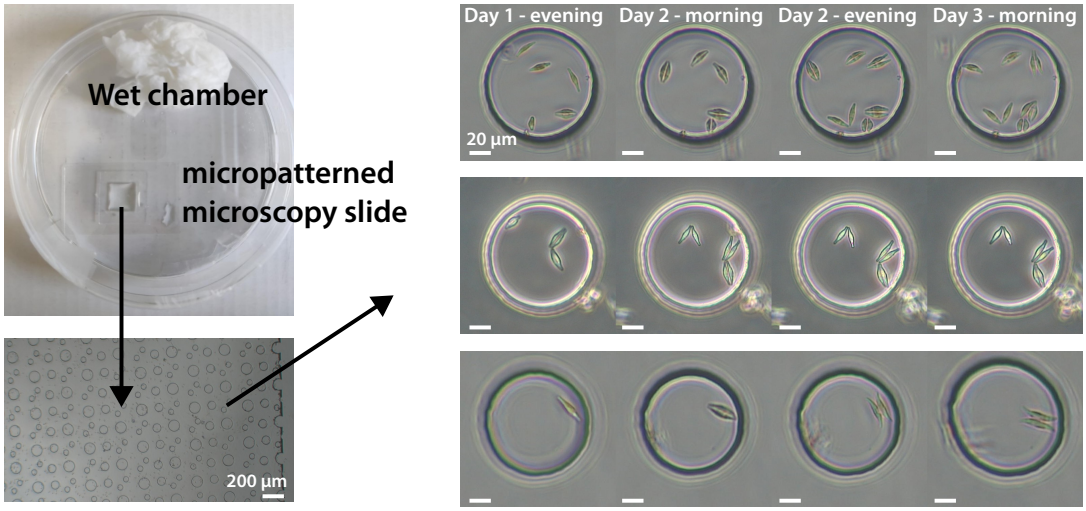

Figure 3.12: Left: Wet chamber containing the microwells used for daily imaging. The microwells are patterned onto a coverslip and surrounded by a PDMS stamp, and immersed in a drop of Pt culture media. Right: Examples of cell divisions over days in some microwells using brightfield microscope.

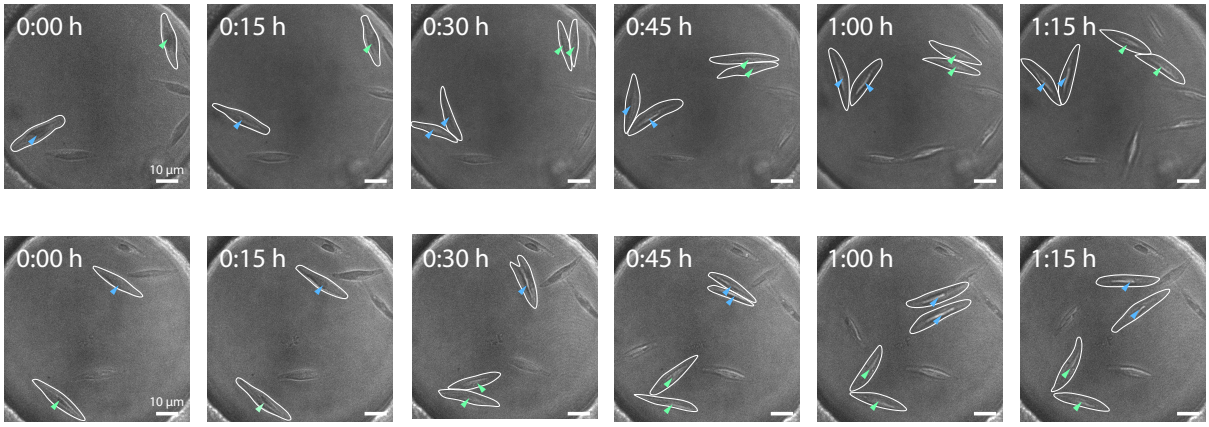

Figure 3.13: Overnight time-lapse of wild-type cells in microwells using spinning disk microscopy. Minimal brightfield and autofluorescence imaging (not shown) reveal several cell divisions (outline and arrows) during the first 6 h.

the microscopy illumination or the setup itself was inhibiting cell division, since many core physiology of Pt is highly dependent of the circadian regulation[166]. This nonetheless proved the setup appropriate for short-to-medium duration (several hours) live-imaging experiments, and sufficient for assessing rapid condensate dynamics.

3.6 Live dissolution of condensates in Pt

We then aimed at using the previously described setup to immobilize cells while being able to image them, and focused on elucidating the dynamics of the DMSO dissolution experiment described before. The live observation of this phenomenon could allow us to discriminate whether a dynamic dissolution is happening, and therefore bring another

hint at the LLPS nature of the observed condensates.

To do so, we used again the microwells system in an ibidi dish described above, since the setup had been proven relevant for short and mid-term timelapses. We performed live experiments using a strain expressing **5Fm** condensates placed inside microwells. After the start of the live imaging, the medium was switched to a medium containing 20% DMSO during acquisition, by slowly adding a 40% DMSO medium into the ibidi dish on top of the cells.

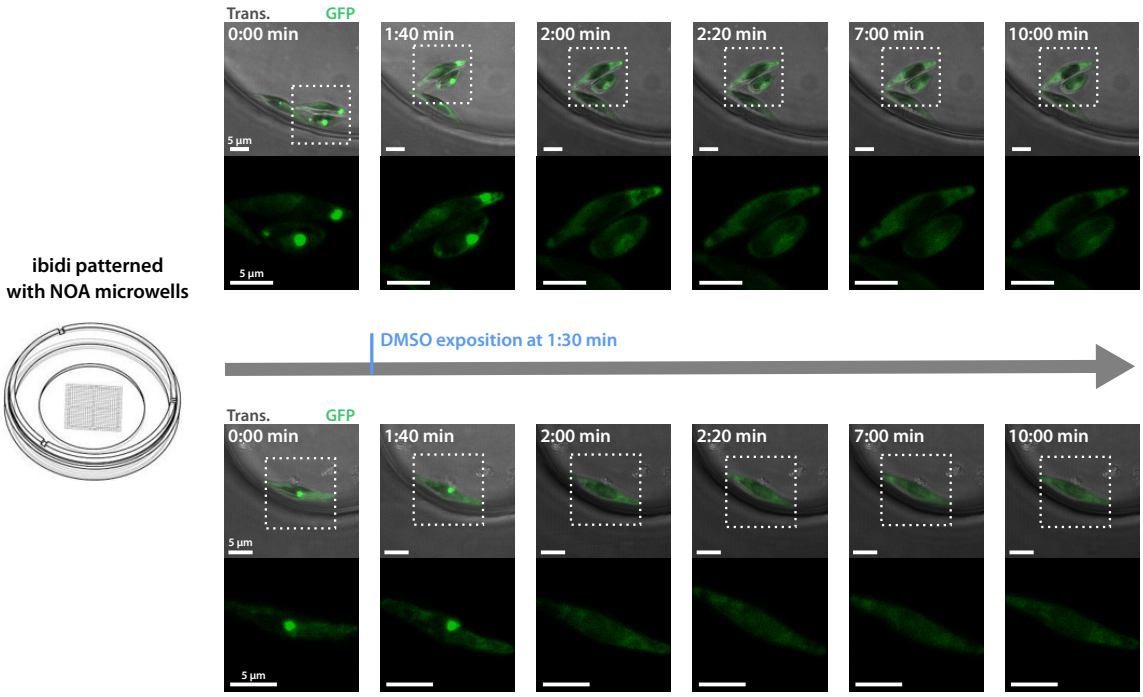

Figure 3.14: Real-time dissolution of condensates upon DMSO addition. **emGFP-5Fm** condensates in strain 6.3 disappear within 30 s after 20 % DMSO is introduced at 1 min 30 s, shifting to uniform cytosolic fluorescence.

As depicted in figure 3.14, we observe here an extremely rapid transition from the presence of the condensate to a uniform cytosolic fluorescence. Additionally, no morphology change is observed in terms of organelles nor membrane integrity right after DMSO addition. After 10 min, we can observe that the cells are starting to be affected by the high concentration of DMSO, with a notable shrink of the plastid. However, the much quicker time scale of condensate disappearance is another hint toward a dynamic object and points therefore toward a chemical LLPS dissociation, compared to a damaged membrane leading to a protein leakage in the cytosol, or a degradation of a protein aggregate.

Altogether, these findings indicate that we managed to recreate the artificial phase-separated condensates **5Fm** and **Fm-Ft** in the microalga *Phaeodactylum tricornutum* by establishing nitrate-inducible stable cell lines. These condensates consistently exhibit hallmarks of LLPS, including spherical morphology, avidity-dependent concentration buffering, and dynamic reversibility under appropriate chemical perturbation, suggesting a LLPS mechanism. However, complementary biophysical characterization such as FRAP would be necessary to definitely confirm the LLPS nature of these condensates.

4 Functionalization of condensates for lipid droplets targeting

We successfully engineered two different kind of artificial liquid-liquid phase separation in *Phaeodactylum tricornutum*. This demonstrates the feasibility of our LLPS-based encapsulation method in Pt, and we aimed next at functionalizing those condensates with LD-specific proteins to reproduce our LD-trapping system in the microalga.

4.1 Functionalization with endogenous LD-associated proteins

Functionalization with StLDP

As a first LD-associated protein candidate, we tested to functionalize the LLPS scaffolds with the Stramenopile Lipid Droplet Protein (StLDP). As described above, this protein has been identified as the major lipid droplet protein in Pt and is reported to localize around lipid droplets[141]. We constructed and introduced plasmids encoding **StLDP-emGFP-5Fm**, **StLDP-Fm-emGFP-Ft**, and the control **StLDP-emGFP** into Pt using the established biolistics protocol. All constructs were under the control of the nitrate-inducible promoter and analyzed after a three-day induction period as presented in the previous section.

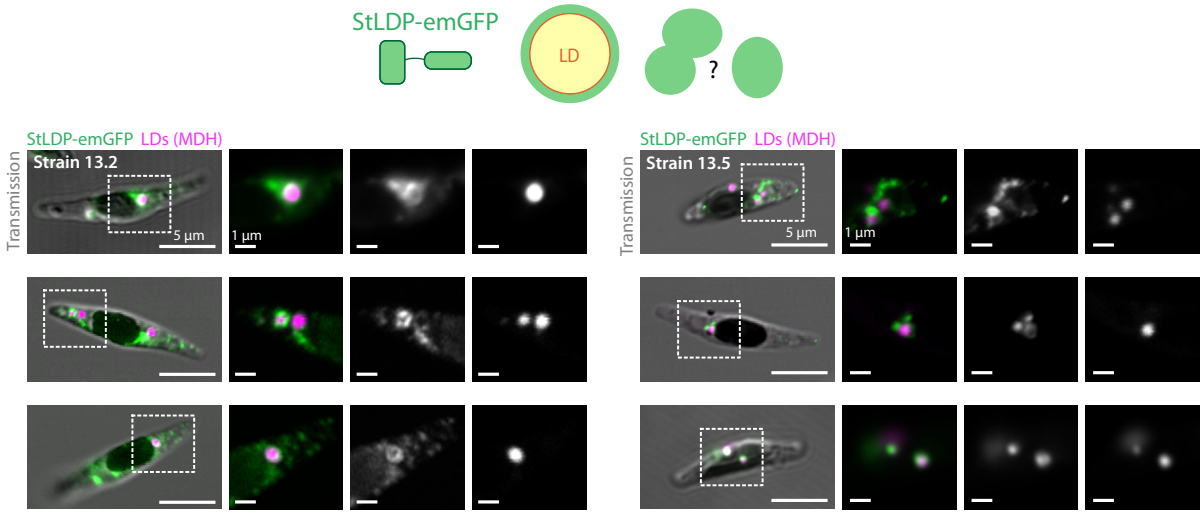

Figure 3.15: Confocal imaging of *P. tricornutum* strains expressing **StLDP-emGFP** after 3 days of nitrate induction. GFP signal localizes to LD surfaces in several cells, while dense cytosolic aggregates can also be observed in the same cells.

In strains expressing **StLDP-emGFP**, we observed heterogeneous localization patterns, as shown in figure 3.15. Some LDs are presenting an enriched GFP signal on their surface as expected. However, in several cells, we also observed accumulation of protein unrelated to LD positions. In these cases, StLDP is likely recruited to the ER, as this localization has also been observed by other teams under non-stressed conditions.

We then investigated the strains expressing **StLDP-emGFP-5Fm** and **StLDP-Fm-emGFP-Ft**, having considered this control StLDP localization.

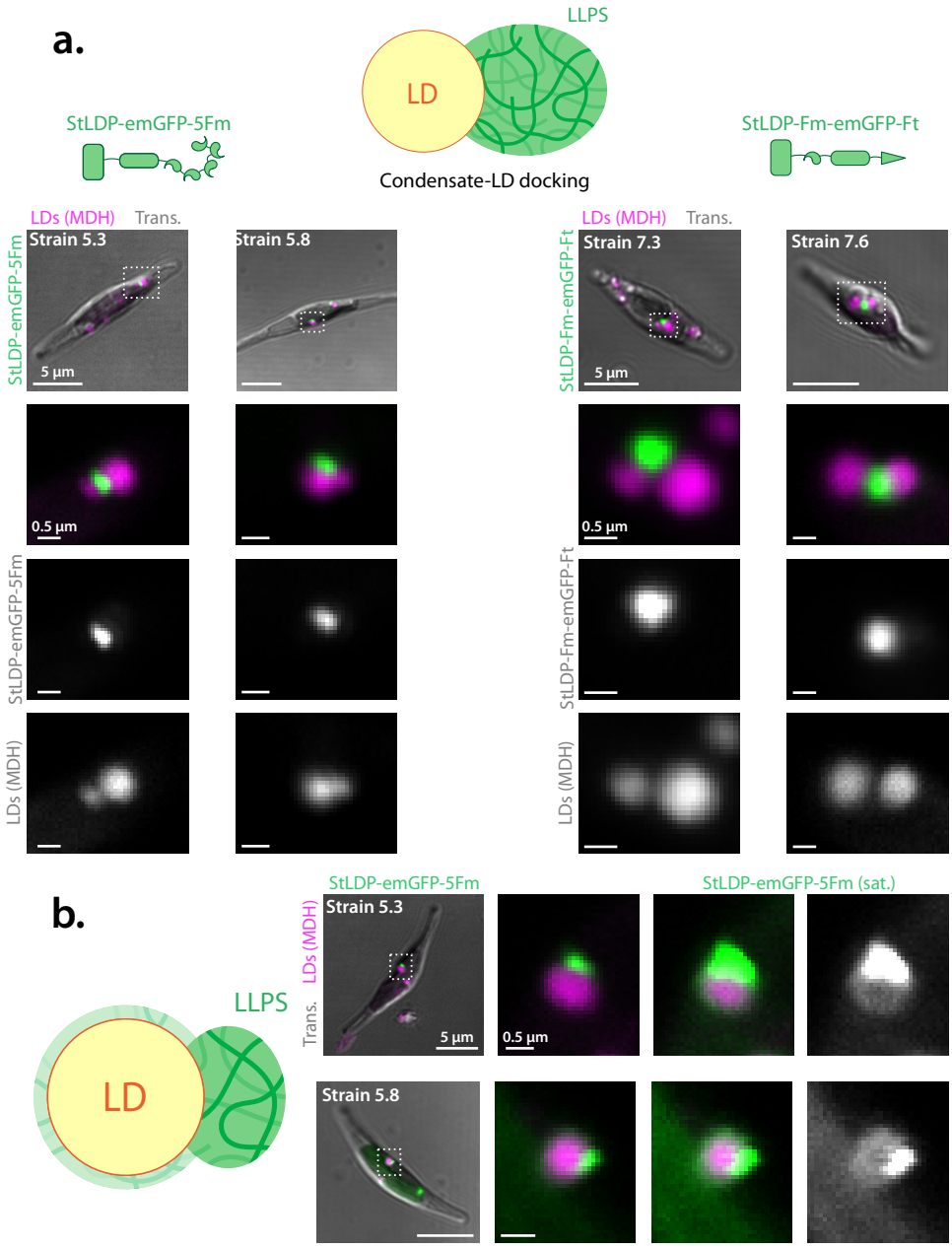

Figure 3.16: Representative confocal images of functionalized StLDP condensates (**StLDP-emGFP-5Fm** and **StLDP-Fm-emGFP-Ft**). Condensates predominantly dock to LDs (**a.**), with occasional partial ring-like structures around LDs in 5Fm (**b.**), indicating scaffold-LD interactions.

Qualitatively, most observed condensates were found adjacent to lipid droplets, indicating that the StLDP tag retained its targeting capability when fused to LLPS scaffold proteins (figure 3.16a.). With the **5Fm** scaffold, we also observed partial ring-like structures around LDs. Only a minority of cells were displaying this phenotype, however this could be a detection issue, since the bright spot of the condensate could mask the faint signal around LDs. On the other hand, no ring around LDs were observed for the **Fm-Ft**

condensates. These morphologies suggest that while full encapsulation is not observed, condensates can dock to LDs with varying degrees of surface contact (figure 3.16b.). One possible explanation is that the lower valency of **5Fm** may favor LD affinity over scaffold-scaffold interaction, whereas the higher multivalency of **Fm-Ft** could bias the protein toward self-association, thereby limiting interactions with LDs.

To evaluate potential toxicity from scaffold expression and functionalized condensate formation, we monitored both growth rate and fluorescence intensity following induction through flow cytometry measurements, as shown in figure 3.17.

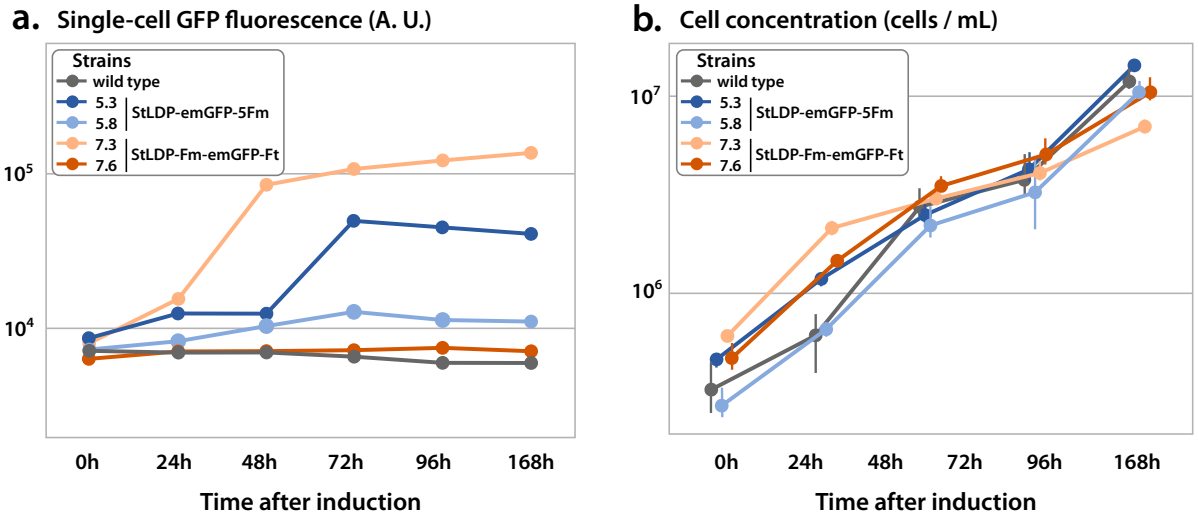

Figure 3.17: **a.** Flow cytometry measurements of StLDP-functionalized strains. Single-cell GFP intensity peaks at 2-3 days post-induction, for strongly and weakly expressing strains. **b.** Growth rate of StLDP-functionalized strains, displaying similar doubling times in induced strains compared to wild-type Pt. Error bars, standard deviation.

These measurements revealed that the maximum single-cell fluorescent intensity is reached after to two to three days. This maximum level varies widely from one strain to another, due to the lack of control on the number of gene copies inserted during biolistic transformation and to the site(s) of insertion. The fluorescent signal in wild-type Pt cells is due to the plastidial autofluorescence and does not vary over time.

Moreover, we observe that the expression of functionalized constructs does not significantly impair growth or reduce cell viability, as no growth defects or abnormal fluorescence signals are observed compared to wild-type Pt. This result confirms that the expression of StLDP-tagged scaffolds is well tolerated by Pt cells in the short term and is compatible with our experimental workflow.

To determine whether the localization of condensates to LDs occurred more frequently than a random distribution, we then performed a colocalization analysis comparing LD-targeted and non-targeted scaffolds.

To carry out this analysis, I developed a quantitative LD detection method using the

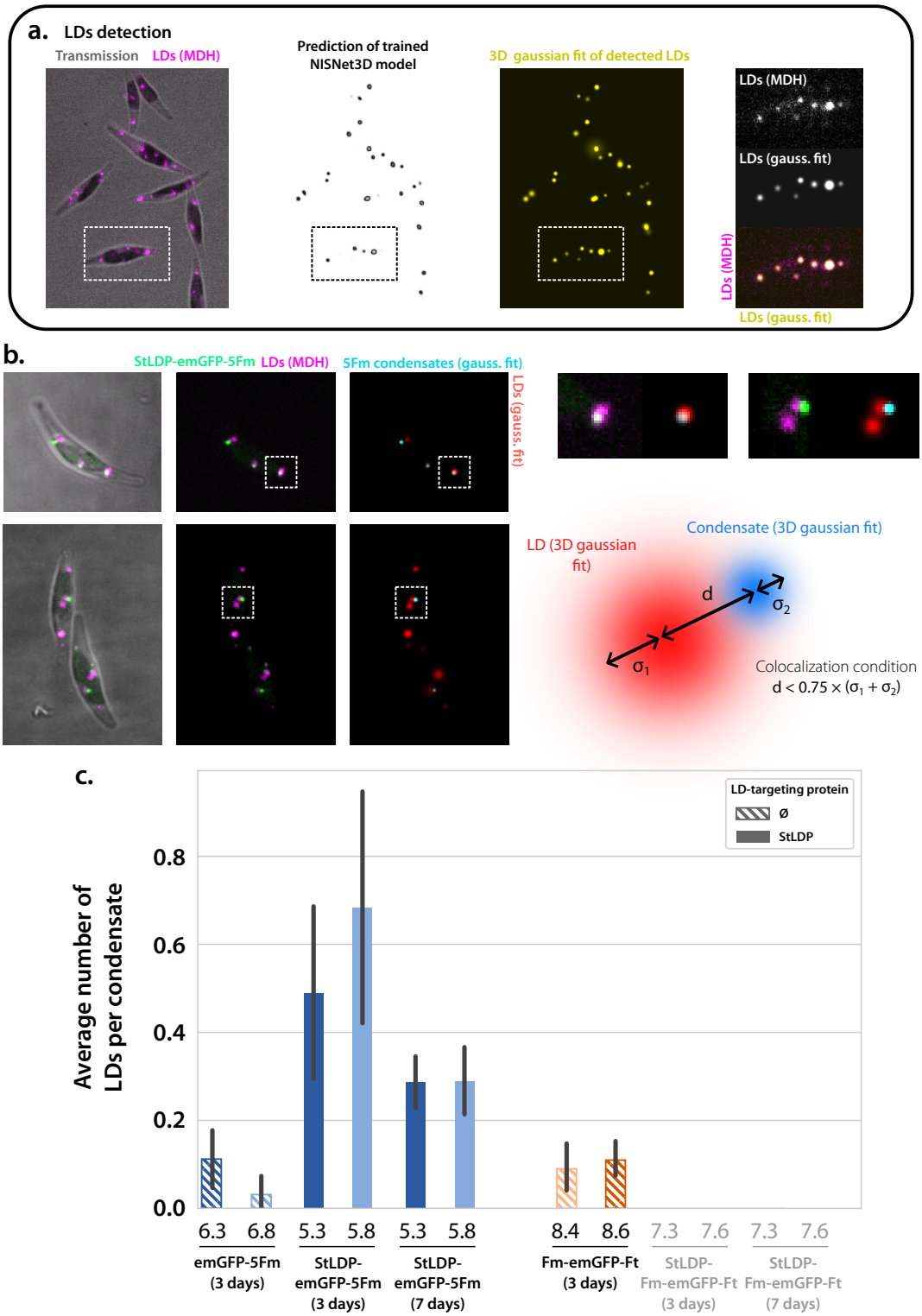

Figure 3.18: Quantitative colocalization analysis of condensates and LDs. **a.** Detection of LDs and condensates in 3D using NISNet3D and Gaussian fitting. **b.** Using fitting on both condensates and LDs allow to detect colocalized objects accurately. **c.** Average number of LDs per condensate, for non-targeted and StLDP-functionalized **5Fm** and **Fm-Ft** condensates. N > 200 cells for each condition. Error bars, standard deviation (preliminary data).

same principle as in section 3.2. Using a NisNet3D model specifically trained on LD images and subsequent fitting analyses, we were able to accurately detect LDs positions and shapes in 3D (figure 3.18a.). Using the previous pipeline, we also fitted the positions of condensates. Using both of these information allowed to compute a colocalization ratio, defined as the average number of LD per condensate that satisfies $d < 0.75 * (\sigma_1 + \sigma_2)$, where d is the distance between the center of the condensate and the center of the LD, and σ_1 and σ_2 are the radii of the respective fitting gaussians of the objects (figure 3.18b.). This ratio is therefore a measure of how many condensates are in close proximity to LDs, compared to a random distribution.

When looking at non-targeted LLPS scaffolds, we can observe a similar average number of condensates associated with LDs, across the 4 studied strains, meaning that around 10% of condensates present a colocalization with LDs, for both **5Fm** and **Fm-Ft** condensates. This analysis demonstrated a significantly higher frequency of LD-associated condensates in strains expressing **StLDP-emGFP-5Fm** compared to those expressing non-functionalized **emGFP-5Fm**. The StLDP-functionalized **Fm-Ft** condensates are ongoing at the time of writing. Altogether, these findings support the hypothesis that StLDP successfully and specifically recruits condensates to LDs.

PtLDP1-based scaffolds

In parallel, we evaluated another LD-associated candidate, PtLDP1, for scaffold targeting. As said earlier, PtLDP1 shares sequence homology with other LD-associated proteins and is predicted to localize at the LD surface. We constructed fusions with LLPS scaffolds and examined their localization after induction. The gene sequence of PtLDP1 was obtained through PCR on wild-type Pt genomic DNA, then fused with emGFP and introduced into Pt via biolistic transformation, and localization was analyzed after three days of nitrate induction.

Unexpectedly, PtLDP1 localized primarily to dense structures rather than LD surfaces. In high-expressing strains, additional membrane-associated patterns were observed around the plastid. This behavior deviates from previously described LD localization and may reflect targeting to a subarea of the plastid, the plastidial compartment or "blob"[167]. Supporting this hypothesis, bioinformatic predictions using Phobius indicated the presence of a signal peptide. Moreover, the targeting sequence ASFAP[167] is found in the protein. We thus hypothetized that these sequences could target PtLDP1 to plastid membranes or internal compartments. Since no clear localization to LDs has been shown, these results suggest that PtLDP1 is not suitable LD-targeting candidate in its current form.

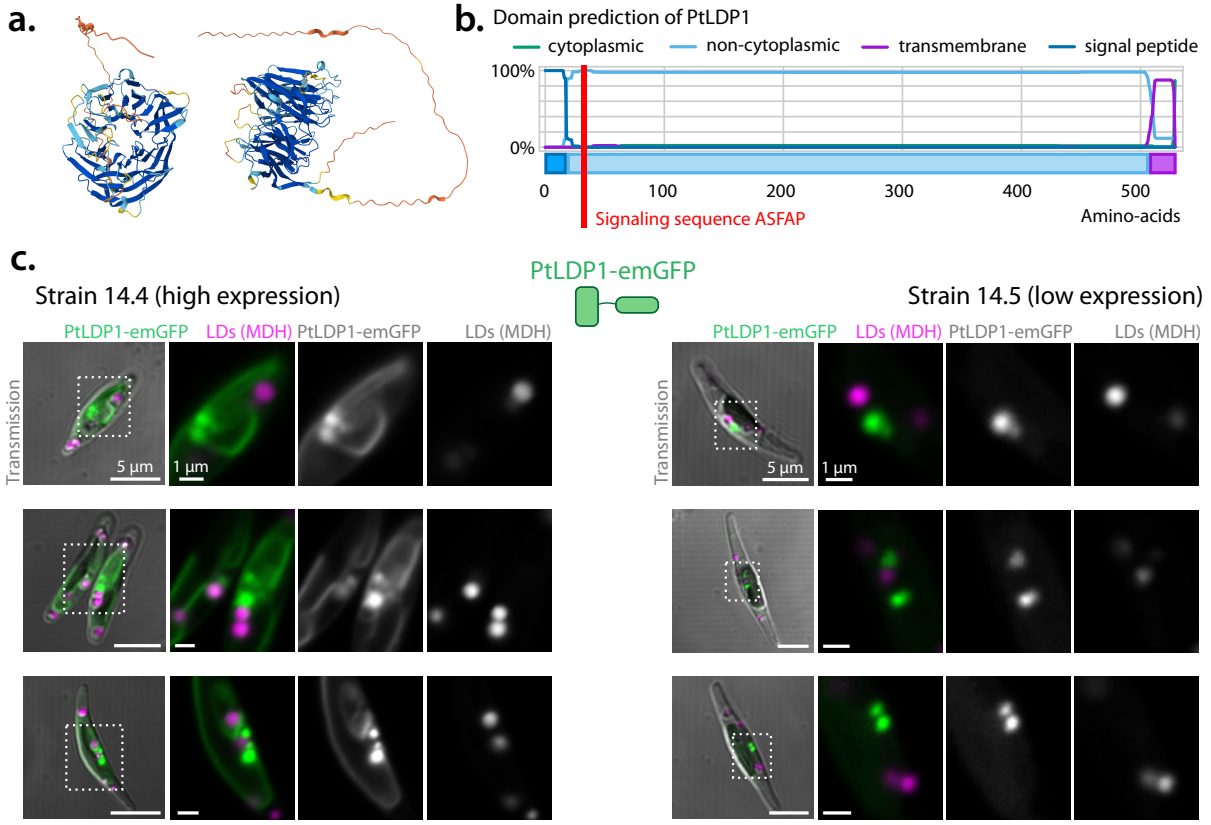

Figure 3.19: **a.** Structure of PtLDP1, predicted by AlphaFold2. **b.** Phobius prediction of functional domains of PtLDP1, showing a signal peptide. A targeting sequence ASFAP is also indicated on the sequence. **c.** Representative localization of PtLDP1-based scaffolds in Pt, for a high-fluorescence and a low-fluorescence strain.

4.2 Optimization of LD-targeting strategies

Towards fine-tuning of StLDP affinity

Given the successful but partial recruitment of condensates to LDs, we next explored whether the affinity of StLDP for LDs could be modulated to force a more efficient LD engulfment. Structural analysis revealed that StLDP is composed of two distinct domains: a N-terminal β-barrel domain and a bundle of α-helices (figure 3.20a.). Moreover, the β-barrel is predicted as a C2 domain[168] and therefore is likely involved in interactions with other membranes. We can therefore hypothetize that this region is responsible of ER interactions. On the other hand, the bundles of α-helices forms a hydrophobic hairpin likely involved in LD interactions.

Using this hypothesis, we investigated if StLDP recruitement to LDs could be impoved by removing the β-barrel domain. We therefore generated a truncated version of StLDP lacking its N-terminal region (figure 3.20). This construct was fused to the scaffold and expressed in Pt as before using nitrate induction. Qualitatively, the localization patterns remained coherent with previous observations, as truncated StLDP were observed in some cases around LDs but mainly scattered in punctas away from LDs. Slightly larger conden-

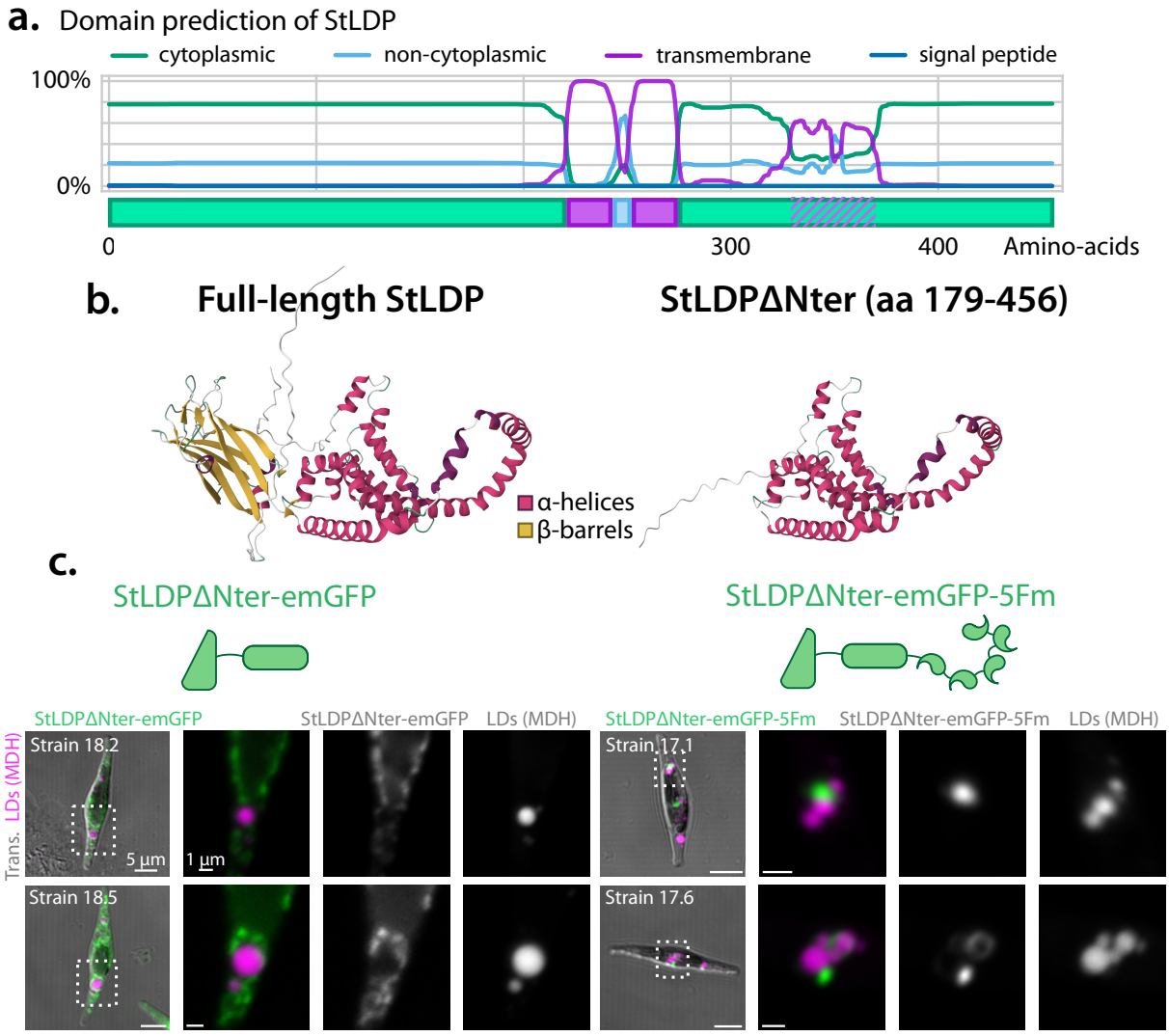

Figure 3.20: Effect of StLDP truncation on condensate targeting. **a.** Phoebius[169] prediction of different StLDP domains. **b.** Proposed trunctation of StLDP for better LD targeting. **c.** Representative confocal images of strains expressing trucated StLDP, with and wihthout **5Fm** scaffold.

sates were often observed in the two **StLDPΔNter-emGFP-5Fm** strains. This could be attributed to an increased availability of the scaffold protein in the cytosol due to altered folding or localization of the truncated tag. If the protein presents a post-translational regulation, the truncated protein could also lose this regulation resulting in an increased expression. However, a conclusive interpretation will require quantitative confirmation via western blots or fluorescence quantification.

HOGP-based scaffolds

Finally, we initiated preliminary testing with a third LD-associated candidate. The protein HOGP (*Haematococcus* Oil Globule Protein) is the main LD associated protein in *Haematococcus pluvialis*, a freshwater green alga. A recent study has shown that HOGP

expression in Pt leads to a localization around LDs, resulting in a homogenous fluorescence ring (figure 3.21a.). The same study highlights that HOGP has to be tagged at N-terminus, otherwise localization to LDs is lost. We therefore adapted our scaffolds as previously, and generated Pt strains expressing **emGFP-HOGP**, **5Fm-emGFP-HOGP** and **Fm-emGFP-Ft-HOGP** under nitrate induction.

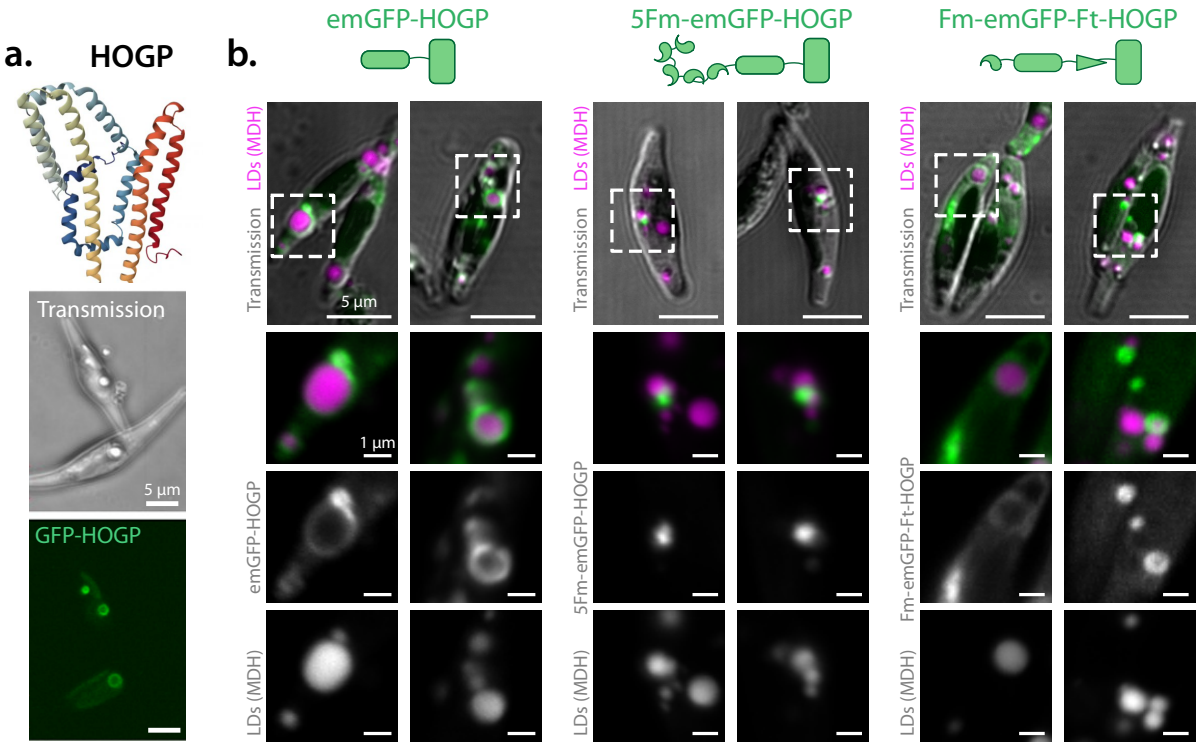

Figure 3.21: **a.** HOGP expression in *Phaeodactylum tricornutum* leads to a uniform covering of LDs, as reported in [Shemesh et al. 2016]. **b.** Confocal imaging of strains expressing **emGFP-HOGP**, **5Fm-emGFP-HOGP** and **Fm-emGFP-Ft-HOGP** scaffolds.

Early observations indicate possible partial LD localization when fused to scaffold proteins, as shown in figure 3.21b. One can observe well formed rings around LDs in **emGFP-HOGP** strains. For the 5Fm-emGFP-HOGP, condensates are often found in close proximity to LDs, in a similar trend with previous investigations. Lastly , the **Fm-Ft** scaffold shows a localization similar with **emGFP-HOGP**: this is likely due to the C-terminus tagging of Ft, whose oligomerization is sensitive to the site and size of other fused modules. Yet, the current data remain insufficient for detailed quantitative analysis. Further experiments are planned to validate these findings and assess the targeting potential of HOGP-based constructs.

Double transformation of StLDP strains

To further increase the efficiency of LD encapsulation, we attempted to increase scaffold concentration around LDs by expressing an excess of non-targeting LLPS scaffolds. This approach was inspired by our mammalian experiments from the previous chapter, where

overexpression of **mCherry-5Fm** helped drive nucleation of LD-targeting scaffolds into LD-encapsulating condensates. We therefore performed a second round of biolistic transformation using previously generated strains expressing **StLDP-emGFP-5Fm**, using plasmids specifically designed for this double transformation:

- mOrange was introduced in place of emGFP to be able to observe both protein locations.
- Zeocin resistance was used instead of Blasticidin, to allow the selection of double transformants, since the strain is already resistant to Blasticidin after the first biolistics transformation.

mOrange was chosen as a fluorescent protein instead of mCherry (which was used in the previous chapter) due to its spectral separation from chlorophyll. We generated strains able to co-express **StLDP-emGFP-5Fm** and **mOrange-5Fm**, and analyzed their localization patterns after nitrate induction.

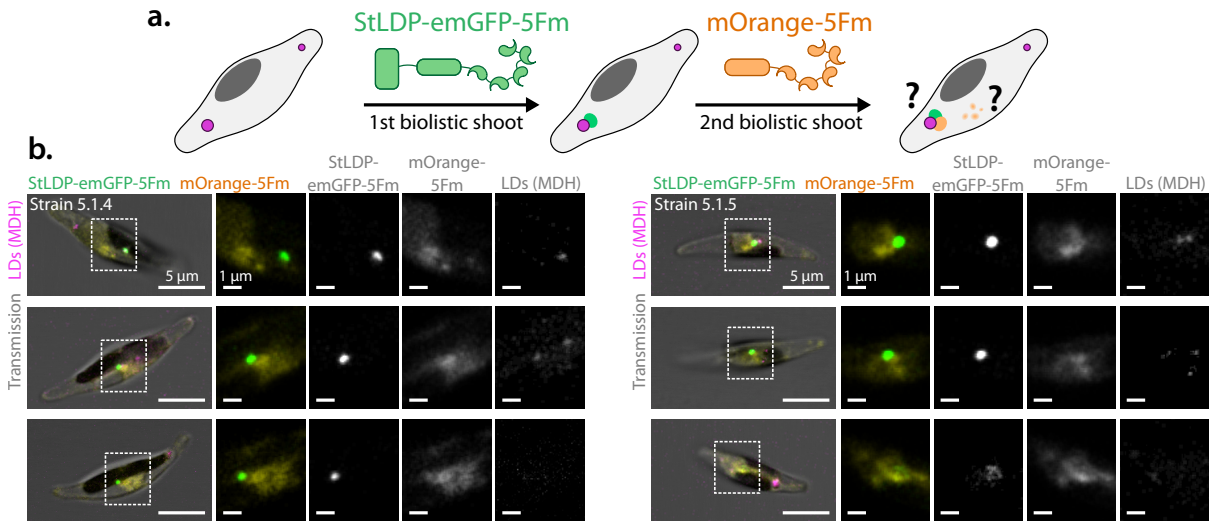

Figure 3.22: **a.** Double transformation of Pt strains result in double expression of LLPS scaffolds. **b.** Representative images of strains co-expressing **StLDP-emGFP-5Fm** and **mOrange-5Fm** with nitrate induction.

As depicted in figure 3.22, despite the successful generation of dual-expressing strains no significant colocalization between **StLDP-emGFP-5Fm** and **mOrange-5Fm** was observed. The mOrange signal remained diffuse throughout the cytosol, suggesting that the two scaffold pools do not mix. A possible explanation could be intracellular compartmentalization or spatial restriction of scaffold access. Ongoing experiments aim to clarify the mechanisms behind this separated localization.

4.3 Induction of bigger LDs to favor StLDP recruitment

Use of phosphate starvation to enlarge LDs

While some docking events and partial LD encapsulations were observed, the diffraction-limited size of LDs in Pt made it difficult to resolve fine localization patterns. To improve visualization and potentially enhance recruitment, we sought to enlarge lipid droplets through metabolic stress. A first way to achieve this is to halt cell division. Specifically, nitrogen and phosphate starvation has been reported to block division while maintaining lipid biosynthesis via photosynthesis[171], leading to an abnormal lipid accumulation. This halted physiological state results in larger LDs which can be observed starting shortly after medium exchange. Moreover, StLDP is reported to better localize on LD surface upon stress events such as this starvation[141]. Since nitrate presence is mandatory to induce the expression of our scaffolds, we chose to use phosphate starvation for this experiment.

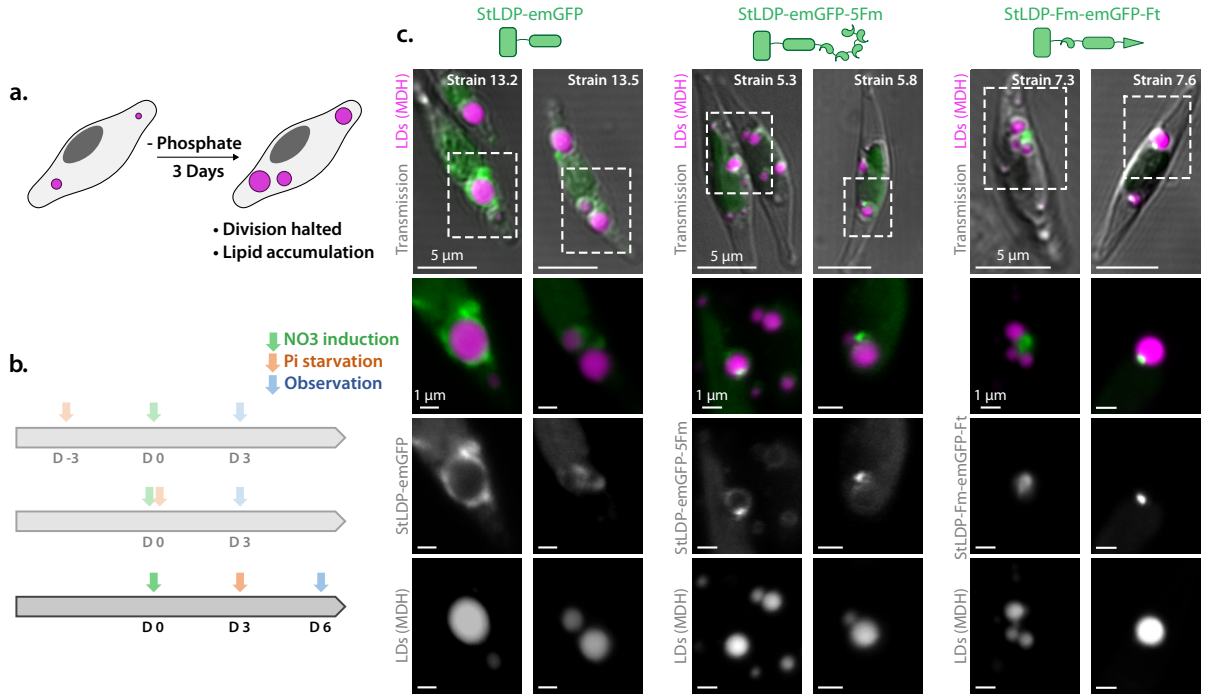

Figure 3.23: **a.** Lipid droplet enlargement by phosphate starvation. Cells starved of phosphate for 3 days results in enlarged LDs. **b.** Different strategies to combine phosphate starvation and nitrate induction. Simultaneous phosphate starvation and nitrate induction impairs scaffold expression, while a two-step protocol allows scaffold expression followed by LD enlargement. **c.** Confocal imaging of cells expressing respectively **StLDP-emGFP**, **StLDP-emGFP-5Fm** and **StLDP-Fm-emGFP-Ft** using the phosphate starvation protocol.

Starvation experiments were performed and are presented in figure 3.23. However, when performing simultaneously phosphate starvation and nitrate induction, we observed a very weak expression of our scaffold, likely induced by an altered metabolism due to starvation. To circumvent this, we applied a two-step protocol: first, nitrate induction

was performed for 3 days to allow scaffold expression, followed by 3 days of phosphate starvation to induce formation of large LDs (see figure 3.23b.). This strategy occasionally resulted in clear ring-like patterns around LDs for **StLDP-emGFP**, and consistent condensate interactions with LDs for **StLDP-emGFP-5Fm** and **StLDP-Fm-emGFP-Ft**. Nonetheless, we did not observe robust engulfment of LDs by condensates, suggesting that further optimization is required for full encapsulation.

Fatty acid feeding to enlarge LDs

Another described method to enlarge LDs in Pt is to feed the cells with exogenous fatty acids. This approach has been reported to efficiently increase LD size in Pt within hours. We therefore tested to form large LDs using palmitoleic acid, using a protocol adapted from the literature[170]. figure 3.24 summarizes the protocol used, and display representative images of cells.

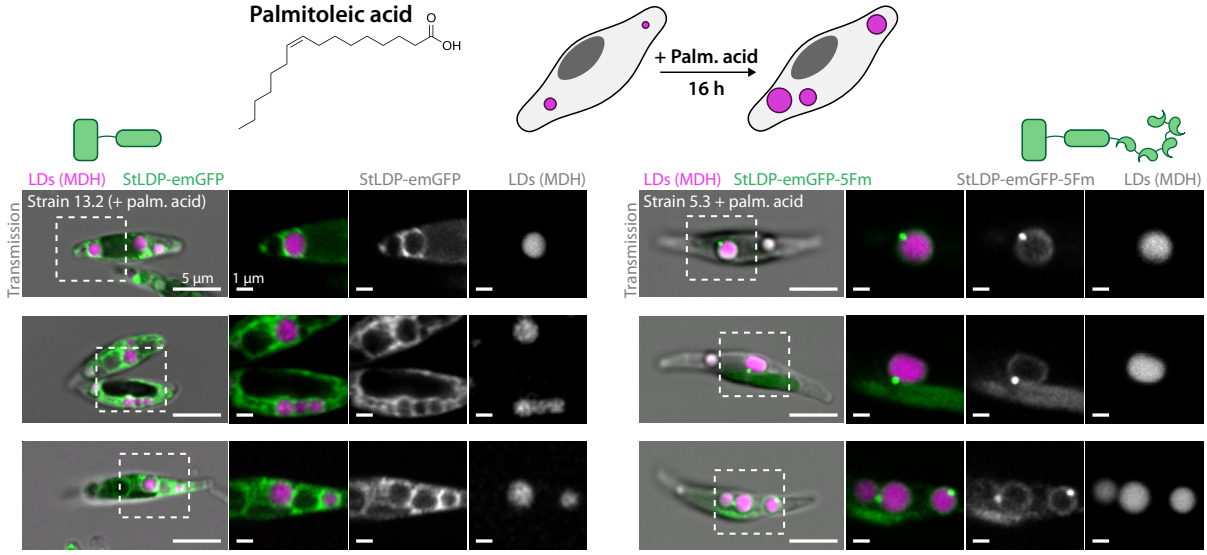

Figure 3.24: **a.** Fatty acid feeding induces the formation of large LDs. **b.** Confocal imaging of strains expressing **StLDP-emGFP** or **StLDP-emGFP-5Fm** fed with 1 mM palmitoleic acid for 16 h, showing large LDs.

A first observation is that the feeding protocol leads to the formation of very large LDs, consistent with previous reports. Moreover, StLDP localization to LDs is more pronounced after feeding, with clear ring-like structures observed in a majority of cells expressing **StLDP-emGFP**. In **StLDP-emGFP-5Fm** strains, condensates are often found in close proximity to LDs, with a fainter ring-like pattern around LDs. Moreover, protein expression is not impaired by nutrient scarcity with these conditions, with qualitative increase in fluorescence signal. However, no full engulfment of LDs by condensates was observed.

5 Discussion and perspectives

In this chapter, we demonstrated that engineered protein scaffolds can drive liquid-liquid phase separation in the marine diatom *Phaeodactylum tricornutum*. Upon induction of transgene expression, the non-targeted scaffolds self-assembled into distinct spherical condensates in the algal cells. We observed some hallmarks of liquid-like condensates such as condensate emergence coinciding with rising scaffold concentration, and the compartments exhibited dynamic behaviors like growth over time. However, to fully assess that the compartments are formed through a LLPS mechanism, we will need to acquire higher-temporal-resolution movies to follow nucleation and growth of single condensates, quantify coalescence events, and measure growth rates. We should also map the apparent saturation concentration by varying scaffold expression and test concentration buffering in the dilute phase, and perform FRAP to measure internal exchange and recovery kinetics. As orthogonal tests, mild physicochemical perturbations, such as 1,6-hexanediol exposure, could probe the weak and multivalent interactions expected for a LLPS.

The successful formation of compartments in *P. tricornutum* confirms that our condensate-based platform can be extended beyond animal cells, underscoring the versatility of phase separation as a tool across divergent eukaryotic phyla. Building on this foundation, we then explored the strategic functionalization of condensates to interact with lipid droplets. We fused our condensate-forming proteins with well-characterized LD-targeting domains, including both endogenous and heterologous LD-associated proteins. These fusion constructs yielded targeted condensates that localized to the surfaces of lipid droplets. Confocal imaging confirmed that condensates bearing an LD-targeting domain formed at or around LDs, even sometimes clustering them. However, the main limitation was to identify the right protein and/or conditions to create a robust LD engulfment in a organisms such as Pt, less well-characterized than mammalian cells. This finding validates the core concept of the ControLD platform in a microalgal system: by functionalizing condensates with appropriate targeting signals, we can direct phase-separated compartments to specific organelles, achieving a new level of control over subcellular organization in diatom cells.

While establishing condensate formation in *P. tricornutum*, we encountered a practical limitation in our choice of promoter used to drive our constructs. All results above relied on the nitrate reductase promoter (pNR), a widely used inducible promoter in *P. tricornutum* that is activated by the presence of nitrate in the growth medium. The pNR promoter proved convenient for temporally controlled expression; it presents however a major drawback for studies related to lipid droplets: pNR is inactive under nitrogen deprivation. This is problematic because *P. tricornutum* (like many microalgae) massively accumulates neutral lipids in LDs during nitrogen starvation, a condition under which we would ideally want to deploy our condensate system. Indeed, pNR-driven expression is known to cease upon nitrate withdrawal, meaning that under nitrogen-starvation conditions (when the

cells induce large LD formation), the current condensate constructs cannot be expressed. This mismatch between promoter activity and physiological LD accumulation restricts our ability to test condensate effects in the most widely used lipid storage context. To overcome this, future experiments should incorporate nitrogen-starvation inducible promoters as a complementary expression system. Rather than completely replacing pNR (which remains useful for normal growth conditions), we envision using an alternative promoter that turns on during nitrogen stress to drive condensate expression when pNR is off. Recent work has identified the *P. tricornutum* promoter of the diacylglycerol acyltransferase 1 (DGAT1) gene, shown to be strongly induced upon nitrogen starvation. This promoter was exploited to achieve transgene expression specifically under N-depleted conditions[170]. In practice, a dual-promoter system could be implemented: pNR-driven constructs would be used for initial validation and observations in N-replete cells, and an N-starvation-inducible promoter (such as DGAT1 or other starvation-upregulated genes) would be activated when shifting cultures into lipid-accumulating conditions.

An intriguing question raised by the creation of LD-targeted condensates is whether associating a condensate to LDs alters the lipid content or composition of those droplets. The fatty acid content of diatom TAGs is well documented for bulk cell extractions and even isolated LD fractions. Key questions include, for instance, if the physical hindrance of LDs by condensates could lead to retention of lipids that would otherwise be catabolized or exchanged with other organelles. The TAG content could also increase or decrease as a result of altered accessibility to lipases or lipogenic enzymes. To address such possibilities, we plan to perform lipidomics measurements on cells expressing LD-targeted condensates. In this forward-looking experiment, we would analyze their lipid composition in detail, and any deviations in the proportion of TAG or phospholipids might reveal how condensate association influences cellular physiology. An especially pertinent analysis would be the fatty acid composition of TAG in condensate-associated LDs: does the presence of condensates skew cells toward storing certain types of fatty acids in LDs? This could occur if, for example, condensate scaffolds sequester enzymes or alter local conditions for lipid synthesis. Prior evidence suggests that modulating LD-associated proteins can indeed impact lipid storage. In a notable case, heterologous expression of HOGP in *P. tricornutum* not only decorated the LDs but also led to an increase in TAG accumulation under nitrogen starvation. This implies that changes to the protein environment of LDs can affect how much neutral lipid the cells stock. While the mechanistic basis is not yet fully understood, it underscores the need to examine whether our condensate-induced LD clustering similarly enhances or impairs lipid storage. Significant changes in lipidomics analysis would point to functional consequences of condensate sequestration beyond spatial repositioning, and would assess whether condensate scaffolding of LDs leads to any biochemical remodeling of the droplets' lipid cargo.

The efficacy of condensate-mediated LD sequestration in *P. tricornutum* can poten-

tially be tuned or improved by exploring a broader range of LD-targeting protein domains. In this study we primarily used StLDP as the targeting module to anchor condensates to LDs, and performed tests on PtLDP1 and HOGP. While StLDP proved effective, it represents just one of many possible ways to bind the surface of a lipid droplet, as each protein can have unique effects on LD behavior. We suggest constructing and testing a panel of condensate fusion proteins incorporating various LD-associated domains, including those from plants and mammals, to compare their targeting efficiency, specificity, and impact on LD morphology in the diatom cell. A recent study[172] highlighted that a broader range of LD-associated proteins localizes with LDs in higher plants, and could be used to identify proteins targeting LDs in *P. tricornutum*. One candidate set comes from plant oleosins, the major LD coat proteins in oilseed plants. Notably, the abundance of oleosins in seeds inversely correlates with LD size: overexpression of certain oleosins leads to many small, stable droplets[173]. Such condensates might trap many tiny LDs within them, which could be beneficial for certain metabolic studies. In addition to plant proteins, we could experiment with mammalian perilipins. These proteins have different binding partners and regulatory roles on LDs. For example, Plin1 in adipocytes is known to tightly restrict lipase access to LDs, while Plin2 is more ubiquitous and constitutive. It is possible that a condensate decorated with different perilipin peptides might attach to LDs differently. We note that plants and algae lack perilipins, so any effects would be novel in this context. Finally, within the diatoms and related algae themselves, there are additional endogenous LD proteins worth exploring: other stramenopile algae possess unique LD proteins (for example, DOAP1 in *Fistulifera* sp. or LDSP in *Nannochloropsis* sp. [131]). Chimeric constructs using those domains could be tested in *P. tricornutum* as well. The goal of these experiments is to diversify the targeting toolkit: by comparing plant oleosins, various perilipins, or even synthetic lipid-binding peptides such as LiveDrop[174], we can determine which yields the best localization at LD interface (leading to a bright, complete coating of all LDs vs. partial or patchy binding) and how each influences the droplets themselves. This systematic exploration will not only optimize our condensate system (choosing the ideal targeting domain for a given application) but also highlight the comparative biology of LD-coating proteins across kingdoms. However, because these proteins are evolutionary distant, it would be interesting to assess whether the algal cell can correctly traffic a condensate tagged with an exogenous protein to LDs, and whether these proteins are mistargeted to other organelles.

An important consideration for our approach is the longer-term impact on cell health. So far, we have shown that *P. tricornutum* cells can survive and proliferate with artificial condensates in their cytosol under standard laboratory conditions. However, it is vital to assess whether the presence of these condensates perturbs the cells' fitness under various stress conditions or over extended timescales. Microalgae frequently encounter fluctuations in nutrients, light intensity, and other environmental factors that induce stress responses, often involving lipid metabolism and LD dynamics. We propose to challenge

condensate-expressing diatom strains with stress conditions to evaluate medium-term viability and physiological impact in presence of condensates associated with LDs. Beyond nutrient stress presented in this study, we should examine oxidative stress and photoinhibition scenarios, since lipid droplets often play protective roles in those contexts. Under high light or oxidative conditions, cells produce reactive oxygen species that can damage membranes and proteins. LDs are known to mitigate oxidative stress by sequestering polyunsaturated fatty acids (which are prone to peroxidation) and by housing antioxidants or sacrificial molecules. If condensates alter the distribution or availability of LDs, the cell's capacity to respond to oxidative stress might change. We can also test this by applying a pro-oxidant treatment (e.g. high light exposure or H_2O_2 addition) to cultures and measuring survival rates, growth, and signs of lipid peroxidation in condensate-expressing vs. normal cells. Similarly, light fluctuations or extended darkness are relevant stresses for a phototroph organism. We may assess whether condensate-containing strains handle transitions from light to dark differently, perhaps due to changes in how carbon is allocated between storage (lipids/carbohydrates) and immediate metabolic use. On the other hand, it is imaginable that condensate-mediated LD sequestration could even prove beneficial under certain stresses, by insulating the LDs or concentrating protective factors, possibly revealing new aspects of how spatial organization of LDs contributes to stress physiology.

Lastly, applied perspectives could as well be envisioned. Microalgae like *P. tricornutum* contribute a large fraction of global carbon fixation and are promising chassis for biofuels and bioproducts. Spatially engineering LDs could partition carbon more efficiently into storage by confining LDs and induce fatty acids channeling directly into TAG, potentially maximizing yields. Prior demonstrations that altering LD-coat proteins boosts oil content (e.g. with HOGP expression) reinforce this perspective. Because LDs also buffer lipotoxicity and oxidative stress, controlling where and how they form may reveal resilience strategies under nutrient or light stress. More broadly, this approach exemplifies intervening in space and time to test "what if" scenarios across systems: it lays a foundation to translate LD control beyond diatoms, uncovering general principles of organelle regulation while opening routes to design intracellular modules that tune metabolism and stress tolerance.

6 Material and methods

Some protocols and methods presented below concerns general *P. tricornutum* experimental techniques, and are adapted from [Gueguen 2022]

P. tricornutum culture conditions

Culture medium

ESAW (Enriched Seawater, Artificial Water) medium is composed as follow: NaCl (326.7 mM), Na_2SO_4 (25 mM), KCl (8.03 mM), KBr (0.725), H_3BO_3 (0.372 mM), NaF (0.0657 mM), $MgCl_2$-$6H_2O$ (47.18 mM), $CaCl_2$-$2H_2O$ (9.134 mM), $SrCl_2$-$6H_2O$ (0.082 mM), Fe-EDTA (8.17 µM), Na_2EDTA-$2H_2O$ (8.3 µM), $ZnSO_4$-$7H_2O$ (0.254 µM), $CoCl_2$-$6H_2O$ (0.0672 µM), $MnCl_2$-$4H_2O$ (2.73 µM), Na_2MoO_4-$2H_2O$ (6.12 nM), Na_2SeO_3 (1 nM), $NiCl_2$-$6H_2O$ (6.27 nM), $CuSO_4$-$5H_2O$ (0.039 nM), vitamin B8 (4.09 nM), vitamin B12 (0.738 nM), vitamin B1 (0.593 µM), $NaNO_3$ **or** NH_4Cl (0.549 mM), and NaH_2PO_4-H2O (0.022 mM). ESAW medium is prepared under sterile conditions from stock solutions sterilized either by autoclaving the solutions or by filtration through a 0.22-µm membrane filter. Under optimal growth conditions, all cultures were conducted using enriched ESAW medium containing 10 times more $NaNO_3$ (resp. NH_4Cl) and NaH_2PO_4, corresponding to a concentration of 5.49 mM and 0.22 mM respectively. This medium was designated as ESAW 10N10P-NO_3^- and 10N10P-NH_4^+. For phosphate deprivation experiments, ESAW 10N0P was used instead.

Culture on solid media

P. tricornutum cells were cultivated in an incubator (MLR-352-PE Climate Chamber) at 20°C under continuous light (50 µmol.m-2.s-1). Cultures of *P. tricornutum* cells on solid medium were performed with ESAW 10N10P-NH_4^+ complemented with Agar (1 % m/v). To guarantee axenic conditions, all media were supplemented with Carbenicillin disodium salt (0.237 µM) to which *P. tricornutum* is naturally resistant. For culture of mutant lines transformed with CRISPR-Cas9 vectors, Zeocin (Invitrogen; 0.07 µM) was added to the media. For overexpressing lines designed in our laboratory, the media were supplemented with Blasticidin (0.028 µM) or Zeocin (0.07 µM).

Culture in liquid media

Cells were transferred from solid to liquid media first in 25-mL, then in 50-mL, 100-mL, and finally 250-mL flasks containing 5 mL, 10 mL, 20 mL, and 50 mL of ESAW 10N10P-NH_4^+ media respectively. Flasks were placed in an incubator (INFORS HT Multitron Pro) at 20°C under gentle agitation (100 rpm), with a light cycle of 12h/12h (40 $\mu mol.m^{-2}.s^{-1}$). Cell concentration was kept between $0.5.10^6$ and 10.10^6 $cell.mL^{-1}$. For phosphate starvation, *P. tricornutum* cells were cultivated in 50 mL of ESAW 10N10P in 250-mL flasks

until a concentration of 3-4.10^6 cell.mL^{-1}. Cultures were transferred to 50-mL polycarbonate tubes and centrifuged at 1,500 g for 10 minutes. Supernatant was removed. Cells were washed with 50 mL of ESAW 0N10P medium 2 times, and centrifuged at 2,000 g for 10 minutes. Supernatant was removed. Cells from each triplicate were then transferred to 250-mL flaks with 50 mL of ESAW 0N10P at a concentration of 2.5-3.10^6 cell.mL^{-1}.

Transformation of *P. tricornutum* and mutant selection

Biolistic transformation

P. tricornutum cells were maintained in exponential growth in a ESAW-NH_4^+ medium for at least two weeks (between 0.5 and 2.10^6 cell.mL^{-1}). Then 150.10^6 cells were collected by gentle centrifugation at 1,000 g for 10 minutes at room temperature, resuspended in 500 µL of ESAW 10N10P (containing ammonium), and spread on a solid media with Carbenicillin. The plate was dried under a sterile hood for 30 minutes, then kept for 24 hours in an incubator (see above) before transformation. Vectors to transform were collected from overnight cultures of *E. coli* 100 mL containing the vector with NucleoBond Xtra Midi kit (MACHEREY-NAGEL) to obtain a concentration of 1 µg.µL-1. Vector preparation before transformation consists in the coating of the vector on microparticles. For each plate to transform, one 1.5-mL tube containing a 50-µL aliquot of 3 mg of tungsten beads M17 (Bio-Rad, Hercules, USA) in glycerol 50 % (v/v) was used. 4 to 5 µg of plasmid, 50 µL of $CaCl_2$ 2.5 M in absolute ethanol and 20 µL of spermidine 0.1 M (Sigma-Aldrich) were added to the tungsten beads. The mix was vigorously mixed using a vortex for 3 min at high speed then incubated at room temperature for 1 minute. Beads were pelleted and the supernatant removed. 140 µL of cold ethanol 70 % were applied on the pellet without resuspending the beads, then removed. Next, 140 µL of cold absolute ethanol were applied on the pellet without resuspending the beads and removed. Finally, 50 µL of cold absolute ethanol were added on the pellet and the beads gently resuspended. Coated beads were kept agitated using a vortex at low speed until use. Biolistic transformation was performed under a sterile laminar flow hood using a Bio-Rad Biolistic PDS-1000/He Particle Delivery System (Bio-Rad) according to manufacturer recommendations (Bio-Rad PDS-1000/He System User Manual). 1550 psi (per square inch) rupture discs were used. All materials for biolistic were sterilized with ethanol 70% beforehand. The plate containing the cells to be transformed was placed at level 2 and 3 of the particle delivery system. For tungsten beads coated with CRISPR-Cas9 constructs, each prepared aliquot was spread on four macrocarriers, and all four macrocarriers were used on a given plate. In other words, tungsten beads from a single aliquot were delivered to a plate through four distinct bombardments. For tungsten beads coated with constructs for overexpression, the aliquot was entirely spread on two macrocarriers only. Rupture disk and macrocarrier were assembled inside the bombardment chamber according to manufacturer recommendations. Briefly, a partial vacuum pressure of 25 inches of mercury was created in the bombardment

chamber of the biolistic system containing the cells to transform. Then, helium gas was sent to a gas acceleration tube, sealed by the rupture disk, above the bombardment chamber. Pressure inside the gas acceleration tube was monitored with a gauge. When the pressure inside the tube reached 1550 psi, the rupture disk burst, creating a helium shock wave inside the bombardment chamber. This causes the macrocarrier coated with the tungsten beads to be propelled downward at high velocity. The macrocarrier was halted after a short distance by a stopping grid, allowing only the tungsten beads to continue their trajectory through the cells to transform on the plate. The penetration of the tungsten beads, coated with the plasmid to transform, in the microalgae cells allowed the potential integration of the plasmid inside the microalga genome.

Transformants selection, screening and purification method

Three days after transformation, transformed cells were transferred to a new ESAW solid medium with Carbenicillin and either Blasticidin or Blasticidin + Zeocin depending of overexpression vector(s). Only cells having successfully integrated the plasmid with the resistance cassette form colonies. Colonies appeared after three to six weeks. Colony PCR (Phire Plant Direct PCR Master Mix, F160, ThermoFisher Scientific) were conducted to analyse the presence of inserted sequences.

Media-shift and nutrient perturbation assays in *P. tricornutum*

Nitrate induction of transgene expression

Cells were cultivated in ESAW 10N10P-NH_4^+ medium as described above until a concentration of 3-4.10^6 cell.mL^{-1}. Cultures were transferred to 15-mL polycarbonate tubes and centrifuged at 1,500 g for 10 minutes. Supernatant was removed. Cells were then transferred to 100-mL flasks with 20 mL of ESAW 10N10P-NO_3^- at a concentration of 0.5.10^6 cell.mL^{-1}, and cultivated with the same parameters. Samples were collected at different time points after induction, depending of the experiment.

Phosphate starvation

For simultaneous phosphate starvation and nitrate induction, cells were cultivated in ESAW 10N10P-NH_4^+ medium until a concentration of 3-4.10^6 cell.mL^{-1}. Cultures were transferred to 50-mL polycarbonate tubes and centrifuged at 1,500 g for 10 minutes. Supernatant was removed. Cells were washed with 50 mL of ESAW 10N0P-NO_3^- medium 2 times, and centrifuged at 2,000 g for 10 minutes. Supernatant was removed. Cells were then transferred to 100-mL flaks with 20 mL of ESAW 10N0P-NO_3^+ at a concentration of 2.10^6 cell.mL^{-1}. For simple phosphate starvation before nitrate induction the same protocol was used, replacing the final medium with ESAW 10N0P-NH_4^+ medium instead, followed three days after by nitrate induction as described above.

Fatty acid feeding

Transformant cells were cultivated according to the nitrate induction protocol described above. After three days, flasks were supplemented with palmitoleic acid (C16:1, ThermoFisher) at a final concentration of 1 mM (from a stock of 100 mg/mL in DMSO). Cell cultures were incubated under these conditions for at least 16 h, and then observed by fluorescence microscopy.

Cytometry measurements

Cell concentration and fluorescence intensity of *P. tricornutum* cells were measured using a NovoCyte Advanteon flow cytometer (Agilent). For each sample, triplicates measurements (3 tubes and 3 measures). emGFP fluorescence was excited with a 488-nm laser and collected with a 525/40-nm bandpass filter. Events were gated using apparent size and granularity (FSC and SSC) of particles, to remove cellular fragments and potential contaminants. Data were analyzed using the NovoExpress software (Agilent).

Live imaging and dissolution

Cells were cultivated as described above. For transformed strains, nitrate induction was performed three days before imaging. 5.10^5 cells were deposited in ibidi patterned with microwells (see section 6), which had been filled with 500 µL of ESAW medium. Cells were left to sediment for 30 min before observation. Live imaging was performed using the Yokogawa spinning-disk confocal microscope described below. For DMSO treatment, a 40% (v/v) solution of DMSO was prepared in ESAW medium. After one minute of imaging, 500 µL of this solution were added to the medium in the ibidi dish, resulting in a final concentration of 20% (v/v) DMSO during live imaging.

Molecular biology

Plasmid construction

All constructs were assembled by Gibson using the pPha-T1 backbone[176] and 40-bp overlaps. Primers carried a 20-bp 5' overlap (40-60% GC, no repeats) plus a $\tilde{2}$0-nt gene-specific 3' tail (T_m $\tilde{6}$2 °C). Inserts and the backbone were amplified with the high-fidelity polymerase Phusion (NEB) and gel-purified on a 1% w/w agarose gel using Monarch DNA Gel Extraction Kit (NEB). Fragments were combined at a 1:2-1:3 vector:insert molar ratio (per junction) in 10 µL reactions with 2x Gibson Master Mix (NEB) and incubated 50 °C for 30-60 min. Assemblies (2-5 µL) were transformed into competent *E. coli* DH5α(NEB) using heat-shock at 42°C for 45 sec, then recovered 1 h in SOC Outgrowth Medium (NEB), and plated on LB with Carbenicillin. Colonies (6-12) were screened by colony PCR; positives were miniprepped (Monarch Plasmid Miniprep Kit, NEB) and verified by restriction analysis and Sanger sequencing across junctions (and full inserts when needed).

DNA extraction and purification

For extraction of genomic DNA from P. tricornutum, a cell pellet corresponding to 100.10^6 cells was resuspended in 500 µL of lysis buffer (250 mM Tris pH 8.2, 100 mM EDTA, 2% SDS, 350 mM NaCl) and transferred to a 1.5-mL tube. The sample was incubated 15 second at 60°C under agitation (450 rpm) using a thermobloc. 500 µL of cold phenol:chloroform:isoamyl alcohol (25:24:1) was added to the sample and homogenized gently by inverting the tube. The sample was centrifuged at 13,000 g at 4°C for 10 minutes to remove debris and form two clearly separated phases (an upper aqueous phase containing the DNA and a lower organic phase). About 300 µL of the upper aqueous phase was transferred to a new 1.5-mL tube. A second extraction was performed by addition of one volume of chloroform:isoamyl alcohol (24:1). The sample was gently mixed before centrifugation at 13,000 g at 4°C for 10 minutes. About 200 µL of the upper aqueous phase was transferred to a final 1.5-mL tube. For DNA precipitation, 30 µL of Na-Acetate 3 M pH 5 and three volumes of absolute ethanol were added, and the sample incubated at -20°C for 20 minutes. The sample was centrifuged for 10 minutes at 13,000 g at 4°C to pellet the precipitated DNA and remove the supernatant. DNA pellet was washed with 700 µL of ethanol 70% and centrifuged at 13,000 g at 4°C for 5 minutes. The supernatant was carefully removed, then the sample was left at room temperature for one hour to air dry the DNA pellet. DNA was resuspended in DNAse-free water. Concentration and purity of the DNA was evaluated using a NanoDrop2000 (ThermoFisher Scientific). Genomic DNA was considered pure for an A260/A280 ratio of 1.8 and a A260/A230 ratio between 1.8 and 2.2. Plasmid extraction from *E. coli* was performed using the NucleoSpin Plasmid kit (MACHEREY-NAGEL) for 2-mL bacteria cultures and the NucleoBond Xtra Midi kit (MACHEREY-NAGEL) for 100-mL bacteria cultures according to manufacturer instructions. DNA purification following PCR, enzyme digestion, or after gel migration was performed using the NucleoSpin Gel and PCR Clean-up kit (740609.250, MACHEREY-NAGEL).

Protein extraction from *P. tricornutum* by phenol precipitation

Make Tanaka buffer with sucrose 0.7 M, Tris 0.5 M, HCl 30 mM, EDTA 50 mM, and KCl 0.1 M; filter (0.22 µm), aliquot 10×50 mL, store at -20°C; just before use, supplement to 2% β-mercaptoethanol, 2 mM PMSF (20 µL of 100 mM per mL), and 1 tablet of protease inhibitors (Roche 05056489001; 1 tablet in 1 mL water; add 20 µL/mL). For each sample, harvest 2.10^8 cells, resuspend the pellet in 700 µL Tanaka (2 samples of 350 µL), add 700 µL phenol pH 7.5, vortex 1 min, centrifuge 5 min at 14.000 rpm at 4°C, recover the upper pigmented phase, precipitate with 1 mL cold 0.1 M ammonium acetate in methanol and incubate at -20°C overnight. Centrifuge 5 min at 14.000 rpm at 4°C, wash pellets 2-3 times with 1 mL 0.1 M ammonium acetate/methanol, rinse with cold 100% acetone, air-dry 30 min, then resuspend in 50 µL lysis buffer (8 M urea, 50 mM Tris-HCl pH 6.8,

1 mM EDTA) freshly supplemented with 5% β-mercaptoethanol and incubate at least 2 h (or at 4°C overnight) before protein quantification.

Western-blot analysis

For the validation of produced LLPS scaffolds, samples containing 8 ²g of P. tricornutum total proteins, 5 µL of Blot LDS Sample Buffer 4X (ThermoFisher Scientific), 2 µL of Sample Reducing Agent 10X (Life technologies), in a total volume of 20 µL adjusted with water were prepared and kept at -20°C until use. Prior electrophoresis, proteins were denatured by heating the samples at 95 °C for 5 minutes. 3 µL of Precision Plus Protein standard (Bio-Rad) were used as protein size markers. Denatured samples and size markers were subjected to electrophoresis on a 15-wells Bolt 4-12% Bis-Tris Plus gel (ThermoFisher Scientific) in a bath containing Blot MES SDS Running buffer (ThermoFisher Scientific). Migration occurred at 100 V for 10 minutes, then 120 V for 1 hour. Proteins were transferred to a 0.2-µm nitrocellulose blotting membrane (Amersham Protran) using a Mini Trans- blot cell (Bio-Rad) with transfer buffer (192 mM Glycine, 25 mM Tri-HCl pH 8.3, 20% ethanol v/v). Transfer was performed at 90V, 35 mA for 1 hour 15 minutes. The membrane was washed in distilled water, and then placed in Red Ponceau preparation (0.2% p/v Red Ponceau, 3% v/v TCA) for 1 minute to visualize protein profile. The membrane was washed again in water and a picture was taken with a Camag TLC Vizualizer (Switzerland). Red Ponceau was removed with TBS buffer (Tris-HCl 20 mM pH 7.5, 150 mM NaCl). Membrane was blocked with TBS milk 5% for 1 hour at room temperature under agitation. For antibody fixation, the membrane was incubated with TBS milk 5% and a 1/1,000 dilution of the antibody at 4°C under agitation overnight. After incubation, the membrane was washed with TBS tween 0.1% three times. Secondary antibody was fixed by incubating the membrane in TBS milk 5% with a 1/10,000 dilution of HRP Goat IGG Anti Rabbit IGG (Interchim) at room temperature under agitation for 3 hours. The membrane was then washed in TBS Tween 0.1%, and finally washed in TBS. For antibody revelation, Clarity Western ECL Substrate (Bio-Rad) was used. Imaging of bands reacting with the antibodies was achieved with an Image Quant 800 (Amersham).

Imaging

Cells were observed using an epifluorescence microscope (Zeiss AxioScope A1) equipped with a Zeiss AxioCam MRc. Images were captured using an oil-immersion x100 objective. Confocal microscopy images were obtained with a microscope Zeiss LSM880 equipped with a 63x/1.4 oil- immersed Plan-Apochromat objective, running Zen 2.3 SP1 acquisition software. Spinning disk microscopy has been performed using a Yokogawa CSU-X1 spinning disk, mounted on a Nikon Ti-E microscope, equipped with a 100X/1.3 oil-immersed Plan-Apochromat objective, and a EM-CCD camera.

Microfabrication of NOA microwells

Microwell masters were fabricated by SU-8 photolithography and replicated in PDMS to produce stamps for NOA molding as follows, retaining the indicated dimensions, times, and temperatures: designs were drawn at target feature sizes (µm) in Inkscape (PDF, white-on-black) or as 8-bit images (1824 x 1140 px in Fiji). Clean glass wafers were spin-coated with SU-8 (3025 or 3050, per desired height), soft-baked at 65 °C then ramped by 5 °C min^{-1} to 95 °C, and exposed either on an inverted microscope with a PRIMO (Alvéole) system using LEONARDO software (manufacturer-recommended UV dose; automatic field stitching when the pattern exceeded the objective field of view) or with a quartz/printed mask on a UV aligner (e.g., KUB2 or MJB4) following SU-8 guidelines. Post-exposure bake was 65 °C with a 5 °C min^{-1} ramp to 95 °C, then 8 min at 95 °C; development under agitation for 30 min; hard-bake 150 °C for 2 h (times given for 25 µm using SU8-3025; adjust per manufacturer for other heights/resists). For PDMS replication, SU-8 molds were silanized (place sample with 5-10 µL silane in a glass desiccator, vacuum 5 min, react 1 h, then bake 100-150 °C for 2 h), degassed PDMS was poured and cured at 70 °C overnight to yield a primary mold, which was itself silanized similarly but baked at 70 °C to avoid PDMS vitrification; fresh degassed PDMS was then cast on this silanized PDMS to obtain PDMS stamps/pillars. Optionally, an epoxy mold was prepared for durability: epoxy resin mixed 100 g:50 g (resin:hardener), centrifuged 5 min at 500 g to remove bubbles, poured into a glass Petri dish; PDMS pillars were pre-vacuumed and brought into contact with the epoxy at an angle (pillars down) to minimize trapped air; cure 48 h at room temperature, then peel PDMS and recast PDMS on the epoxy mold to generate new pillars. For NOA microwells, coverslips (VWR) were cleaned by wiping with 96% ethanol, rinsing in Milli-Q water, sonicating 30 min at 60 °C in 2% Hellmanex, rinsing in a large volume (2 L) of water with agitation for 30 min, and drying with compressed air. PDMS stamps from section 1.2 were cut as rectangles (õ0.6 cm x 1 cm; single sharp scalpel cut), cleaned with compressed air, and gently pressed onto clean coverslips (or ibidi dish) to exclude trapped air (primary PDMS molds should be used less than 4-5 times; prefer epoxy molds for longer use). NOA was dispensed to one side of the stamp and allowed to fill by capillarity; excess NOA was aspirated; UV exposure was 12 min at maximum power, the cured NOA around wells was cut with straight scalpel lines, followed by a second UV exposure of 2 min at maximum power; final curing was performed on a hot plate at 110-115 °C for more than 2 h or at 60 °C overnight; finished microwells can be stored at room temperature for days to weeks. Protocol adapted from [Vianay et al. 2025]. When using ibidi dishes (35 mm, ibidi), follow the same protocol but skip the coverslip cut step after first irradiation.

Conclusion and perspectives

Conclusion – Cross-system similarities, divergences, and interpretation

Across mammalian cells and *Phaeodactylum tricornutum*, this work establishes a generalizable strategy: multivalent, protein-based scaffolds can nucleate intracellular dynamic condensates, and functionalization with appropriate lipid droplet-targeting modules brings these condensates into proximity with LDs.

In mammalian cells, ControLD demonstrates all the hallmarks of a tunable and dynamic compartment: assemblies are created past a concentration threshold, capture LDs via perilipin tags, and can be rapidly and reversibly dissolved by small-molecule competition, with seconds-scale dissolution dynamics. Functionally, transient confinement of LDs acts as a physical barrier on organelle crosstalk: LD-mitochondria contacts are selectively reduced during trapping and re-established after dissolution. Conceptually, these behaviors are consistent with the modern view of biomolecular condensates as dynamic, multivalent assemblies that organize biochemistry while maintaining rapid molecular exchange. In *Pt*, we similarly established intracellular phase separation using two scaffold architectures (5Fm and Fm-Ft), quantified their appearance and growth over induction time, confirming the relevance and portability of those phase-separated structures. Before functionalization, condensates did not show nonspecific LD bias, mimicking the results of the non-targeted condensates in mammalian cells. Upon coupling to a LD coat protein, condensates frequently docked to LDs and occasionally displayed partial ring-like morphologies, demonstrating controlled engineering of condensate-LD interactions in a photosynthetic microalga. Moreover, this meshwork could as well alter LD remobilization dynamics in Pt, pointing to metabolism interference.

Across both systems, condensates form once scaffold concentrations cross a multivalency threshold, and LD-targeting modules redirect these condensates to lipid-droplet surfaces resulting in dynamic assemblies. Together, these features show that the mesoscale organization of LD accessibility can be engineered and toggled in living cells, and validate

the relevance of porting the approach across distant organisms and place LLPS-based perturbation alongside established tools for probing LD biology.

However, although robust similarities emerged across the different systems, important differences emerged in *Pt* relative to mammalian cells. *Pt* cells typically display a single condensate after induction, in contrast to the multiple assemblies commonly observed in mammalian cells under comparable conditions. Moreover, even with StLDP functionalization, *Pt* condensates predominantly dock to LDs and only rarely show partial ring-like wetting; robust, complete LD engulfment readily seen in mammalian cells is not observed in *Pt* despite attempts to enlarge LDs and to optimize the induction/starvation schedule. These divergences indicate that lineage-specific LD surface chemistry, organelle geography, and expression kinetics set the boundary conditions for condensate morphology and function.

Several factors could mechanistically explain the prevalence of docking—and the absence of full engulfment in *Pt* compared to mammalian cells. A first important lead is organelle organization in photosynthetic cells: *Pt* LDs are embedded within ER networks that are contiguous with a complex plastid, creating LD–ER–plastid triads where chemical cues and steric constraints vary at the subdomain scale. Such anisotropic, multi-organelle proximities promote subdomain-specific affinities and oriented docking sites rather than the large, symmetric wraps that would lead to uniform scaffold access around the droplet surface. Another factor is lineage-specific surface chemistries and targeting competitions. Diatoms lack perilipins; instead, StLDP-like coats can partition between LD surfaces and neighboring ER membranes. When used as targeting modules, this multiple localization could drain scaffold material away from the LD, limiting sustained residence and favoring transient docking. By contrast, in mammalian cells perilipin tags furnish a strong, LD-selective interface that supports near-complete enclosure and the reversible exclusion of non-target organelles. Moreover, the population of LD-associated proteins is different between mammals and microalgae, which could lead to different encapsulation behaviour. Finally, expression kinetics and LLPS thresholding impose a temporal filter: under nitrate induction, condensates emerge only after scaffold levels surpass a phase-separation threshold, while nutrient regimens that enlarge LDs (e.g., phosphate starvation) can depress protein synthesis. The double condition of high scaffold concentration and large LDs could restrict nucleation to few sites and biases the steady state toward docking rather than engulfment.

Nonetheless, this work shows that *controlling access* independently of specific enzymatic perturbations can provide a clean, reversible handle on LD physiology. In mammals, ControLD demonstrates that physical sequestration alone can reprogram organelle interactions and lipid utilization on demand. In *Pt*, the approach exposes fundamental biophysical behaviors and sets the stage for future metabolic studies. These results establish ControLD as a versatile platform to probe LD biology across diverse organisms.

Perspectives and Future directions

Several avenues exist to apply and extend the ControLD system beyond its current scope. These perspectives open up new possibilities for both fundamental research and technological innovation in organelle manipulation.

Cell biology perspectives

Lipid droplets play central roles in both normal physiology and disease, serving as hubs for energy storage, stress adaptation, and host-pathogen interactions. The ControLD system's ability to synchronize and pause LD dynamics allow probing these roles across diverse biological contexts. By using ControLD to temporarily trap and release LDs, one could dissect how synchronized lipid release influences cell survival during metabolic challenges. For example, LDs buffer lipid toxicity in neurons and support synaptic function, thus ControLD could clarify how timed LD release impacts neuronal health and plasticity. Beyond normal physiology, pathological contexts stand to benefit from this approach. LD dysregulation is implicated in metabolic disorders (e.g. fatty liver disease and insulin resistance) as well as infectious and inflammatory conditions. During infections, cells often rewire lipid metabolism to use LDs for their replication. By deploying ControLD in infected or stressed cells, researchers could temporally lock and release LDs to observe how this impacts pathogen proliferation or immune responses. In cancer biology, where tumor cells often reprogram their lipid storage and LDs can support rapid growth, ControLD could allow investigation of how synchronized lipid release or retention influences tumor cell metabolism. More broadly, the ability to manipulate LD positioning and contacts on demand represents a powerful tool for examining disease mechanisms.

Moreover, the ControLD strategy could be targeted to control other organelles like mitochondria or lysosomes. Mitochondria are highly dynamic, constantly moving, fusing, and interacting with LDs and the ER. A mitochondria-targeted system (using a mito outer membrane protein as an anchor) could reversibly cluster or immobilize mitochondria. This would allow tests of how synchronized mitochondrial positioning affects energy distribution, calcium signaling, or apoptotic sensitivity. In a similar fashion, one could imagine trapping lysosomes or endosomes to study their contribution to autophagy and trafficking in a timed manner. Such organelle-specific traps would mirror ControLD's ability to disrupt and restore contact sites: it is therefore a generalizable tool toward precise control of organelle behavior in living systems to explore complex biological processes.

ControLD for simpler LD purification

Beyond its cell-biological uses, ControLD could be developed into a novel biochemical tool for isolating LDs and their molecular partners. Traditionally, purifying lipid droplets from cells involves lengthy ultracentrifugation steps exploiting their low density. While

effective, density-based isolation is time-consuming, requires specialized equipment, and can suffer from the loss of certain interactors. ControLD's ability to cluster and segregate LDs opens new methodological leads for capturing LDs more easily. By aggregating LDs into a single compartment within cells, ControLD creates a concentrated cluster of LDs that could be harvested without ultracentrifugation. For example, cells could be gently lysed and the large protein-LD condensates collected by low-speed centrifugation or even simple sedimentation, or by engineering a tag on the condensate protein to pull down entire LD condensates from cell extracts, dramatically reducing the time and cost compared to high-speed gradients.

Another powerful extension is subpopulation-selective trapping. LD pools differ by size, composition, and coat proteins, implying specialized functions[177, 178]. Swapping the targeting domain in ControLD enables selective confinement of defined subsets: PLIN1 (large, lipolysis-regulated adipocyte LDs) versus PLIN2/PLIN3 (ubiquitous storage droplets) would allow selective trapping of LDs based on their accessibility; ACSL3 or Seipin could be used to capture nascent LDs forming at the ER and dissect early deposition steps. Resolving subset-specific roles would enable researchers to isolate the nascent LD population and study early lipid content separately from older LDs. Selective LD trapping thus offers a refined method to examine how each droplet cohort contributes to cellular metabolism and signaling.

ControLD-mediated clusters could also be used to capture interactors that associate transiently with LDs. Any proteins weakly bound to LDs, or even RNAs and ribonucleoproteins that transiently dock on LD surfaces, would co-purify. Notably, LDs are known to sequester unexpected molecules - for instance, Drosophila embryos store a cache of maternal histone proteins on LDs via the protein Jabba[179]. There is evidence that certain mRNAs localize to LDs as well (e.g. Oskar mRNA in fruit fly oocytes, or lncRNAs in mammals). By immobilizing the LD and its partners in a condensate, condensates might recover weak or fleeting contacts (such as a lipase that adsorbs transiently to LDs), and ControLD-based pull-down could help identify such LD-associated RNAs or proteins, expanding our knowledge of LD "interactomes" beyond the core proteome.

ControLD as a model for endogenous LD assemblies

Perhaps the most intriguing perspective is using ControLD as a model system to mimic contact sites between endogenous specific organelles, by reproducing complex interactions from the nanometer to micrometer scales. In recent years, cell biologists have discovered that cells often organize organelles into higher-order assemblies or condensates to realize specific functions. Interesting parallels exist between ControLD-induced LD clusters and several natural organelle assemblies observed in cells.

One well-known endogenous mechanism that clusters lipid droplets is mediated by

the protein CIDEC (also called FSP27) in adipocytes. CIDEC localizes to the interfaces between adjacent LDs and tethers droplets together to promote lipid exchange [180]. In white adipose tissue, this is critical for forming one giant droplet per cell. Genetic studies show that without CIDEC, adipocytes instead display many small droplets. How CIDEC causes small LDs to coalesce into a big one was unclear until recently. Ganeva et al. (2023) visualized these LD-LD contacts and found that CIDEC brings LD membranes into extremely close proximity. This creates a "lipid bridge" through two monolayers, allowing triglycerides to flow from the smaller droplet into the larger droplet, a phenomenon called Ostwald ripening. Morphologically, ControLD is able to form "bead-on-a-string" phenotypes, where LDs are densely packed and connected by thin layers of LLPS scaffolds (presented in Extended Fig. 1 of the article discussed in chapter 2), which can be viewed as an LD-clustering system analogous to CIDEC. It would be interesting to compare ControLD clusters with CIDEC clusters. For instance, CIDEC-mediated contacts are specialized to enable lipid mixing; ControLD's protein condensate might hold LDs slightly further apart (potentially inhibiting lipid exchange). One could imagine engineering the condensate to mimic a CIDEC interface, with membrane-binding or amphipathic motifs (similar to those in CIDEC) to promote closer LD apposition. By doing so, ControLD might induce not just clustering but actual lipid transfer between droplets - effectively reconstituting the lipid fusion that CIDEC accomplishes. Even without that modification, studying ControLD-induced LD clusters can yield insight into the biophysical properties of tethered LDs.

Since clustering of organelles via phase separation is not limited to lipid metabolism, one can broaden the scope to other organelles. Synaptic vesicles (SVs), which carry neurotransmitters, are known to form large clusters at presynaptic nerve terminals (the reserve pool of vesicles). Recent research has updated this view by showing that synapsin proteins phase-separate with synaptic vesicles, forming liquid-like condensates[181]. In these SV-synapsin condensates, the vesicles are held in a densely packed cluster, yet they remain dynamic and mobile within the assembly, a hallmark of a biocondensate.

The synapsin/SV paradigm is highly analogous to ControLD and LDs: in both cases, a biomolecular condensate group organelles into a concentrated, yet reversible assembly. This parallel suggests that the physical rules governing ControLD assemblies likely mirror those of natural condensates. For instance, synapsin's condensation can be modulated by signaling (synapsins disperse upon phosphorylation during intense activity, releasing vesicles), a property reflected in ControLD reversibility. Questions about the material properties of such condensates (viscosity, surface tension, fusion/fission dynamics) can be addressed in the ControLD system and compared to known behaviors of synapsin-SV condensates, insights which could be relevant to neuroscience.

These examples show that cells natively deploy phase separation to regulate organelle access, which strengthens the rationale for our synthetic modeling. They also open con-

crete, testable perspectives: can an orthogonal, chemically addressable condensate be used to compete with, disrupt, or even substitute for a native condensate to restore a lost function? This would let us separate the effect of physical organization from the effect of enzymatic activity in the function of endogenous condensates.

Annexes

Tools of the trade

https://doi.org/10.1038/s41580-025-00880-x

Condensate-mediated intracellular organelle sequestration



Compartmentalization is essential for the correct function of eukaryotic cells, and many biomolecules and biochemical events are localized in organelles, which are in a dynamic flux of material or information with other cellular compartments. Understanding the interplay between organelles and the orchestration of these fluxes is a major challenge of cellular biology. A widespread approach to studying these questions is perturbing the system, for example using genetic, chemical or physical approaches. However, most of these techniques lack specificity or temporal resolution, requiring the development of new tools.

We have developed a novel approach to impair the ability of organelles to exchange and communicate with other cellular components. We called this method ControLD after our organelle of interest, lipid droplets (LDs), which are ubiquitous organelles with many essential roles from energy storage to oxidative stress protection. The ControLD system consists of artificial, engineered proteins containing a bio-orthogonal liquid–liquid phase separation (LLPS) domain. Following overexpression in different cell types, these scaffold proteins can self-organize into micrometric dense liquid-like structures once their concentration crosses a scaffold-specific threshold. By fusing these self-organization domains to an LD-specific protein, we were able to generate a dense protein meshwork around nearly all LDs of a living cell, effectively isolating them from other organelles. We demonstrated that sequestered LDs are not consumed when the cell initiates lipid mobilization and are therefore metabolically unavailable. Importantly, this LLPS-mediated confinement meshwork is easily reversible using the chemical FK506 to disrupt the LLPS, releasing LDs rapidly. ControLD provides an efficient and versatile approach to physically isolate an organelle of interest. This perturbative approach does not rely on prior knowledge or hypotheses on the proteins or pathways involved in inter-organelle communication and is instead focused on building a physical barrier around a target organelle. This method presents the advantage of biological orthogonality, compared to chemical inhibitors disrupting an entire signalling cascade, while remaining highly specific to organelles and fully reversible. We envision that this tool could be used to gain a better understanding of how and when organelles exchange biomolecules, and of the implications of organelle sequestration for the biochemistry of the cell.

Emma Pasquier ✉ **& Chems Amari** ✉
Chemistry Department, Ecole Normale Supérieure, Paris, France.
✉e-mail: emma.pasquier@ens.fr; chems.amari@normalesup.org

Competing interests
The authors declare no competing interests.

Original Article: Amari, C. et al. Controlling lipid droplet dynamics via tether condensates. *Nat. Chem. Biol.* https://doi.org/10.1038/s41589-025-01915-2 (2025)

Related Article: Cochard, A. et al. RNA at the surface of phase-separated condensates impacts their size and number. *Biophys. J.* **121**, 1675–1690 (2022)

CREDIT: MOTAZKATTAN/ROOM/GETTY

2 Protein domains sequences

Table 5.2: Amino-acid sequences of protein domains, and nucleic sequences of promoters presented throughout the study.

Protein	Full name	Protein sequence
blasR	Blasticydin resistance	MAKPLSQEESTLIERATATINSIPISEDYSVASA ALSSDGRIFTGVNVYHFTGGPCAELVVLGTAA AAAAGNLTCIVAIGNENRGILSPCGRCRQVLL DLHPGIKAIVKDSDGQPTAVGIRELLPSGYVW EG
emGFP	Emerald Green Fluorescent Protein	MVSKGEELFTGVVPILVELDGDVNGHKFSVSG EGEGDATYGKLTLKFICTTGKLPVPWPTLVT TLTYGVQCFARYPDHMKQHDFFKSAMPEGY VQERTIFFKDDGNYKTRAEVKFEGDTLVNRIE LKGIDFKEDGNILGHKLEYNYNSHKVYITADK QKNGIKVNFKTRHNIEDGSVQLADHYQQNTPI GDGPVLLPDNHYLSTQSALSKDPNEKRDHMV LLEFVTAAGITLGMDELYK
Fm	Human FKBP with point mutation F36M	MGVQVETISPGDGRTFPKRGQTCVVHYTGML EDGKKMDSSRDRNKPFKFMLGKQEVIRGWEE GVAQMSVGQRAKLTISPDYAYGATGHPGIIPP HATLVFDVELLKLEE
Ft	Human light-chain ferritin	MNYSTDVEAAVNSLVNLYLQASYTYLSLGFYF DRDDVALEGVSHFFRELAEEKREGYERLLKM QNQRGGRALFQDIKKPAEDEWGKTPDAMKA AMALEKKLNQALLDLHALGSARTDPHLCDFLE THFLDEEVKLIKKMGDHLTNLHRLGGPEAGL GE
mOrange	Monomeric orange fluorescent protein	MVSKGEENNMAIIKEFMRFKVRMEGSVNGHE FEIEGEGEGRPYEGFQTAKLKVTKGGPLPFA WDILSPHFTYGSKAYVKHPADIPDYFKLSFPE GFKWERVMNYEDGGVVTVTQDSSLQDGEFIY KVKLRGTNFPSDGPVMQKKTMGWEASSERM YPEDGALKGKIKMRLKLKDGGHYTSEVKTTY KAKKPVQLPGAYIVDIKLDITSHNEDYTIVEQY ERAEGRHSTGGMDELYK

Continued on next page

Protein	Full name	Protein sequence
HOGP	*Haematococcus* oil globule protein	MSEKQLKRLGFVHQGASYAYSYTGTAEKLYK TARSFAPTFVEPTLAQVEDRVVAITAPVVAQA QDLSEKALHIADDQVDCILNTTDKAVADGKK GVVDCMNGVKEMHEKNMQTYIATSNSYFEYI KGISDWAKDKLNPIKGGQHALDTLNAAIAKA QEATDPDVAAKMALDAWNSFASVPVVAKVL ETADPVTQTGLSSFYKLHDTLVSWPLYSKVVS TGVSTLSWATTTMPYKLGAQYMYPLVQPVA DPALAKITNSKVINGTLSYWKPTASAA
PtLDP1	*Phaeodactylum Tricornutum* Lipid Droplet Protein 1	MKILSSLVLATIALANGQITYLDAPVEGWRASF APMEQGNGVFLSPDGSMVVAIASNCLVRAFG QATGEVRWTSNPPPGDGSSSCNGGITFNDNA DIPYFTYMVNDNVQGTISTRVIMGDIDTGDVL MTSEVLAGSSAGSPQTTLDGRHIMFTHNDGG TGMFSILDTMQDPDMSGMTPIISPIFSESNATE PFSAVGVFHDPNGGNYAGGLTTNRNDIFVWS LATNFDVNNTRPPVGEAGVFGFQFPVDFNNT GDDLDILYFGSFSFQATTRPVLASNGTSMYWG VTRGEYRAWFQRAFDRPITELVTLSRDNVVPS LGARAAVTLSSDPINPIVFGPGPNEEFFRGNSD FSETTIISTSPSDASPYGEGIVSGRAAVSPDDQF VYYATQGGLLTQAETDALASVWTTGGAANIT IESVRGDLAISRDGSRVFVPDTVSASGFVIAVQ VAEVGETPPPTGAPISMDMSMAPSGADGSSG TAAPSLPDGATAPPNAEGTDAPGSTPAPAPAS SAIRASMIALVASLLVFVF
StLDP	*Stramenopile*-type LD protein	MPSSSNPNGIKASSSMTTPLLSSGSSRTARRGE QKGQLTAVVLSAYDLPSREPPLYVKISIPEKYA AQTGPPCQRHKDRNSFKFGSNGASSSTADNQI SLRAPLPELYTSTLRVDVVSDGPESATLTATY RLEQLQVGVATWLILNLEESTPSSAVVPDTSD VVPPTLRLQMTLDGPYRTEIGALVNWGQAW FRFVDQLEASGANFFSKLPLSIFAIFNSQWMLV LVVPIVAVLVVSAPIWVGFLAVTLPMLLPLLV AGAAVLFTVATVLLILYASTNAGREQVSGICM PVVHTLLASRSGQRLVYQTGPRPTPVGVAKA ILPVSLWQKLFVSLWIDFMGSASYLLPIVGEGL DIAWAPLQTILIMAMYDTTSPNLKYISFLEEILP FTDIVPSATAGWLKEFGVPLLFGPGHGEPME VKDLMKVLLSPPRTGSPTQSSKPPPAASSATP MLVPAS

Continued on next page

Protein	Full name	Protein sequence
StLDPΔNter	StLDP with Nter truncation (aa 179-456)	MRTEIGALVNWGQAWFRFVDQLEASGANFFS KLPLSIFAIFNSQWMLVLVVPIVAVLVVSAPIW VGFLAVTLPMLLPLLVAGAAVLFTVATVLLIL YASTNAGREQVSGICMPVVHTLLASRSGQRLV YQTGPRPTPVGVAKAILPVSLWQKLFVSLWID FMGSASYLLPIVGEGLDIAWAPLQTILIMAMY DTTSPNLKYISFLEEILPFTDIVPSATAGWLKE FGVPLLFGPGHGEPMEVKDLMKVLLSPPRTG SPTQSSKPPPAASSATPMLVPAS
ZeoR	Zeocine resistance	MAKLTSAVPVLTARDVAGAVEFWTDRLGFSR DFVEDDFAGVVRDDVTLFISAVQDQVVPDNT LAWVWVRGLDELYAEWSEVVSTNFRDASGP AMTEIGEQPWGREFALRDPAGNCVHFVAEEQ D

Promoter	Full name	Promoter sequence
pfcpA	FcpA promoter	atttaggtgacactatagaaccagatcccccgggctgcaggacgcaat ggaggattatcaccgcaaaaatgaacttcgaaaaaaactttcgagcga ccatggaaaaggaggatcagattcagattacaacagtggattgctctg gtagcaaatatcttctgctagattggctcatggtcggttttggacgttcg aagctcaccgtcaaaagaaacaaaagagaagaatgacgtcttcgtgac gtagaatctacgactgtactcggatctgggaaatgaattgactcacggt cttcttcgagtcctgttacaggcccttggtccgaaccccacacgatttt gcaccaaagatttgcttcaatttgctggatgttttgactgcaagatcagc tggcctagcaagagtgctcgtgttgcttcgtcgggaatccctacgaattt cagttctgcacaaatttgtctgccgtttcga
pNR	Nitrate reductase promoter	agcgaacagaagacccaatcgtggagcagtcatcatcattgtggaaat gtgtcctagactgttgcagacagtcaccaacggaatgctttcgttaaga gcaaggcgacaacggttccttcgttgagatggtggttccactgtgcagg tcacgtagtgaagtgatgttgcggtagtctgcaatcccgctagatacac gtcattcgtgaaaggcctgttgttttcatgtccgggtctgcacgggcact agaaggaaggaagcaaagacgaacggaagtgactgtaaacgagaag tgcacgaagccttttcttgtgacgtcacaacccgaatagccctacgtgg cgtgcgactttccggcactttggatatcgttgccctatatgtattgggtg tatacatgtcgtattccaactacgacagaaaacagtcagttacgggtat tcgaacttccggcacctgcagcgaggagttttgtgtccgtcgcacatcct ccgtgctttcggcacctacgtaggcggcaaacttcctgccttccgccccc gccttgcggcattccggctccgggccagaattgcccgggtgttcacaat tttgcctcctcacgaaaaaacgttctactttgtattttggtcgggtttcgg atccttccagcaaccattctcattcaaagtcaccacttgtgcgaacg

References

[1] Michal Eisenberg-Bord, Nadav Shai, Maya Schuldiner, and Maria Bohnert. "A Tether Is a Tether Is a Tether: Tethering at Membrane Contact Sites". *Developmental Cell* 39.4 (2016), pp. 395–409. pmid: 27875684 (cit. on pp. 5–7, 11).

[2] Alice L. Baillie, Anna-Lena Falz, Stefanie J. Müller-Schüssele, and Imogen Sparkes. "It Started With a Kiss: Monitoring Organelle Interactions and Identifying Membrane Contact Site Components in Plants". *Frontiers in Plant Science* 11 (2020), p. 517. pmid: 32435254 (cit. on pp. 5, 19).

[3] G.K. Voeltz, E.M. Sawyer, G. Hajnóczky, and W.A. Prinz. "Making the Connection: How Membrane Contact Sites Have Changed Our View of Organelle Biology". *Cell* 187.2 (2024), pp. 257–270 (cit. on p. 6).

[4] Maya Schuldiner and Maria Bohnert. "A Different Kind of Love – Lipid Droplet Contact Sites". *Biochimica et Biophysica Acta (BBA) - Molecular and Cell Biology of Lipids*. Recent Advances in Lipid Droplet Biology 1862 (10, Part B 2017), pp. 1188–1196 (cit. on pp. 7, 21).

[5] Miguel Sánchez-Álvarez, Miguel Ángel del Pozo, Marta Bosch, and Albert Pol. "Insights Into the Biogenesis and Emerging Functions of Lipid Droplets From Unbiased Molecular Profiling Approaches". *Frontiers in Cell and Developmental Biology* 10 (2022), p. 901321. pmid: 35756995 (cit. on pp. 7, 8, 21–24).

[6] Patricia Gomez-Suaga, Sebastien Paillusson, Radu Stoica, Wendy Noble, Diane P. Hanger, and Christopher C.J. Miller. "The ER-Mitochondria Tethering Complex VAPB-PTPIP51 Regulates Autophagy". *Current Biology* 27.3 (2017), pp. 371–385. pmid: 28132811 (cit. on pp. 8, 12).

[7] Benjamin E. Housden, Matthias Muhar, Matthew Gemberling, Charles A. Gersbach, Didier Y. R. Stainier, Geraldine Seydoux, et al. "Loss-of-Function Genetic Tools for Animal Models: Cross-Species and Cross-Platform Differences". *Nature reviews. Genetics* 18.1 (2017), pp. 24–40. pmid: 27795562 (cit. on pp. 9, 10).

[8] Mohamed A. El-Brolosy and Didier Y. R. Stainier. "Genetic Compensation: A Phenomenon in Search of Mechanisms". *PLOS Genetics* 13.7 (13 juil. 2017), e1006780 (cit. on p. 9).

[9] J. Lytton, M. Westlin, and M. R. Hanley. "Thapsigargin Inhibits the Sarcoplasmic or Endoplasmic Reticulum Ca-ATPase Family of Calcium Pumps." *Journal of Biological Chemistry* 266.26 (1991), pp. 17067–17071 (cit. on p. 10).

[10] Benoît Kornmann, Erin Currie, Sean R. Collins, Maya Schuldiner, Jodi Nunnari, Jonathan S. Weissman, et al. "An ER-mitochondria Tethering Complex Revealed by a Synthetic Biology Screen". *Science (New York, N.Y.)* 325.5939 (2009), pp. 477–481. pmid: 19556461 (cit. on p. 11).

[11] Hossein Moghimianavval, Chintan Patel, Sonisilpa Mohapatra, Sung-Won Hwang, Tunc Kayikcioglu, Yashar Bashirzadeh, et al. "Engineering Functional Membrane–Membrane Interfaces by InterSpy". *Small* 19.13 (2023), p. 2202104 (cit. on p. 12).

[12] Chi-Lun Chang, Aubrey V. Weigel, Maria S. Ioannou, H. Amalia Pasolli, C. Shan Xu, David R. Peale, et al. "Spastin Tethers Lipid Droplets to Peroxisomes and Directs Fatty Acid Trafficking through ESCRT-III". *Journal of Cell Biology* 218.8 (2019), pp. 2583–2599 (cit. on p. 12).

[13] Helen D. Wu, Masaki Kikuchi, Onur Dagliyan, Adam K. Aragaki, Hideki Nakamura, Nikolay V. Dokholyan, et al. "Rational Design and Implementation of a Chemically Inducible Heterotrimerization System". *Nature Methods* 17.9 (2020), pp. 928–936 (cit. on pp. 12, 14, 15).

[14] D. M. Spencer, T. J. Wandless, S. L. Schreiber, and G. R. Crabtree. "Controlling Signal Transduction with Synthetic Ligands". *Science (New York, N.Y.)* 262.5136 (1993), pp. 1019–1024. pmid: 7694365 (cit. on p. 12).

[15] J. Liang, J. Choi, and J. Clardy. “Refined Structure of the FKBP12–Rapamycin–FRB Ternary Complex at 2.2 Å Resolution”. *Acta Crystallographica Section D: Biological Crystallography* 55.4 (1999), pp. 736–744 (cit. on p. 12).

[16] Takafumi Miyamoto, Robert DeRose, Allison Suarez, Tasuku Ueno, Melinda Chen, Tai-ping Sun, et al. “Rapid and Orthogonal Logic Gating with a Gibberellin-Induced Dimerization System”. *Nature Chemical Biology* 8.5 (2012), pp. 465–470 (cit. on pp. 13, 15).

[17] Sang-Youl Park, Jingde Qiu, Shuang Wei, Francis C. Peterson, Jesús Beltrán, Angélica V. Medina-Cucurella, et al. “An Orthogonalized PYR1-based CID Module with Reprogrammable Ligand-Binding Specificity”. *Nature Chemical Biology* 20.1 (2024), pp. 103–110 (cit. on p. 13).

[18] Toru Komatsu, Igor Kukelyansky, J. Michael McCaffery, Tasuku Ueno, Lidenys C. Varela, and Takanari Inoue. “Organelle-Specific, Rapid Induction of Molecular Activities and Membrane Tethering”. *Nature Methods* 7.3 (2010), pp. 206–208 (cit. on p. 13).

[19] Takanari Inoue, Won Do Heo, Joshua S. Grimley, Thomas J. Wandless, and Tobias Meyer. “An Inducible Translocation Strategy to Rapidly Activate and Inhibit Small GTPase Signaling Pathways”. *Nature Methods* 2.6 (2005), pp. 415–418 (cit. on p. 14).

[20] Divyanshu Mahajan, Hieng Chiong Tie, Bing Chen, and Lei Lu. “Dopey1-Mon2 Complex Binds to Dual-Lipids and Recruits Kinesin-1 for Membrane Trafficking”. *Nature Communications* 10 (2019), p. 3218. pmid: 31324769 (cit. on p. 14).

[21] Andrei V. Karginov, Yan Zou, David Shirvanyants, Pradeep Kota, Nikolay V. Dokholyan, Douglas D. Young, et al. “Light Regulation of Protein Dimerization and Kinase Activity in Living Cells Using Photocaged Rapamycin and Engineered FKBP”. *Journal of the American Chemical Society* 133.3 (2011), pp. 420–423 (cit. on p. 14).

[22] Zachary B Hill, Alexander J Martinko, Duy P Nguyen, and James A Wells. “Human Antibody-Based Chemically Induced Dimerizers for Cell Therapeutic Applications”. *Nature chemical biology* 14.2 (2018), pp. 112–117. pmid: 29200207 (cit. on p. 15).

[23] Wignand W. D. Mühlhäuser, Maximilian Hörner, Wilfried Weber, and Gerald Radziwill. “Light-Regulated Protein Kinases Based on the CRY2-CIB1 System”. *Methods in Molecular Biology (Clifton, N.J.)* 1596 (2017), pp. 257–270. pmid: 28293892 (cit. on p. 15).

[24] Daphne L. Che, Liting Duan, Kai Zhang, and Bianxiao Cui. “The Dual Characteristics of Light-Induced Cryptochrome 2, Homo-oligomerization and Heterodimerization, for Optogenetic Manipulation in Mammalian Cells”. *ACS synthetic biology* 4.10 (2015), pp. 1124–1135. pmid: 25985220 (cit. on pp. 15, 16, 18).

[25] Liting Duan, Daphne Che, Kai Zhang, Qunxiang Ong, Shunling Guo, and Bianxiao Cui. “Optogenetic Control of Molecular Motors and Organelle Distributions in Cells”. *Chemistry & Biology* 22.5 (2015), pp. 671–682. pmid: 25963241 (cit. on pp. 16, 18).

[26] Laura B Motta-Mena, Anna Reade, Michael J Mallory, Spencer Glantz, Orion D Weiner, Kristen W Lynch, et al. “An Optogenetic Gene Expression System with Rapid Activation and Deactivation Kinetics”. *Nature Chemical Biology* 10.3 (2014), pp. 196–202 (cit. on p. 16).

[27] Clare E. Buckley, Rachel E. Moore, Anna Reade, Anna R. Goldberg, Orion D. Weiner, and Jonathan D. W. Clarke. “Reversible Optogenetic Control of Subcellular Protein Localization in a Live Vertebrate Embryo”. *Developmental Cell* 36.1 (2016), pp. 117–126. pmid: 26766447 (cit. on pp. 17, 18).

[28] Andrea Flores-Ibarra, Raiza N. A. Maia, Bence Olasz, Jonathan R. Church, Guillaume Gotthard, Igor Schapiro, et al. “Light-Oxygen-Voltage (LOV)-Sensing Domains: Activation Mechanism and Optogenetic Stimulation”. *Journal of Molecular Biology*. Photosensory Receptors-Mechanisms and Effects 436.5 (2024), p. 168356 (cit. on p. 17).

[29] Oana I. Lungu, Ryan A. Hallett, Eun Jung Choi, Mary J. Aiken, Klaus M. Hahn, and Brian Kuhlman. “Designing Photoswitchable Peptides Using the AsLOV2 Domain”. *Chemistry & Biology* 19.4 (2012), pp. 507–517. pmid: 22520757 (cit. on p. 17).

[30] Gurkan Guntas, Ryan A. Hallett, Seth P. Zimmerman, Tishan Williams, Hayretin Yumerefendi, James E. Bear, et al. “Engineering an Improved Light-Induced Dimer (iLID) for Controlling the Localization and Activity of Signaling Proteins”. *Proceedings of the National Academy of Sciences* 112.1 (2015), pp. 112–117 (cit. on p. 17).

[31] Taras A. Redchuk, Maksim M. Karasev, Evgeniya S. Omelina, and Vladislav V. Verkhusha. “Near-Infrared Light-Controlled Gene Expression and Protein Targeting in Neurons and Non-neuronal Cells”. *ChemBioChem* 19.12 (2018), pp. 1334–1340 (cit. on p. 17).

[32] Kangqiang Qiu, Weiwei Zou, Hongbao Fang, Mingang Hao, Kritika Mehta, Zhiqi Tian, et al. “Light-Activated Mitochondrial Fission through Optogenetic Control of Mitochondria-Lysosome Contacts”. *Nature Communications* 13.1 (2022), p. 4303 (cit. on pp. 17, 18).

[33] Luhao Zhang, Xuechun Liu, Min Zhu, Yuanfa Yao, Zhichao Liu, Xianming Zhang, et al. “Optogenetic Control of Mitochondrial Aggregation and Function”. *Frontiers in Bioengineering and Biotechnology* 12 (2025) (cit. on p. 18).

[34] Xin Deng, Wei Wang, Dandan Peng, Luhao Zhang, Zhihao Ma, Junfen Fu, et al. “Optogenetic Perturbation of Lipid Droplet Localization Affects Lipid Metabolism and Development in Drosophila”. *Journal of Lipid Research* 66.8 (2025), p. 100848. pmid: 40545239 (cit. on p. 18).

[35] Imogen Sparkes. “Lessons from Optical Tweezers: Quantifying Organelle Interactions, Dynamics and Modelling Subcellular Events”. *Current Opinion in Plant Biology*. Cell Biology 46 (2018), pp. 55–61 (cit. on pp. 19, 20).

[36] Samuel H. Chung, Damon A. Clark, Christopher V. Gabel, Eric Mazur, and Aravinthan DT Samuel. “The Role of the AFD Neuron in C. Elegans Thermotaxis Analyzed Using Femtosecond Laser Ablation”. *BMC Neuroscience* 7.1 (2006), p. 30 (cit. on p. 19).

[37] Jan Brugués, Benoit Maugis, Jaume Casademunt, Pierre Nassoy, François Amblard, and Pierre Sens. “Dynamical Organization of the Cytoskeletal Cortex Probed by Micropipette Aspiration”. *Proceedings of the National Academy of Sciences* 107.35 (2010), pp. 15415–15420 (cit. on p. 19).

[38] Rosalind A. Coleman. “The "Discovery" of Lipid Droplets: A Brief History of Organelles Hidden in Plain Sight”. *Biochimica Et Biophysica Acta. Molecular and Cell Biology of Lipids* 1865.9 (2020), p. 158762. pmid: 32622088 (cit. on p. 21).

[39] Eva Jarc and Toni Petan. “Lipid Droplets and the Management of Cellular Stress”. *The Yale Journal of Biology and Medicine* 92.3 (2019), pp. 435–452. pmid: 31543707 (cit. on pp. 21, 28–30).

[40] Yujie Zhao, Rui Cao, Jincheng Li, Yingying Xu, Lijuan Zhou, and Yajin Ye. “Lipid Droplets in Plants: Turnover and Stress Responses”. *Frontiers in Plant Science* 16 (2025) (cit. on pp. 22, 27, 28).

[41] R.Mankamna Kumari, Amit Khatri, Ritika Chaudhary, and Vineet Choudhary. “Concept of Lipid Droplet Biogenesis”. *European journal of cell biology* 102.4 (2023), p. 151362. pmid: 37742390 (cit. on pp. 22, 24, 25, 30).

[42] Congyan Zhang and Pingsheng Liu. “The New Face of the Lipid Droplet: Lipid Droplet Proteins”. *PROTEOMICS* 19.10 (2019), p. 1700223 (cit. on p. 22).

[43] James A. Olzmann and Pedro Carvalho. “Dynamics and Functions of Lipid Droplets”. *Nature Reviews Molecular Cell Biology* 20.3 (2019), pp. 137–155 (cit. on p. 22).

[44] Chao-Wen Wang. “Lipid Droplet Dynamics in Budding Yeast”. *Cellular and Molecular Life Sciences: CMLS* 72.14 (2015), pp. 2677–2695. pmid: 25894691 (cit. on p. 22).

[45] Michele Wölk and Maria Fedorova. “The Lipid Droplet Lipidome”. *FEBS Letters* 598.10 (2024), pp. 1215–1225 (cit. on p. 22).

[46] Natalie Krahmer, Yi Guo, Florian Wilfling, Maximiliane Hilger, Susanne Lingrell, Klaus Heger, et al. “Phosphatidylcholine Synthesis for Lipid Droplet Expansion Is Mediated by Localized Activation of CTP:Phosphocholine Cytidylyltransferase”. *Cell metabolism* 14.4 (2011), pp. 504–515. pmid: 21982710 (cit. on pp. 22, 30).

[47] Qiang Gao, Derk D. Binns, Lisa N. Kinch, Nick V. Grishin, Natalie Ortiz, Xiao Chen, et al. “Pet10p Is a Yeast Perilipin That Stabilizes Lipid Droplets and Promotes Their Assembly”. *Journal of Cell Biology* 216.10 (2017), pp. 3199–3217 (cit. on p. 23).

[48] Imen Bouchnak, Denis Coulon, Vincent Salis, Sabine D’Andréa, and Claire Bréhélin. “Lipid Droplets Are Versatile Organelles Involved in Plant Development and Plant Response to Environmental Changes”. *Frontiers in Plant Science* 14 (2023) (cit. on p. 23).

[49] Muhammad Arifur Rahman, Ravinder Kumar, Enrique Sanchez, and Taras Y. Nazarko. “Lipid Droplets and Their Autophagic Turnover via the Raft-Like Vacuolar Microdomains”. *International Journal of Molecular Sciences* 22.15 (2021), p. 8144. pmid: 34360917 (cit. on pp. 23, 32).

[50] Yury S. Bykov, Nir Cohen, Natalia Gabrielli, Hetty Manenschijn, Sonja Welsch, Petr Chlanda, et al. “High-Throughput Ultrastructure Screening Using Electron Microscopy and Fluorescent Barcoding”. *Journal of Cell Biology* 218.8 (2019), pp. 2797–2811 (cit. on p. 24).

[51] Horst Robenek, Oliver Hofnagel, Insa Buers, Mirko J. Robenek, David Troyer, and Nicholas J. Severs. “Adipophilin-Enriched Domains in the ER Membrane Are Sites of Lipid Droplet Biogenesis”. *Journal of Cell Science* 119.20 (2006), pp. 4215–4224 (cit. on p. 24).

[52] Hsiao-Ching Wan, Rossana C. N. Melo, Zhoung Jin, Ann M. Dvorak, and Peter F. Weller. "Roles and Origins of Leukocyte Lipid Bodies: Proteomic and Ultrastructural Studies". *The FASEB Journal* 21.1 (2007), pp. 167–178 (cit. on p. 24).

[53] Vineet Choudhary and Roger Schneiter. "Lipid Droplet Biogenesis from Specialized ER Subdomains". *Microbial Cell* 7.8 (), pp. 218–221. pmid: 32743002 (cit. on p. 24).

[54] Florian Wilfling, Huajin Wang, Joel T. Haas, Natalie Krahmer, Travis J. Gould, Aki Uchida, et al. "Triacylglycerol Synthesis Enzymes Mediate Lipid Droplet Growth by Relocalizing from the ER to Lipid Droplets". *Developmental Cell* 24.4 (2013), pp. 384–399. pmid: 23415954 (cit. on p. 25).

[55] Hui Qian, Yuanying Chen, Zongqian Nian, Lu Su, Haoyong Yu, Feng-Jung Chen, et al. "HDAC6-mediated Acetylation of Lipid Droplet–Binding Protein CIDEC Regulates Fat-Induced Lipid Storage". *The Journal of Clinical Investigation* 127.4 (2017), pp. 1353–1369 (cit. on p. 25).

[56] Jiunn Song, Arda Mizrak, Chia-Wei Lee, Marcelo Cicconet, Zon Weng Lai, Wei-Chun Tang, et al. "Identification of Two Pathways Mediating Protein Targeting from ER to Lipid Droplets". *Nature Cell Biology* 24.9 (2022), pp. 1364–1377 (cit. on p. 25).

[57] Jose Verdezoto Mosquera, Meghan C. Bacher, and James R. Priess. "Nuclear Lipid Droplets and Nuclear Damage in Caenorhabditis Elegans". *PLOS Genetics* 17.6 (2021), e1009602 (cit. on p. 25).

[58] Yoann Combot, Veijo T. Salo, Gilliane Chadeuf, Maarit Hölttä, Katharina Ven, Ilari Pulli, et al. "Seipin Localizes at Endoplasmic-Reticulum-Mitochondria Contact Sites to Control Mitochondrial Calcium Import and Metabolism in Adipocytes". *Cell Reports* 38.2 (2022). pmid: 35021082 (cit. on p. 25).

[59] Alexandra Grippa, Laura Buxó, Gabriel Mora, Charlotta Funaya, Fatima-Zahra Idrissi, Francesco Mancuso, et al. "The Seipin Complex Fld1/Ldb16 Stabilizes ER–Lipid Droplet Contact Sites". *Journal of Cell Biology* 211.4 (2015), pp. 829–844 (cit. on p. 25).

[60] Roger Schneiter and Vineet Choudhary. "Seipin Collaborates with the ER Membrane to Control the Sites of Lipid Droplet Formation". *Current Opinion in Cell Biology* 75 (2022), p. 102070 (cit. on p. 25).

[61] Zhe Cao, Yan Hao, Chun Wing Fung, Yiu Yiu Lee, Pengfei Wang, Xuesong Li, et al. "Dietary Fatty Acids Promote Lipid Droplet Diversity through Seipin Enrichment in an ER Subdomain". *Nature Communications* 10.1 (2019), p. 2902 (cit. on p. 25).

[62] Bhumika Bhatt-Wessel, T. William Jordan, John H. Miller, and Lifeng Peng. "Role of DGAT Enzymes in Triacylglycerol Metabolism". *Archives of Biochemistry and Biophysics* 655 (2018), pp. 1–11 (cit. on p. 26).

[63] Albert Herms, Marta Bosch, Nicholas Ariotti, Babu J. N. Reddy, Alba Fajardo, Andrea Fernández-Vidal, et al. "Cell-to-Cell Heterogeneity in Lipid Droplets Suggests a Mechanism to Reduce Lipotoxicity". *Current Biology* 23.15 (2013), pp. 1489–1496. pmid: 23871243 (cit. on pp. 26, 30).

[64] Abdou Rachid Thiam and Elina Ikonen. "Lipid Droplet Nucleation". *Trends in Cell Biology* 31.2 (2021), pp. 108–118. pmid: 33293168 (cit. on p. 26).

[65] Vineet Choudhary, Namrata Ojha, Andy Golden, and William A. Prinz. "A Conserved Family of Proteins Facilitates Nascent Lipid Droplet Budding from the ER". *Journal of Cell Biology* 211.2 (2015), pp. 261–271 (cit. on p. 26).

[66] Michel Becuwe, Laura M. Bond, Antonio F.M. Pinto, Sebastian Boland, Niklas Mejhert, Shane D. Elliott, et al. "FIT2 Is an Acyl–Coenzyme A Diphosphatase Crucial for Endoplasmic Reticulum Homeostasis". *Journal of Cell Biology* 219.10 (2020), e202006111 (cit. on p. 27).

[67] Robin W. Klemm, Justin P. Norton, Ronald A. Cole, Chen S. Li, Seong H. Park, Matthew M. Crane, et al. "A Conserved Role for Atlastin GTPases in Regulating Lipid Droplet Size". *Cell Reports* 3.5 (2013), pp. 1465–1475. pmid: 23684613 (cit. on p. 27).

[68] David Barneda and Mark Christian. "Lipid Droplet Growth: Regulation of a Dynamic Organelle". *Current Opinion in Cell Biology*. Cell Organelles 47 (2017), pp. 9–15 (cit. on p. 27).

[69] Chems Amari, Marta Carletti, Siqi Yan, Morgane Michaud, and Juliette Salvaing. "Lipid Droplets Degradation Mechanisms from Microalgae to Mammals, a Comparative Overview". *Biochimie*. Lipids, from Molecular Mechanisms to Diseases 227 (2024), pp. 19–34 (cit. on p. 27).

[70] Mandeep P. Gaidhu, Nicole M. Anthony, Prital Patel, Thomas J. Hawke, and Rolando B. Ceddia. "Dysregulation of Lipolysis and Lipid Metabolism in Visceral and Subcutaneous Adipocytes by High-Fat Diet: Role of ATGL, HSL, and AMPK". *American Journal of Physiology-Cell Physiology* 298.4 (2010), pp. C961–C971 (cit. on p. 27).

[71] Melanie Korbelius, Nemanja Vujic, Vinay Sachdev, Sascha Obrowsky, Silvia Rainer, Benjamin Gottschalk, et al. "ATGL/CGI-58-Dependent Hydrolysis of a Lipid Storage Pool in Murine Enterocytes". *Cell Reports* 28.7 (2019), 1923–1934.e4. pmid: 31412256 (cit. on p. 27).

[72] Xuwen Xiang, Jing Chen, and Lin Che. "Emerging Roles and Therapeutic Implications of Lipid Droplet Protein Perilipin 2 in Liver Disease". *Genes & Diseases* (2025), p. 101712 (cit. on pp. 27, 35).

[73] Christoph F. Kurat, Klaus Natter, Julia Petschnigg, Heimo Wolinski, Kim Scheuringer, Harald Scholz, et al. "Obese Yeast: Triglyceride Lipolysis Is Functionally Conserved from Mammals to Yeast*". *Journal of Biological Chemistry* 281.1 (2006), pp. 491–500 (cit. on p. 27).

[74] Peter J. Eastmond. "SUGAR-DEPENDENT1 Encodes a Patatin Domain Triacylglycerol Lipase That Initiates Storage Oil Breakdown in Germinating Arabidopsis Seeds". *The Plant Cell* 18.3 (2006), pp. 665–675. pmid: 16473965 (cit. on p. 28).

[75] Carl Ward, Nuria Martinez-Lopez, Elsje G. Otten, Bernadette Carroll, Dorothea Maetzel, Rajat Singh, et al. "Autophagy, Lipophagy and Lysosomal Lipid Storage Disorders". *Biochimica Et Biophysica Acta* 1861.4 (2016), pp. 269–284. pmid: 26778751 (cit. on pp. 28, 29, 31).

[76] Tim van Zutphen, Virginia Todde, Rinse de Boer, Martin Kreim, Harald F. Hofbauer, Heimo Wolinski, et al. "Lipid Droplet Autophagy in the Yeast Saccharomyces Cerevisiae". *Molecular Biology of the Cell* 25.2 (2014), pp. 290–301. pmid: 24258026 (cit. on p. 28).

[77] Irene Álvarez-Guerra, Emma Block, Filomena Broeskamp, Sonja Gabrijelčič, Terence Infant, Ana de Ory, et al. "LDO Proteins and Vac8 Form a Vacuole-Lipid Droplet Contact Site to Enable Starvation-Induced Lipophagy in Yeast". *Developmental Cell* 59.6 (2024), 759–775.e5. pmid: 38354739 (cit. on p. 28).

[78] Yushi Yoshitake, Hiroyuki Ohta, and Mie Shimojima. "Autophagy-Mediated Regulation of Lipid Metabolism and Its Impact on the Growth in Algae and Seed Plants". *Frontiers in Plant Science* 10 (2019) (cit. on pp. 29, 32, 33).

[79] Aaron M. Hosios, Meghan Wilkinson, Molly C. McNamara, Krystle C. Kalafut, Margaret E. Torrence, John M. Asara, et al. "mTORC1 Regulates a Lysosome-Dependent Adaptive Shift in Intracellular Lipid Species". *Nature metabolism* 4.12 (2022), pp. 1792–1811. pmid: 36536136 (cit. on p. 30).

[80] Irfan J. Lodhi, Li Yin, Anne P. L. Jensen-Urstad, Katsuhiko Funai, Trey Coleman, John H. Baird, et al. "Inhibiting Adipose Tissue Lipogenesis Reprograms Thermogenesis and PPARγ Activation to Decrease Diet-Induced Obesity". *Cell Metabolism* 16.2 (2012), pp. 189–201. pmid: 22863804 (cit. on p. 31).

[81] Dana M. Gwinn, David B. Shackelford, Daniel F. Egan, Maria M. Mihaylova, Annabelle Mery, Debbie S. Vasquez, et al. "AMPK Phosphorylation of Raptor Mediates a Metabolic Checkpoint". *Molecular cell* 30.2 (2008), pp. 214–226. pmid: 18439900 (cit. on p. 31).

[82] Maryam Ahmadian, Marcia J. Abbott, Tianyi Tang, Carolyn S. S. Hudak, Yangha Kim, Matthew Bruss, et al. "Desnutrin/ATGL Is Regulated by AMPK and Is Required for a Brown Adipose Phenotype". *Cell Metabolism* 13.6 (2011), pp. 739–748. pmid: 21641555 (cit. on p. 31).

[83] Sana Raza, Sangam Rajak, Paul M. Yen, and Rohit A. Sinha. "Autophagy and Hepatic Lipid Metabolism: Mechanistic Insight and Therapeutic Potential for MASLD". *npj Metabolic Health and Disease* 2.1 (2024), p. 19 (cit. on p. 31).

[84] Arnold Y Seo, Pick-Wei Lau, Daniel Feliciano, Prabuddha Sengupta, Mark A Le Gros, Bertrand Cinquin, et al. "AMPK and Vacuole-Associated Atg14p Orchestrate μ-Lipophagy for Energy Production and Long-Term Survival under Glucose Starvation". *eLife* 6 (2017). Ed. by Vojo Deretic, e21690 (cit. on p. 31).

[85] Isaac Tamargo-Gómez and Guillermo Mariño. "AMPK: Regulation of Metabolic Dynamics in the Context of Autophagy". *International Journal of Molecular Sciences* 19.12 (2018), p. 3812 (cit. on p. 31).

[86] Lianggong Ding, Wenfei Sun, Miroslav Balaz, Anyuan He, Manuel Klug, Stefan Wieland, et al. "Peroxisomal β-Oxidation Acts as a Sensor for Intracellular Fatty Acids and Regulates Lipolysis". *Nature Metabolism* 3.12 (2021), pp. 1648–1661 (cit. on p. 32).

[87] Chandramohan Chitraju, Niklas Mejhert, Joel T. Haas, L. Grisell Diaz-Ramirez, Carrie A. Grueter, Jason E. Imbriglio, et al. "Triglyceride Synthesis by DGAT1 Protects Adipocytes from Lipid-Induced ER Stress during Lipolysis". *Cell Metabolism* 26.2 (2017), 407–418.e3. pmid: 28768178 (cit. on p. 32).

[88] Yi Jin, Yanjie Tan, Lupeng Chen, Yan Liu, and Zhuqing Ren. "Reactive Oxygen Species Induces Lipid Droplet Accumulation in HepG2 Cells by Increasing Perilipin 2 Expression". *International Journal of Molecular Sciences* 19.11 (2018), p. 3445 (cit. on p. 32).

[89] Jingshu Zhang, Yun Lan, and Sumana Sanyal. “Modulation of Lipid Droplet Metabolism—A Potential Target for Therapeutic Intervention in Flaviviridae Infections”. *Frontiers in Microbiology* 8 (2017) (cit. on p. 32).

[90] Christin Wallstab, Dimitra Eleftheriadou, Theresa Schulz, Georg Damm, Daniel Seehofer, Jürgen Borlak, et al. “A Unifying Mathematical Model of Lipid Droplet Metabolism Reveals Key Molecular Players in the Development of Hepatic Steatosis”. *The FEBS journal* 284.19 (2017), pp. 3245–3261. pmid: 28763157 (cit. on p. 32).

[91] Zhongshuai Gai, Yu Wang, Yiqian Ding, Wenjun Qian, Chen Qiu, Hui Xie, et al. “Exogenous Abscisic Acid Induces the Lipid and Flavonoid Metabolism of Tea Plants under Drought Stress”. *Scientific Reports* 10.1 (2020), p. 12275 (cit. on p. 32).

[92] Stephanie P. Mueller, Daniel M. Krause, Martin J. Mueller, and Agnes Fekete. “Accumulation of Extra-Chloroplastic Triacylglycerols in Arabidopsis Seedlings during Heat Acclimation”. *Journal of Experimental Botany* 66.15 (2015), pp. 4517–4526 (cit. on p. 33).

[93] Rubén Fernández-Santos, Yovanny Izquierdo, Ana López, Luis Muñiz, Marta Martínez, Tomás Cascón, et al. “Protein Profiles of Lipid Droplets during the Hypersensitive Defense Response of Arabidopsis against Pseudomonas Infection”. *Plant and Cell Physiology* 61.6 (2020), pp. 1144–1157 (cit. on p. 33).

[94] Amit Kumar Sharma, Shivangi Jaryal, Shubham Sharma, Archana Dhyani, Bhagya Sindhu Tewari, and Neelima Mahato. “Biofuels from Microalgae: A Review on Microalgae Cultivation, Biodiesel Production Techniques and Storage Stability”. *Processes* 13.2 (2025), p. 488 (cit. on p. 33).

[95] Alberto Rock, Lucie Novoveská, and David Green. “Synthetic Biology Is Essential to Unlock Commercial Biofuel Production through Hyper Lipid-Producing Microalgae: A Review”. *Applied Phycology* 2.1 (2021), pp. 41–59 (cit. on p. 33).

[96] Min Wang, Xiaoxue Ye, Hongwen Bi, and Zhongbao Shen. “Microalgae Biofuels: Illuminating the Path to a Sustainable Future amidst Challenges and Opportunities”. *Biotechnology for Biofuels and Bioproducts* 17.1 (2024), p. 10 (cit. on p. 33).

[97] Michael R. Connor and Shota Atsumi. “Synthetic Biology Guides Biofuel Production”. *Journal of Biomedicine and Biotechnology* 2010 (2010), p. 541698. pmid: 20827393 (cit. on p. 34).

[98] Jing-Yuan Lin, Xiao Bu, Yi-Bin Lan, Chang-Qing Duan, and Guo-Liang Yan. “Combined Metabolic Engineering and Lipid Droplets Degradation to Increase Vitamin A Production in Saccharomyces Cerevisiae”. *Microbial Cell Factories* 23 (2024), p. 317. pmid: 39581972 (cit. on p. 34).

[99] Thomas Vanhercke, Anna El Tahchy, Qing Liu, Xue-Rong Zhou, Pushkar Shrestha, Uday K. Divi, et al. “Metabolic Engineering of Biomass for High Energy Density: Oilseed-like Triacylglycerol Yields from Plant Leaves”. *Plant Biotechnology Journal* 12.2 (2014), pp. 231–239 (cit. on p. 34).

[100] Pengxiang Zhao, Zichen Zhao, Ziwei Yu, Lupeng Chen, Yi Jin, Jian Wu, et al. “Application of Synthetic Lipid Droplets in Metabolic Diseases”. *Clinical and Translational Medicine* 13.11 (2023), e1441. pmid: 37997538 (cit. on p. 34).

[101] Diego A. Miranda, Ji-Hyun Kim, Long N. Nguyen, Wang Cheng, Bryan C. Tan, Vera J. Goh, et al. “Fat Storage-inducing Transmembrane Protein 2 Is Required for Normal Fat Storage in Adipose Tissue*”. *Journal of Biological Chemistry* 289.14 (2014), pp. 9560–9572 (cit. on p. 35).

[102] Xinyue Jiang, Hongzhan Wang, Kexin Nie, Yang Gao, Shen Chen, Yueheng Tang, et al. “Targeting Lipid Droplets and Lipid Droplet-Associated Proteins: A New Perspective on Natural Compounds against Metabolic Diseases”. *Chinese Medicine* 19.1 (2024), p. 120 (cit. on p. 35).

[103] Zhangnan Liu, Meichen Liu, Ming Fan, Sijing Pan, Shaowei Li, Mingliang Chen, et al. “Metabolomic-Proteomic Combination Analysis Reveals the Targets and Molecular Pathways Associated with Hydrogen Sulfide Alleviating NAFLD”. *Life Sciences* 264 (2021), p. 118629 (cit. on p. 35).

[104] Ana-Belén Blázquez, Patricia Mingo-Casas, Ernesto Quesada, Eva María Priego, María-Jesús Pérez-Perez, and Miguel A. Martín-Acebes. “Lipid-Targeting Antiviral Strategies: Current State and Future Perspectives”. *Antiviral Research* 236 (2025), p. 106103 (cit. on p. 35).

[105] Michael S. Haney, Róbert Pálovics, Christy Nicole Munson, Chris Long, Patrik K. Johansson, Oscar Yip, et al. “APOE4/4 Is Linked to Damaging Lipid Droplets in Alzheimer’s Disease Microglia”. *Nature* 628.8006 (2024), pp. 154–161 (cit. on p. 36).

[106] Clifford P. Brangwynne, Christian R. Eckmann, David S. Courson, Agata Rybarska, Carsten Hoege, Jöbin Gharakhani, et al. “Germline P Granules Are Liquid Droplets That Localize by Controlled Dissolution/Condensation”. *Science* 324.5935 (2009), pp. 1729–1732 (cit. on p. 56).

[107] Yongdae Shin and Clifford P. Brangwynne. “Liquid Phase Condensation in Cell Physiology and Disease”. *Science* 357.6357 (2017), eaaf4382 (cit. on pp. 56, 58).

[108] Tetsuro Hirose, Kensuke Ninomiya, Shinichi Nakagawa, and Tomohiro Yamazaki. “A Guide to Membraneless Organelles and Their Various Roles in Gene Regulation”. *Nature Reviews Molecular Cell Biology* 24.4 (2023), pp. 288–304 (cit. on pp. 56, 59, 60).

[109] Saroj Kumar Nandi, Daniel Österle, Meta Heidenreich, Emmanuel D. Levy, and Samuel A. Safran. “Affinity and Valence Impact the Extent and Symmetry of Phase Separation of Multivalent Proteins”. *Physical Review Letters* 129.12 (2022), p. 128102 (cit. on p. 57).

[110] Pilong Li, Sudeep Banjade, Hui-Chun Cheng, Soyeon Kim, Baoyu Chen, Liang Guo, et al. “Phase Transitions in the Assembly of Multivalent Signalling Proteins”. *Nature* 483.7389 (2012), pp. 336–340 (cit. on pp. 57, 62).

[111] Denes Hnisz, Krishna Shrinivas, Richard A. Young, Arup K. Chakraborty, and Phillip A. Sharp. “A Phase Separation Model for Transcriptional Control”. *Cell* 169.1 (2017), pp. 13–23. pmid: 28340338 (cit. on p. 57).

[112] Jun-Qi Li, Zeng-Shuai Yan, Yu-Qiang Ma, and Hong-Ming Ding. “Sequence-Dependent Biomolecular Phase Separation Driven by Short-Range Interaction: From Material Properties to Coarsening Dynamics”. *Physical Review E* 111.5 (2025), p. 054403 (cit. on p. 58).

[113] Alex S. Holehouse and Simon Alberti. “Molecular Determinants of Condensate Composition”. *Molecular Cell*. Focus on Patterns in Molecular Biology 85.2 (2025), pp. 290–308 (cit. on p. 58).

[114] Daniele Notarmuzi and Emanuela Bianchi. “Liquid-Liquid Phase Separation Driven by Charge Heterogeneity”. *Communications Physics* 7.1 (2024), p. 412 (cit. on p. 58).

[115] Tebbe de Vries, Mihajlo Novakovic, Yinan Ni, Izabela Smok, Clara Inghelram, Maria Bikaki, et al. “Specific Protein-RNA Interactions Are Mostly Preserved in Biomolecular Condensates”. *Science Advances* 10.10 (2024), eadm7435 (cit. on p. 58).

[116] Xiaotian Wang, Zhiguang Xiao, Jiahao Niu, and Yujie Sun. “FRAP4ICBS: FRAP Analysis Method to Evaluate Dominant Effects for Biomolecular Condensate Formation”. *Analytical Chemistry* 97.25 (2025), pp. 13229–13238 (cit. on p. 59).

[117] Salman F. Banani, Hyun O. Lee, Anthony A. Hyman, and Michael K. Rosen. “Biomolecular Condensates: Organizers of Cellular Biochemistry”. *Nature Reviews Molecular Cell Biology* 18.5 (2017), pp. 285–298 (cit. on p. 59).

[118] Aleksandr Ivanovich Oparin. *The Origin of Life*. New York: The Macmillan Company, 1938. viii pp. (cit. on p. 61).

[119] D. E. Meyer and A. Chilkoti. “Purification of Recombinant Proteins by Fusion with Thermally-Responsive Polypeptides”. *Nature Biotechnology* 17.11 (1999), pp. 1112–1115. pmid: 10545920 (cit. on p. 61).

[120] Yongdae Shin, Joel Berry, Nicole Pannucci, Mikko P. Haataja, Jared E. Toettcher, and Clifford P. Brangwynne. “Spatiotemporal Control of Intracellular Phase Transitions Using Light-Activated optoDroplets”. *Cell* 168.1–2 (2017), 159–171.e14. pmid: 28041848 (cit. on pp. 63, 64).

[121] Dan Bracha, Mackenzie T. Walls, Ming-Tzo Wei, Lian Zhu, Martin Kurian, José L. Avalos, et al. “Mapping Local and Global Liquid Phase Behavior in Living Cells Using Photo-Oligomerizable Seeds”. *Cell* 175.6 (2018), 1467–1480.e13. pmid: 30500534 (cit. on pp. 63, 65).

[122] Yongdae Shin, Yi-Che Chang, Daniel S. W. Lee, Joel Berry, David W. Sanders, Pierre Ronceray, et al. “Liquid Nuclear Condensates Mechanically Sense and Restructure the Genome”. *Cell* 175.6 (2018), 1481–1491.e13. pmid: 30500535 (cit. on p. 63).

[123] Elliot Dine, Agnieszka A. Gil, Giselle Uribe, Clifford P. Brangwynne, and Jared E. Toettcher. “Protein Phase Separation Provides Long-Term Memory of Transient Spatial Stimuli”. *Cell Systems* 6.6 (2018), 655–663.e5. pmid: 29859829 (cit. on p. 63).

[124] Hideki Nakamura, Albert A. Lee, Ali Sobhi Afshar, Shigeki Watanabe, Elmer Rho, Shiva Razavi, et al. “Intracellular Production of Hydrogels and Synthetic RNA Granules by Multivalent Molecular Interactions”. *Nature Materials* 17.1 (2018), pp. 79–89 (cit. on pp. 64, 66).

[125] Yifan Dai, Mina Farag, Dongheon Lee, Xiangze Zeng, Kyeri Kim, Hye-in Son, et al. “Programmable Synthetic Biomolecular Condensates for Cellular Control”. *Nature Chemical Biology* 19.4 (2023), pp. 518–528 (cit. on p. 65).

[126] Maruša Ramšak, Dominique A. Ramirez, Loren E. Hough, Michael R. Shirts, Sara Vidmar, Kristina Eleršič Filipič, et al. “Programmable de Novo Designed Coiled Coil-Mediated Phase Separation in Mammalian Cells”. *Nature Communications* 14.1 (2023), p. 7973 (cit. on p. 66).

[127] Marina Garcia-Jove Navarro, Shunnichi Kashida, Racha Chouaib, Sylvie Souquere, Gérard Pierron, Dominique Weil, et al. “RNA Is a Critical Element for the Sizing and the Composition of Phase-Separated RNA–Protein Condensates”. *Nature Communications* 10.1 (2019), p. 3230 (cit. on pp. 67, 103).

[128] Audrey Cochard, Marina Garcia-Jove Navarro, Leonard Piroska, Shunnichi Kashida, Michel Kress, Dominique Weil, et al. "RNA at the Surface of Phase-Separated Condensates Impacts Their Size and Number". *Biophysical Journal* 121.9 (2022), pp. 1675–1690. pmid: 35364105 (cit. on p. 67).

[129] Leonard Piroska, Alexis Fenyi, Scott Thomas, Marie-Aude Plamont, Virginie Redeker, Ronald Melki, et al. "α-Synuclein Liquid Condensates Fuel Fibrillar α-Synuclein Growth". *Science Advances* 9.33 (2023), eadg5663 (cit. on p. 68).

[130] Chems Amari, Damien Simon, Emma Pasquier, Theodore Bellon, Marie-Aude Plamont, Sylvie Souquere, et al. "Controlling Lipid Droplet Dynamics via Tether Condensates". *Nature Chemical Biology* (2025), pp. 1–10 (cit. on p. 70).

[131] Nolwenn Guéguen, Damien Le Moigne, Alberto Amato, Juliette Salvaing, and Eric Maréchal. "Lipid Droplets in Unicellular Photosynthetic Stramenopiles". *Frontiers in Plant Science* 12 (2021) (cit. on pp. 97–99, 133).

[132] Grégory Francius, Benoît Tesson, Etienne Dague, Véronique Martin-Jézéquel, and Yves F. Dufrêne. "Nanostructure and Nanomechanics of Live Phaeodactylum Tricornutum Morphotypes". *Environmental Microbiology* 10.5 (2008), pp. 1344–1356 (cit. on p. 97).

[133] Serena Flori, Pierre-Henri Jouneau, Giovanni Finazzi, Eric Maréchal, and Denis Falconet. "Ultrastructure of the Periplastidial Compartment of the Diatom *Phaeodactylum Tricornutum*". *Protist* 167.3 (2016), pp. 254–267 (cit. on p. 97).

[134] Damien Le Moigne, Marta Carletti, Chems Amari, Rachel Bonnarde, Fabien Richard, Catherine Albrieux, et al. "Functional Study of Phaeodactylum Tricornutum Seipin Highlights Specificities of Lipid Droplets Biogenesis in Diatoms". *New Phytologist* 247.5 (2025), pp. 2245–2269 (cit. on pp. 96, 99, 101).

[135] Victor Murison, Josiane Hérault, Martine Côme, Sabrina Guinio, Alexis Lebon, Christophe Chamot, et al. "Comparison of Two Phaeodactylum Tricornutum Ecotypes under Nitrogen Starvation and Resupply Reveals Distinct Lipid Accumulation Strategies but a Common Degradation Process". *Frontiers in Plant Science* 14 (2023) (cit. on pp. 96–99).

[136] Thomas Butler, Rahul Vijay Kapoore, and Seetharaman Vaidyanathan. "Phaeodactylum Tricornutum: A Diatom Cell Factory". *Trends in Biotechnology* 38.6 (2020), pp. 606–622. pmid: 31980300 (cit. on p. 98).

[137] Valeria Villanova, Antonio Emidio Fortunato, Dipali Singh, Davide Dal Bo, Melissa Conte, Toshihiro Obata, et al. "Investigating Mixotrophic Metabolism in the Model Diatom Phaeodactylum Tricornutum". *Philosophical Transactions of the Royal Society B: Biological Sciences* 372.1728 (2017), p. 20160404 (cit. on p. 98).

[138] Victor Murison, Josiane Hérault, Justine Marchand, and Lionel Ulmann. "Diatom Triacylglycerol Metabolism: From Carbon Fixation to Lipid Droplet Degradation". *Biological Reviews of the Cambridge Philosophical Society* 100.4 (2025), pp. 1423–1443. pmid: 40065527 (cit. on p. 98).

[139] Kohei Yoneda, Masaki Yoshida, Iwane Suzuki, and Makoto M. Watanabe. "Identification of a Major Lipid Droplet Protein in a Marine Diatom Phaeodactylum Tricornutum". *Plant & Cell Physiology* 57.2 (2016), pp. 397–406. pmid: 26738549 (cit. on p. 98).

[140] Yogesh Taparia, Achintya Kumar Dolui, Sammy Boussiba, and Inna Khozin-Goldberg. "Multiplexed Genome Editing via an RNA Polymerase II Promoter-Driven sgRNA Array in the Diatom Phaeodactylum Tricornutum: Insights Into the Role of StLDP". *Frontiers in Plant Science* 12 (2022), p. 784780 (cit. on p. 99).

[141] Kohei Yoneda, Reika Oishi, Masaki Yoshida, Yusuke Matsuda, and Iwane Suzuki. "Stramenopile-Type Lipid Droplet Protein Functions as a Lipid Droplet Scaffold Protein in the Marine Diatom Phaeodactylum Tricornutum". *Plant and Cell Physiology* 64.7 (2023), pp. 803–813 (cit. on pp. 99, 120, 129).

[142] Xiang Wang, Ting-Bin Hao, Srinivasan Balamurugan, Wei-Dong Yang, Jie-Sheng Liu, Hong-Po Dong, et al. "A Lipid Droplet-Associated Protein Involved in Lipid Droplet Biogenesis and Triacylglycerol Accumulation in the Oleaginous Microalga Phaeodactylum Tricornutum". *Algal Research* 26 (2017), pp. 215–224 (cit. on p. 99).

[143] Veijo T. Salo. "Seipin—Still a Mysterious Protein?" *Frontiers in Cell and Developmental Biology* 11 (2023) (cit. on p. 99).

[144] Lu Liu, Qingqing Jiang, Xuhong Wang, Yuxi Zhang, Ruby C.Y. Lin, Sin Man Lam, et al. "Adipose-Specific Knockout of Seipin/Bscl2 Results in Progressive Lipodystrophy". *Diabetes* 63.7 (2014), pp. 2320–2331 (cit. on p. 99).

[145] Ben Leyland, Aliza Zarka, Shoshana Didi-Cohen, Sammy Boussiba, and Inna Khozin-Goldberg. "High Resolution Proteome of Lipid Droplets Isolated from the Pennate Diatom Phaeodactylum

Tricornutum (Bacillariophyceae) Strain Pt4 Provides Mechanistic Insights into Complex Intracellular Coordination during Nitrogen Deprivation". *Journal of Phycology* 56.6 (2020), pp. 1642–1663 (cit. on p. 99).

[146] Antoine Jaussaud, Josselin Lupette, Juliette Salvaing, Juliette Jouhet, Olivier Bastien, Marina Gromova, et al. "Stepwise Biogenesis of Subpopulations of Lipid Droplets in Nitrogen Starved Phaeodactylum Tricornutum Cells". *Frontiers in Plant Science* 11 (2020) (cit. on p. 99).

[147] Yufeng Mao, Li Guo, Yan Luo, Zhihong Tang, Wei Li, and Wen Dong. "Sexual Reproduction Potential Implied by Functional Analysis of SPO11 in Phaeodactylum Tricornutum". *Gene* 757 (2020), p. 144929. pmid: 32622990 (cit. on p. 100).

[148] Zhiqian Yi, Yixi Su, Maonian Xu, Andreas Bergmann, Saevar Ingthorsson, Ottar Rolfsson, et al. "Chemical Mutagenesis and Fluorescence-Based High-Throughput Screening for Enhanced Accumulation of Carotenoids in a Model Marine Diatom Phaeodactylum Tricornutum". *Marine Drugs* 16.8 (2018), p. 272. pmid: 30081564 (cit. on p. 100).

[149] K. E. Apt, P. G. Kroth-Pancic, and A. R. Grossman. "Stable Nuclear Transformation of the Diatom Phaeodactylum Tricornutum". *Molecular & general genetics: MGG* 252.5 (1996), pp. 572–579. pmid: 8914518 (cit. on pp. 100, 103).

[150] Mado Miyahara, Masaki Aoi, Natsuko Inoue-Kashino, Yasuhiro Kashino, and Kentaro Ifuku. "Highly Efficient Transformation of the Diatom Phaeodactylum Tricornutum by Multi-Pulse Electroporation". *Bioscience, Biotechnology, and Biochemistry* 77.4 (2013), pp. 874–876. pmid: 23563551 (cit. on p. 100).

[151] Bogumil J. Karas, Rachel E. Diner, Stephane C. Lefebvre, Jeff McQuaid, Alex P. R. Phillips, Chari M. Noddings, et al. "Designer Diatom Episomes Delivered by Bacterial Conjugation". *Nature Communications* 6.1 (2015), p. 6925 (cit. on p. 100).

[152] Marianne Nymark, Amit Kumar Sharma, Torfinn Sparstad, Atle M. Bones, and Per Winge. "A CRISPR/Cas9 System Adapted for Gene Editing in Marine Algae". *Scientific Reports* 6.1 (2016), p. 24951 (cit. on p. 100).

[153] M. Serif, B. Lepetit, K. Weißert, P. G. Kroth, and C. Rio Bartulos. "A Fast and Reliable Strategy to Generate TALEN-mediated Gene Knockouts in the Diatom *Phaeodactylum Tricornutum*". *Algal Research* 23 (2017), pp. 186–195 (cit. on p. 100).

[154] Jidnyasa Joshi-Deo, Matthias Schmidt, Ansgar Gruber, Wolfram Weisheit, Maria Mittag, Peter G. Kroth, et al. "Characterization of a Trimeric Light-Harvesting Complex in the Diatom Phaeodactylum Tricornutum Built of FcpA and FcpE Proteins". *Journal of Experimental Botany* 61.11 (2010), pp. 3079–3087. pmid: 20478968 (cit. on p. 103).

[155] Sarah R. Smith, Chris L. Dupont, James K. McCarthy, Jared T. Broddrick, Miroslav Oborník, Aleš Horák, et al. "Evolution and Regulation of Nitrogen Flux through Compartmentalized Metabolic Networks in a Marine Diatom". *Nature Communications* 10.1 (2019), p. 4552 (cit. on p. 103).

[156] N. J. Antia, B. R. Berland, D. J. Bonin, and S. Y. Maestrini. "Comparative Evaluation of Certain Organic and Inorganic Sources of Nitrogen for Phototrophic Growth of Marine Microalgae". *Journal of the Marine Biological Association of the United Kingdom* 55.3 (1975), pp. 519–539 (cit. on p. 103).

[157] Lili Chu, Daniela Ewe, Carolina Río Bártulos, Peter G. Kroth, and Ansgar Gruber. "Rapid Induction of GFP Expression by the Nitrate Reductase Promoter in the Diatom Phaeodactylum Tricornutum". *PeerJ* 4 (2016), e2344. pmid: 27635322 (cit. on pp. 103, 104).

[158] Chenxi Zhang, Xiaorong Zhang, and Guanghua Zhao. "Ferritin Nanocage: A Versatile Nanocarrier Utilized in the Field of Food, Nutrition, and Medicine". *Nanomaterials* 10.9 (2020), p. 1894 (cit. on p. 104).

[159] Olaf Ronneberger, Philipp Fischer, and Thomas Brox. *U-Net: Convolutional Networks for Biomedical Image Segmentation*. 2015. arXiv: 1505.04597 [cs]. URL: http://arxiv.org/abs/1505.04597 (visited on 04/30/2025). Pre-published (cit. on p. 105).

[160] Liming Wu, Alain Chen, Paul Salama, Seth Winfree, Kenneth W. Dunn, and Edward J. Delp. "NISNet3D: Three-Dimensional Nuclear Synthesis and Instance Segmentation for Fluorescence Microscopy Images". *Scientific Reports* 13.1 (2023), p. 9533 (cit. on p. 106).

[161] Marius Pachitariu and Carsen Stringer. "Cellpose 2.0: How to Train Your Own Model". *Nature Methods* 19.12 (2022), pp. 1634–1641 (cit. on p. 107).

[162] C. H. Li and C. K. Lee. "Minimum Cross Entropy Thresholding". *Pattern Recognition* 26.4 (1993), pp. 617–625 (cit. on p. 113).

[163] Christopher E. Spiese, Triet Le, Robert L. Zimmer, and David J. Kieber. "Dimethylsulfide Membrane Permeability, Cellular Concentrations and Implications for Physiological Functions in Marine Algae". *Journal of Plankton Research* 38.1 (2016), pp. 41–54 (cit. on p. 114).

[164] Peter Burkhard, Paul Taylor, and Malcolm D Walkinshaw. "X-Ray Structures of Small Ligand-FKBP Complexes Provide an Estimate for Hydrophobic Interaction Energies1". *Journal of Molecular Biology* 295.4 (2000), pp. 953–962 (cit. on p. 114).

[165] Benoit Vianay, Christophe Guérin, Laurène Gressin, Magali Orhant-Prioux, Laurent Blanchoin, Manuel Théry, et al. *Fabrication of Microcompartments with Controlled Size and Shape for Encapsulating Active Matter*. 2025. URL: https://www.biorxiv.org/content/10.1101/2025.04.23.650156v1 (visited on 05/07/2025). Pre-published (cit. on pp. 115, 141).

[166] Alessandro Manzotti, Raphaël Monteil, Soizic Cheminant Navarro, Dany Croteau, Lucie Charreton, Antoine Hoguin, et al. "Circadian Regulation of Key Physiological Processes by the RITMO1 Clock Protein in the Marine Diatom Phaeodactylum Tricornutum". *New Phytologist* 246.4 (2025), pp. 1724–1739 (cit. on p. 117).

[167] Ansgar Gruber, Sascha Vugrinec, Franziska Hempel, Sven B. Gould, Uwe-G. Maier, and Peter G. Kroth. "Protein Targeting into Complex Diatom Plastids: Functional Characterisation of a Specific Targeting Motif". *Plant Molecular Biology* 64.5 (2007), pp. 519–530. pmid: 17484021 (cit. on p. 124).

[168] John A. Corbin, John H. Evans, Kyle E. Landgraf, and Joseph J. Falke. "Mechanism of Specific Membrane Targeting by C2 Domains: Localized Pools of Target Lipids Enhance Ca2+ Affinity". *Biochemistry* 46.14 (2007), pp. 4322–4336. pmid: 17367165 (cit. on p. 125).

[169] Lukas Käll, Anders Krogh, and Erik L. L. Sonnhammer. "A Combined Transmembrane Topology and Signal Peptide Prediction Method". *Journal of Molecular Biology* 338.5 (2004), pp. 1027–1036. pmid: 15111065 (cit. on p. 126).

[170] Zachor Shemesh, Stefan Leu, Inna Khozin-Goldberg, Shoshana Didi-Cohen, Aliza Zarka, and Sammy Boussiba. "Inducible Expression of *Haematococcus* Oil Globule Protein in the Diatom *Phaeodactylum Tricornutum*: Association with Lipid Droplets and Enhancement of TAG Accumulation under Nitrogen Starvation". *Algal Research* 18 (2016), pp. 321–331 (cit. on pp. 127, 130, 132).

[171] Heni Abida, Lina-Juana Dolch, Coline Meï, Valeria Villanova, Melissa Conte, Maryse A. Block, et al. "Membrane Glycerolipid Remodeling Triggered by Nitrogen and Phosphorus Starvation in Phaeodactylum Tricornutum". *Plant Physiology* 167.1 (2015), pp. 118–136 (cit. on p. 129).

[172] Florent Fontaine. "Functional Study of Lipid Droplet (LD) Addressing Domains to Improve the Purification of Recombinant Proteins". PhD thesis. Université Paris-Saclay, 2025 (cit. on p. 133).

[173] Yiwu Zhao, Qingdi Dong, Yuhu Geng, Changle Ma, and Qun Shao. "Dynamic Regulation of Lipid Droplet Biogenesis in Plant Cells and Proteins Involved in the Process". *International Journal of Molecular Sciences* 24.8 (2023), p. 7476 (cit. on p. 133).

[174] Huajin Wang, Michel Becuwe, Benjamin E. Housden, Chandramohan Chitraju, Ashley J. Porras, Morven M. Graham, et al. "Seipin Is Required for Converting Nascent to Mature Lipid Droplets". *eLife* 5 (2016), e16582. pmid: 27564575 (cit. on p. 133).

[175] Nolwenn Gueguen. "Caractérisation Des Monogalactosyldiacylglycérol Synthases Chez La Diatomée Modèle Phaeodactylum Tricornutum". These de doctorat. Université Grenoble Alpes, 2022 (cit. on p. 135).

[176] Lioudmila A. Zaslavskaia, J. Casey Lippmeier, Peter G. Kroth, Arthur R. Grossman, and Kirk E. Apt. "Transformation of the Diatom *Phaeodactylum Tricornutum* (Bacillariophyceae) with a Variety of Selectable Marker and Reporter Genes". *Journal of Phycology* 36.2 (2000), pp. 379–386 (cit. on p. 138).

[177] Shuyan Zhang, Yang Wang, Liujuan Cui, Yaqin Deng, Shimeng Xu, Jinhai Yu, et al. "Morphologically and Functionally Distinct Lipid Droplet Subpopulations". *Scientific Reports* 6.1 (2016), p. 29539 (cit. on p. 146).

[178] Rebekah Rakotonirina-Ricquebourg, Vítor Costa, and Vitor Teixeira. "Hello from the Other Side: Membrane Contact of Lipid Droplets with Other Organelles and Subsequent Functional Implications". *Progress in Lipid Research* 85 (2022), p. 101141 (cit. on p. 146).

[179] Zhihuan Li, Katharina Thiel, Peter J. Thul, Mathias Beller, Ronald P. Kühnlein, and Michael A. Welte. "Lipid Droplets Control the Maternal Histone Supply of Drosophila Embryos". *Current biology : CB* 22.22 (2012), pp. 2104–2113. pmid: 23084995 (cit. on p. 146).

[180] Iva Ganeva, Koini Lim, Jerome Boulanger, Patrick C. Hoffmann, Olivia Muriel, Alicia C. Borgeaud, et al. “The Architecture of Cidec-mediated Interfaces between Lipid Droplets”. *Cell Reports* 42.2 (2023), p. 112107 (cit. on p. 147).

[181] Christian Hoffmann, Jakob Rentsch, Taka A. Tsunoyama, Akshita Chhabra, Gerard Aguilar Perez, Rajdeep Chowdhury, et al. “Synapsin Condensation Controls Synaptic Vesicle Sequestering and Dynamics”. *Nature Communications* 14.1 (2023), p. 6730 (cit. on p. 147).

ABSTRACT

Lipid droplets (LDs) are central hubs for lipid storage and exchange, interfacing with the ER, mitochondria, peroxisomes, and lysosomes, and governing energy balance, signaling, and stress responses. Despite rich descriptive mapping, causally linking LD surface interactions to lipid fluxes remains challenging. In this PhD thesis, we developed a perturbative framework called ControLD: an engineered, specific, programmable system that encapsulates LDs within a liquid-liquid phase-separated (LLPS) protein meshwork. By combining phase-separating scaffolds with LD-targeting modules, ControLD builds a tunable, reversible steric barrier at the LD surface, blocking interactions without chemical inhibitors. In mammalian cells, live imaging shows rapid, specific recruitment to LDs and controlled meshwork formation with minimal off-target assembly; LLPS enables on-demand trapping and release. We quantify how encapsulation remodels organelle interfaces and metabolism: limiting surface availability reduces neutral lipid influx under nutrient abundance, while trapped LDs resist consumption during starvation. Pharmacological and nutrient challenges highlight state-dependent roles of the LD surface in buffering lipid availability. To test portability across lineages, we translated ControLD to the diatom *Phaeodactylum tricornutum* (Pt), adapting targeting domains (including endogenous LD-binding proteins) and expression strategies. In Pt, ControLD forms robustly under multiple conditions; we compare encapsulation behaviors between models and infer potential physiological causes. Methodologically, this thesis delivers a modular toolkit for surface-localized LLPS meshworks with controlled affinity, coupling physical hindrance to metabolic readouts. By constraining LD accessibility rather than deleting components, ControLD isolates physical proximity from signaling and enzymatic partners. This establishes organelle trapping by engineered condensates as a general approach to probe organelle interfaces and lipid homeostasis.

KEYWORDS

Lipid droplets, liquid-liquid phase separation, perturbative approach, synthetic biology tools, lipid metabolism

RÉSUMÉ

Les gouttelettes lipidiques (LDs) sont des carrefours centraux de stockage et d'échange, en interface avec le réticulum endoplasmique, les mitochondries, les peroxysomes et les lysosomes, et régulent l'équilibre énergétique, la signalisation et les réponses au stress. Malgré une cartographie riche, établir un lien causal entre les interactions de surface des LDs et les flux lipidiques reste difficile. Dans cette thèse, nous avons développé une approche perturbative appelée ControLD : un système spécifique et programmable qui encapsule les LDs dans un réseau protéique issu d'une séparation de phase liquide-liquide (LLPS). En combinant des protéines de séparation de phase et des modules de ciblage des LDs, ControLD crée une barrière stérique réversible à leur surface, bloquant les interactions sans inhibiteurs chimiques. Dans les cellules de mammifères, un recrutement rapide et spécifique vers les LDs et une formation contrôlée du réseau sont observés; la LLPS permet un piégeage et une libération à la demande. Nous quantifions comment l'encapsulation remodèle les interfaces d'organites et le métabolisme : limiter l'accessibilité réduit l'afflux de lipides neutres en situation d'abondance nutritive, tandis que les LDs piégées résistent à la consommation lors d'une carence. Pour tester la portabilité inter-espèces, nous avons transposé ControLD chez la diatomée *Phaeodactylum tricornutum* (Pt), en adaptant les domaines de ciblage et les stratégies d'expression. Chez Pt, ControLD se forme de façon robuste ; nous comparons les encapsulations entre modèles et en inférons des causes physiologiques. Méthodologiquement, cette thèse fournit une boîte à outils modulaire pour cibler la formation de réseaux protéiques sur une surface. En restreignant l'accessibilité des LDs plutôt qu'en supprimant des composants, ControLD découple la proximité physique et les partenaires enzymatiques. Cela établit le piégeage d'organites par condensats artificiels en tant qu'approche générale pour sonder les interfaces d'organites et l'homéostasie lipidique.

MOTS CLÉS

Gouttelettes lipidiques, séparation de phase liquide-liquide, approche perturbative, outils de biologie synthétique, métabolisme lipidique